Understanding the Role of Macrophage Phenotype in Biomaterial-Mediated Tissue Regeneration

A Thesis

Submitted to the Faculty

of

Drexel University

by

Pamela Leigh Graney

in partial fulfillment of the

requirements for the degree

of

Doctor of Philosophy

January 2018

Dedications

To the loving memory of my father,

Stephen T. Kubinski

Acknowledgements

First and foremost, I would like to acknowledge my family, who have made this academic journey possible. To my husband, Sean, for his unwavering support, love and patience as I traveled the world and dedicated my time to this thesis. His selflessness enabled me to make my dreams a reality, and for that I will be forever grateful. To my parents and stepparents, who have always encouraged me to reach for the moon, and given me the discipline, confidence, and faith to get there. To my sister, Jenn, for the unbreakable bond we share. To my brother, Andrew, who taught me that nothing is impossible. To my loving in-laws for accepting me into their wonderful family. And, of course, Ellie, who is a daily source of inspiration and joy.

I am also tremendously grateful to my advisor, Dr. Kara Spiller, for taking me under her wing. Her leadership, dedication, and confidence in me has not only driven me to achieve a higher level of research, but also created opportunities for me that I never thought possible. She has been an excellent mentor and a role model for success. I would also like to give my utmost gratitude to Dr. Hala Zreiqat and Dr. Shulamit Levenberg, for guiding me in this work and allowing me to spend many months conducting research in their labs. My time abroad has had a profound impact on my life, both professionally and personally. I would also like to thank my committee members, Dr. Alisa Morss Clyne, Dr. Kenneth Barbee, Dr. Yinghui Zhong, and Dr. Lin Han, for advising me in this work.

I would also like to acknowledge the members of the Biomaterials and Regenerative Medicine Laboratory at Drexel, the Biomaterials and Tissue Engineering Research Unit at the University of Sydney, and the Stem Cell and Tissue Engineering Laboratory at the Technion-Israel Institute of Technology. I have been blessed to be surrounded by brilliant and hard-working peers, who have not only pushed me to excel,

but also provided me with lasting friendships. I am especially thankful to Dr. Sina Nassiri, Claire Witherel, Emily Lurier, Shahar Ben Shaul, Kate Wofford, Dr. Valerie Tutwiler, Bhavani Singh, Tony Yu, Amanda Pentecost, Dr. Anamika Bajpai, Carly Deusenbery, Nicole Ferraro, Nathan Tessema, Jessica Eager, Erin O'Brien, Greg Risser, Alicia Clark, Thant Soe, Kieran O'Donnell, Edgar Cardenas, Shira Landau, Ariel Szklanny, Tom Ben Arye, Dr. Luba Perry, Dr. Inbal Michael, Dr. Galia Ben David, Uri Merdler, Rita Beckerman, Barak Zohar, Dr. Seyed-Iman Roohani-Esfahani, and Peter Newman.

Additionally, I would like to take this opportunity to express my gratitude to the U.S.-Israel Binational Science Foundation, for awarding me with a Prof. Rahamimoff Travel Grant, to the Louis and Bessie Stein Family Foundation for a 2015-2016 Stein Fellowship, and for funding provided by the Koerner Family Foundation.

Finally, I could not have completed this work without the technical assistance of Dr. Sylvain Le Marchand and Dr. Marita Chakhtoura. I also owe a debt of gratitude to Dr. John Bethea for graciously providing me with the bench space needed to make this research possible in my final year at Drexel.

Table of Contents

List of Tables

List of Figures

Abstract

Understanding the Role of Macrophage Phenotype in
Biomaterial-Mediated Tissue Regeneration

Pamela Leigh Graney
Kara L. Spiller, Ph.D.

The underlying goal of tissue engineering is to functionally repair and regenerate complex tissues and organs. One of the major challenges in engineering viable tissues is forming functional and stable blood vessel networks (angiogenesis) within the tissue, which supply oxygen and nutrients to the cells. Following implantation, these networks must subsequently connect with the body's existing vasculature (anastomosis) for continued survival. Currently, there is no known way to control anastomosis, preventing the translation of many potentially useful biomaterials for tissue engineering applications. Macrophages, the primary cells of the inflammatory response, are major contributors to vascularization and regulate the response to implanted biomaterials; however, macrophages are highly plastic cells that alter their behavior in response to local stimuli, and the contributions of macrophage phenotype to these processes are poorly understood. Therefore, the overarching goals of this work were to (1) understand how regenerative biomaterials modulate macrophage behavior and (2) delineate the impact of changing macrophage phenotype on biomaterial vascularization.

First, the *in vitro* response of primary human macrophages to biomaterials proven to enhance tissue regeneration in animal models was evaluated. Interestingly, biomaterials more successful in promoting tissue repair induced a phenotypic shift in macrophage behavior toward an anti-inflammatory "M2" state. The modulatory effects of these scaffolds were predominantly due to direct cell-scaffold interactions, as only modest changes in macrophage gene expression were observed by soluble factors derived from

the scaffolds. Importantly, these findings provide evidence that regenerative biomaterials modulate macrophage behavior. Then, to elucidate the effects of changing macrophage phenotype on biomaterial vascularization, crosstalk between macrophages and vascular endothelial cells (ECs) was assessed via transwell co-culture. Interestingly, the angiogenic behavior of ECs was differentially influenced by macrophage phenotype; specifically, macrophages stimulated toward M1 and M2c activation induced EC up-regulation of genes related to vessel sprouting, while M2a and M2f macrophages altered genes related to vessel branching and extracellular matrix disassembly, respectively. Finally, the functional consequences of changing macrophage phenotype on biomaterial vascularization were ascertained through development of a 3D *in vitro* model of vascular growth. Self-assembly of ECs and support cells into vascular structures was achieved by co-culture on commercially available Gelfoam® scaffolds, to which macrophages were seeded at different stages of vessel development. Consistent with the previous study, M1 and, to a lesser extent, M2, macrophages increased vessel sprouting and the number of connected vessels relative to vascular networks without macrophages. Preliminary studies also demonstrated the potential for temporal control over macrophage activation to enhance vascularization.

Collectively, these findings can be used to inform the design of biomaterials that harness the inflammatory response to promote vascularization and improve healing outcomes. This work also has important implications for treating diseases characterized by extensive blood vessel growth, such as cancer and autoimmune conditions, whereby vascularization of the tissue facilitates disease progression.

CHAPTER 1: INTRODUCTION

1.1 Tissue Engineering

Organ transplantation as a field has achieved major advances over the last several decades that have not only allowed for successful long-term survival of transplanted tissue, but also significantly reduced the risk of implant rejection. Despite these accomplishments, there remains a staggering gap between the number of patients in need of life-saving organs and the number of donors worldwide. By the end of 2015, there were 122,071 patients on the national transplant waiting list in the United States alone [1]; however, only 30,975 transplants were performed, with organs recovered from 15,068 donors. Historically, this gap continues to widen every year, creating a global organ shortage crisis. As a result, there is a growing interest in developing engineered tissues and organs to meet this rising demand.

Tissue Engineering refers to “an interdisciplinary field that applies the principles of engineering and the life sciences toward the development of biological scaffolds that restore, maintain, or improve tissue function” [2]. The underlying goal of tissue engineering is to functionally repair and regenerate complex tissue and organs. This is traditionally achieved by combining cells derived from the patient or another individual, with growth factors or bioactive signals, on or within a 3-dimensional (3D) support or scaffold that is naturally derived or synthetic in origin. The scaffold, also referred to as a biomaterial, serves as a template to guide tissue formation and plays a fundamental role in creating a suitable microenvironment that orchestrates this process. Biomaterials are generally selected for tissue engineering applications based on several criteria, including first and foremost, biocompatibility, biodegradability, mechanical properties, and architecture.

Biocompatibility refers to the ability of the scaffold or tissue engineered construct to perform while eliciting an appropriate host response, which is inevitably initiated upon implantation. For many decades, biomaterials were designed with the intention of evading or minimizing the host response to avoid potentially detrimental immune reactions that could inhibit integration of the implant with the host tissue. Recently, however, there has been a paradigm shift away from these immuno-inert materials, toward biomaterials designed to harness and direct this response for improved tissue regeneration and healing outcomes.

1.2 Host Response to Biomaterials

Biomaterial implantation causes injury to vascularized tissue, which activates the inflammatory response and subsequent wound healing cascade [3, 4]. This cascade involves a series of coordinated events that can be divided into four phases: coagulation, inflammation, proliferation, and remodeling with scar tissue formation [5, 6]. The coagulation phase begins immediately post-injury, during which platelets adhere to damaged blood vessels and initiate a blood-clotting cascade to limit blood loss and provide a fibrin-based provisional matrix at the tissue-implant interface [3, 6]. In addition, platelets release a multitude of growth factors and cytokines that activate and recruit inflammatory cells to the injury site, representing the beginning of the inflammatory phase of healing. Neutrophils are the first cells to infiltrate the injury site and clear the wound of bacteria and foreign particles via release of enzymes and reactive oxygen species [6]. In the case of biomaterials, neutrophils are unable to engulf the implant due to its size, but activate in response to proteins that coat the biomaterial surface immediately upon implantation [7]. This activation stimulates the release of bioactive signals that recruit macrophages to the injury site. Neutrophils later undergo apoptosis and are removed by phagocytosis, or

uptake, by infiltrating macrophages. Macrophages are also phagocytic inflammatory cells, and act as key regulators in wound healing through release of growth factors that direct other cells in the tissue, including keratinocytes, fibroblasts and endothelial cells [6]. Following the inflammation phase is the proliferative phase, involving the formation of granulation tissue. During this time, fibroblasts are recruited to the injury site and begin to deposit extracellular matrix (ECM) that replaces the provisional matrix originally established, and further supports migration of dermal and epidermal cells [5, 6].

A critical component of the wound healing process is the development of an adequate blood supply, which not only provides cells with oxygen and nutrients, but also removes waste from the tissue. Upon injury to the tissue, the vascular supply is disrupted, creating an environment with low oxygen, referred to as hypoxia. The lack of oxygen, in addition to blood vessel damage, stimulates the release of signals that initiate vessel sprouting from nearby, undamaged vasculature. The establishment of new blood vessel occurs during all phases of the repair process and facilitates survival of the tissue and re-epithelialization [5, 6]. As the granulation tissue becomes vascularized and perfused, the surrounding matrix undergoes remodeling through a delicate balance of ECM synthesis and degradation by tissue degrading enzymes released by inflammatory cells and fibroblasts, and their corresponding tissue inhibitors. The wound begins to contract, which further facilitates remodeling and organizing of the matrix as the native tissue properties are restored. As healing progresses, fibroblasts undergo apoptosis, leaving behind relatively acellular scar tissue with a decreased number of blood vessels [6].

With respect to biomaterial implantation, an inability of macrophages to break down and phagocytose the material can lead to persistent inflammation. During this chronic inflammatory response, macrophages become frustrated and fuse to form multinucleated giant cells, which deposit a fibrous matrix around the implant, walling it off

from the rest of the body [7, 8]. This is referred to as fibrous capsule formation and impedes implant integration with host tissue and consequently, tissue regeneration.

1.3 Vascularization of Engineered Tissues

1.3.1 Vascularization is Required for Biomaterial-Mediated Tissue Repair

Despite significant advances in our understanding of the host response to biomaterial-tissue interactions, the potential of tissue engineering to develop complex 3D tissues has not yet been realized. Indeed, the translation of many regenerative medicine strategies has been limited by poor tissue vascularization and perfusion following implantation. This is especially true in large implants, as cells within the engineered tissue must rely on diffusion of oxygen for survival in the absence of an established vasculature network. However, oxygen diffusion is limited to 150-200 μm from the nearest capillary [9, 10], and vascular ingrowth is limited to several tenths of micrometers per day [11]. As a result, it can take weeks for an implanted tissue to be fully vascularized, during which time oxygen and nutrient deficiencies deep within the tissue can lead to cell death and impaired tissue integration and function. Since the natural rate of vessel growth is often too slow to support long-term implant survival, several strategies are being explored to enhance engineered tissue vascularization. Importantly, blood vessels must not only form within the engineered tissue, a process referred to as angiogenesis, but also connect or anastomose with the surrounding host vasculature in order to achieve perfusion and continued tissue survival.

1.3.2 Blood Vessel Development

Blood vessels are tubular structures lined with endothelial cells (ECs) that are surrounded by a layer of perivascular support cells and a basement membrane [12].

Formation of blood vessels can occur through two underlying processes: vasculogenesis and angiogenesis [9, 13, 14]. Vasculogenesis refers to the *de novo* formation of blood vessels that occurs predominantly during early development [15]. During this process, endothelial progenitor cells differentiate into mature ECs, proliferate in avascular areas and assemble to create a primitive vessel network [9]. In contrast, angiogenesis refers to the sprouting of new capillaries from pre-existing blood vessels and mainly contributes to physiological and pathological blood vessel growth that occurs in post-natal life [15].

Angiogenesis involves a complex and dynamic multi-stage cascade that broadly involves degradation of the basement membrane and surrounding ECM by tissue degrading enzymes called matrix metalloproteinases (MMPs), EC migration from the vessel walls driven by gradients of vascular endothelial growth factor (VEGF) – a potent angiogenic stimulator [16], and EC proliferation and tube formation guided by complex cell signaling [17, 18]. Newly formed neighboring vessels then fuse, or anastomose, followed by synthesis of a new basement membrane and recruitment of support cells that stabilize the vessel wall and regulate blood pressure. During this process, ECs display functional heterogeneity, and compete with each other to dynamically acquire specialized phenotypes that allow for coordinated blood vessel growth [19, 20]. ECs that lead vascular sprouts are called tip cells, which display extended filopodia and migratory behavior, and respond to direction cues from the local milieu [19]. Following the tip cells are stalk cells, which maintain the integrity of the network [15]. In contrast to tip cells, stalk cells display fewer filopodia, and are highly proliferative; additionally, they are responsible for establishing tight junctions to maintain the stability and integrity of the new sprout, while forming the budding vessel lumen [19]. Once the newly formed vessels have matured and blood flow is established, ECs enter a quiescent state during which migration and proliferation ceases [13].

The differentiation of ECs into tip and stalk cells is dynamic, and regulated in part by the VEGF/Notch pathway. Tip cells are enriched for Delta-like ligand 4 (DLL4), a transmembrane protein that binds to Notch receptor on adjacent cells, VEGF Receptor 2 (VEGFR2, also known as KDR), and platelet-derived growth factor-beta (PDGFB), among others [19]; whereas, stalk cells are enriched for the ligand Jagged-1 (Jag1), which also binds to Notch receptor but with opposing effects compared to DLL4 [21]. VEGF stimulation (usually in response to hypoxia) causes activation of VEGFR2 on tip cells, which then induces DLL4 expression. DLL4 on these tip cells subsequently binds to Notch receptor on adjacent cells, leading to down-regulation of VEGF receptors, consequently reducing their ability to bind to VEGF and activate VEGFR2 [13]. This action ultimately impedes the differentiation of these adjacent cells into sprouting tip cells. In contrast, Jag1 on stalk cells binds to Notch receptor on tip cells, preventing activation of Notch signaling on these tip cells. Hence, DLL4 suppresses EC sprouting and proliferation, while VEGF and Jag1 promote angiogenic EC behavior. Interestingly, stalk cells also produce VEGFR1, which acts as a decoy receptor to locally deplete VEGF and maintain a gradient of higher VEGF levels ahead of the sprouting tip cells [13]. Moreover, data suggests that although stalk cells proliferate, this proliferation does not push the tip cell forward; rather, tip cells are believed to interact with the surrounding matrix and pull themselves in the direction of the growing sprout [22]. Nevertheless, proliferation is needed to enable further outgrowth of the vessel, as reduced stalk cell proliferation is associated with vessel regression [23].

When two sprouting vessels come in contact, the tip cells form new inter-cellular junctions that facilitate the process of vessel fusion, or anastomosis. Although VE-cadherin has been implicated in this process [24], the mechanisms behind anastomosis remain unknown. Indeed, studies have also implicated other cells, including macrophages,

in this process [25], based on the reciprocal expression of several receptor-ligand candidates that could facilitate macrophage-EC interaction. For example, Notch, Tyrosine-protein kinase receptor (TIE2), and C-X-C chemokine receptor type 4 (CXCR4) are all expressed on macrophages, while their counterparts DLL4, Angiopoietin-2 (ANGPT2), and Stromal cell-derived factor-1 (SDF1) are expressed on endothelial cells [26-29].

Post-anastomosis, the immature vessels undergo stabilization through deposition of ECM around the vessel and recruitment of mural support cells, such as pericytes, in response to tip-cell derived PDGFB [12, 30]. Recruited mural cells are believed to undergo differentiation in response to including transforming growth factor-beta 1 (TGFB1) [31], and deliver vascular stabilizing factors, such as tissue inhibitor of metalloproteinase 3 (TIMP3) and ANGPT1. ANGPT1 signaling through TIE on ECs is thought to stabilize the vessels and reduce leakiness, possibly by promoting DLL4 and activating Notch signaling, which subsequently suppressed VEGFR2 and induced expression of Notch regulated ankyrin repeat protein (NRARP) [13, 31, 32]. NRARP promotes Wnt signaling in stalk cells, which then leads to stabilization of tight junctions [23].

Once the vessels undergo stabilization, remodeling and pruning occur in order to facilitate patterning of the vasculature. Currently, the process of vascular remodeling and regression is not well understood, and there is a lack of consensus regarding the drivers of this process. It is plausible that regression occurs due to the removal or absence of pro-survival factors like VEGF and VE-cadherin [33], as well as through active signaling pathways that induce cell death [34, 35]; however, recent studies suggest that EC apoptosis removes only non-perfused vessel segments but does not regulate vessel regression in murine retinal angiogenesis [36]. Alternatively, it was recently proposed that vessel regression is the result of directed migration of ECs, resembling anastomosis in

reverse [37]. In addition to these findings, it has been documented that mechanical activation imparted by blood flow also influences EC survival and angiogenesis [38, 39].

Nevertheless, as the matured vessels become organized and perfused, ECs enter a state of quiescence that prevents excessive and aberrant vascularization.

1.3.3 Strategies to Improve Biomaterial Vascularization

The establishment of a functional blood vessel network within engineered tissues is a necessity to ensure survival and integration post-implantation. As a result, strategies that improve biomaterial vascularization are paramount to advance the field of tissue engineering and regenerative medicine. Significant efforts are being made to address this challenge, and for a detailed review of this strategies, the reader is referred to Ref. [9, 10, 14, 40]; a few of the most common current approach being explored are outlined briefly here.

1.3.3.1 Growth Factor-Releasing Biomaterials

A common approach to improve vascularization *in vivo* is to design a system that facilitates release of one or more pro-angiogenic growth factors. For example, Cao *et al.* demonstrated that transient exposure of PDGFB and fibroblast growth factor (FGF)-2 in a rat or rabbit hind-limb ischemia model promoted the long-term development of stable and functional blood vessels, even after removal of the stimuli [41]. Likewise, Awada *et al.* designed a controlled release system for the sequential delivery of VEGF and PDGF [42]. By embedding VEGF in a fibrin gel, and PDGF in a heparin-based coacervate distributed within the fibrin gel, the authors demonstrated improved angiogenesis and cardiac function with reduced fibrosis and inflammation in a rat model of myocardial infarction [42]. In other work, simultaneous delivery of VEGF and ANGPT2, followed by delivery of PDGF and

ANGPT1 from a macroporous polymer not only enhanced vessel maturation, but also promote vascular remodeling following subcutaneous implantation in mice [43]. However, the same effects were not observed if all factors were delivered at the time, demonstrating that temporal control over growth factor release can be used to control vascularization. Similar effects were reported by others following the sequential delivery of VEGF, FGF2 and PDGF in chorioallantoic membrane (CAM) angiogenesis *in vivo* [44]. In a slightly different approach, Hsu *et al*. implanted polymeric hydrogel discs containing VEGF or PDGF with FGF in a murine cornea model of angiogenesis, and found that the combination of PDGF and FGF induced recruitment of macrophages. Interestingly, dynamic interactions between macrophages and ingressing blood vessels increased the density, organization and perfusion of the vessels, compared to VEGF alone [45].

1.3.3.2 Pre-Vascularization of Biomaterials

An alternative strategy to delivering growth factors is to form a vascular network within the construct prior to implantation. This serves to accelerate anastomosis and subsequent perfusion of the implant, and is commonly achieved by co-culturing endothelial cells and support cells on a 3D structure to self-assemble into a vascular network. The construct is then implanted with the aim of achieving anastomosis between the engineered and host vasculature [46]. This concept was demonstrated in seminal work by Levenberg *et al*., in which human umbilical vein endothelial cells (HUVECs) were co-seeded with myoblasts and embryonic fibroblasts on a porous polymer scaffold comprised of poly(L-lactic acid) (PLLA) and poly(lactic-glycolic acid) (PLGA) [47]. After 2 weeks, the engineered muscle constructs were implanted subcutaneously in mice, or intramuscularly into rat muscle; the authors demonstrated that pre-vascularization significantly improved perfusion of the tissue and survival of muscle constructs. A similar concept was explored

by Chen *et al*., in which HUVECs and fibroblasts were seeded together in fibrin gel and vascular networks were established over 1 week *in vitro* [48]. Subcutaneous implantation in a dorsal window in mice revealed a significantly greater presence of blood vessels within the engineered tissue by day 5, compared to constructs that were not pre-vascularized which required 14 days for perfusion. Likewise, HUVECs, embryonic fibroblasts, and human embryonic stem cell (hESC)-derived cardiomyocytes have been tri-cultured on PLLA/PLGA scaffolds for 2 weeks, and then engrafted to cardiac tissue in rats, resulting in formation of donor and rat-derived vasculature within the graft that were functionally integrated [49]. More recently, Kusuma *et al*. demonstrated that human pluripotent stem cells (hPSCs), induced to co-differentiate into early vascular cells, can develop into ECs and pericytes and self-assemble into microvascular networks on 3D engineered tissue [50]; upon subcutaneous implantation in mice, the engineered tissue was integrated and perfusable.

In vivo pre-vascularization approaches have also been explored, to a lesser extent. For example, Zhang *et al.* embedded VEGF in PLGA/poly(ethylene glycol) microspheres, and seeded them on a collagen-chitosan scaffold containing human adipose-derived stem cells; following implantation around a vascular pedicle in nude rats, the construct supported the development of a vascularized soft tissue flap, which has potential to be transferred to a recipient site [51].

1.3.3.3 Microfabrication of Engineered Vascularization

Vessels have also been engineered using microfabrication techniques. For example, Kolesky *et al*. used 3D bioprinting to generate vascularized tissues exceeding 1-cm in thickness, that were perfusable on a chip for several weeks [52]. Specifically, human mesenchymal stem cells (MSCs) and fibroblasts were co-printed within a cross-

linked gelatin-fibrin matrix with sacrificial ink, which was removed to create a hollow network within the matrix that was subsequently perfused and lined with ECs. The authors demonstrated that the engineered tissue supported the differentiation of MSCs. In other work, Miller *et al*. used a biocompatible sacrificial material to 3D print engineered tissues containing living cells, thereby generating tubular networks that could be perfused and endothelialized [53].

1.4 Macrophages Regulate Healing

As noted earlier, the inflammatory response plays a critical role in the host response to implanted biomaterials. Macrophages are monocyte-derived myeloid cells originating from the bone marrow, and have long been recognized as the primary cells of the inflammatory response and crucial regulators of healing [54]. Indeed, depletion of macrophages from wounds has been proven to impair adult salamander limb regeneration [55], as well as murine skeletal muscle regeneration [56] and tissue repair post-myocardial injury in mice[57]. While macrophage depletion causes drastically reduced angiogenesis [25, 58, 59] and healing, exogenous addition of macrophages promotes angiogenesis [60, 61]. Consistent with these findings, macrophages have been demonstrated to play an important role in the repair of bone – one of the most highly vascularized tissues in the body. For example, in a murine femoral fracture model, macrophage depletion abolished callus formation – which stimulates angiogenesis and the healing cascade, demonstrating the importance of macrophages to endochondral ossification [62]. Macrophages also mediate *in vivo* woven bone deposition and mineralization [63] and enhance differentiation of mesenchymal progenitors [64] during fracture repair.

This multifaceted behavior stems from the inherent plasticity of macrophages, which exist on a spectrum of activation states or phenotypes [65]. Macrophages exert

control over all phases of tissue regeneration and alter their behavior in response to changing environmental stimuli [66]. This plasticity suggests that biomaterials that modulate macrophage behavior have potential to direct the response to implanted tissues, thereby promoting integration and healing outcomes. Although there are a multitude of phenotypes that likely exist *in vivo*, macrophages classification is commonly oversimplified to discriminate between classically activated, or pro-inflammatory, “M1” macrophages and alternatively activated, or anti-inflammatory, “M2” macrophages. However, the M2 classification has recently been expanded to include essentially all other distinct phenotypes, including M2a, M2c, and M2f, all of which contribute to tissue repair [67-70]. There are also several other phenotypes that have been described in response to different stimuli [71-73], as well as those associated with tumors [74] and hybrid M1/M2 profiles [75]. M1 macrophages are believed to clear the injury of pathogens and cellular debris, and can be activated *in vitro* in the presence of lipopolysaccharide (LPS) and interferon-γ (IFNγ). In contrast, M2 macrophages contribute to tissue repair processes, including tissue deposition and breakdown, but their roles are incompletely understood [70]. M2a macrophages have been implicated in fibrous capsule formation and fibrosis in various tissues [76-78], while M2c macrophages have been shown to display a higher capacity to phagocytose apoptotic cells [79], and secrete an array of tissue degrading MMPs [80]. M2f macrophages secrete anti-inflammatory mediators and have been linked to angiogenesis [Brecht 2011]. M2 macrophages can be stimulated *in vitro* by the presence of interleukin (IL)-4 and IL13 for M2a activation; IL10 for M2c activation; and apoptotic cells for M2f activation [Spiller 2014, Voll 1997].

Importantly, in the normal healing process of many tissues, including bone, the macrophage population shifts from predominantly M1 to predominantly M2 over time [81]

[82], which may be related to their proposed roles in angiogenesis [70, 83]. However, it is not clear whether phenotypic shifts in macrophage activation result from the same macrophage population, or represent a new influx of macrophages recruited to the injury site. Moreover, with many studies failing to discern among M2 phenotypes, it is not clear if the shift toward M2 activation holds true for all M2 macrophages. In fact, recent studies have provided evidence suggesting that M2c macrophages act early in the repair process [80, 84]. It is clear that temporal profile of macrophage activation plays a critical role in tissue regeneration, as studies have shown that selective depletive of macrophages at different times during wound healing drastically alters the repair process [85]. Moreover, evidence suggests that the balance of M1 and M2 macrophages can be used to predict not only healing in chronic diabetic ulcers [86], but also the extent of biomaterial-mediated tissue repair [87, 88].

1.5 Macrophages Affect Biomaterial Vascularization

It is widely appreciated that inflammation and angiogenesis are intimately linked processes [89]. Indeed, studies have shown that pre-seeding monocytes on a biphasic bone substitute led to increased vessel ingrowth and maturation upon subcutaneous implantation in mice [90]. Likewise, addition of murine-derived macrophages to peptide-modified PEG matrixes seeded with ECs has been demonstrated to enhance EC tubule volume relative to scaffolds without macrophages [91]; moreover, macrophages were observed to both wrap around vessels and bridge ECs, as others have shown. Nevertheless, the cell-specific contributions between these dynamic processes are still unclear.

Importantly, macrophages have been implicated at multiple stages of the angiogenic cascade, and have been called the “architects of development” [92]. Recently,

a murine cornea model of macrophage recruitment revealed dynamic interactions of macrophages and ingressing blood vessels that simultaneously up-regulated both M1- and M2-related genes [45]. This was consistent with prior findings that macrophages can act as bridging cells to support anastomosis [25], as well as guide sprouting vessels by forming tunnels within the local extracellular matrix [93, 94] However, the relative contributions of macrophage phenotypes remain unclear. For example, $CCR2^{+}$ (M1) macrophages are critical for inducing vascular sprouting by VEGF secretion at early stages of healing in murine skin wounds [95], and M1 conditioned media has been shown to promote vascular tube formation *in vitro* [70]. In contrast, bone marrow-derived M1 macrophages inhibited tube formation in a Matrigel plug implanted subcutaneously in mice, while M2a and M2c macrophages enhanced angiogenesis, but through different mechanisms [96]. Others report the presence of both M1 and M2 phenotypes in vascularizing engineered soft tissue flaps, where M2 macrophages were localized in the remodeled tissue and M1 were found mostly in the engineered tissue [51]. Recently, it has been shown that M1 macrophages stimulated *in vitro* secrete the highest levels of the angiogenic stimulator VEGF, while M2a secrete large quantities of the chemoattractant PDGFBB, and M2c produce the highest levels of ECM-degrading MMP9 [70]; not surprisingly, several studies have demonstrated that proper temporal regulation of these factors is needed for successful angiogenesis [18, 43]. Taken together, these findings suggest that M1, M2a and M2c macrophages play unique roles in angiogenesis and anastomosis, both temporally and spatially.

1.6 Macrophage Modulation as a Therapeutic Strategy

Proper temporal control over macrophage activation is crucial for healing. It is well established that excessive M1 activation leads to chronic inflammation, while insufficient

M1 activation delays healing due to accumulation of cell debris and poor vascularization [97, 98]; likewise, excessive M2a activation can lead to fibrosis and encapsulation of the implant [99, 100], but insufficient M2a activation disrupts angiogenesis and causes chronic wound formation. Based on this precedence, there has been a paradigm shift toward the design of biomaterials that pro-actively direct the inflammatory response to promote healing of chronic wounds, tissue defects, and inflammatory conditions (Reviewed in [101, 102]). These includes strategies that modulate M1 activation, M2 activation, or temporal modulation of both phenotypes.

1.6.1 Modulation of M1 Activation

For example, researchers have used biomaterials to delivery anti-TNF small interfering RNA (siRNA) in order to inhibit TNF production by M1 macrophages in murine models of collagen-induced arthritis (CIA) and inflammatory bowel disease (IBD) [103, 104]. Inhibition of macrophage TNF prevented arthritis-induced bone loss 7 weeks post-treatment, and inhibited the onset of colitis. Alternatively, treatments designed to enhance IL10 expression, an anti-inflammatory cytokine, have been used to suppress inflammation in a rat adjuvant arthritis model [105]. Delivery of nanoparticles containing plasmid RNA enhanced expression of M2 marker Cluster of Differentiation 163 (CD163), and reduced tissue levels of pro-inflammatory cytokines, including tumor necrosis factor-alpha (TNF), IL6, and IL1B.

Importantly, inhibiting M1 activation is not always beneficial, despite higher levels of baseline inflammatory activity in chronic inflammatory conditions, like diabetic wounds. It is suspected that M1 macrophages may enter a state of low-grade chronic inflammation, through which they become hypo-responsive to inflammatory stimuli and cannot mount an appropriate response to stimulate tissue repair [106-108]. Indeed, administering IL1B-

stimulated M1 macrophages into subdermal wounds in a diabetic mouse model led to increased granulation tissue formation and promoted lymphatic vessel development in work conducted by Maruyama *et al*. [108]. Likewise, Yin *et al*. have shown that recruitment of a fresh population of M1 macrophages via release of monocyte chemotactic protein 1 (MCP1) from gelatin/polyglycolic acid scaffolds in a diabetic murine model facilitated the development of epithelial tissue and improved healing rates [109].

Collectively, these and other studies provide evidence that biomaterial-mediated modulation of abnormal macrophage behavior in chronically inflamed tissues can promote healing.

1.6.2 Modulation of M2 Activation

As an alternative to inhibiting M1 responses, researchers have also explored strategies to promote tissue repair by modulating M2 activation. For example, antibodies targeting IL4 – a potent activator of the M2a phenotype *in vitro*, were injected into poly(etherurethane urea cages) implanted subcutaneously in mice, leading to reduced foreign body giant formation around the cages [77]. While this study supports the contribution of M2a macrophages in fibrous capsule formation, the role of this phenotype in the foreign body response is controversial, as others have delivered IL4 from chitosan/dermatan sulfate-coated polypropylene mesh implanted subcutaneously and demonstrated reduced fibrosis and enhanced tissue remodeling that correlated with reduced M1 activation and transiently enhanced M2a activity [110]. Together, these studies demonstrate the importance of a properly controlled M2 response to mitigate the foreign body response.

Biomaterial-mediated modulation of M2 activation has also been used to repair cardiac tissue post-myocardial infarction (MI). Inspired by the ability of apoptotic cells to

promote secretion of anti-inflammatory factors, Harel-Adar *et al.* prepared liposomes presenting phosphatidylserine (PS) – a ligand recognized by macrophages that is expressed on the surface of apoptotic cells, to induce M2 activation in a rat model of acute MI [111]. Post-intraperitoneal (IP) injection in mice, PS-presenting liposomes elicited enhanced macrophage engulfment; moreover, intramyocardial injection of PS-presenting liposomes immediately after MI significantly enhanced macrophage production of anti-inflammatory IL10 and TGFB. Corresponding to these effects, tail vein injection of PS-presenting liposomes 48 h after MI was also shown to prevent ventricular dilatation and remodeling. This work demonstrates that modulation of cardiac macrophages toward M2f activation can improve infarct repair.

Improved biomaterial-tissue integration has also been demonstrated by release of microsphere-encapsulated IL4 from collagen scaffolds implanted subcutaneously in mice, which enhanced infiltration of M2a macrophages into the scaffold 24 h post-implantation [112]; however, up-regulation of genes related to both M1 and M2a activation observed after 3 days, which may suggest a synergistic role for multiple macrophage phenotypes.

Taken together, these studies suggest that modulating the behavior of a single macrophage phenotype can improve healing outcomes.

1.6.3 Temporal Modulation of M1 and M2 Activation

Although the strategies described above have potential to enhance tissue repair, recent evidence suggests both M1 and M2 phenotypes are required for biomaterial integration with host tissue [70]. Indeed, M1 macrophages have been shown to initiate angiogenesis [70] and may prime fibroblasts for ECM deposition [113]; and M2a macrophages have been suggested to stabilize angiogenesis [70] and promote ECM

deposition [114]. These findings, coupled with the known M1-to-M2 phenotypic transition that occurs during the normal healing process of many tissues, has motivated researches to develop strategies that actively target both M1 and M2 macrophages, in a temporally controlled manner, to enhance biomaterial-mediated tissue regeneration.

This approach was recently explored by Spiller *et al.* via sequential delivery of M1- and M2a-stimulating cytokines from bone scaffolds following subcutaneous implantation in mice [83]. The authors first used biotin-streptavidin binding to conjugate IL4, an M2a stimulator, to the surface of decellularized bone, followed by physical adsorption of IFNγ. Although individual release of the cytokines *in vitro* promoted up-regulation of genes associated with the M1 or M2a phenotypes, sequential release of IFNγ and IL4 did not induce robust activation of either phenotype, perhaps due to overlapping release profiles. This study underscores the need for proper temporal control over macrophage phenotype.

In other work, temporally controlled delivery of MCP1 and IL4 was demonstrated using multidomain peptides that self-assemble to form fibrous mesh and, consequently, nanofibrous hydrogels [115]. In this study, MCP1 was used to recruit macrophage to the implant, while IL4 served to direct M2a activation. Notably, subcutaneous implantation in rats demonstrated enhanced macrophage filtration after 3 days, and increased expression of M2 markers, CD206 and CD163, by day 7. Moreover, biphasic release of MCP1 and IL4 led to distinct blood vessel formation 1 week post-implantation, and were completely resorbed by day 14. Overall, these findings provide evidence that temporally controlled activation of M1 and M2 phenotypes has potential to enhance biomaterial-mediated tissue repair.

A similar concept was applied by Kim *et al*. using gelatin hydrogels to simultaneously deliver a macrophage recruiting agent, SEW2871, and platelet-rich

plasma (PRP), as a means to promote angiogenesis and enhance bone repair in a rat critical-size defect. Release of SEW2871 and PRP led to an influx of macrophages and enhanced collagen deposition within 3 days post-implantation. Intriguingly, these hydrogels also promoted transient up-regulation of pro-inflammatory TNF, and sustained up-regulation of IL10 after 10 days *in vivo*, which correlated with the most pronounced bone formation, relative to control constructs.

Based on these findings, an early but transient M1 response that shifts toward M2 activation may be a suitable approach to direct biomaterial-mediated tissue repair. However, the contributions of macrophage phenotypes are still largely undefined, due in part to an underappreciation for the many distinct M2 phenotypes that are simply denoted as M2. Nevertheless, it is clear that macrophages play a role in vascularization and biomaterial-mediated tissue regeneration. If we can advance our understanding of the roles that macrophage phenotypes play in these processes, this knowledge could be applied to improve the translation of many biomaterials that are currently unviable due to insufficient perfusion and integration with host tissue.

1.7 Bone as a Model Vascularized Tissue

One approach to understand the relationship between macrophage phenotype, vascularization, and tissue repair is to investigate these processes in tissue that has an innate ability to heal itself, such as bone. Bone represents a unique tissue with an innate capacity to self-repair small fractures, without fibrous scarring [116]; however, large, critical-size defects are generally unable to heal without intervention [117]. While treatment most commonly involves the transplantation of either allografts or autografts, harvested from other locations in the body, into the defect, these strategies are associated with many drawbacks, including infection, limited tissue supply, donor site morbidity and poor

integration[118]. As a result, tremendous efforts have been made to use tissue engineering approaches that can be used to regenerate the native tissue. Most commonly, this involves culturing cells on 3D scaffolds *in vitro*, which are later implanted into the defect. Despite major advances in the field, realization of this strategy has been severely hampered due to the lack of a functional vasculature supply, which, not surprisingly, is considered a major pitfall of engineered bone tissue [119]. This is a major hurdle considering that bone is a metabolically active and highly vascularized tissue, in which skeletal integrity relies on the close proximity of blood vessels.

1.8 The Inflammatory Response is Critical for Bone Repair

Upon injury to bone, fracture healing occurs through a complex cascade of events that is initiated by a trauma-induced inflammatory response followed by ossification and bone remodeling [120-123]. Post-fracture, vascular endothelial damage leads to hematoma formation at the injury site, which is then infiltrated by inflammatory cells. This cascade leads to formation of an avascular cartilaginous callus and stimulates angiogenesis. The fracture callus is subsequently mineralized and replaced by woven bone as the fracture site is revascularized [123, 124]. The woven bone is later remodeled to restore the original tissue structure and mechanical integrity. Establishment of an active blood vessel network is a prerequisite for proper bone repair [125]. Indeed, studies have shown that the absence of VEGF reduces angiogenesis, bone formation, and callus mineralization; whereas, addition of VEGF enhances blood vessel formation and new bone maturation [126]. Similar to other tissues, this process is initiated and regulated by the inflammatory response, which consequently plays a central role in bone repair. Indeed, it has been shown that, at early times after injury, removal of the fracture hematoma, which initiates the inflammatory cascade, impairs healing [127, 128]. Similarly, the absence of

pro-inflammatory signals, like TNF, following injury leads to delayed chondrogenic differentiation and resorption of the mineralized cartilage, resulting in altered fracture healing [129], perhaps due to the role of TNF in coordinating the expression of angiogenic factors and MMPs [130]. Alternatively, infusion of TNF to murine bone fractures at early times after injury significantly accelerates healing [131], and the addition of inflammatory cytokines TNF and interleukin-1β (IL1β) to cell culture media causes increased osteogenesis of mesenchymal stem cells (MSCs) [132]. However, prolonged inflammation also leads to impaired healing in bone [133]. For example, acute exposure of adipose-derived stem cells to TNF has been shown to promote vascularization *in vitro*, whereas continuous exposure and high doses inhibit vascular growth [134]. Collectively, these data emphasize the importance of a precisely controlled inflammatory response, and consequently vascularization, for bone regeneration.

1.9 Macrophage-Biomaterial Interactions Affect Bone Repair

Given the interplay of the inflammatory response and angiogenesis [135], a number of studies have started to explore the interactions of macrophages with biomaterials for bone regeneration.

However, the role of macrophage phenotype in bone repair is still unclear. Ceramic-based materials inducing M2c activation have been shown to promote osteogenic differentiation of MSCs *in vitro* [136, 137], whereas others have found that increased recruitment of M1 but limited M2 macrophages leads to greater bone formation [138, 139]. Unfortunately, many of these studies fail to distinguish between M2a and M2c phenotypes, which may account for some of the conflicting literature and may warrant further investigation. Moreover, it is still unclear how biomaterials, including ceramic bone substitutes, impact the microenvironment to modulate macrophage behavior and affect

healing outcomes, though ion release [136, 140], surface topography [141] microstructure [142], and mechanical properties [143, 144] have all been shown to influence macrophage activation. Identifying the properties of biomaterials that regulate inflammatory cell behavior would have important implications for biomaterial-mediated bone repair strategies.

CHAPTER 2: RESEARCH GOALS

The overarching goals of this work were to 1) understand how macrophages respond to biomaterials used in tissue regeneration, using bone as a model vascularized tissue, and 2) interrogate the effects of changing macrophage behavior on biomaterial vascularization. The overall hypothesis of this work was that sequential activation of M1 and M2 macrophages promotes enhanced biomaterial-mediated tissue regeneration and vascularization. This hypothesis was tested through the following 3 specific aims:

Specific Aim 1: Determine how regenerative biomaterials regulate macrophage phenotype over time. Using ceramic scaffolds proven to promote tissue regeneration *in vivo* in comparison to less successful controls, the temporal response of unactivated macrophages in direct contact or transwell co-culture with the scaffolds was determined. In addition, mechanisms of macrophage modulation were investigated by varying scaffold properties. It was hypothesized that scaffolds most successful in promoting tissue regeneration induce an M1-to-M2 phenotypic transition over time.

Specific Aim 2: Characterize the effects of macrophage phenotype on vascular endothelial cells *in vitro*. Using a 2D transwell co-culture system *in vitro*, the effects of M1, M2a and M2c macrophages on endothelial cell behavior were assessed. It was hypothesized that M1 and M2c macrophages promote up-regulation of genes related to tip cell selection and vessel sprouting, while M2a macrophages promote up-regulation of genes related to vessel stabilization and maturation.

Specific Aim 3: Develop a platform to delineate the contribution of macrophage phenotype to tissue vascularization *in vitro*. A previously established 3D model of biomaterial vascularization was adapted for a novel application, the study of macrophage phenotype in angiogenesis. This model was subsequently used *in vitro* to identify the individual roles of M1, M2a and M2c macrophages, as well as the effects of sequential M1 and M2 activation, in promoting angiogenesis. It was hypothesized that M1 and M2c macrophages promote sprouting, and M2a macrophages facilitate anastomosis and vessel thickening.

Achieving sufficient and functional vascularization is a major challenge in engineering tissues for regenerative medicine. Establishing the role of the inflammatory response to biomaterial-mediated tissue regeneration can be used to inform the design of new biomaterials that promote vascularization and healing. Moreover, understanding how the inflammatory response regulates vascularization would have important implications for treating diseases and chronic inflammatory conditions associated with extensive blood vessel growth, such as cancer and many autoimmune conditions [89], whereby vascularization of the tissue facilitates disease progression.

CHAPTER 3: TEMPORAL RESPONSE OF MACROPHAGES TO REGENERATIVE BIOMATERIALS

3.1 Introduction

More than 6 million bone fractures occur annually in the United States alone [145, 146], and 5-10% of these fail to heal adequately due to bone loss, failed fixation, infection and poor vascularization [145]. Bone is a unique tissue in that small fractures can self-repair, without fibrous scarring [116], but large, critical-sized bone defects remain a challenge [117]. Therefore, there is a significant need for tissue engineering strategies that utilize artificial materials to harness the intrinsic ability of bone to repair itself. Despite efforts to engineer bone tissue to address this challenge, the lack of functional vasculature remains a major cause of failure [119].

Although it is well established that macrophages regulate the inflammatory response to implanted biomaterials by rapidly shifting their phenotype in response to environmental stimuli [66], it is not clear how biomaterials alter the microenvironment in fracture healing to modulate macrophage behavior and affect vascularization and healing outcomes. Studies have shown that the structural and mechanical properties of biomaterials can induce macrophage activation [142, 147, 148], but such effects are not limited to direct contact between biomaterial-cell interfaces, as ions have also been shown to modulate macrophage behavior [149, 150]. As an initial step to understand how biomaterials regulate macrophage phenotype in bone repair, the interactions between macrophages and model biomaterials proven to enhance bone regeneration in animal models were studied.

For this work, Baghdadite ($Ca_3ZrSi_2O_9$) and Strontium-Hardystonite-Gahnite (Sr-HT Gahnite, Sr-$Ca_2ZnSi_2O_7$-$ZnAl_2O_4$) scaffolds were selected as two materials that enhance bone regeneration in critical size defects compared to clinically used tricalcium

phosphate-hydroxyapatite (TCP-HA) manufactured to the same specifications [151, 152]. Both Baghdadite and Sr-HT Gahnite have been shown to result in extensive new bone formation and complete bridging of critical-sized radial segmental defects in rabbits 12 weeks post-implantation, compared to only partial bridging demonstrated by TCP-HA [151-153]. In sheep segmental defect models, Baghdadite scaffolds also showed 80% bridging of the critical-sized defect with evidence of bone infiltration and remodeling within the scaffold implant [154]. Baghdadite scaffolds not only supported bioactivity of primary human osteoblasts and endothelial cells, but also promoted the differentiation of monocytes to form functional osteoclasts *in vitro* [155]. Intriguingly, while direct contact between Baghdadite and either osteoblasts or adipose-derived stem cells (ASCs) promoted osteogenic gene expression and bone morphogenetic protein 2 (BMP2) secretion *in vitro*, these scaffolds also modulated the cross talk between osteoblasts and ASCs to promote osteogenic behavior in an indirect co-culture system [156]. By comparison, the unique microstructural design of Sr-HT Gahnite enabled this scaffold to elicit bioactivity with osteoblasts, while reproducing the mechanical properties of native bone [152]. Sr-HT Gahnite has also been shown to support adhesion and osteogenic differentiation of ASCs, as well as enhanced angiogenic activity by ASCs and human microvascular endothelial cells *in vitro* and *in vivo* [157]. While these scaffolds are known to directly affect osteogenic cells involved in bone formation, their effects on recruited macrophages are unknown.

Therefore, the goal of this aim was to characterize macrophage activation in vitro in response to these scaffolds, with the hypothesis that biomaterials with different properties induce different macrophage responses, through both direct and indirect mechanisms; it was anticipated that these changes would be correlated with the ability of the scaffolds to promote bone repair in vivo. To test this hypothesis, the temporal response

of unactivated (M0) macrophages in direct contact with the scaffolds was evaluated to determine the potential of the scaffolds to modulate macrophage behavior. Then, to explore potential mechanisms of macrophage modulation, the effects of soluble factors released from the scaffolds on macrophage activation were compared. Finally, scaffold grain size was investigated as a potential contributing factor to macrophage modulation, since topographical and mechanical cues are known to affect macrophage phenotype. Macrophage response was evaluated in terms of gene expression for a panel of markers indicative of the M1, M2a and M2c phenotypes, because of their distinct roles in promoting vascularization and tissue repair[70], as well as genes involved more generally in angiogenesis, tissue remodeling, and osteogenesis.

This work has been published in the Journal of the Royal Society Interface [158].

3.2 Experimental Section

3.2.1 Experimental Design

A schematic of the experimental design is provided in **Figure 3.1**. Primary human monocytes were differentiated into macrophages *in vitro* for 5 days. *Study 1: Temporal effects.* Unactivated (M0) macrophages were seeded directly onto Baghdadite, Sr-HT Gahnite and TCP-HA scaffolds for 6 days, and macrophage gene expression was assessed at early (day 2) and late (day 6) stages of contact. *Study 2: Direct vs. indirect Interactions*. Unactivated macrophages were seeded either directly onto the scaffolds or onto the bottom of a 24-well ultra-low attachment plate containing transwell inserts loaded with the scaffolds. Macrophage gene expression was evaluated on day 6. *Study 3: Grain size effects.* The grain size of Baghdadite scaffolds was varied and the resulting temporal effects on

3.2.2 Fabrication of Scaffolds

TCP-HA, Baghdadite, and Sr-HT-Gahnite scaffolds were prepared by the Biomaterials and Tissue Engineering Research Unit at the University of Sydney (PI: Prof. Hala Zreiqat) according to previously described methods [151, 152]. A sintering temperature of 1380°C was applied for shorter (3 h) or longer (12 h) periods of time to vary Baghdadite grain size, yielding 2 μm and 4 μm grains, respectively. All scaffolds were autoclaved and pre-equilibrated in media prior to macrophage seeding.

3.2.3 Monocyte Isolation and Differentiation

Primary human monocytes were either isolated from blood (obtained from the New York Blood Center) using sequential density gradient centrifugations of Ficoll-Paque™ PLUS and 46% Percoll™ PLUS (GE Healthcare), or purchased from the University of Pennsylvania Human Immunology Core (Philadelphia, PA). Monocytes were cultured in ultra-low attachment flasks for 5 days in Roswell Park Memorial Institute (RPMI) 1640 media, supplemented with 10% heat-inactivated human serum, 1% penicillin streptomycin and 20 ng/mL macrophage colony stimulating factor (MCSF) to induce macrophage differentiation as previously described [70]. Unactivated M0 macrophages were gently scraped and collected on day 5.

3.2.4 Temporal Effects of Scaffolds on Macrophage Activation

M0 macrophages (1×10^6 cells) were seeded directly onto the scaffolds in 15 μL and allowed to attach for 1 h at 37°C and 5% CO_2, as described previously [49, 159, 160]. After 1 h, the culture media was adjusted to a final volume of 1 mL and the samples were

incubated for an additional 2 to 6 days in the presence of 20 ng/mL MSCF. M0 macrophages exposed to culture media alone served as a control. Media was replenished on day 3 and, on days 2 and 6, the scaffolds were transferred into 1 mL TRIzol and stored at -20°C until RNA extraction. Control cells, not exposed to scaffolds (M0), were gently scraped and collected, and centrifuged at 400×g for 7 min. Cell pellets were re-suspended in Buffer RLT (RNeasy Micro Kit, Qiagen), and stored at -20°C until RNA extraction.

3.2.5 Indirect Effects of Scaffolds on Macrophage Activation

To identify whether any soluble factors released from the scaffolds, such as dissolved ions, affect macrophage gene expression, scaffolds were separated from the macrophages by placing them in the apical chamber of transwell inserts (Millipore) in 24 well ultra-low attachment plates in 250 μL culture media. M0 macrophages (1×10^5 cells) were seeded in the basolateral chamber in 750 μL of culture media. The scaffolds and cells were co-cultured in this way at 37°C and 5% CO_2 for 6 days, with media exchange on days 1, 3 and 6. On day 6, cells were lysed directly in the well in Buffer RLT (RNeasy Micro Kit, Qiagen) and stored at -20°C overnight. All samples were cultured in media containing 20 ng/mL MCSF.

3.2.6 Effects of Grain Size on Macrophage Behavior

To better understand the material properties that contribute to macrophage behavior, the effects of Baghdadite grain size on macrophage activation were studied *in vitro.* Baghdadite was selected for this study based on its ability to modulate macrophage behavior in study 1. M0 macrophages (1×10^6 cells) were seeded directly onto the scaffolds in 15 μL culture media and allowed to attach for 25 min at 37°C and 5% CO_2. Following

attachment, the culture media was adjusted to a final volume of 2 mL, to completely submerge the scaffolds, and the samples were incubated for an additional 2 to 6 days, with media exchange on day 3. All media contained 20 ng/mL MSCF for macrophage differentiation. On days 2 and 6, the media was collected and stored at -80°C for analysis of secreted proteins.

As controls, 0.5×10^6 M0 macrophages were seeded in a 24-well ultra-low attachment plate and differentiated into the M0, M1, M2a and M2c phenotypes in the presence of 20 ng/mL MCSF for 6 days. Differentiation was achieved by addition of interferon-γ (IFN-γ, 100 ng/mL) and lipopolysaccharide (LPS, 100 ng/mL) for M1 activation, interleukin-4 (IL-4, 40 ng/mL) and interleukin-13 (IL-13, 20 ng/mL) for M2a activation, and interleukin-10 (IL-10, 40 ng/mL) for M2c activation [70].

3.2.7 RNA Extraction and cDNA Synthesis

Scaffolds in TRIzol were thawed on ice, vortexed briefly and allowed to stand at room temperature for 5 min. Chloroform was added to the supernatants and the samples were vigorously shaken by hand for 15 s. After an additional 3 min at room temperature, the samples were centrifuged at 12,000×g and 4°C for 15 min. The aqueous layer was collected, mixed with an equal volume of 70% ethanol and the precipitated RNA was purified on an RNeasy mini-spin column (Qiagen) according to the manufacturer's instructions. Cells lysed without scaffolds were thawed on ice, vortexed briefly, mixed with an equal volume of 70% ethanol and directly loaded onto an RNeasy mini-spin column (Qiagen) for purification. RNA was eluted in a final volume of 30 μL and stored at -80°C until used for reverse transcription. The RNA was subsequently quantified on a NanoQuant plate (Tecan) and treated with DNAse I, Amplification Grade (Invitrogen) for

DNA removal according to the manufacturer's protocol. cDNA was synthesized from 1 μg RNA ($A_{260/280}$ > 1.8) using a High-Capacity cDNA Reverse Transcription Kit (Applied Biosystems) according to the manufacturer's protocol and stored at -80°C until analysis of gene expression.

3.2.8 Gene Expression Analysis

Quantitative RT-PCR was performed using 20 ng cDNA and Fast SYBR Green Master Mix (Applied Biosystems) according to the manufacturer's protocol, with n=2 technical replicates. Mean quantification cycle (C_q) values were calculated and the expression of target genes was normalized to the reference gene, *GAPDH*. Data shown represent the mean fold change ± SEM (n≥4). All primers (**Table 3.1**) were synthesized by Life Technologies.

3.2.9 Principal Component Analysis

To visualize the global representation of gene expression data and emphasize variation in macrophage behavior, principal component analysis (PCA) was implemented using Matlab® software (MathWorks, Natick, MA). PCA is a multivariate data analysis approach that reduces the dimensionality of a data set by capturing most of the variation in the data set into new variables known as principal components [[161]]. Samples can then be plotted using a few of these uncorrelated principal components in order to detect the hidden phenomena in the data set, including similarities and dissimilarities among samples. Prior to analysis, the data were standardized using z-scores to enable comparison across the data set.

3.2.10 Combinatorial M1/M2 Scoring

The relative M1 and M2 character of macrophages in response to the scaffolds was determined by combining data from a panel of genes into a single M1/M2 score, based on an algorithm that has been previously shown to accurately predict healing of human diabetic ulcers [86]. The score is defined as the ratio of the sum of the raw values of M1 gene expression (*CCR7*, *IL1B*, *TNF*, *and VEGF*) to the sum of the raw values of M2a gene expression (*MRC1*, *PDGFB* and *TIMP3*) such that higher scores represent increased pro-inflammatory (M1) behavior with respect to M2a behavior.

3.2.11 Protein Secretion

Media collected from the scaffolds or cells was analyzed for the presence of proteins using commercially available kits, according to the manufacturers' instructions. Human tumor necrosis factor (TNF), vascular endothelial growth factor (VEGF), platelet-derived growth factor beta polypeptide (PDGFB) and bone morphogenetic protein 2 (BMP2) Mini ELISA Development kits were purchased from Peprotech (Rocky Hill, NJ). Human matrix metalloproteinase 7 (MMP7) and matrix metalloproteinase 9 (MMP9) Quantikine ELISA kits were purchased from R&D Systems, Inc. (Minneapolis, MN). TIMP metalloproteinase inhibitor 3 (TIMP3, MIG-5) Human ELISA kits were purchased from Abcam® (Cambridge, MA).

3.2.12 Statistical Analysis

Data are represented as mean ± SEM. Statistical analysis for all studies was performed in GraphPad Prism (GraphPad Software, Inc., La Jolla, CA). Prior to analysis, fold change in gene expression data were log-transformed. Data were analyzed using one-way or two-way ANOVA, with Tukey's post-hoc analysis. A multiple t-test analysis

was performed on protein secretion data using the Holm-Sidak method. In all analyses, $p<0.01$ was considered significant.

3.3 Results and Discussion

3.3.1 Temporal Effects of Scaffolds on Macrophage Activation

3.3.1.1 Principal Component Analysis and Combinatorial Scoring

To test the hypothesis that Baghdadite, Sr-HT-Gahnite, and TCP-HA scaffolds differentially regulate macrophage behavior, the response of primary human monocyte-derived macrophages on these scaffolds was evaluated over time *in vitro*.

Principal component 1 (PC 1) captured 25.6% of the variance within the gene expression set, and clustered the data based on time (**Figure 3.2a**). Interestingly, PC 2 distinguished the M0 control on day 2 from all other macrophage responses, which accounted for 20.9% of the variance in the data. Not surprisingly, these results indicate that macrophages behave very differently when cultured in 3D on ceramic scaffolds compared to 2D culture on ultra-low attachment plastic. The leading drivers of the variance retained within PC 1 were *MARCO*, *BGLAP*, *TNFSF11* and *VCAN*, while *MMP9*, *TGFB1*, *TIE1* and *MMP7* were major contributors to the variance of PC 2; coefficients of all genes projected onto the principal components are provided in **Figure 3.3a**. Extending the analysis to PC 3 and PC4, which captured 14.3% and 9.7% of the variance, respectively, revealed scaffold type as the third largest source of variation in the data (**Figure 3.2b**). More specifically, PC 3 separated macrophage interactions with Baghdadite scaffolds from all other groups at both time points. PC 3 also separated macrophage interactions with TCP-HA scaffolds from all other groups on day 6. The genes most contributing to the variance of PC 3 were *CD163*, *CCR7*, *VEGF* and *SPP1*; genes driving the variance of PC 4 included *CCL22*, *ALPL*, and *TIMP3* (**Figure 3.3b**). Importantly, these results show that

Baghdadite scaffolds elicited different macrophage activation compared to Sr-HT-Gahnite, and both scaffolds were different in their responses compared to TCP-HA scaffolds, strongly suggesting that scaffold chemistry differentially regulates macrophage phenotype.

Intriguingly, Baghdadite scaffolds resulted in a significant reduction in the M1/M2a score over time (**Figure 3.2c**), which may suggest that these scaffolds promote a phenotypic transition in macrophage activation. In contrast, TCP-HA scaffolds appeared to promote prolonged pro-inflammatory activation with an increasing M1/M2a score between days 2 and 6, which was significantly higher than all other groups.

3.3.1.2 Temporal Changes in Gene Expression

Analysis of expression levels of individual genes revealed interesting differences between macrophages cultured on the different scaffolds. Compared to the M0 control, TCP-HA scaffolds caused up-regulation of the pro-inflammatory M1 markers *TNF* at day 2, and *VEGF* and *IL1B* at day 6 (**Figure 3.4**). *CCR7* was downregulated at day 6 by macrophages on TCP-HA scaffolds. Baghdadite caused up-regulation of *TNF* at day 2 and of *IL1B* at day 6, with down-regulation of *VEGF* at day 2 relative to the M0 control. Sr-HT-Gahnite caused up-regulation of *TNF* at day 2 and down-regulation of *CCR7* at day 6. Differences in gene expression of M1 markers between scaffolds were also noted, with Baghdadite promoting higher expression of *CCR7* and *TNF* relative to TCP-HA at day 2, which then returned to baseline by day 6.

TCP-HA scaffolds promoted significant down-regulation of all M2a markers at day 6 (**Figure 3.5**), which was likely the major contributing factor to the increasing M1/M2a score over time. All scaffolds promoted down-regulation of the M2a marker *CCL22* compared to the M0 control at both days 2 and 6, with the exception of Sr-HT-Gahnite

scaffolds at day 2. Gene expression of M2a markers *PDGFBB* and *TIMP3* was unaffected by Baghdadite scaffolds at either time point, but *MRC1* was down-regulated at day 6 relative to the M0 control. Sr-HT-Gahnite scaffolds promoted down-regulation of *CCL22*, *MRC1*, and *TIMP3* at day 6. With respect to differences between scaffolds, macrophages cultured on TCP-HA scaffolds expressed lower levels of 3 of the 4 M2a markers compared to macrophages on Baghdadite or Sr-HT-Gahnite scaffolds at both time points.

In addition to promoting down-regulation of many M2a markers, TCP-HA scaffolds also promoted down-regulation of several M2c markers at day 6 (*CD163*, *MMP7*, *MMP9*, and *SPP1*) relative to the M0 control (**Figure 3.6**). In contrast, Baghdadite scaffolds promoted up-regulation of two M2c markers at day 6 (*CD163* and *VCAN*), as well as down-regulation of *MARCO* at day 2 and *MMP7* at day 6, although to a lesser extent than TCP-HA. Sr-HT-Gahnite scaffolds promoted down-regulation of *MMP7* and *MMP9* at day 6, also to a lesser extent than did TCP-HA scaffolds. In general, macrophages cultured on Baghdadite scaffolds expressed higher levels of the M2c genes than macrophages on the other scaffolds, especially at the later time point. While the role of M2c macrophages in tissue regeneration is still poorly understood, recent studies suggest that they are involved in tissue remodeling [162], which plays an important role in bone repair. The fracture healing cascade involves formation of a cartilaginous fracture callus, mineralization and resorption of the callus, and production of woven bone as the fracture site is revascularized, which is later remodeled through a coordinated process of bone resorption and formation to restore the native tissue. Several studies have shown that the absence of the tissue-remodeling enzyme, MMP9, following injury delays endochondral ossification and alters healing [163, 164]. Similarly, the absence of osteopontin, encoded by SPP1 and believed to facilitate the uptake of mineralized matrix [165], causes altered tissue remodeling in mice and, consequently, reduced biomechanical properties [166].

Taken together, these results suggest that TCP-HA scaffolds promote the highest levels of M1-related gene expression, while Baghdadite and Sr-HT-Gahnite scaffolds promote a shift toward M2-related gene expression, especially at the later time point. On the other hand, the only genes that showed different trends in terms of direction of expression for Baghdadite and TCP-HA, relative to the M0 control, were *CCR7* and *CD163*, and hybrid activation states that were not distinctly M1 or M2 were observed for all scaffolds. The fact that many genes were regulated in the same direction and to similar extents suggests that more studies are needed to confirm if these changes correspond to functional differences.

Nevertheless, the potential of these scaffolds to differentially regulate macrophage behavior may have important implications for harnessing the natural healing ability of bone. Promoting proper vascularization following injury is a major challenge of tissue engineering strategies for fracture healing. Considering that the inflammatory response plays an important role in stimulating angiogenesis and healing, and previous work has demonstrated that sequential M1 and M2 macrophage activation is required to support these processes [70, 81], scaffolds that promote early M1- and late M2-like activation would also be expected to promote bone repair. Indeed, Baghdadite and Sr-HT-Gahnite scaffolds have been previously shown to be more successful in promoting bone regeneration in a critical-sized bone defect model in rabbits [151, 152]. However, a direct correlation between macrophage phenotype and biomaterial-mediated vascularization in bone repair remains to be demonstrated.

Further extending the analysis to genes more generally related to angiogenesis and osteogenic processes revealed only minor changes in markers of angiogenesis, and did not provide any indication of osteoblast- or osteoclast-like behavior induced by TCP-HA, Baghdadite or Sr-HT-Gahnite scaffolds (**Figure 3.7**).

Overall, these findings suggest that different scaffold chemistries differentially influence macrophage activation *in vitro*, which also been shown for materials used in chronic wound care [160]. Changing activation states of macrophages in response to implanted materials would be expected to have profound effects on bone formation given the importance of macrophages for bone repair [81].

3.3.2 Effects of Soluble Factors on Macrophage Activation

3.3.2.1 Principal Component Analysis

Baghdadite, Sr-HT-Gahnite and TCP-HA scaffolds have different mechanical properties, microstructure and ion dissolution profiles [158]. As an initial step toward investigating why macrophages behaved differently on each scaffold, the effects of released soluble factors on macrophage activation were tested by culturing the macrophages and scaffolds in separate chambers of a transwell culture system. Again, PCA was used to visualize the gene expression data, enabling us to identify patterns and emphasize variation among the scaffolds.

Interestingly, PC 1, PC 2, and PC 3 failed to separate macrophages cultured in transwell with any of the scaffolds (**Figure 3.8**). These three principal components captured 88.1% of the variation in the data, suggesting that soluble signals released from the scaffolds do not account for differences in gene expression of macrophages.

3.3.2.2 Gene Expression

Individual gene analysis revealed minor changes in gene expression of *CCL22, IL1B,* and *MMP7* by macrophages cultured in transwell with the scaffolds (**Figure 3.9**, **Figure 3.10**), in agreement with the principal component analysis results. In general,

differences in gene expression were much more pronounced for macrophages cultured in direct contact with the scaffolds.

Nevertheless, the immunomodulatory effects of metal ions like titanium, zinc, zirconium and strontium are now widely appreciated, resulting in a paradigm shift away from inert bone substitutes [167]. In one study, conditioning macrophages in β-tricalcium phosphate extracts increased the osteogenic differentiation of MSCs, supporting the role of macrophages in biomaterial-induced osteogenesis [136]. Although the mechanisms behind metal ion-induced bone regeneration are not well understood (reviewed in Ref. [140]), the presence of ions likely affects macrophages. Zirconia (in Baghdadite) has been shown to be pro-inflammatory [168], while strontium and zinc (in Sr-HT-Gahnite) have been shown to affect bone remodeling [150, 169] and promote anti-inflammatory activity [170]. Additional studies are needed to determine if the presence of these ions contributed to the differential activation of macrophages observed in this work.

3.3.3 Grain Size Effects on Macrophage Activation

Considering released factors had only minor effects on macrophage gene expression, it was hypothesized that changing topography of the scaffolds would affect macrophages in direct contact with the scaffolds. To test this hypothesis, the grain size within Baghdadite scaffolds was varied, and protein secretion analysis was implemented instead of gene expression analysis to confirm that macrophages secrete the protein products of these genes at appreciable levels. While all proteins evaluated were secreted at the expected levels based on previous reports [70, 83], varying grain size had only a modest effect on macrophage activation (**Figure 3.11**). For example, macrophages cultured on large grain Baghdadite scaffolds secreted higher levels of TNF at day 2

($p<0.05$). As a comparison, control macrophages cultured on ultra-low attachment plastic yielded differential protein production across phenotypes (**Figure 3.12**).

While the effects of modifying scaffold architecture on macrophage activation were modest in this work, which may be due to the less than marginal change in mechanical properties between small and large grain Baghdadite scaffolds [158], others have demonstrated that surface topography can alter macrophage phenotype. Previously it was shown that macrophages accumulated on rough but not smooth titanium surfaces, though both led to bone formation in a rat subcutaneous model, suggesting differences in the mechanism of healing [141]. Other studies have also demonstrated the role of microstructure and surface topography in promoting anti-inflammatory behavior in human macrophages [142, 171, 172]. In this work, only modest effects of changing Baghdadite grain size on the activation of macrophages were observed. However, these findings are limited to the small region of grain sizes tested in this study and additional work is necessary to draw conclusions regarding the influence of grain size on macrophage-Baghdadite interactions. It is also possible that grain size plays a role in macrophage responses to other materials not investigated in the present study. Additional work is needed to elucidate the effects of surface topography on M1, M2a and M2c activation in greater detail.

Macrophage regulation could also be caused by mechanical properties. To date, the effect of scaffold stiffness on macrophage phenotype has been relatively underexplored and remains unclear. Irwin *et al.* attempted to shed light on the ambiguous relationship between inflammatory cells and substrate modulus using the THP-1 cell line, a human monocytic cell line that can be differentiated into macrophages [148]. Although cells attached preferentially to stiffer substrates, secretion of pro-inflammatory cytokines was variable. In contrast, another study found that stiffness of poly(ethylene glycol) (PEG)

substrates did not affect *in vitro* attachment of RAW 264.7 macrophages; however, stiffer substrates promoted pro-inflammatory gene expression in primary murine macrophages when stimulated with LPS [143]. More recently, Guo *et al*. showed that the modulus of poly(ester urethane) scaffolds implanted subcutaneously in rats can be tailored to modulate macrophage phenotype [144]. Given the potential for the ceramic scaffolds investigated in the present study to modulate macrophage behavior, future studies to specifically isolate substrate modulus would be interesting.

It is worth noting that there were several limitations to this work. Because of the complexity of these scaffolds, it was not possible to isolate any one variable that contributes to modulation of macrophage behavior. The goal was to explore the response of macrophages to different scaffolds that have been successful in regenerating vascularized tissue in order to identify the most promising areas for more detailed investigation in future studies. Thus, it is recommended that subsequent work focus on carefully defining how changing scaffold ion content, topography, and mechanical properties affect macrophage activation, which could have major effects on the design of scaffolds for bone regeneration. Another major limitation is that only a small subset of the thousands of genes involved in bone regeneration were evaluated. Moreover, although gene expression has been shown to be an excellent indicator of cell identity and physiological state [173], especially for discerning macrophage activation [65, 174, 175], additional work is needed to confirm phenotypic changes in macrophages on a functional level. Finally, the effects of these scaffolds on only macrophages were investigated, but other immune cells, including dendritic cells and resident tissue macrophages, as well as cells specific to bone repair, would be expected to interact with macrophages and have major effects on bone regeneration. Future studies should explore the interactions

between macrophages, activated by bone substitutes, and other cells involved in the fracture healing cascade. Despite these limitations, this study suggests that scaffold properties differentially activate macrophages, and that with further investigation, it may be possible to proactively modulate macrophage behavior using scaffold design as a means to promote tissue vascularization and regeneration.

3.4 Conclusions

In this work, the effects of pro-regenerative scaffolds on macrophage activation were investigated. Overall, the findings suggest that macrophage phenotype is influenced by scaffold properties. To this end, Baghdadite and Sr-HT-Gahnite scaffolds were shown to regulate macrophage responses differently compared to TCP-HA scaffolds, which caused up-regulation of inflammatory (M1) genes and down-regulation of M2 genes (both M2a and M2c). Though additional work is needed to confirm these findings on a functional level, the ability of Baghdadite and Sr-HT-Gahnite scaffolds to modulate macrophage behavior would be expected to have important implications for bone regeneration. In addition, the ability of these scaffolds to regulate macrophage phenotype was demonstrated to result from a combination of direct and indirect cell-scaffold interactions, with direct interactions having the dominant effects.

Although it is currently unknown how these changes in macrophage activation subsequently affect biomaterial-mediated tissue regeneration, improved understanding of the interactions between scaffolds that regenerate tissue *in vivo* and cells of the inflammatory response can aid in the design of biomaterials that promote healing outcomes.

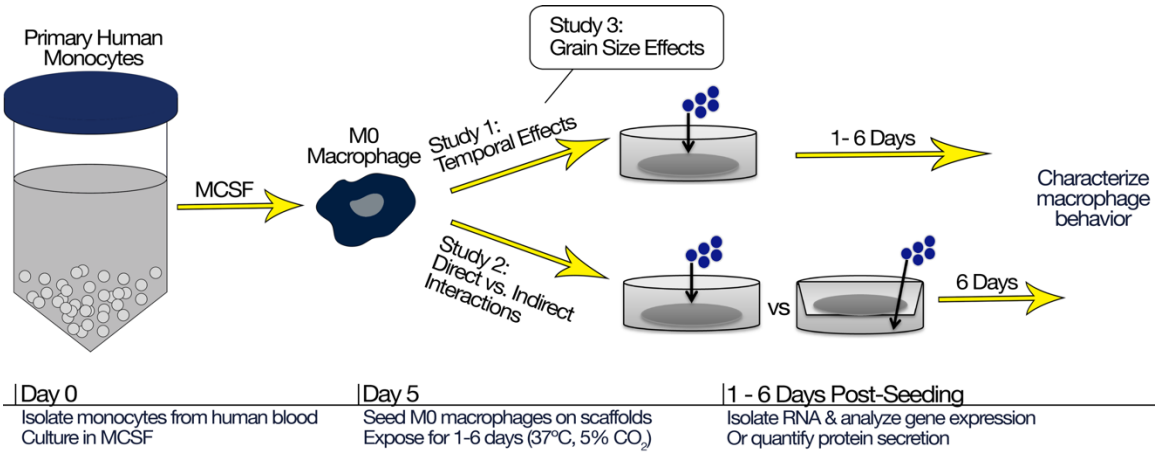

Figure 3.1. Schematic of study design. Study 1: Temporal effects. Unactivated macrophages were seeded directly on Baghdadite, Sr-HT-Gahnite and TCP-HA scaffolds for 6 days, and characterized in terms of gene expression at early and late times of direct cell-scaffold contact. Study 2: Effects of soluble factors. Unactivated macrophages were seeded directly onto scaffolds or co-cultured using a transwell insert to discern the contributions to macrophage gene expression patterns stemming from physical scaffold properties and those resulting from ion dissolution. Study 3: Grain size effects. The grain size of Baghdadite scaffolds was varied and the ensuing temporal response on macrophage protein secretion was assessed at early and late stages of contact.

Table 3.1. Primers used for quantitative RT-PCR.

Gene	Forward Primer (5' - 3')	Reverse Primer (5' - 3')
GAPDH	AAGGTGAAGGTCGGAGTCAAC	GGGGTCATTGATGGCAACAATA
TNF	CCTCTCTCTAATCAGCCCTCTG	GAGGACCTGGGAGTAGATGAG
CCR7	TGAGGTCACGGACGATTACAT	GTAGGCCCACGAAACAAATGAT
IL1B	ATGATGGCTTATTACAGTGGCAA	GTCGGAGATTCGTAGCTGGA
CD80	AAACTCGCATCTACTGGCAAA	GGTTCTTGTACTCGGGCCATA
CCL22	GCGTGGTGTTGCTAACCTTCA	AAGGCCACGGTCATCAGAGT
MRC1	AAGGCGGTGACCTCACAAG	AAAGTCCAATTCCTCGATGGTG
CD163	TTTGTCAACTTGAGTCCCTTCAC	TCCCGCTACACTTGTTTTCAC
VCAN	GCAAGTGATGCGGGTCTTTAC	TTGCCGCCCTGTAGTGAAAC
MARCO	CAGCGGGTAGACAACTTCAC	TTGCTCCATCTCGTCCCATAG
VEGF	AGGGCAGAATCATCACGAAGT	AGGGTCTCGATTGGATGGCA
PDGF	CTCGATCCGCTCCTTTGATGA	CGTTGGTGCGGTCTATGAG
TIE1	AAGCAGACAGACGTGATCTGG	GCACGATGAGCCGAAAGAAG
MMP7	GAGTGAGCTACAGTGGGAACA	CTATGACGCGGGAGTTTAACAT
MMP9	GTACTCGACCTGTACCAGCG	TCAGGGCGAGGACCATAGAG
TIMP3	ACCGAGGCTTCACCAAGATG	CATCATAGACGCGACCTGTCA
ALPL	TTTATAAGGCGGCGGGGGTG	AGCCCAGAGATGCAATCGAC
BGLAP	ATGAGAGCCCTCACACTCCTCG	GTCAGCCAACTCGTCACAGTCC
RUNX2	TGGCAGTCACATGGCAGATT	GACCCTGACTTTTCGGGGAG
SPP1	TTCCAAGTAAGTCCAACGAAAG	GTGACCAGTTCATCAGATTCAT
TNFSF11	TCAGAAGATGGCACTCACTG	AACATCTCCCACTGGCTGTA

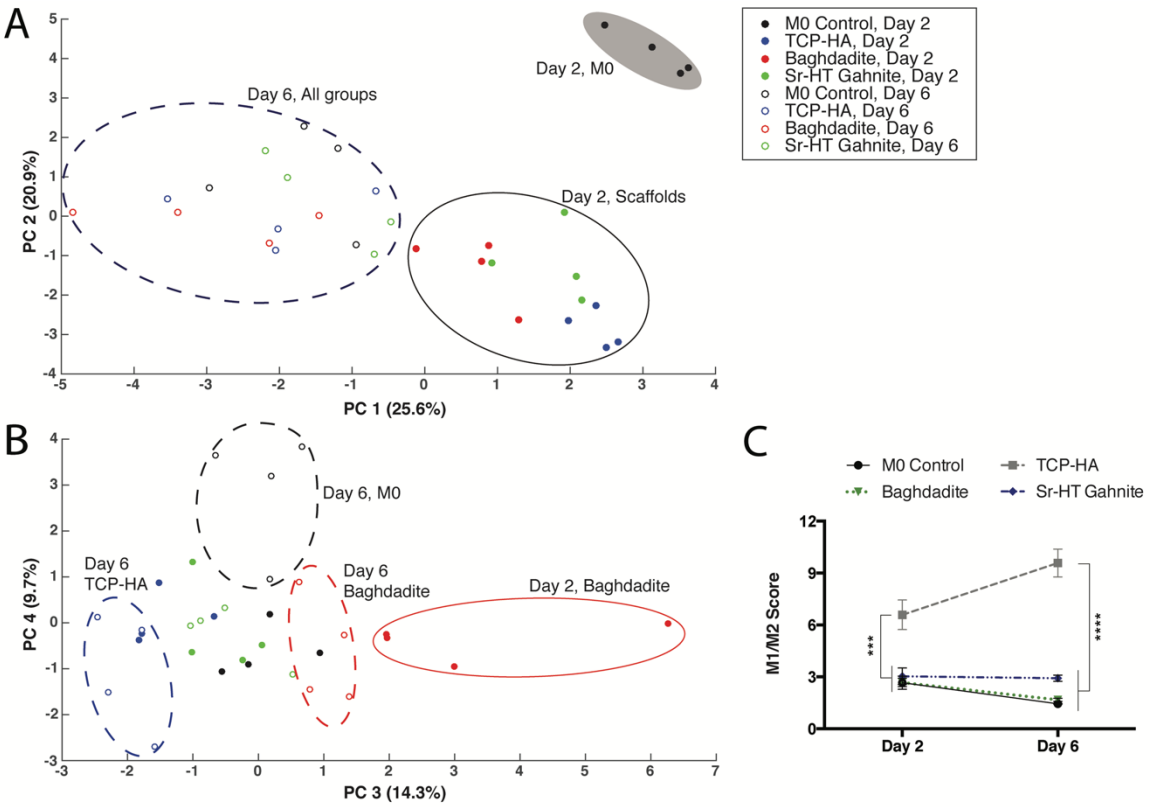

Figure 3.2. Multivariate analysis of gene expression data. (A-B) PCA of the temporal effects of Baghdadite, Sr-HT-Gahnite and TCP-HA scaffolds on macrophage gene expression. (A) Score plot of PC 1 and 2 depicted, capturing 25.6% and 20.9% of the variance within the data, respectively. Solid line encloses all scaffold-activated macrophages on day 2; shaded region highlights unactivated M0 control macrophages on day 2; dashed line captures all day 6 responses. (B) Score plot of PC 3 and 4, capturing 14.3% and 9.7% of the variance, respectively. Shaded region represents Baghdadite-activated macrophages on day 2; dashed lines enclose day 6 macrophage responses from Baghdadite (red), TCP-HA (blue) and the M0 control (black). (C) M1/M2 scoring of scaffold-activated macrophages over time. Data represent mean score ± SEM. Statistical analysis completed using two-way ANOVA with Tukey's post-hoc analysis. ***$p < 0.001$, ****$p < 0.0001$; $n = 4$. Differences between day 1 and 6 were compared for each scaffold using a multiple t-test analysis via the Holm-Sidak method; Baghdadite scaffolds were significantly different ($p<0.01$).

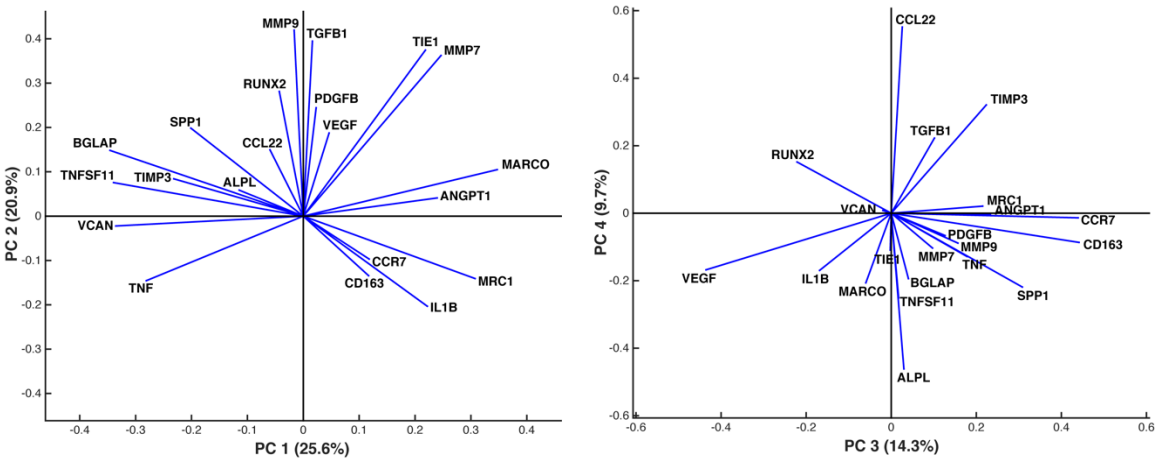

Figure 3.3. Principal component analysis biplots. Plots illustrate the gene loadings for the first four principal components projected onto PC 1 and PC 2 (left), as well as PC 3 and PC 4 (right).

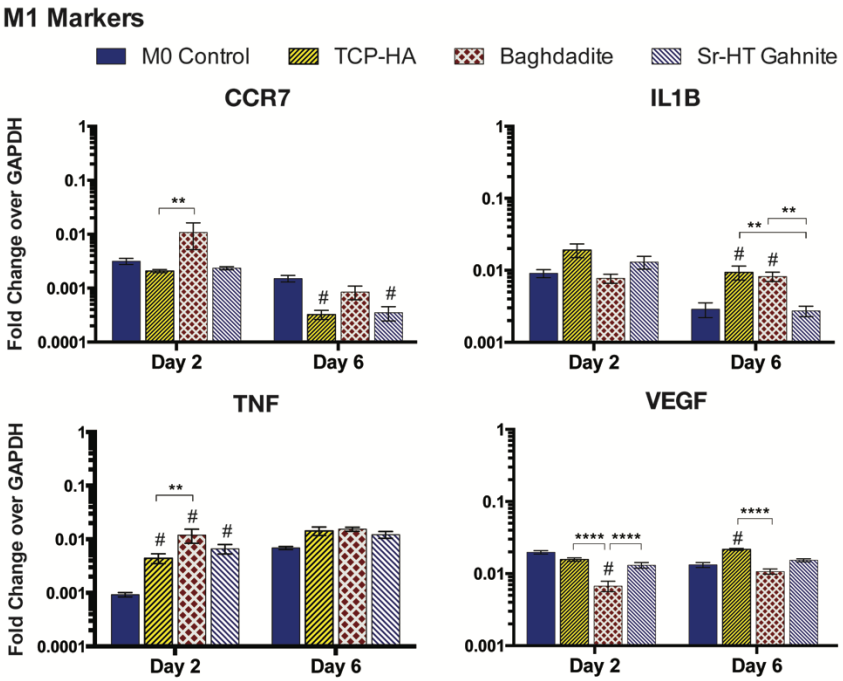

Figure 3.4. Gene expression of macrophages exposed to Baghdadite, Sr-HT-Gahnite and TCP-HA scaffolds over 6 days, based on markers indicative of the M1 phenotype. Data represent mean fold change over *GAPDH* ± SEM. Statistical analysis was performed on log-transformed data using two-way ANOVA with Tukey's post-hoc analysis. # denotes significance ($p < 0.01$) relative to the M0 control. **$p < 0.01$, ***$p < 0.001$, ****$p < 0.0001$; $n = 4$.

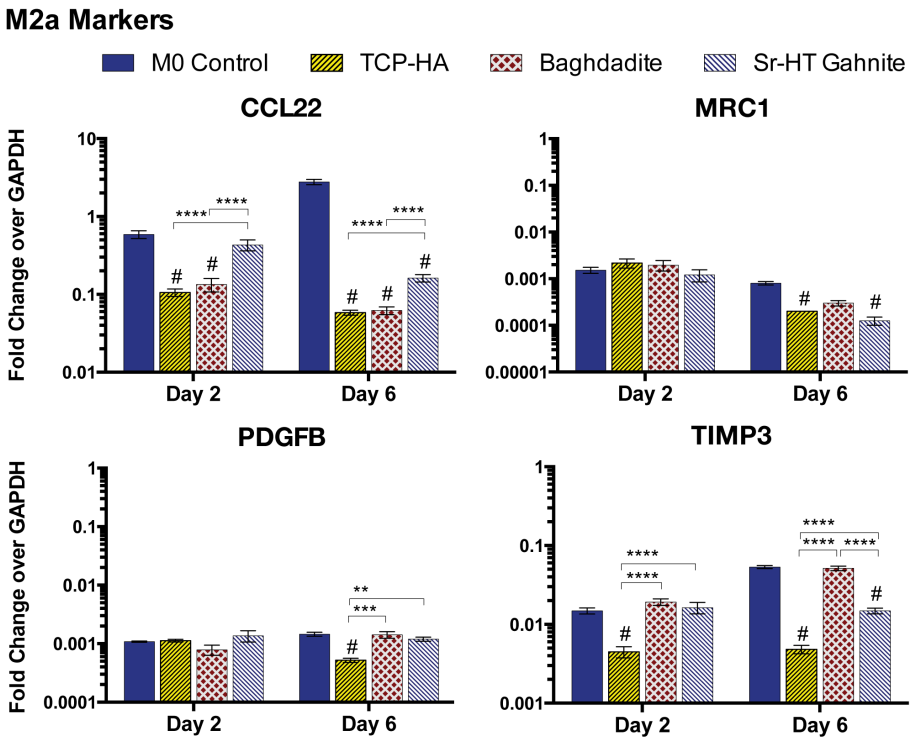

Figure 3.5. Gene expression of macrophages exposed to Baghdadite, Sr-HT-Gahnite and TCP-HA scaffolds over 6 days, based on markers indicative of the M2a phenotype. Data represent mean fold change over *GAPDH* ± SEM. Statistical analysis was performed on log-transformed data using two-way ANOVA with Tukey's post-hoc analysis. # denotes significance ($p < 0.01$) relative to the M0 control. **$p < 0.01$, ***$p < 0.001$, ****$p < 0.0001$; $n = 4$.

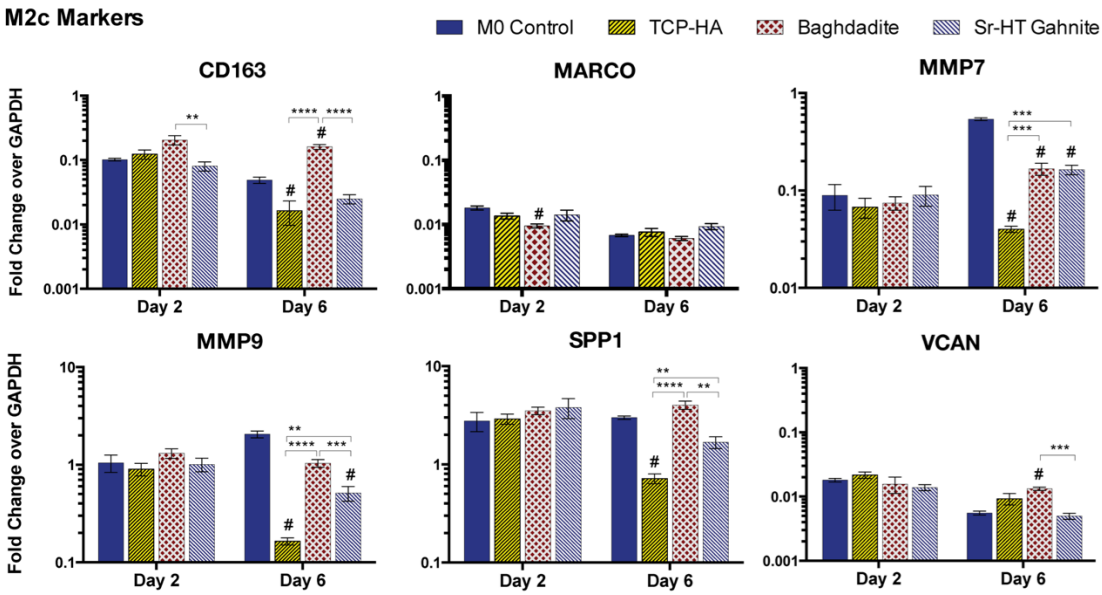

Figure 3.6. Gene expression of macrophages exposed to Baghdadite, Sr-HT-Gahnite and TCP-HA scaffolds over 6 days, based on markers indicative of the M2c phenotype. Data represent mean fold change over *GAPDH* ± SEM. Statistical analysis was performed on log-transformed data using two-way ANOVA with Tukey's post-hoc analysis. # denotes significance ($p < 0.01$) relative to the M0 control. **$p < 0.01$, ***$p < 0.001$, ****$p < 0.0001$; $n = 4$.

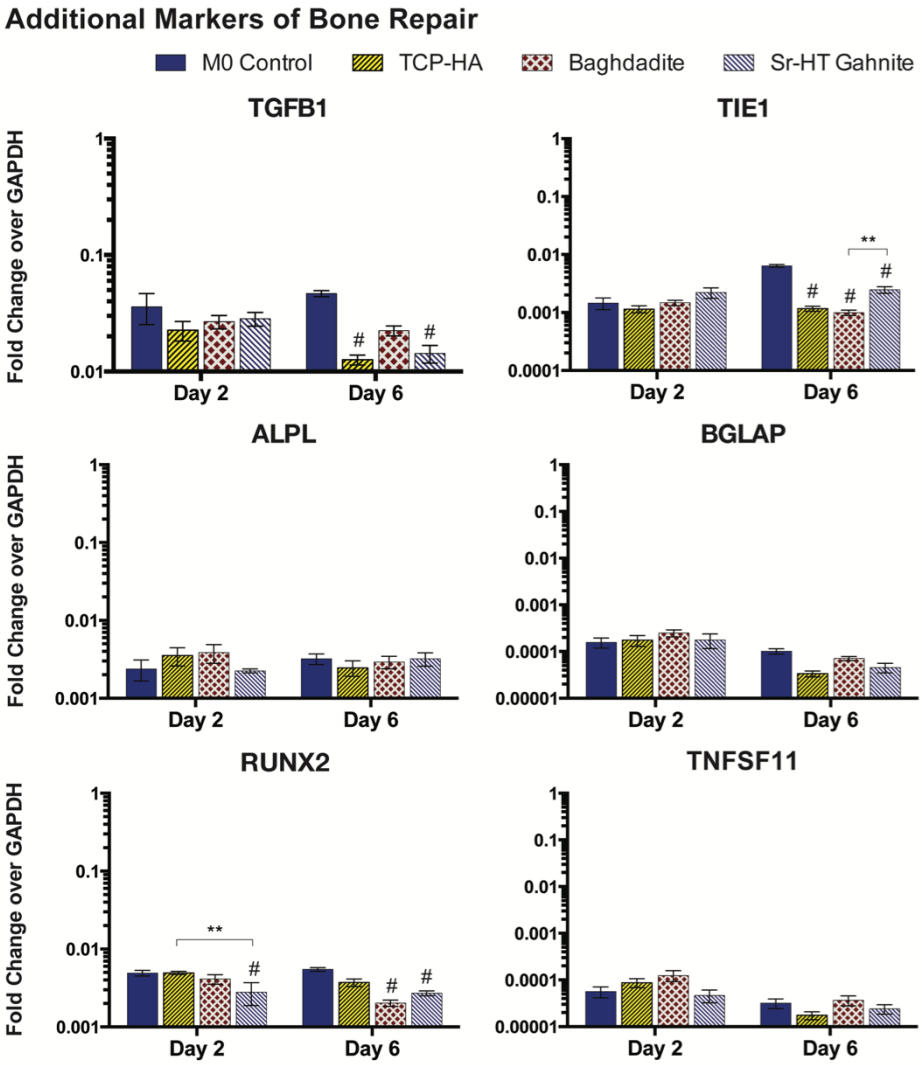

Figure 3.7. Gene expression profiles of macrophages exposed to Baghdadite, Sr-HT Gahnite and TCP-HA scaffolds over 6 days, based on a panel of markers related to bone repair. Data represent mean fold change over GAPDH ± SEM. Statistical analysis was performed on log-transformed data using two-way ANOVA with Tukey's post-hoc analysis. # denotes significance ($p < 0.01$) relative to the M0 control. **$p < 0.01$, ***$p < 0.001$, ****$p < 0.0001$; $n = 4$.

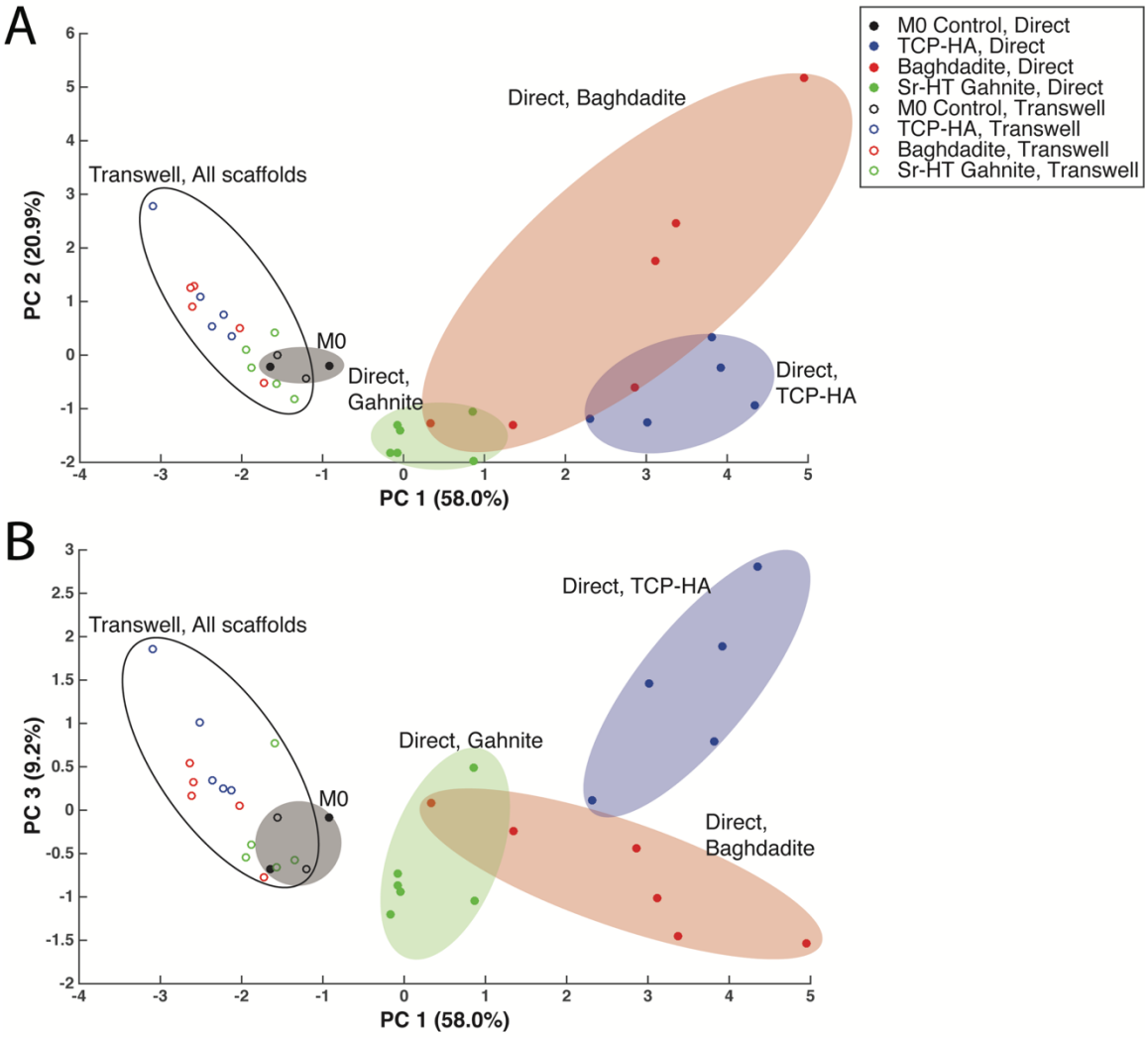

Figure 3.8. PCA of direct and indirect (transwell) interactions on macrophage gene expression. (A) Score plot of PC 1 and 2 depicted, capturing 58.0% and 20.9% of the variance within the data, respectively. (B) Score plot of PC 1 and 3, which captured 9.2% of the variance. Shaded regions highlight direct effects of Baghdadite (red), TCP-HA (blue), Sr-HT-Gahnite (green) and unactivated M0 control (black). Solid line indicates clustering of all transwell effects.

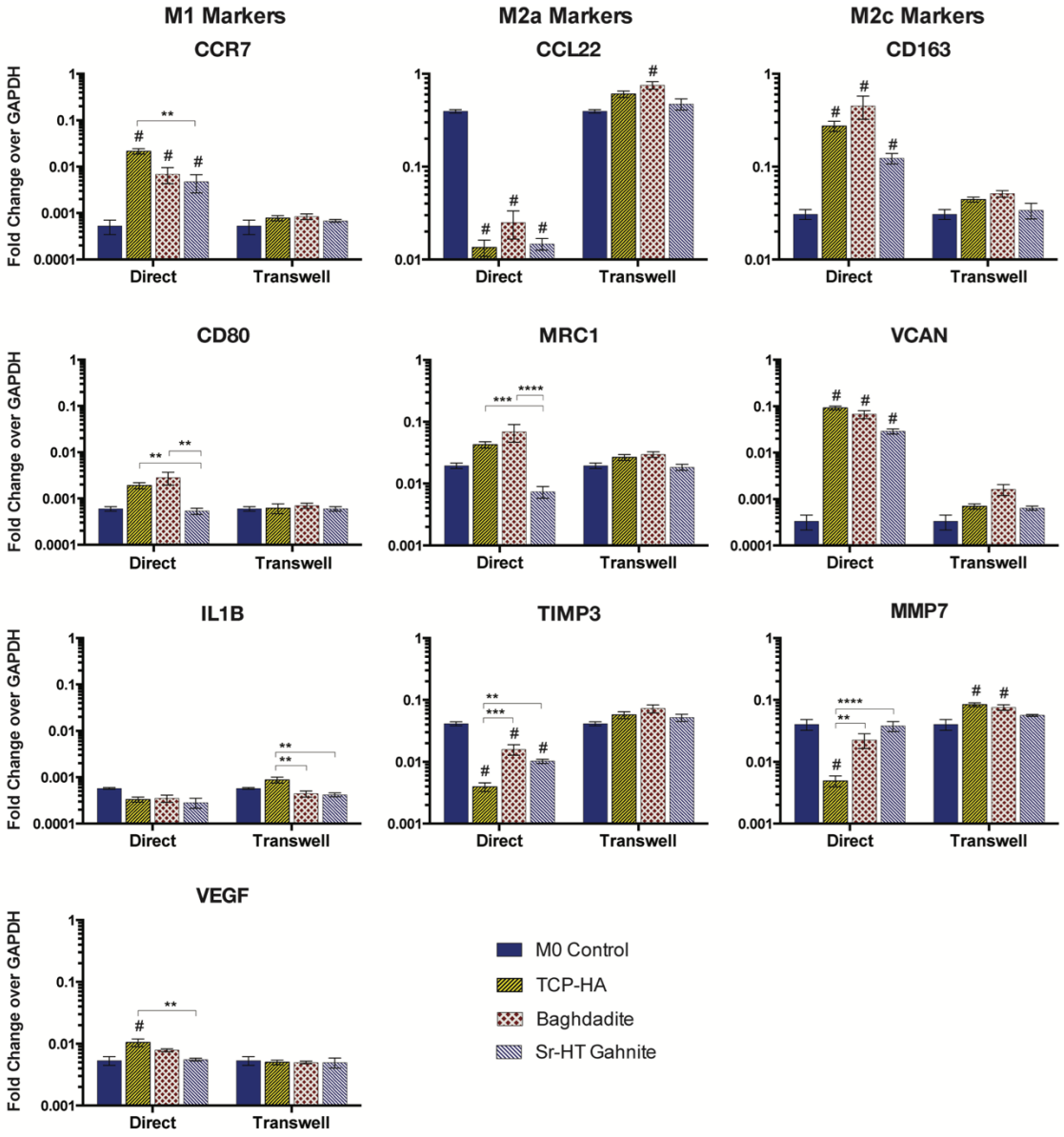

Figure 3.9. Effects of soluble factors on macrophage gene expression. Data represent mean fold change over *GAPDH* ± SEM. Statistical analysis was performed on log-transformed data using one-way ANOVA with Tukey's post-hoc analysis. # denotes significance ($p < 0.01$) relative to the M0 control. **$p < 0.01$, ***$p < 0.001$, ****$p < 0.0001$; $n \geq 4$.

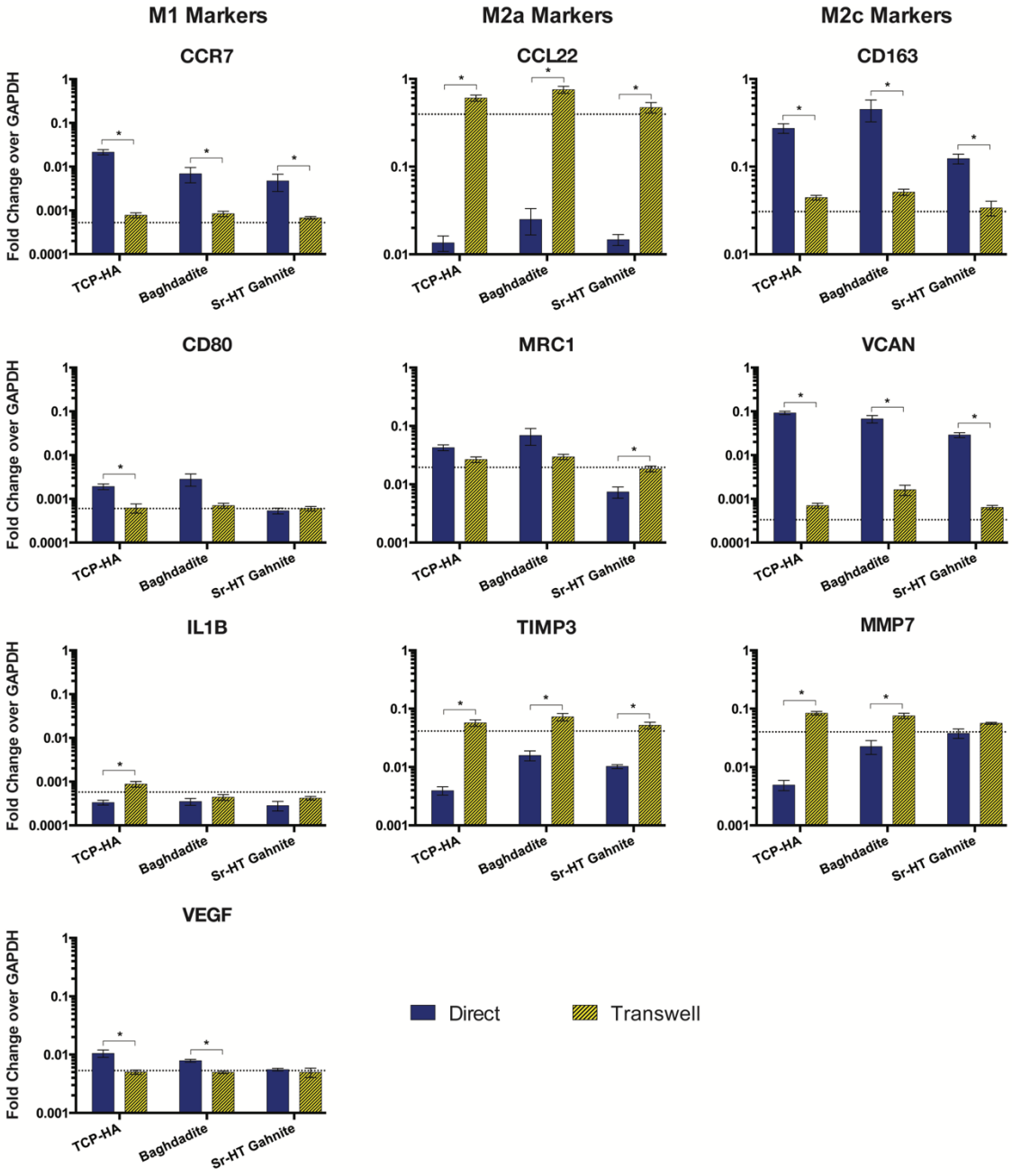

Figure 3.10. Comparison of direct and indirect effects on macrophage gene expression for Baghdadite, Sr-HT Gahnite and TCP-HA scaffolds. Data represent mean fold change over *GAPDH* ± SEM. Statistical analysis was performed on log-transformed data using the Holm-Sidak method; *$p < 0.01$, $n \geq 4$. The dashed line represents the unactivated M0 control.

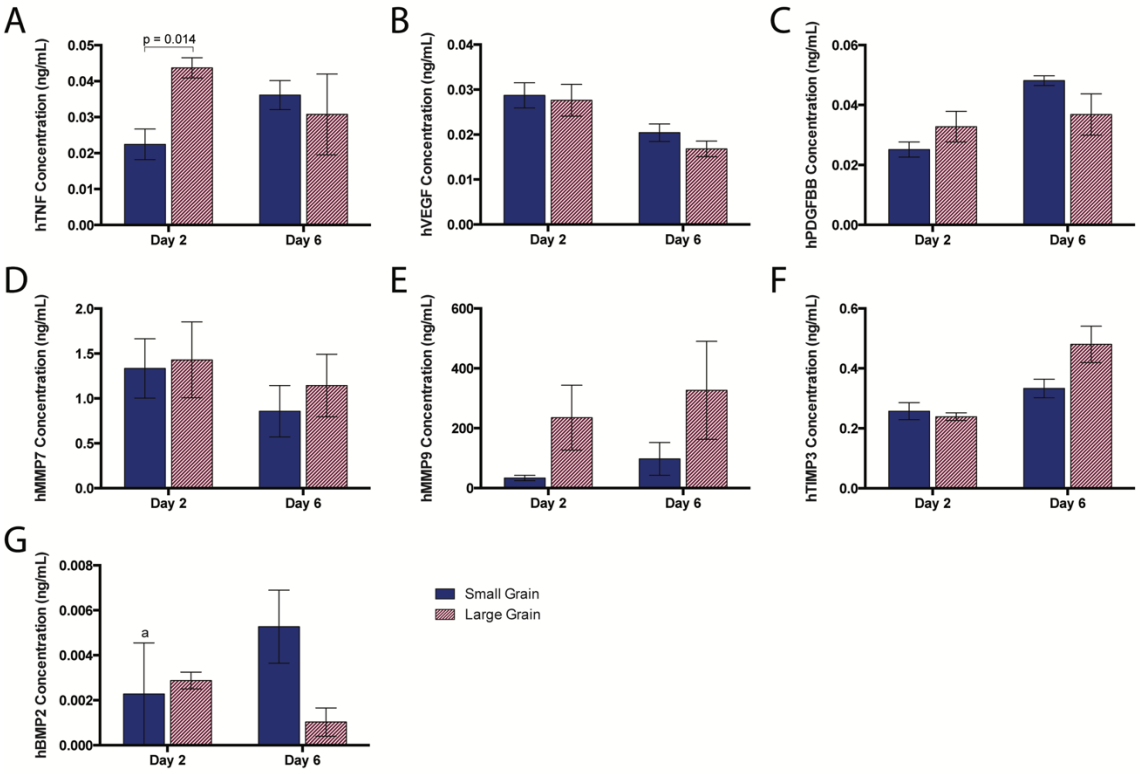

Figure 3.11. Protein secretion analysis for Baghdadite grain size effects on macrophage behaviour over time. Proteins measured include TNF (A), VEGF (B), PDGFB (C), MMP7 (D), MMP9 (E), TIMP3 (F) and BMP2 (G). Data represent mean±SEM. A multiple t-test analysis was completed using the Holm-Sidak method to determine significant differences; *$p < 0.01$, $n = 3$. 'a' indicates protein secretion below limit of detection; these samples were assumed to be 0 ng/mL.

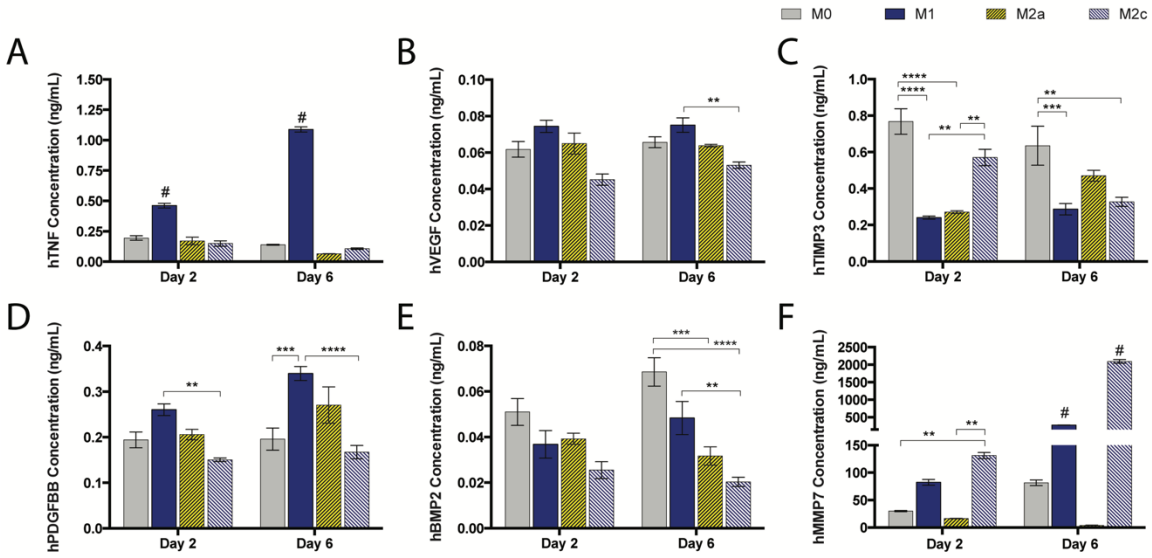

Figure 3.12. Protein secretion for macrophage phenotype controls cultured on ultra-low attachment plates for 6 days. Proteins measured include TNF (A), VEGF (B), TIMP3 (C), PDGFB (D), BMP2 (E), and MMP7 (F). Data represent mean ± SEM. Statistical analysis completed using two-way ANOVA with Tukey's post-hoc analysis. # denotes significance ($p < 0.05$) relative to all other phenotypes. *$p < 0.05$, **$p < 0.01$, ***$p < 0.001$, ****$p < 0.0001$; $n = 3$.

CHAPTER 4: EFFECTS OF MACROPHAGE PHENOTYPE ON VASCULAR ENDOTHELIAL CELLS IN VITRO

4.1. Introduction

Accumulating evidence suggests that macrophages play important roles during vascularization through bidirectional interactions with endothelial cells (ECs), involving both direct physical contact as well as crosstalk via paracrine signaling. For instance, direct contact with endothelial cells (ECs) *in vitro* has been shown to instruct macrophage differentiation toward an M2-like phenotype, and subcutaneous injection of these macrophages with RM1 cancer cells significantly increased tumor vascularity in mice [176]. There is also data demonstrating that direct contact with ECs can stimulate the differentiation of monocytes and macrophages into endothelial-like cells [177]. However, macrophage activation is not limited to direct cell contact as transwell co-culture of ECs and human monocytes also modulates the anti-inflammatory behavior of macrophages, which has been attributed to the secretion of extracellular vesicles [178]. Notch signaling, which is activated in ECs during angiogenesis, is thought to mediate the crosstalk between ECs and macrophages [27], and has been shown to control macrophage recruitment in a murine model of retinal angiogenesis [26].

Macrophages also reciprocally act on endothelial cells to promote vascularization. For example, M1, M2a and M2c macrophages have been shown to secrete large quantities of VEGF, PDGF, and MMPs, respectively [70], all of which are involved in the angiogenic cascade. In addition to these factors, TNF, a hallmark indicator of M1 macrophages, has been proven to induce endothelial tip cell differentiation [18], while other pro-inflammatory factors, like FGF, have been shown to prime EC responses to cytokines that modulate vascular morphogenesis [179]. Likewise, osteopontin (OPN), produced by M2c macrophages [180], is a known immunomodulator that enhances VEGF

expression in ECs and promotes proliferation, migration and tube formation of ECs *in vitro* [181].

In addition to these M1-, M2a-, and M2c-associated factors, macrophages activated in response to uptake of apoptotic cells (referred to as M2f) have been shown to promote EC migration *in vitro* and vessel formation *in vivo* [67]. It is also well established that M2f macrophages up-regulate TGFB1 [182], which has been implicated in endothelial crosstalk with support cells to modulate vessel stabilization [183].

Collectively, these studies support the ability of macrophages to respond to signals from ECs and facilitate vascularization. However, the unique contributions of macrophage phenotype in this process are not well defined and poorly understood. Therefore, the goal of this aim was to delineate the effects of M1, M2a, M2c and M2f on regulating the angiogenic behavior of endothelial cells, with the hypothesis that macrophage phenotypes differentially modulate the endothelial cell gene expression; these phenotypes were selected based on their established roles in tissue repair and suspected contributions to angiogenesis. To test this hypothesis, macrophage-endothelial crosstalk was assessed over 3 days *in vitro* utilizing a transwell co-culture system to facilitate isolation of cells without the need for significant processing.

4.2. Experimental Section

4.2.1. Neutrophil Culture and Induction of Apoptosis

Human promyelocytic leukemia (HL-60) cells were purchased from ATCC (Manassas, VA) and expanded in Iscove's Modified Dulbecco's Medium (ATCC, #30-2005^{TM}) supplemented with 25% fetal bovine serum (FBS) and 1% penicillin/streptomycin in a humidified chamber at 37°C and 5% CO_2. Neutrophils were maintained at a density

of 1×10^5 cells/mL via media exchange every 3 days, and trypan blue exclusion was performed to assess cell viability, which was routinely > 85%. To induce apoptosis, HL-60 cells were first re-suspended in culture media without FBS for 2 h for cell synchronization. Following serum-deprivation, 800 μM H_2O_2 (Sigma Aldrich, #H1009) was added to the cells and incubated for an additional 3 h. Apoptosis was confirmed via flow cytometry using an APO-BrdU™ TUNEL assay kit (Thermo Fisher Scientific, #A23210), according to the manufacturer's instructions, and compared to healthy neutrophil controls. All apoptotic HL-60 cells were washed in 1X PBS prior to incubation with macrophages, as detailed below.

4.2.2. Monocyte Isolation and Differentiation

Primary human monocytes from 4 healthy donors were purchased from the University of Pennsylvania Human Immunology Core (Philadelphia, PA). Monocytes (0.5×10^6) were cultured at a concentration of 1×10^6 cells/mL in ultra-low attachment well plates for 8 days in RPMI 1640 media, supplemented with 10% heat-inactivated human serum, 1% penicillin streptomycin and 20 ng/mL MCSF as previously described [70, 162]. Media was replenished on days 3 and 5. On day 5, macrophages were stimulated into the M0, M1, M2a, and M2c by addition of IFN-γ (100 ng/mL) and LPS (100 ng/mL) for M1 activation, IL-4 (40 ng/mL) and IL-13 (20 ng/mL) for M2a activation, and IL-10 (40 ng/mL) for M2c activation [70]. For M2f activation, macrophages were co-cultured with apoptotic HL-60 cells in a 1:5 ratio of macrophages to neutrophils. On day 8, all macrophages were washed to remove polarizing stimuli. To confirm differentiation, n=4 biological replicates per phenotype were lysed in 350 μL Buffer RLT (RNeasy Micro Kit, Qiagen) and stored at -80°C for downstream gene expression analysis.

4.2.3. Endothelial Cell Culture

Human adipose microvascular endothelial cells expressing dTomato fluorescent protein (HAMEC-dTom) were generously provided by the Levenberg Lab (Technion, Israel) and cultured at 5,000-7,000 cells/cm^2 in Endothelial Cell Medium (ECM, SciencCell, #1001) supplemented with 5% fetal bovine serum (FBS), 1% endothelial cell growth supplement, and 1% penicillin/streptomycin solution. HAMEC-dTom were routinely subcultured via trypsinization at 90% confluency and used within 7 passages. All cells were cultured in a humidified chamber at 37°C and 5% CO_2.

4.2.4. Transwell Assay

To investigate macrophage-endothelial cell crosstalk, a transwell co-culture system was utilized, allowing cell-cell communication via paracrine signaling. A schematic of the experimental design is provided in **Figure 4.1**. HAMEC-dTom (25,000) were seeded in the apical chamber of transwell inserts (0.4 μm pore size, 6.5 mm diameter) in 100 μL ECM and allowed to attach for 1 h at 37°C and 5% CO_2. Media was removed from all macrophage-seeded wells and replaced with 100 μL co-culture media (1:1 ratio of ECM to cRPMI 1640 with MCSF) to support cell survival. Transwell inserts containing HAMEC-dTom were transferred to macrophage-seeded wells (n=4 per phenotype). An additional 500 μL and 100 μL co-culture media were added to the basolateral and apical chambers, respectively. All samples were incubated for 1-3 days at 37°C and 5% CO_2. Controls included HAMEC-dTom cultured in transwell inserts in the absence of macrophages, as well as M0, M1, M2a, M2c, and M2f macrophages cultured in the absence of endothelial cells. All controls were cultured in equal volumes of co-culture media to account for changes in cell behavior induced by media supplements.

On days 1 and 3, transwell inserts were transferred to clean 24-well plates and stored on ice. Conditioned media was collected from the basolateral and apical chambers and stored at -80°C, and all samples were washed in 1X PBS to remove residual media. Macrophages were lysed directly in the wells in 350 μL Buffer RLT (RNeasy Micro Kit, Qiagen) with gentle scraping, and HAMEC-dTom were lysed directly in the inserts in 200 μL Buffer RLT (Qiagen). All lysates were transferred to 1.5 mL PCR-clean tubes and stored at -80°C until RNA extraction.

4.2.5. RNA Extraction and Purification

All HAMEC-dTom and macrophage lysates were thawed on ice and vortexed briefly. An additional 150 μL Buffer RLT were added to HAMEC-dTom lysates to bring final volume to 350 μL. Samples were mixed with an equal volume of 70% ethanol and directly loaded onto an RNeasy mini-spin column (RNeasy Micro Kit, Qiagen) for purification, according to the manufacturer's instructions. RNA was eluted in a final volume of 14 μL RNase-free water and stored at -80°C until multiplex gene expression analysis.

4.2.6. Multiplex Gene Expression Analysis

RNA was thawed on ice and quantified using a NanoDrop 1000 (Thermo Scientific). Multiplex gene expression analysis was performed via NanoString using two custom nCounter XT CodeSets (NanoString Technologies, Seattle, WA), inclusive of 54 endogenous genes for macrophage RNA, 38 endogenous genes for HAMEC-dTom RNA, 4 housekeeping genes, 8 External RNA Control Consortium (ERCC) negative controls, and 6 ERCC positive controls. All genes included in the endothelial cell and macrophage CodeSets are listed in **Table 4.1** and **Table 4.2**, respectively. These genes were selected

based on literature demonstrating their association with various processes involved in angiogenesis, including regulation of endothelial cell differentiation into tip and stalk phenotypes, regulation of the potent angiogenic stimulator, VEGF, tube formation, vessel stabilization and maturation, hypoxia, and apoptosis. Hybridization reactions were prepared with 100 ng RNA for all samples, according to the manufacturer's instructions. Raw count data were extracted using nSolver™ Analysis Software 3.0 (NanoString Technologies, Seattle, WA).

4.2.7. Data Normalization and Analysis

Raw count data were first normalized to the ERCC positive controls, as recommended by the manufacturer, to normalize all platform associated sources of variation. The geometric mean of the positive controls was calculated for each sample, and averaged across all samples. This average was divided by the geometric mean of the positive controls for each sample, yielding a sample-specific scaling factor. Subsequently, all gene counts for each sample were multiplied by corresponding sample-specific scaling factor. These data were imported into R studio and normalized using the *voomWithQualityWeights* function within the *limma* package, which assigns a weight factor to each sample before performing a global normalization [184]. Prior to analysis, genes not expressed above the ERCC negative controls were identified. The geometric mean of the negative controls was calculated for each sample, and averaged across all samples. This average was then subtracted from the normalized gene counts for each sample, yielding negative count values for genes expressed below the limit of detection. Genes with undetectable expression for all samples were excluded from further analysis.

To better understand how changes in gene expression induced by macrophage-endothelial cell crosstalk relate to processes involved in angiogenesis, Gene Ontology

(GO) Enrichment Analysis was performed on groups of genes up-regulated or down-regulated in endothelial cells by macrophage phenotype [185-187]. GO enrichment was performed via the PANTHER Overrepresentation Test (release 20171205) with the GO Ontology database released 2017-11-28. The default homo sapiens reference list, including all genes in the database, was used with the GO biological process complete data set. Overrepresented genes were determined using Fisher's Exact with FDR multiple test correction for $p<0.05$.

4.2.8. Statistical Analysis

All data are represented as mean ± SEM, where a y-axis value of 0 represents the limit of detection for gene expression. Statistical analysis of the normalized gene expression data was performed in GraphPad Prism (GraphPad Software, Inc., La Jolla, CA). To determine the effects of macrophages on endothelial cells, all HAMEC-dTom data were analyzed using a two-way ANOVA, and the False Discovery Rate was controlled for post-hoc analysis. The two-stage linear step-up method of Benjamini, Krieger and Yekutieli was used with Q=0.1 to control for the number of false positives resulting from multiple comparisons [188]. To assess changes in macrophage behavior in response to endothelial cells, a multiple t-test analysis was performed on all macrophage data using the Holm-Sidak method, in which $p < 0.01$ was considered statistically significant.

4.3. Results and Discussion

4.3.1. Effects of Macrophage Phenotype on Endothelial Cells

Of the 38 genes included in the CodeSet to analyze changes in endothelial cell (EC) behavior, 6 genes were excluded from the analysis due to undetectable gene count

levels. These included *CD36*, *Jag1*, *MMP9*, *PDGFB*, *VEGFD*, and *WNT7B*. For all other genes, the effects of macrophage phenotype on ECs are shown in **Figure 4.2**.

In general, differential gene expression induced in ECs by macrophage phenotype was most notable at the early time point, but abolished by day 3. Specifically, M0 macrophages down-regulated early EC expression of *BAX*, *KDR*, and *PECAM1* compared to all other phenotypes, as well as *NRP1* relative to M1, M2a and M2c, and *ANGPT2, Endoglin*, and *ERG* relative to M1 and M2c macrophages. In contrast, M1 and M2c macrophages up-regulated *CXCR4* and *NRARP* relative to the other phenotypes. Modest up-regulation of CTNNB1 was also induced by the M1 and M2a phenotypes. Aside from these differences, M1 and M2a macrophages promoted greater expression of *NOTCH3* relative to the M2f phenotype, for which expression was undetectable. After 3 days, the only phenotype-specific differences among the groups was down-regulated expression of *ETS1* induced by M1, relative to M2c macrophages, and down-regulated expression of *TGFB1* induced by M2f, relative to the M0 phenotype.

4.3.1.1. Effects of M0 Macrophages on Endothelial Cells

Importantly, while differential effects were observed by different macrophage phenotypes, only a few of these changes were different relative to the EC control without macrophages. To gain a better understanding of how each macrophage phenotype modulates changes in EC behavior, the genes altered by each phenotype relative to the EC-only control were identified. As shown in **Figure 4.3**, 7 out of the 32 genes expressed by ECs were altered by the presence of M0 macrophages. By in large, genes affected by the M0 phenotype were down-regulated at one or both time points, with the exception of pro-apoptotic *BAX*, which was initially down-regulated on day 1 and later up-regulated on day 3. Specifically, M0 macrophages induced early down-regulation of *PECAM1* and *TEK*,

late down-regulation of *ETS1* and *PDGFB*, and sustained down-regulation of *MMP2* and *NRCAM*.

PECAM-1, an endothelial cell-cell adhesion molecule, is known to play a fundamental role in vessel formation *in vitro* [189] and *in vivo* [190], and may stimulate EC motility by promoting filopodia formation [191]. *TEK*, commonly referred to as TIE2, belongs to the receptor tyrosine kinase family and is expressed on ECs, as well as pro-angiogenic macrophages [192-194]. Tyrosine kinase receptors bind angiopoietin cytokines, represent a major signaling system in regulating angiogenesis. Indeed, TIE2-deficiency has been reported to causes aberrant network organization with poor vessel branching, remodeling and maturation [195], perhaps related to altered interactions between ECs and stabilizing support cells [196].

ETS-1 is expressed on stalk cells [197], and has been shown to direct EC differentiation into an angiogenic phenotypic [198] and regulate the expression of matrix metalloproteinases to facilitate vascular EC migration [198, 199]. In addition to these roles, ETS-1 has been linked to EC apoptosis via modulation of apoptosis-related genes [200], and was recently reported to play an important role in VEGF transcriptional regulation [201].

PDGFB is widely appreciated to act on PDGF β-receptor (PDGFR-beta), promoting endothelial tube formation *in vitro* [202]. For example, PDGFB has been demonstrated to regulate the release of tube formation-promoting extracellular vesicles by mesenchymal stem cells *in vitro* [203]. In addition, PDGFB plays an important role in recruitment of pericytes and vascular support cells that stabilize the vessel wall [30].

Expression of *MMP2*, along with other matrix metalloproteinases, plays a crucial role in sprouting angiogenesis that involves degradation of both the basement membrane and the surrounding extracellular matrix to create space necessary for lumen formation

[204]. Indeed, *MMP2* expression is correlated with increased metastasis and angiogenesis of lung [205] and gastric carcinomas [206], and *in vitro* models of retinoblastoma [207].

NRCAM is a neural cell adhesion molecule expressed by tubular ECs during the early stages of tube formation [208, 209], possibly related to cell-cell communication involved in sprouting angiogenesis.

GO enrichment analysis of EC genes down-regulated by exposure to M0 macrophages on day 1 confirmed their association with blood vessel development and morphogenesis, as well as cell migration. Similarly, analysis of genes down-regulated on day 3 indicated their association with vasculature development, as well as the positive regulation of vascular smooth muscle cell proliferation. Overall, these data may suggest that M0 macrophages induce anti-angiogenic behavior in endothelial cells.

4.3.1.2. Effects of M1 Macrophages on Endothelial Cells

In contrast, M1 macrophages modulated the expression of 8 out of the 32 genes expressed by ECs (**Figure 4.4**). With the exception of *ETS1*, which was down-regulated on both day 1 and day 3, M1 macrophages promoted up-regulation of markers associated with angiogenesis in ECs. These changes included early up-regulation of *ANGPT2*, *CDH2*, *CXCR4*, *KDR*, *NRARP*, and *TP53*, in addition to late up-regulation of *CTNNB1* as a result of EC crosstalk with M1 macrophages.

As mentioned earlier, ANGPT2 binds to TIE2 on endothelial cells and acts as an antagonist to ANGPT1-TIE2 signaling [210]; however, the effects of this interaction are largely dependent on the surrounding cytokine milieu. For instance, ANGPT2 promotes angiogenesis in the presence of endogenous VEGF *in vivo*, but induces vessel regression in its absence [211, 212]. In addition to its direct effects on ECs, ANGPT2 has been reported to enhance the pro-angiogenic behavior of *TIE2*-expressing monocytes and

macrophages [28]. A detailed review of the ANGPT-TIE system has been provided elsewhere [213].

CDH2 belongs to the cadherin family, and is reported to support angiogenesis by mediating intercellular adhesion, as well as regulating expression of monocyte chemoattractant protein (*MCP1*) [214]. For example, inhibition of CDH2 during brain angiogenesis in the chicken was correlated with defective adhesion between endothelial cells and pericytes, and abnormal vascular morphogenesis [215]. Similarly, CDH2 deletion in an *in vitro* model of embryonic stem cell differentiation confirmed that CDH2 was not required for sprouting angiogenesis, but led to impaired pericyte coverage of endothelial outgrowths [216]. These data implicate CDH2 in vessel maturation via pericyte interaction.

CXCR4, a chemokine receptor, is a marker of endothelial tip cells that has been shown to play a role in mediating tip cell morphology and vascular patterning in a neonatal retina model of angiogenesis [217]. There is also evidence suggesting CXCR4 promotes tumor angiogenesis by inducing expression of VEGF [218]. *KDR*, also called VEGF receptor 2 (VEGFR2), is also enriched in tip cells and mediates VEGF-stimulated filopodia extension [16]. Studies have demonstrated that KDR not only mediates VEGF-induced angiogenesis and tumor development in murine hepatocellular carcinoma [219], but also plays a vital role in vasculogenesis in mice [220]. Notably, differential VEGFR levels only affect tip cell selection in the presence of Notch signaling by controlling DLL4 expression [20].

NRARP, or Notch-Regulated Ankyrin Repeat Protein, is expressed in stalk cells at branch points and contributes to the regulation of vessel stabilization and regression [221]. In order to promote elongation of vessel branches, Notch signaling in stalk cells induces expression of *NRARP*, which subsequently counteracts Notch signaling and promotes

Wnt/CTNNB1 signals in stalk cells [23]. This coordination ultimately leads to vessel stabilization.

TP53, also known as p53 tumor suppressor, is appreciated as a protective protein that responds to stress signals by inducing DNA repair, cell cycle arrest, and apoptosis. However, TP53 has also been linked to many processes involved in angiogenesis, such as inhibition of new blood vessel development [222]. Other studies have provided evidence for a dual role in regulating VEGF during hypoxia, whereby TP53 initially promotes VEGF expression in response to hypoxia but indirectly down-regulates VEGF in response to sustained hypoxia [223].

Consistent with the individual roles of these genes, GO enrichment analysis on genes up-regulated on days 1 or 3 in response to M1 crosstalk linked these changes to the positive regulation of chemotaxis and response to stimulus, blood vessel morphogenesis, sprouting angiogenesis, vasculogenesis, adherens junction organization, the response to hypoxia, cell migration, regulation of cell adhesion, and positive regulation of cell differentiation. Collectively, these data support a pro-angiogenic effect of M1 macrophages on endothelial cells, possibly related to tip cell regulation.

4.3.1.3. Effects of M2a Macrophages on Endothelial Cells

Changes in EC gene expression caused by M2a exposure are provided in **Figure 4.5** and included 7 genes. Unlike the M0 and M1 phenotypes, which generally induced changes in gene expression in a single direction, M2a macrophages induced both up-regulation and down-regulation of genes, and many of these changes occurred only after several days of macrophage-endothelial cell interaction. For example, M2a macrophages promoted late down-regulation of *ANGPT2*, *ETS1*, *MMP2*, and *NRCAM*.

However, M2a macrophages also supported late up-regulation of *CTNNB1*, early up-regulation of *NRP1*, and pro-longed up-regulation of *NRARP*.

As mentioned earlier, *ANGPT2* acts as an antagonist to ANGPT1-TIE2 signaling [210], to promote angiogenesis or induce vessel regression depending on the presence or absence of VEGF [211, 212]. *ETS1*, a stalk cell marker, and *MMP2* facilitate EC migration and sprouting [198, 199] [204], and *NRCAM* is a neural cell adhesion molecule related to tube formation [208].

CTNNB1 encodes for the Wnt signaling protein beta-catenin, which has been proven to modulate vascular remodeling by regulating DLL4 transcription and Notch signaling [224]. Indeed, inactivation of *CTNNB1* in ECs reduced intercellular adhesion and altered the vascular patterning in mice [225].

Neuropilin 1 (NRP1) encodes for a receptor that interacts with VEGFR2. Studies have shown that NRP1 not only promotes endothelial tip cell function during vessel sprouting in the brain [226], but also suppresses stalk cell differentiation [227]. Consistent with these findings, loss of macrophage *NRP1* also has been shown to inhibit tumor progression [228].

As before, GO enrichment analysis was performed on the genes up-regulated on days 1 or 3 in response to M2a macrophages, in order to better understand the collective effects of M2a on endothelial cell behavior. The analysis linked these genes to branching involved in blood vessel morphogenesis; likewise, analysis of genes down-regulated on day 1 in response to M2a macrophages indicated an association with blood vessel morphogenesis and development, as well as the response to hypoxia. These data may support a role for M2a macrophages in regulating vessel branching.

4.3.1.4. Effects of M2c Macrophages on Endothelial Cells

Similar to the changes observed by the M1 phenotype, crosstalk between ECs and M2c macrophages modulated the expression of 6 genes. With the exception of *ETS1*, which was down-regulated on both day 1 and day 3, M2c macrophages promoted early or pro-longed up-regulation of genes involved in angiogenesis (**Figure 4.6**). Specifically, *CXCR4*, *KDR*, *NOTCH1*, and *NRARP* were all enhanced relative to the EC only control on day 1, while expression of *NRP1* was elevated on both day 1 and day 3.

As discussed above, *CXCR4*, *KDR*, and *NRP1* promote tip cell function and vascular patterning [16, 217, 226], while *NRARP* is expressed by stalk cells and regulates vessel stabilization and regression [221].

Similar to these genes, *NOTCH1* encodes for a transmembrane receptor that regulates tip and stalk cell selection via interaction with DLL4 and Jagged ligands [21]; DLL4-Notch signaling inhibits sprouting, whereas Jagged-Notch signaling promotes sprouting. Not surprisingly, Notch1 is indispensable for VEGF-induced angiogenesis [229, 230].

GO enrichment analysis indicated association of genes up-regulated by M2c with blood vessel endothelial cell differentiation, VEGF signaling and cellular response to VEGF stimulus, EC migration involved in sprouting angiogenesis, positive regulation of cell junction assembly, branching involved in blood vessel morphogenesis, vasculogenesis, and positive regulation of EC proliferation. As with the M1 phenotype, these data indicate that M2c macrophages mediate pro-angiogenic endothelial cell responses, likely related to tip cell selection and regulation.

4.3.1.5. Effects of M2f Macrophages on Endothelial Cells

With respect to the M2f phenotype, 8 genes were differentially expressed in ECs as a result of transwell co-culture (**Figure 4.7**). Similar to the M2a phenotype, genes affected by M2f macrophages were not collectively altered in a single direction. For example, *BAX*, *CXCR4* and *TIE1* were all up-regulated on day 1, whereas *CDH2* expression was elevated on day 3. In contrast, *ANGPT2*, *TGFB1*, and *ETS1* were all down-regulated on day 3, along with sustained down-regulation of *NRCAM* at both times.

With respect to up-regulated markers, *BAX* is a pro-apoptotic marker, *CXCR4* is a tip cell marker that mediates vascular patterning [217] and may induce expression of VEGF [218], and *CDH2* mediates intercellular adhesion [214] and vessel maturation [216]. *TIE1*, as mentioned earlier, is part of the angiopoietin/TIE system that regulates vascular remodeling. Recent studies posit a milieu-dependent role of Tie1, in which Tie1 interacts with Tie2 during inflammation to regulate ANGPT-induced vascular remodeling, but in the absence of an inflammatory environment, Tie1 is cleaved causing a loss of ANGPT activity and promoting vascular stability [231, 232].

With respect to down-regulated markers, *ANGPT2* antagonizes ANGPT1-TIE2 signaling [210] to promote angiogenesis or induce vessel regression depending levels of VEGF [211, 212]. *ETS-1* is expressed on stalk cells [197], promotes angiogenic EC behavior [198, 199], and has been linked to EC apoptosis via modulation of apoptosis-related genes [200]. Lastly, *TGFB1* (transforming growth factor-beta 1) has been shown to induce angiogenesis, but requires VEGF/VEGFR2-mediated apoptosis of endothelial cells [233].

Based on GO enrichment analysis, genes up-regulated in response to the M2f phenotype were associated with cellular membrane fusion; whereas, down-regulated genes were associated with regulation of extracellular matrix disassembly, regulation of

endothelial cell migration, blood vessel morphogenesis, and the response to mechanical stimulus and hypoxia. These findings may suggest a role for M2f macrophages in vessel regression.

Notably, the changes observed in endothelial cell behavior were different across all phenotypes investigated, with M1 and M2c macrophages exerting the most similar effects. Although gene expression is thought to reflect cell identify and physiological state [173, 209], additional work is required to confirm how these changes affect endothelial cell behavior on a functional level. Nevertheless, these data support the notion that macrophage phenotypes contribute uniquely to the angiogenic behavior of endothelial cells, which would be expected to have profound effects on vascularization.

4.3.2. Effects of Microvascular Endothelial Cells on Macrophages

Of the 50 genes included in the CodeSet to analyze changes in macrophage phenotype in response to ECs, 9 genes were excluded from the analysis due to undetectable gene count levels. These included *CD200R1*, *CD80*, *DLL4*, *PLOD2*, *PTGER3*, *RGS5*, *STAB1*, *VEGFC*, and *WNT7B*. For all other genes related to angiogenesis, the effects of ECs on macrophages are shown in **Figure 4.8** as compared to untreated phenotype controls. In addition, effects of ECs on macrophages with respect to markers indicative of the M1, M2a, and M2c phenotypes are provided in **Figure 4.9 - Figure 4.11**; for comparison, M1, M2a, and M2c markers for the macrophage-only controls were also evaluated (**Figure 4.13 - Figure 4.15**).

Surprisingly, ECs had only modest effects on macrophage phenotype compared to corresponding phenotype controls. As **Figure 4.8** shows, ECs caused down-regulation of *CXCR4* expression by M2a macrophages on day 3, as well as down-regulation of *Jag1*

by M0 macrophages on day 1, followed by up-regulation on day 3. In addition to these changes, ECs inhibited M2c expression of *PDGFA* on day 1.

Similarly, only minor changes in markers of macrophage phenotype were detectable. With respect to markers indicative of the M1 phenotype, there were no changes in M1 behavior, but transwell co-culture of HAMEC-dTom and M2 macrophages significantly enhanced M2a expression of *TNF* at both time points (**Figure 4.9**). *IL1B* and *CCR7* also appeared up-regulated, though not significantly, compared to M2a-only controls on day 1. Yet, early expression of IL6 was reduced in M2a macrophages. With respect to markers indicative of the M2a phenotype, there were no observable differences between macrophages exposed to HAMEC-dTom compared to their phenotype controls (**Figure 4.10**). Likewise, the only effect of ECs on markers indicative of M2c activation was reduced expression of *MMP8* by M2c macrophages on day 1 (**Figure 4.11**).

All macrophage genes affected by transwell co-culture with HAMEC-dTom are summarized according to phenotype in **Figure 4.12**.

As discussed above, *Jag1* (Jagged1) is a Notch ligand that competes with DLL4 to regulate blood vessel growth. Deletion of *Jag1* in mice not only reduces EC proliferation, but also compromises vessel stability [21], which may be related to its role in pericyte and vascular smooth muscle cell differentiation [234, 235]. Consistent with these studies, Jagged1 has also been demonstrated to antagonize DLL4 regulation of vessel branching and modulate vascular growth and maturation to accelerate wound healing in mice [236].

Likewise, *CXCR4* mediates endothelial tip cell behavior and vascular patterning [217], and both *CXCR4* and *IL6* have been shown to induce VEGF [218, 237]. Recent work also supports a role for IL6 in promoting vessel sprouting to a comparable extent as VEGF, but these sprouts had aberrant pericyte coverage leading to defective angiogenesis [238].

MMP8, like other matrix metalloproteinases, plays an important role in angiogenesis. There is evidence that knockdown of MMP8 in ECs impedes tube formation, cell proliferation and migration *in vivo*, and is associated with impaired angiogenesis *in vivo* [239]. Other *ex vivo* work supports a role of MMP8 in vascular smooth muscle cell proliferation and migration [240].

Lastly, *PDGFA* has been shown to induce angiogenesis in murine corneas; though *PDGFA* was considerably less potent than *PDGFB* and other isoforms in promoting neovascularization, it was associated with a greater percentage of vessels staining positive for mural cells [241].

Collectively, these data may suggest that ECs do not significantly influence macrophage phenotype through secreted factors; however, the lack of effects observed in this study may be attributed to the low seeding density of HAMEC-dTom, especially considering that others have demonstrated suppressed M1 activation [178] and enhanced M2 activation in response to ECs [176].

Evaluation of macrophage phenotypes not exposed to ECs confirmed their differential expression of genes indicative of the M1 (**Figure 4.13**), M2a (**Figure 4.14**), and M2c (**Figure 4.15**) phenotypes even after 3 days *in vitro* without polarizing stimuli.

It should be noted that this study has several limitations. For example, the investigation of macrophage-EC crosstalk was conducted using a 2D assay without tube formation or the presence of other cells, like pericytes and MSCs, which are vital for angiogenesis and have been shown to also regulate macrophage recruitment and activation [242], [243]. In addition, the co-culture media used was supplemented with growth factors to support EC survival and macrophage differentiation. It is conceivable

that the presence of these factors supersedes the changes induced by cellular crosstalk, thereby masking the effects of macrophage-EC interactions.

4.4. Conclusions

This study provides evidence that macrophage phenotype differentially influences the angiogenic behavior of microvascular ECs. In general, M1 and M2c macrophages affected genes broadly associated with tip cell behavior, which may suggest a role for these phenotypes in vessel sprouting. In contrast, M2a macrophages affected genes related to vessel morphogenesis, perhaps related to vessel branching, while M2f macrophages altered genes correlated with apoptosis and vascular remodeling, which may implicate M2f in vessel regression. On the other hand, EC down-regulation of genes in response to M0 macrophages may suggest that the M0 phenotype is anti-angiogenic.

Given the distinct effects of macrophage phenotype on endothelial cell behavior, it is tempting to speculate that modulation of macrophage behavior can be used to pro-actively control vascularization, addressing a major challenge for many engineered tissues in regenerative medicine.

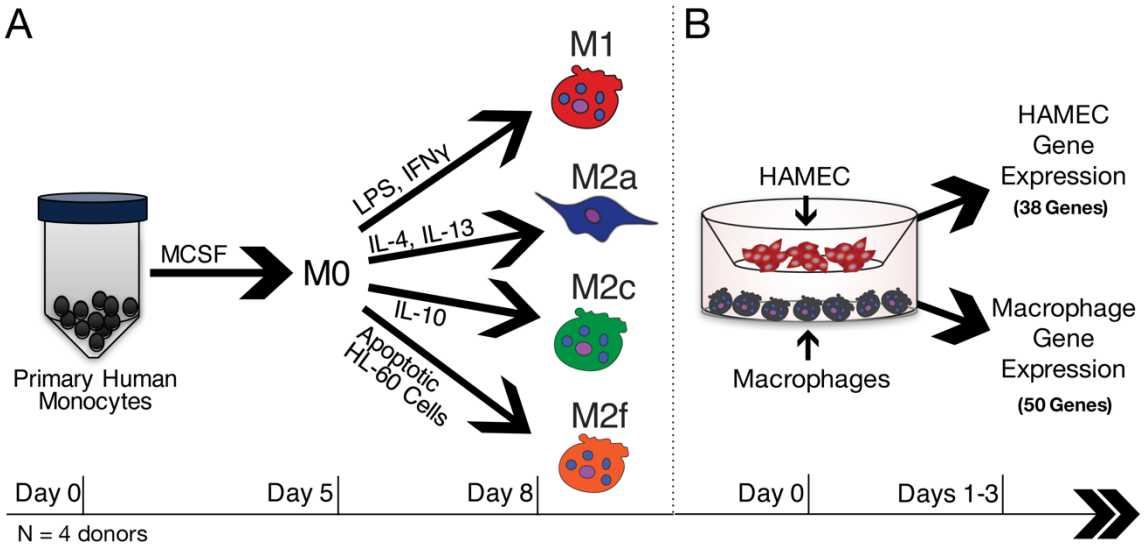

Figure 4.1. Schematic of Study Design. Primary human monocytes were isolated from 4 healthy donors and differentiated into M0, M1, M2a, M2c, and M2f macrophages *in vitro* via stimulation with macrophage colony stimulating factor (MCSF) and polarizing factors for 3 days, on ultra-low attachment plastic. HAMEC-dTom were subsequently placed in the apical chamber of a transwell insert, and co-cultured with M0, M1, M2a, M2c, or M2f macrophages in HAMEC-dTom-macrophage co-culture media, containing MCSF, at 37°C and 5% CO_2. After an additional 1-3 days, the cells were washed and lysed for gene expression analysis via custom nCounter XT CodeSets (NanoString Technologies). Untreated macrophages and endothelial cells served as controls.

Table 4.1. List of Genes Included in Custom CodeSet for Analysis of Endothelial Cell mRNA.

	Gene Name	Class Name	Accession No.		Gene Name	Class Name	Accession No.
1	ANGPT1(Ang1)	Endogenous	NM_001146.3	29	PECAM1(CD31)	Endogenous	NM_000442.3
2	ANGPT2(Ang2)	Endogenous	NM_001147.2	30	RGS5	Endogenous	NM_003617.2
3	BAX	Endogenous	NM_138761.3	31	TEK(TIE2)	Endogenous	NM_000459.3
4	CCL5	Endogenous	NM_002985.2	32	TGFB1	Endogenous	NM_000660.3
5	CD34	Endogenous	NM_001025109.1	33	TIE1	Endogenous	NM_005424.2
6	CD36	Endogenous	NM_000072.3	34	TP53	Endogenous	NM_000546.2
7	CDH2(N-Cadherin)	Endogenous	NM_001792.3	35	VEGFA	Endogenous	NM_001025366.1
8	COL4A1	Endogenous	NM_001845.4	36	VEGFC	Endogenous	NM_005429.2
9	CTNNB1	Endogenous	NM_001098210.1	37	VEGFD	Endogenous	NM_004469.2
10	CXCR4	Endogenous	NM_003467.2	38	WNT7B	Endogenous	NM_058238.1
11	DLL4	Endogenous	NM_019074.2	39	PSMB2	Housekeeping	NM_002794.3
12	Endoglin(CD105)	Endogenous	NM_001114753.1	40	PSMB4	Housekeeping	NM_002796.2
13	ERG	Endogenous	NM_001136155.1	41	SDHA	Housekeeping	NM_004168.1
14	ETS1	Endogenous	NM_005238.3	42	VCP	Housekeeping	NM_007126.2
15	FLT1(VEGR1)	Endogenous	NM_002019.4	43	NEG_A	Negative	ERCC_00096.1
16	HIF1a	Endogenous	NM_001530.2	44	NEG_B	Negative	ERCC_00041.1
17	Jag1	Endogenous	NM_000214.2	45	NEG_C	Negative	ERCC_00019.1
18	KDR(VEGFR2)	Endogenous	NM_002253.2	46	NEG_D	Negative	ERCC_00076.1
19	MMP2	Endogenous	NM_004530.2	47	NEG_E	Negative	ERCC_00098.1
20	MMP9	Endogenous	NM_004994.2	48	NEG_F	Negative	ERCC_00126.1
21	Notch1	Endogenous	NM_017617.3	49	NEG_G	Negative	ERCC_00144.1
22	NOTCH3	Endogenous	NM_000435.2	50	NEG_H	Negative	ERCC_00154.1
23	NRARP	Endogenous	NM_001004354.2	51	POS_A	Positive	ERCC_00117.1
24	NRCAM	Endogenous	NM_005010.4	52	POS_B	Positive	ERCC_00112.1
25	NRP1	Endogenous	NM_003873.5	53	POS_C	Positive	ERCC_00002.1
26	PDGFA	Endogenous	NM_002607.5	54	POS_D	Positive	ERCC_00092.1
27	PDGFB	Endogenous	NM_033016.2	55	POS_E	Positive	ERCC_00035.1
28	PDGFR-beta	Endogenous	NM_002609.3	56	POS_F	Positive	ERCC_00034.1

Table 4.2. List of Genes Included in Custom CodeSet for Analysis of Macrophage mRNA.

	Gene Name	Class Name	Accession No.		Gene Name	Class Name	Accession No.
1	BAX	Endogenous	NM_138761.3	35	PTGES	Endogenous	NM_004878.4
2	CABLES1	Endogenous	NM_001100619.2	36	RAMP1	Endogenous	NM_005855.2
3	CCL5	Endogenous	NM_002985.2	37	RGS5	Endogenous	NM_003617.2
4	CCR7	Endogenous	NM_001838.2	38	STAB1	Endogenous	NM_015136.2
5	CD163	Endogenous	NM_004244.4	39	SYK	Endogenous	NM_003177.5
6	CD200R1	Endogenous	NM_138806.3	40	TEK(TIE2)	Endogenous	NM_000459.3
7	CD34	Endogenous	NM_001025109.1	41	TGFB1	Endogenous	NM_000660.3
8	CD36	Endogenous	NM_000072.3	42	TIMP1	Endogenous	NM_003254.2
9	CD80	Endogenous	NM_005191.3	43	TNF	Endogenous	NM_000594.2
10	CLEC10A	Endogenous	NM_182906.2	44	TNFRSF11A	Endogenous	NM_003839.3
11	CXCR4	Endogenous	NM_003467.2	45	TP53	Endogenous	NM_000546.2
12	DACT1	Endogenous	NM_001079520.1	46	VCAN	Endogenous	NM_004385.3
13	DLL4	Endogenous	NM_019074.2	47	VEGFA	Endogenous	NM_001025366.1
14	ETS1	Endogenous	NM_005238.3	48	VEGFC	Endogenous	NM_005429.2
15	FLT1(VEGR1)	Endogenous	NM_002019.4	49	WNT5A	Endogenous	NM_003392.3
16	HIF1a	Endogenous	NM_001530.2	50	WNT7B	Endogenous	NM_058238.1
17	IDO1	Endogenous	NM_002164.3	51	PSMB2	Housekeeping	NM_002794.3
18	IL1B	Endogenous	NM_000576.2	52	PSMB4	Housekeeping	NM_002796.2
19	IL6	Endogenous	NM_000600.3	53	SDHA	Housekeeping	NM_004168.1
20	Jag1	Endogenous	NM_000214.2	54	VCP	Housekeeping	NM_007126.2
21	LYVE1	Endogenous	NM_006691.3	55	NEG_A	Negative	ERCC_00096.1
22	MARCO	Endogenous	NM_006770.3	56	NEG_B	Negative	ERCC_00041.1
23	MMP2	Endogenous	NM_004530.2	57	NEG_C	Negative	ERCC_00019.1
24	MMP7	Endogenous	NM_002423.3	58	NEG_D	Negative	ERCC_00076.1
25	MMP8	Endogenous	NM_002424.2	59	NEG_E	Negative	ERCC_00098.1
26	MMP9	Endogenous	NM_004994.2	60	NEG_F	Negative	ERCC_00126.1
27	MRC1	Endogenous	NM_002438.2	61	NEG_G	Negative	ERCC_00144.1
28	Notch1	Endogenous	NM_017617.3	62	NEG_H	Negative	ERCC_00154.1
29	NRP1	Endogenous	NM_003873.5	63	POS_A	Positive	ERCC_00117.1
30	PDGFA	Endogenous	NM_002607.5	64	POS_B	Positive	ERCC_00112.1
31	PDGFB	Endogenous	NM_033016.2	65	POS_C	Positive	ERCC_00002.1
32	PECAM1(CD31)	Endogenous	NM_000442.3	66	POS_D	Positive	ERCC_00092.1
33	PLOD2	Endogenous	NM_182943.2	67	POS_E	Positive	ERCC_00035.1
34	PTGER3	Endogenous	NM_000957.2	68	POS_F	Positive	ERCC_00034.1

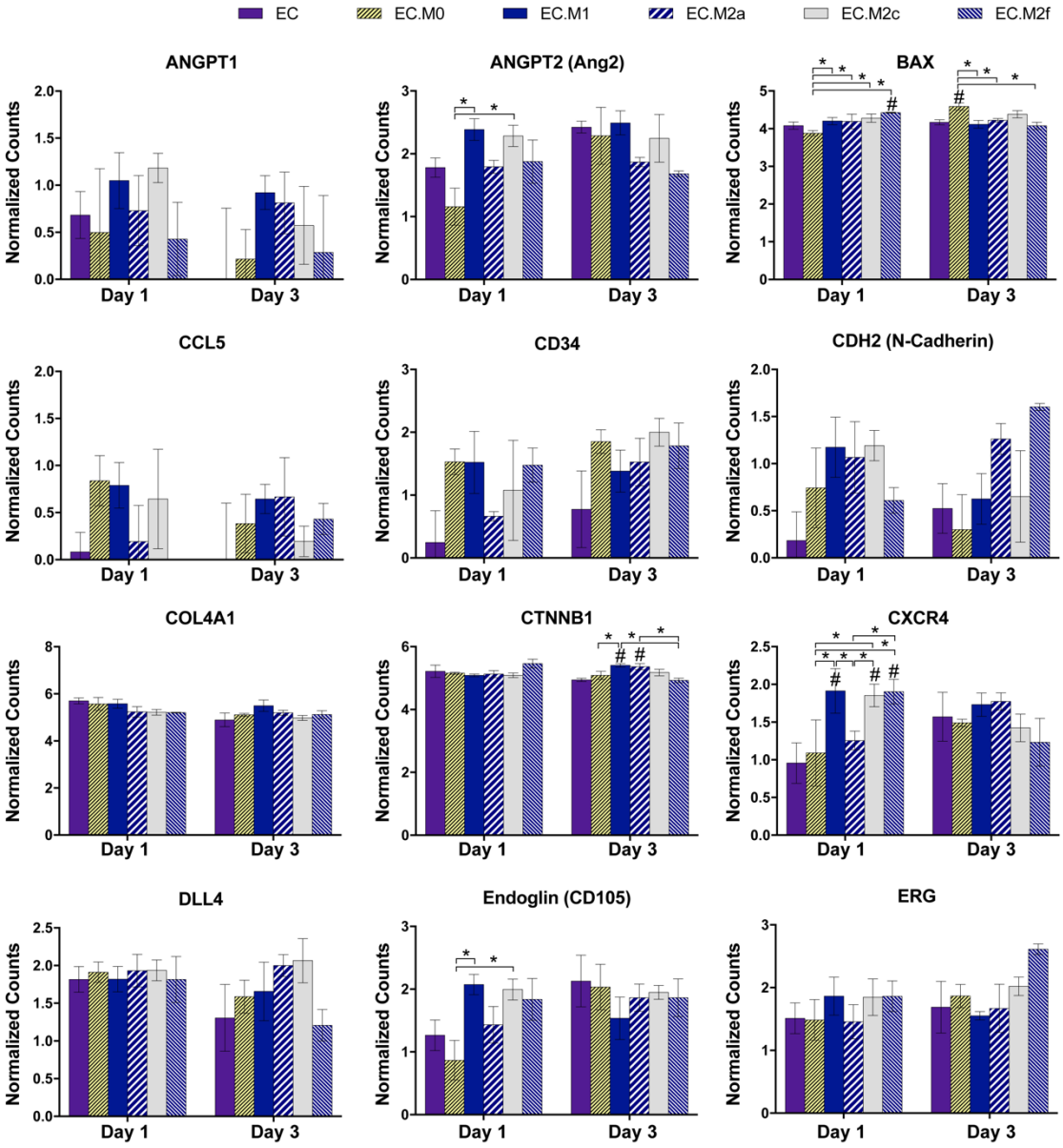

Figure 4.2. Endothelial gene expression in response to transwell co-culture with M0, M1, M2a, M2c, or M2f macrophages for 3 days. Data represent mean normalized counts ± SEM. Statistical analysis was performed on normalized gene expression data using two-way ANOVA and FDR post-hoc analysis with Q = 0.1. # denotes discovery ($p < 0.05$) relative to the EC-only control. *adjusted $p < 0.05$; n = 4.

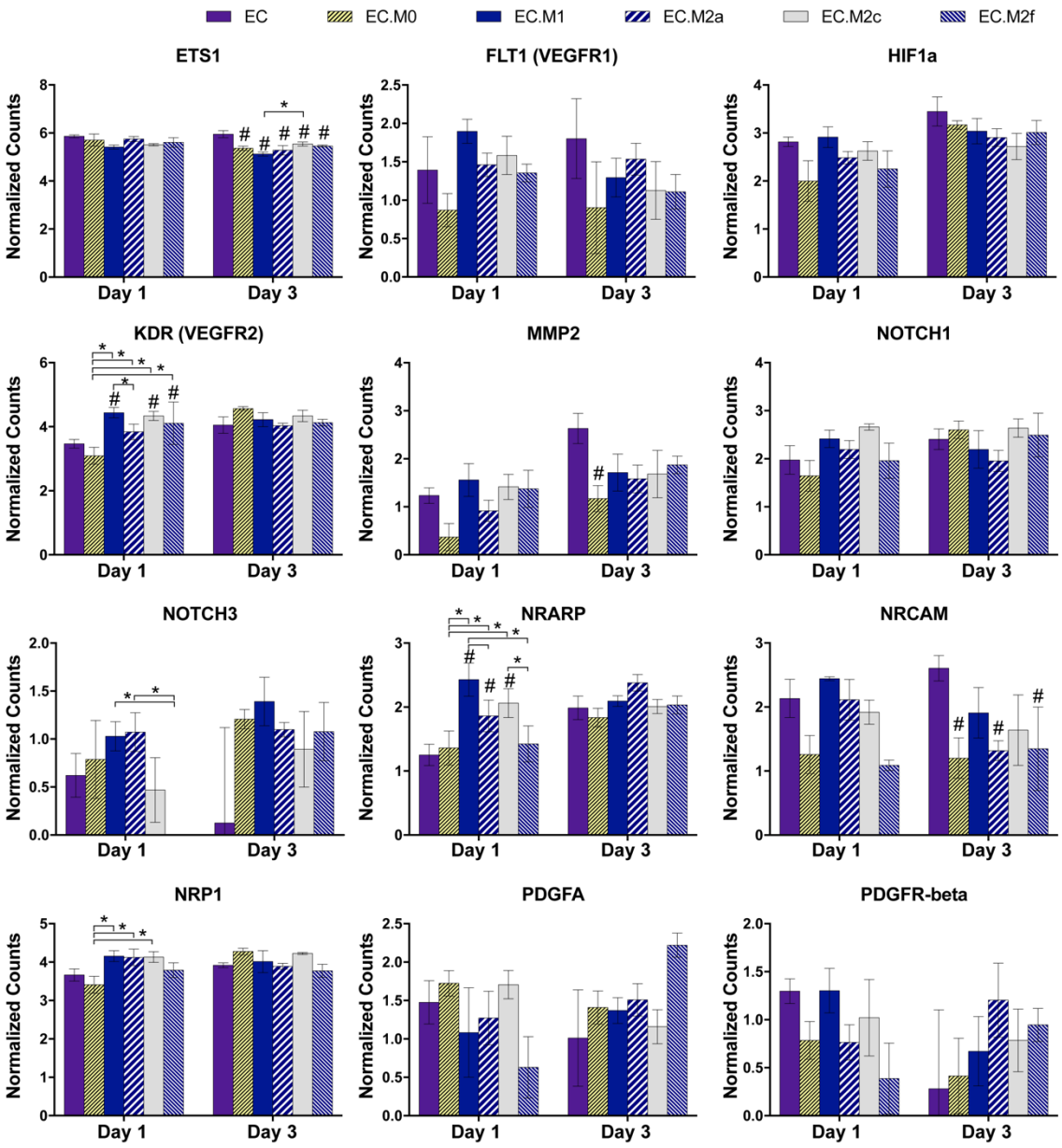

Figure 4.2. (Continued).

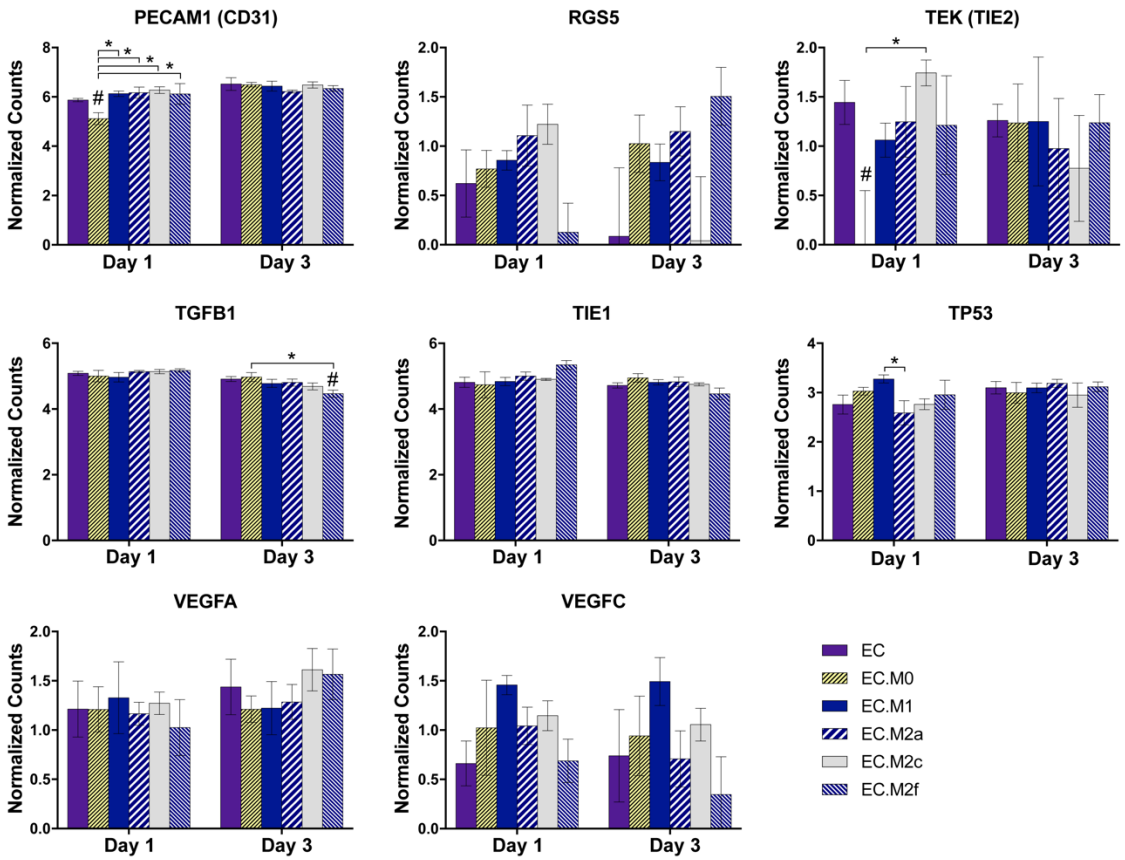

Figure 4.2. (Continued).

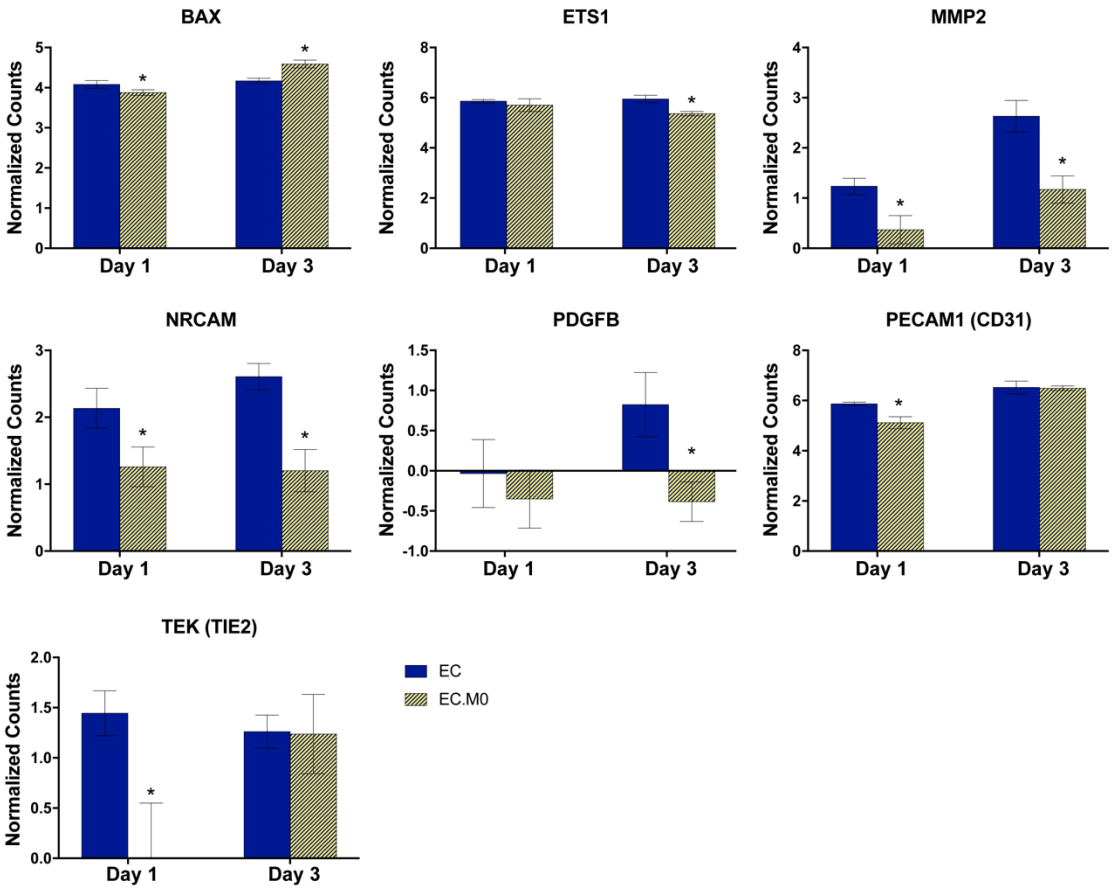

Figure 4.3. M0-induced changes in endothelial gene expression by transwell co-culture for 3 days. Data represent mean normalized counts ± SEM. Statistical analysis was performed on normalized gene expression data using two-way ANOVA and FDR post-hoc analysis with Q = 0.1. # denotes discovery ($p < 0.05$) relative to the EC-only control. *adjusted $p < 0.05$; n = 4.

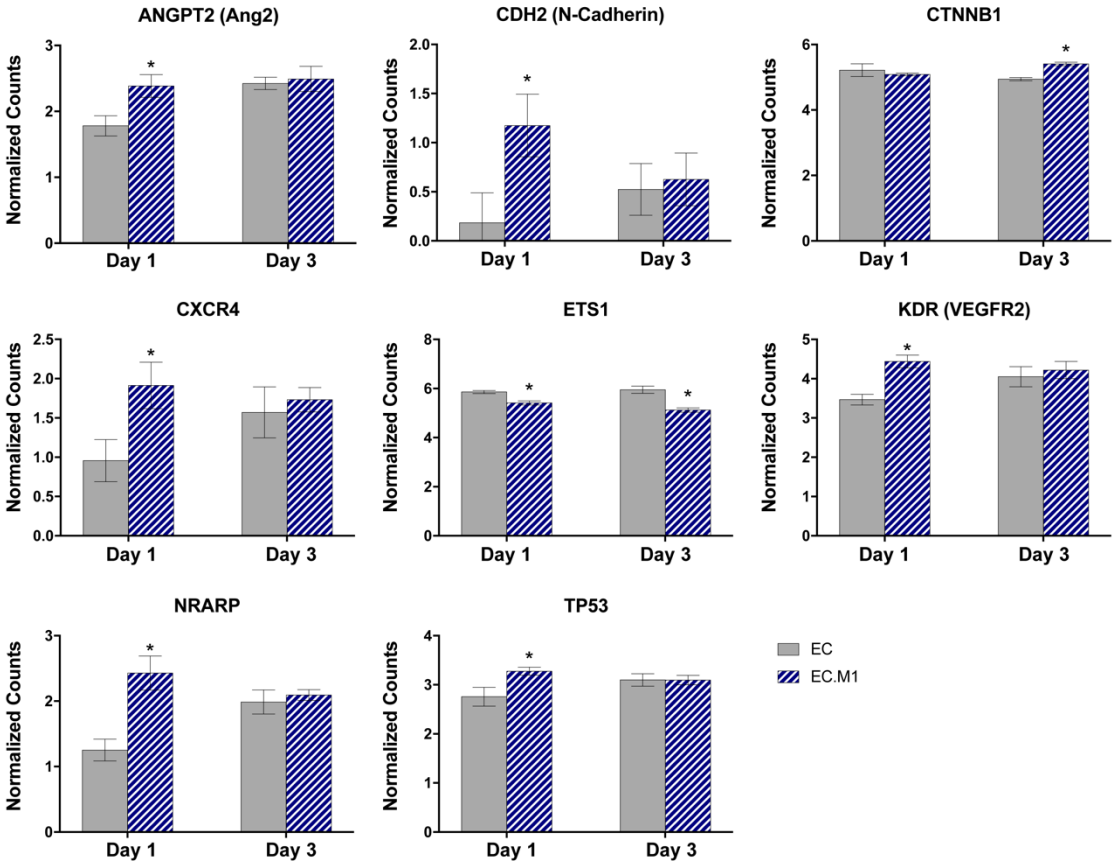

Figure 4.4. M1-induced changes in endothelial gene expression by transwell co-culture for 3 days. Data represent mean normalized counts ± SEM. Statistical analysis was performed on normalized gene expression data using two-way ANOVA and FDR post-hoc analysis with Q = 0.1. # denotes discovery ($p < 0.05$) relative to the EC-only control. *adjusted $p < 0.05$; n = 4.

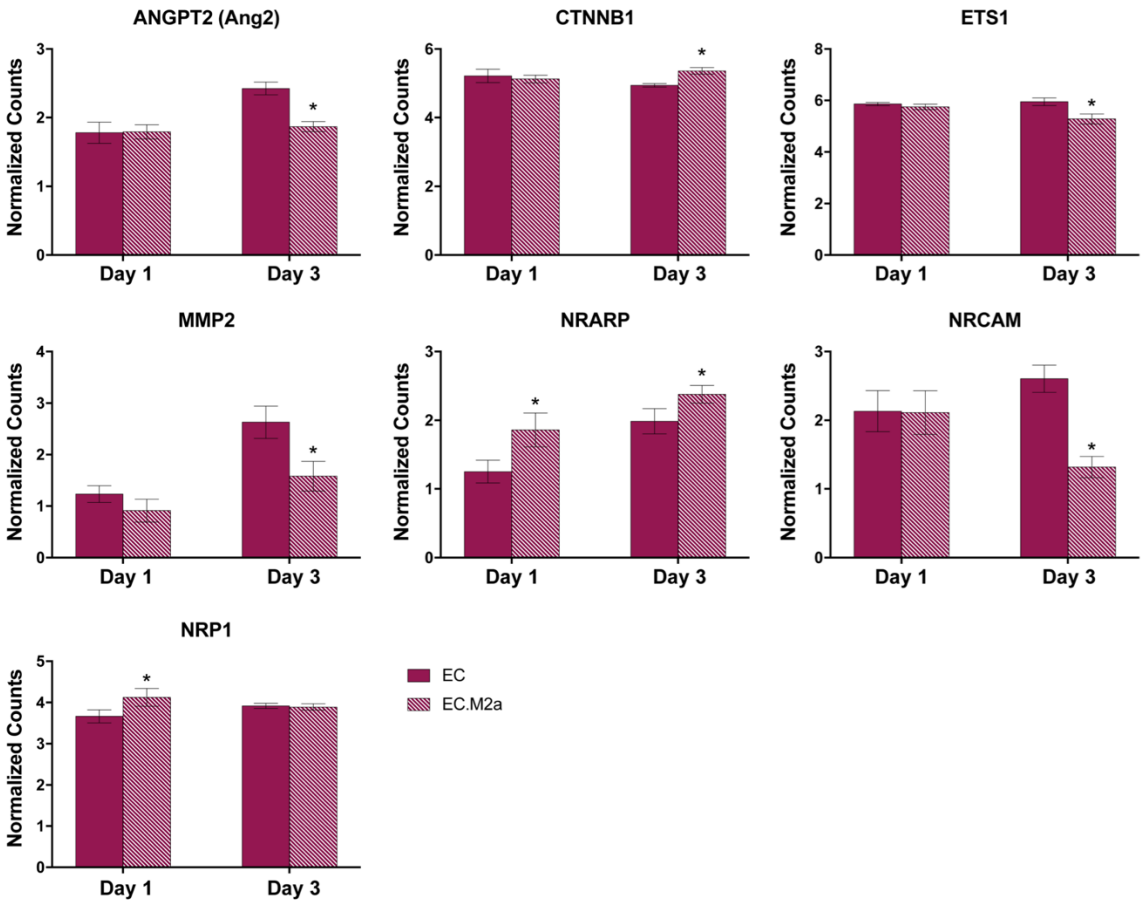

Figure 4.5. M2a-induced changes in endothelial gene expression by transwell co-culture for 3 days. Data represent mean normalized counts ± SEM. Statistical analysis was performed on normalized gene expression data using two-way ANOVA and FDR post-hoc analysis with Q = 0.1. # denotes discovery ($p < 0.05$) relative to the EC-only control. *adjusted $p < 0.05$; n = 4.

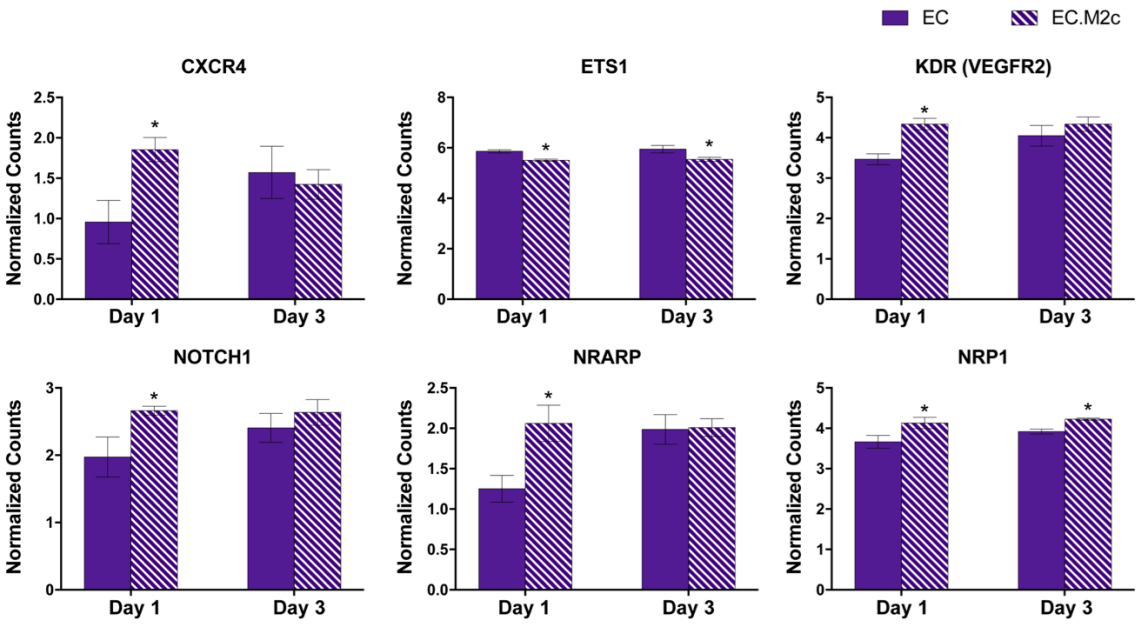

Figure 4.6. M2c-induced changes in endothelial gene expression by transwell co-culture for 3 days. Data represent mean normalized counts ± SEM. Statistical analysis was performed on normalized gene expression data using two-way ANOVA and FDR post-hoc analysis with Q = 0.1. # denotes discovery ($p < 0.05$) relative to the EC-only control. *adjusted $p < 0.05$; n = 4.

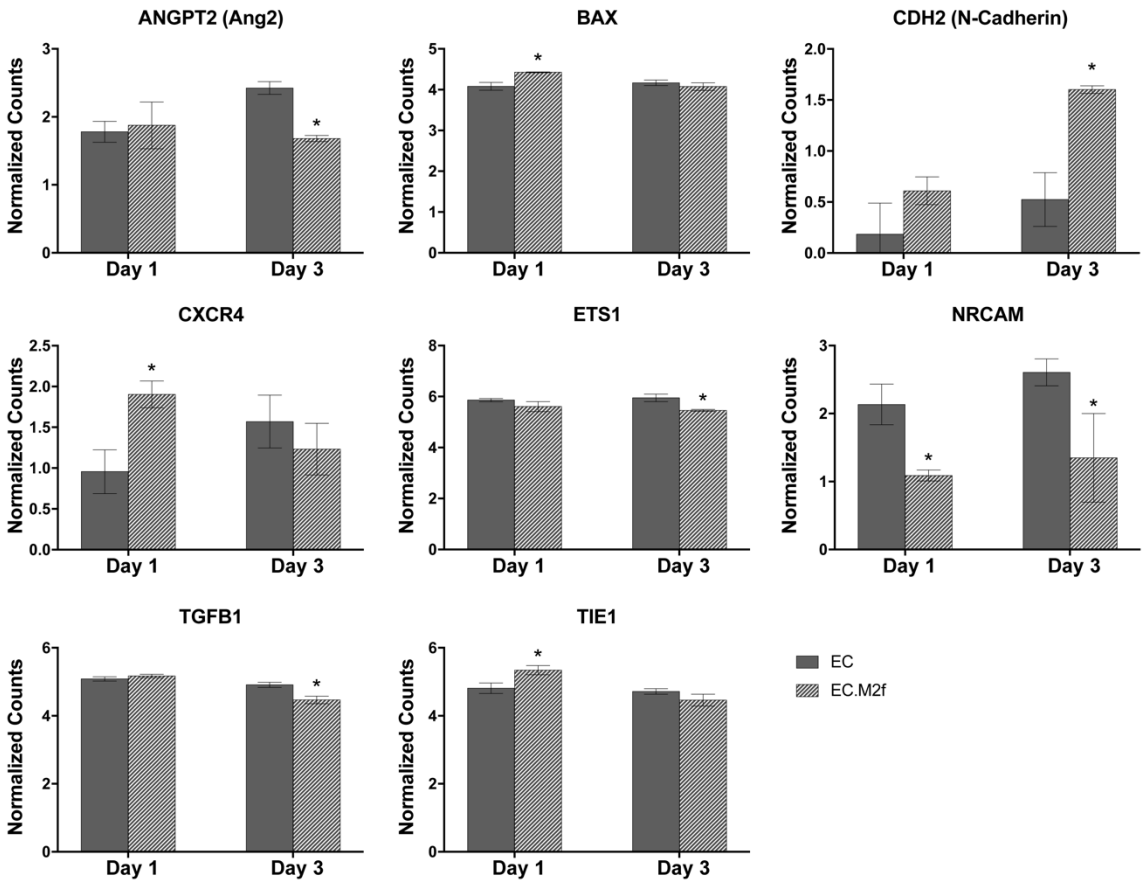

Figure 4.7. M2f-induced changes in endothelial gene expression by transwell co-culture for 3 days. Data represent mean normalized counts ± SEM. Statistical analysis was performed on normalized gene expression data using two-way ANOVA and FDR post-hoc analysis with Q = 0.1. # denotes discovery ($p < 0.05$) relative to the EC-only control. *adjusted $p < 0.05$; n = 4.

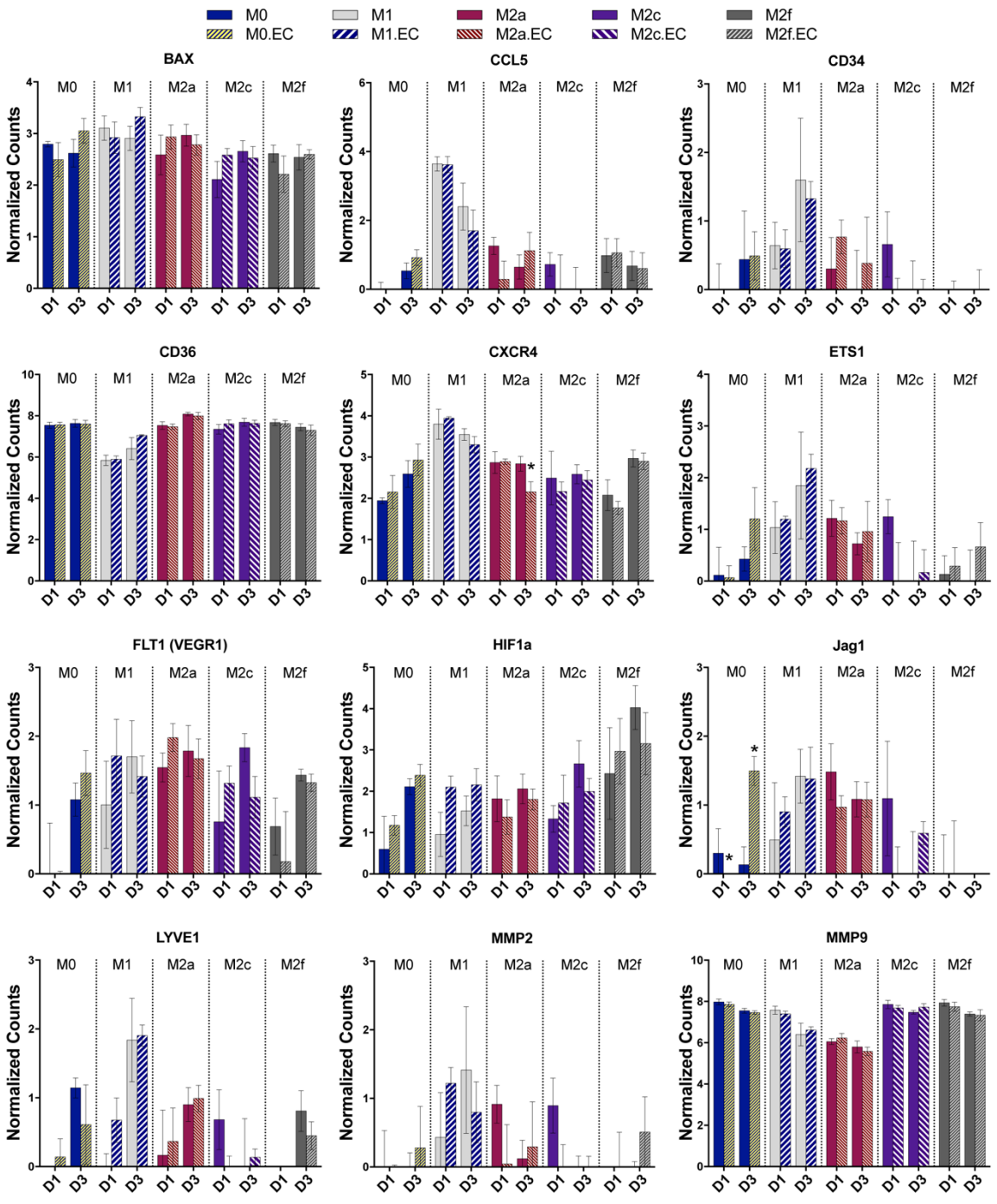

Figure 4.8. Summary of macrophage gene expression for all angiogenic genes in response to transwell co-culture with endothelial cells for 3 days. Data represent mean normalized counts ± SEM. Statistical analysis was performed on normalized gene expression data by multiple t-test analysis via the Holm-Sidak method; *$p < 0.01$; $n = 4$.

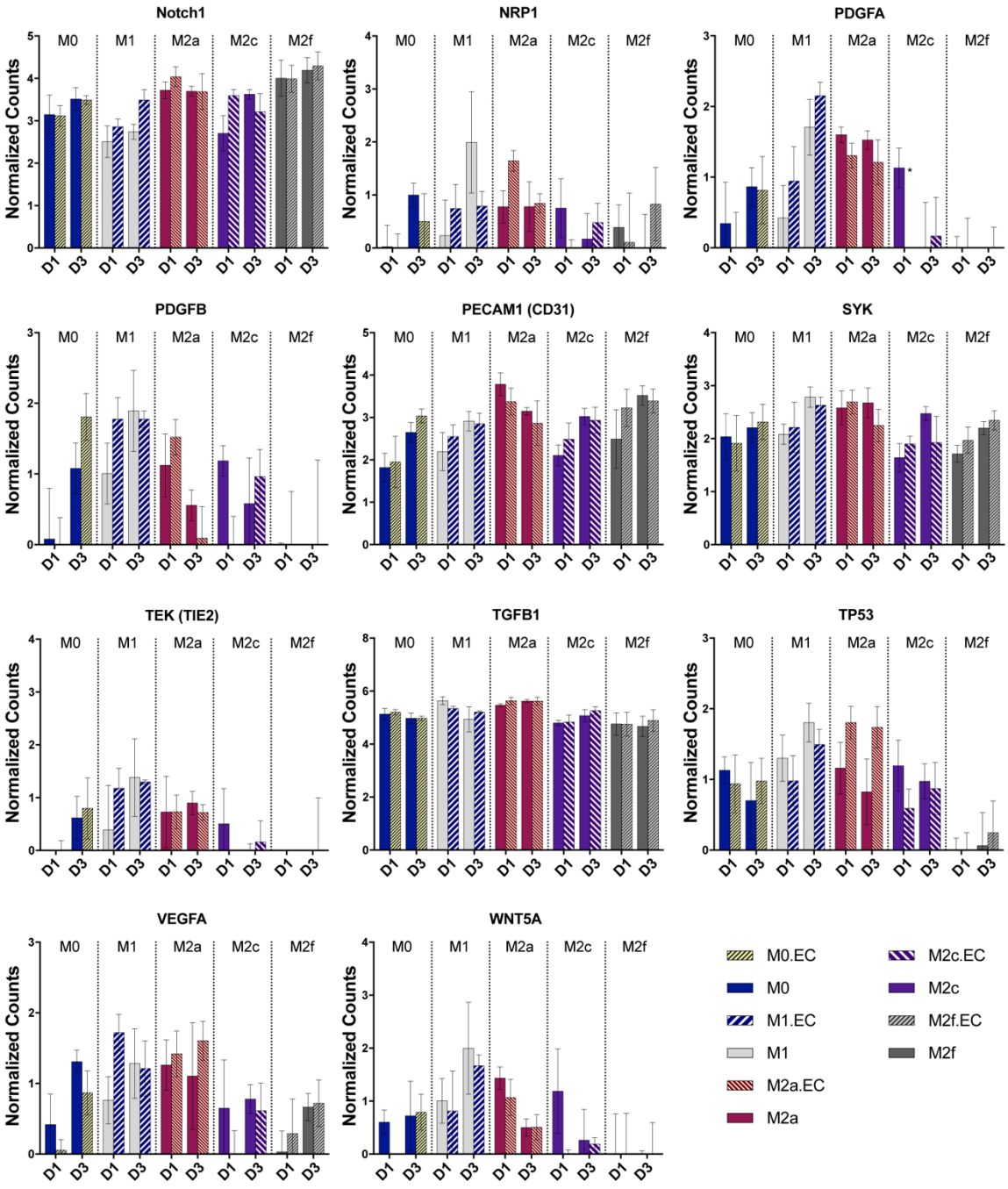

Figure 4.8. (Continued).

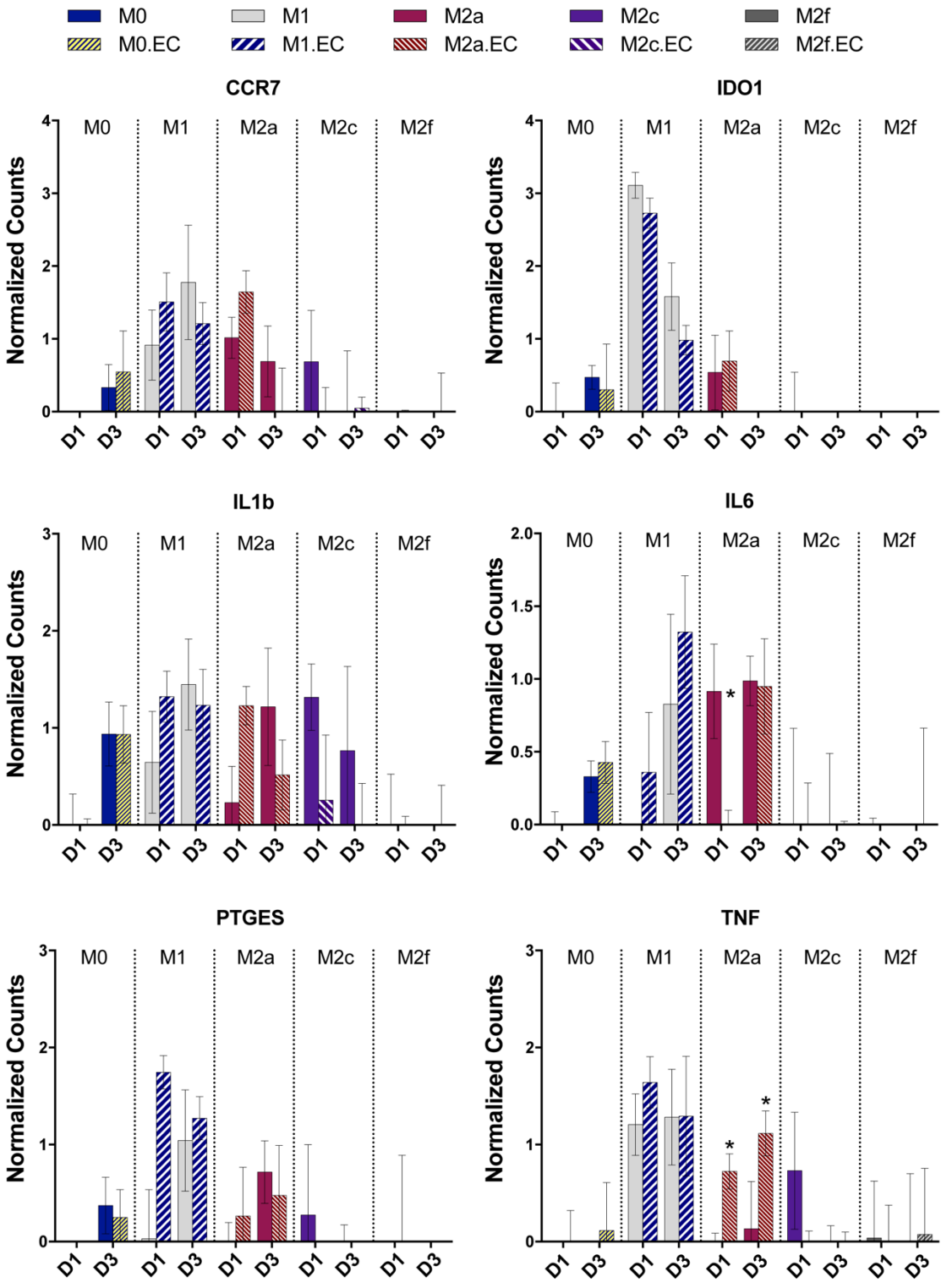

Figure 4.9. Macrophage expression of M1 genes in response to transwell co-culture with endothelial cells for 1 (D1) and 3 (D3) days. Data represent mean normalized counts ± SEM. Statistical analysis was performed on normalized gene expression data by multiple t-test analysis via the Holm-Sidak method; *$p < 0.01$; $n = 4$.

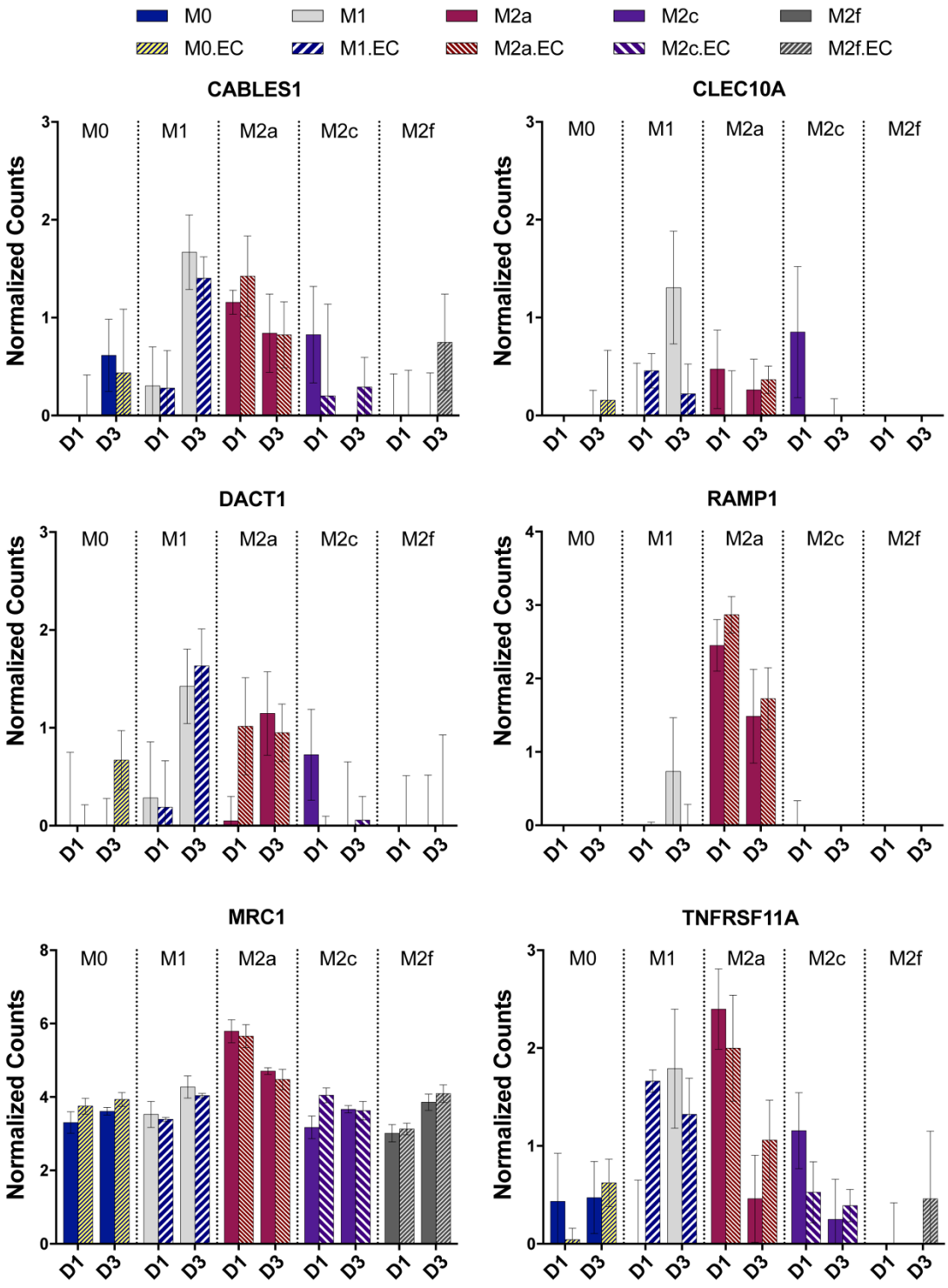

Figure 4.10. Macrophage gene expression of M2a genes in response to transwell co-culture with endothelial cells for 1 (D1) and 3 (D3) days. Data represent mean normalized counts ± SEM. Statistical analysis was performed on normalized gene expression data by multiple t-test analysis via the Holm-Sidak method; *$p < 0.01$; $n = 4$.

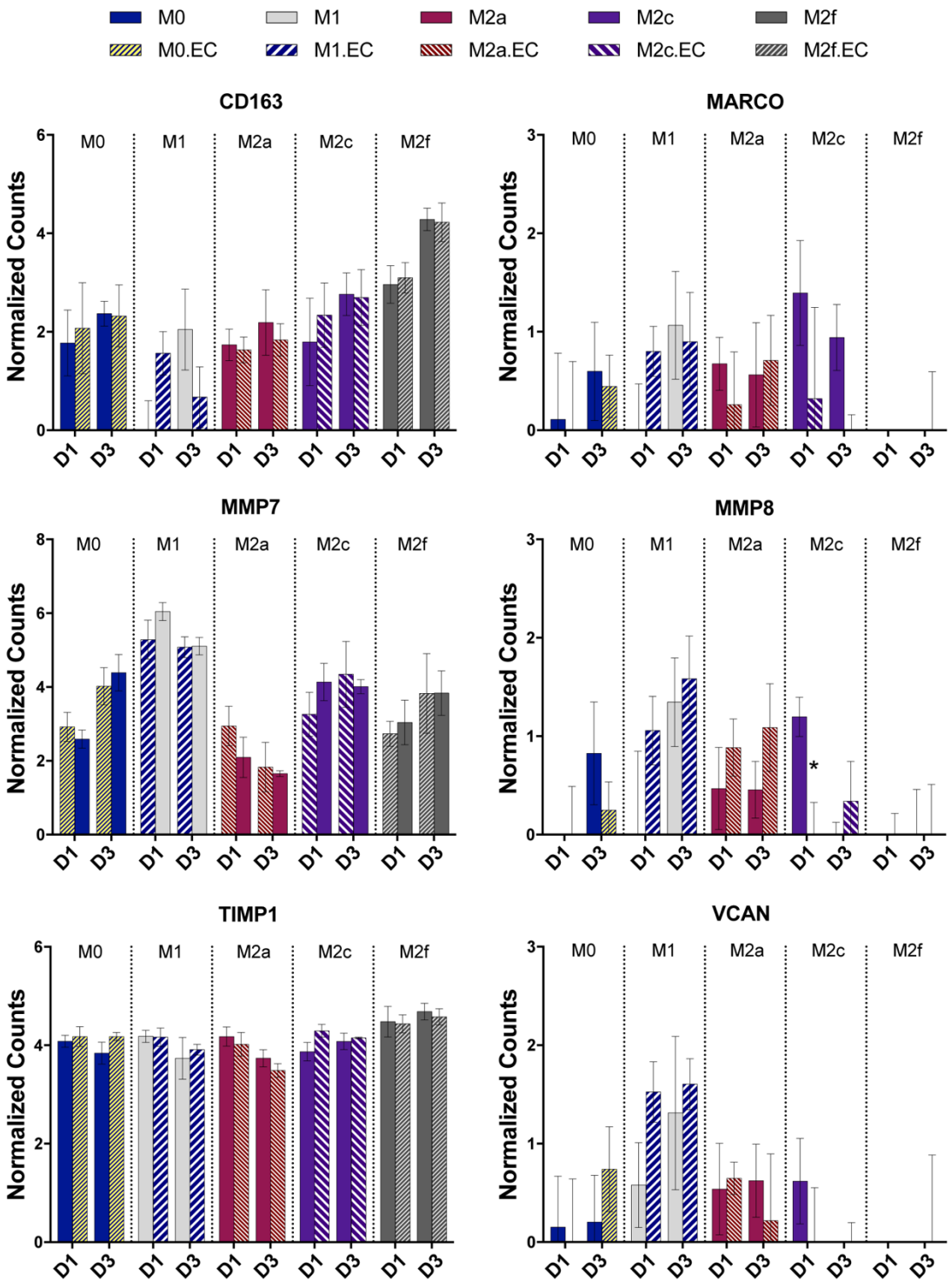

Figure 4.11. Macrophage gene expression of M2c genes in response to transwell co-culture with endothelial cells for 1 (D1) and 3 (D3) days. Data represent mean normalized counts ± SEM. Statistical analysis was performed on normalized gene expression data by multiple t-test analysis via the Holm-Sidak method; *$p < 0.01$; $n = 4$.

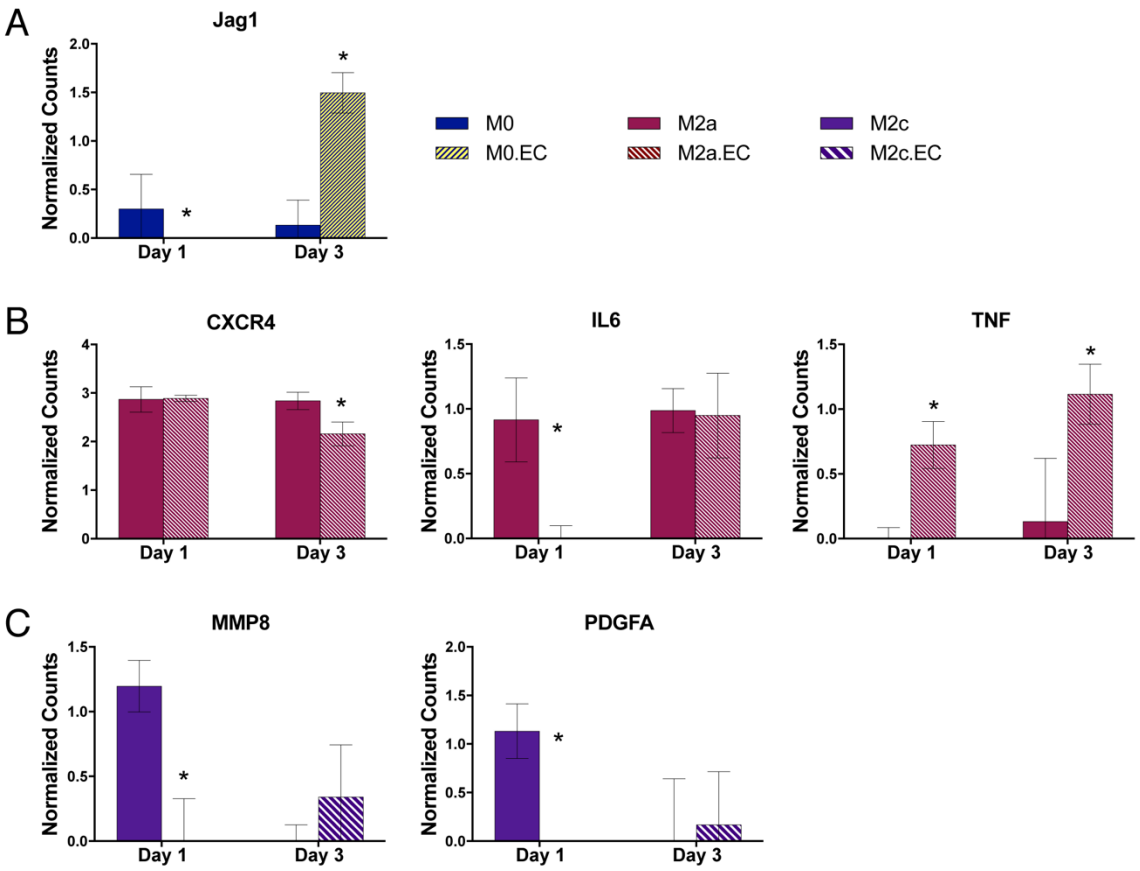

Figure 4.12. Summary of all endothelial cell-induced changes in (A) M0, (B) M2a, and (C) M2c gene expression, relative to untreated phenotype controls. Transwell co-culture with HAMEC-dTom did not affect expression of genes by M1 or M2f macrophages. Data represent mean normalized counts ± SEM. Statistical analysis was performed on normalized gene expression data by multiple t-test analysis via the Holm-Sidak method; *$p < 0.01$; $n = 4$.

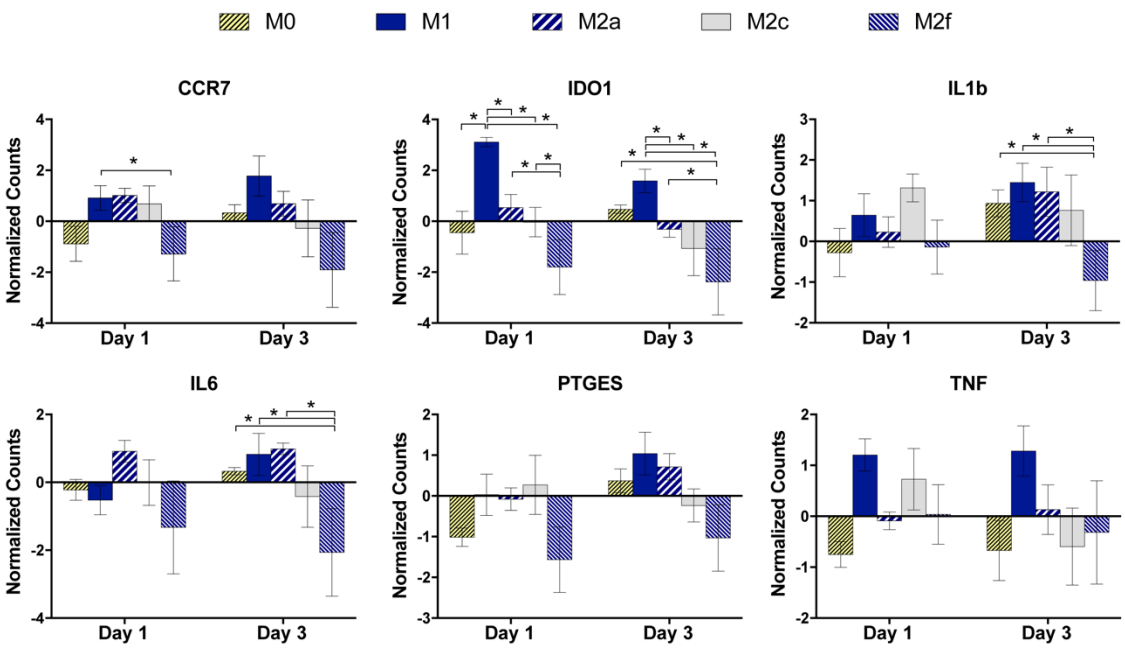

Figure 4.13. Expression of M1 genes by macrophage controls cultured in co-culture media only, without HAMEC-dTom, for 3 days. Data represent mean normalized counts ± SEM; y-value = 0 represents the limit of detectable expression. Statistical analysis was performed on normalized gene expression data using two-way ANOVA and FDR post-hoc analysis with Q = 0.1; *adjusted $p < 0.05$ and n = 4.

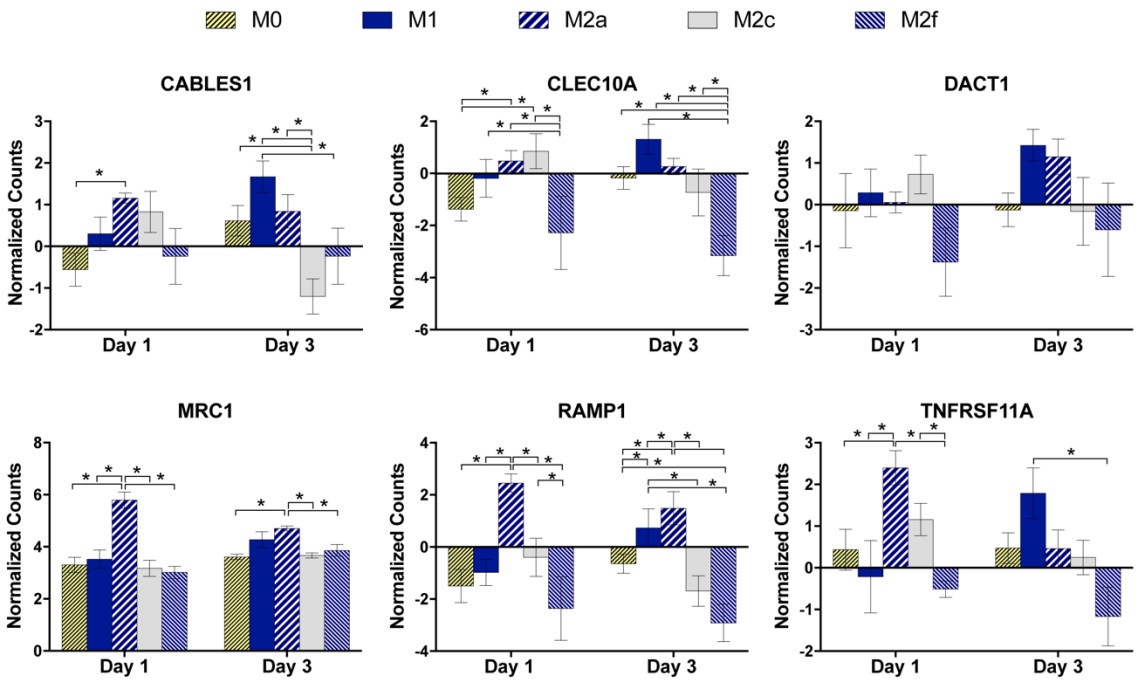

Figure 4.14. Expression of M2a genes by macrophage controls cultured in co-culture media only, without HAMEC-dTom, for 3 days. Data represent mean normalized counts ± SEM; y-value = 0 represents the limit of detectable expression. Statistical analysis was performed on normalized gene expression data using two-way ANOVA and FDR post-hoc analysis with Q = 0.1; *adjusted $p < 0.05$ and n = 4.

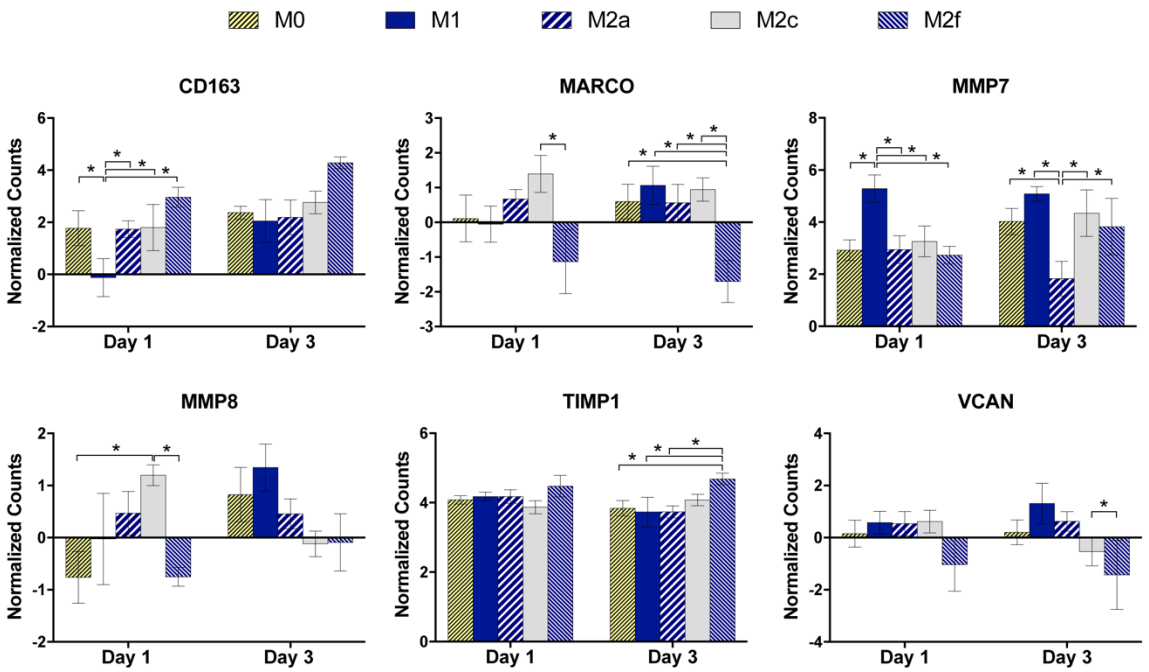

Figure 4.15. Expression of M2c genes by macrophage controls cultured in co-culture media only, without HAMEC-dTom, for 3 days. Data represent mean normalized counts ± SEM; y-value = 0 represents the limit of detectable expression. Statistical analysis was performed on normalized gene expression data using two-way ANOVA and FDR post-hoc analysis with Q = 0.1; *adjusted $p < 0.05$ and n = 4.

CHAPTER 5: CONTRIBUTION OF MACROPHAGE PHENOTYPE TO TISSUE VASCULARIZATION IN VITRO

5.1. Introduction

Given the heterogeneity in macrophage responses to different biomaterial stimuli, it is critical to understand how changes in macrophage activation subsequently influence vascularization and integration of biomaterials upon implantation. In the previous aim, evidence was collected in support of the unique actions of macrophage phenotypes in stimulating angiogenic EC responses *in vitro*, at least at the gene expression level; though these findings support other reports implicating macrophages in angiogenesis *in vivo*, the distinct functional roles of macrophage phenotypes to biomaterial vascularization remain obscure.

For instance, several studies have demonstrated that macrophages physically interact with blood vessels, and not only contribute to fusion of sprouting vessels [25, 45], but also mediate the repair of ruptured vascular though adhesion and mechanical traction [244]. Though the mechanisms behind anastomosis are still unknown, M2a macrophages have been shown to generate significantly more traction force compared to the M1 phenotype [245]. Other studies have also discovered macrophage tunneling, in which monocytes and macrophages form tubular structures [92, 93] and functional vascular channels that lack endothelium [246]. Still, others have discovered that TIE1-expressing macrophages integrate into vessel walls and are recruited to sites of vascular remodeling [247]. CD206+ macrophages have also been shown to surround remodeling vessels [248]. In addition to these actions, macrophages are also known to influence angiogenesis via paracrine signaling, as discussed in the previous chapter, possibly related to the distinct secretory profiles of VEGF and FGF, PDGF, MMPs and OPN, and TGFB1 by M1, M2a, M2c, and M2f macrophages, respectively [70, 80, 180, 182].

Despite these reports, there is still a lack of consensus regarding the angiogenic potential of different macrophage phenotypes. While evidence suggests that M1 macrophages promote endothelial tube formation *in vitro* [70], others report that M1 macrophages secrete both pro- and anti-angiogenic factors and only M2 macrophages promote angiogenesis *in vivo* [96]. In contrast, both M1 and M2 macrophages have been reported to recruit vessel-associated stem cells *in vitro* via secretion of TNF and high mobility group box 1 (HMBG1, M1), and MMP9 (M2a and M2c) [249]. It is clear that the roles of macrophage phenotype in vascularization are poorly defined, perhaps because M1, M2a, M2c and M2f macrophages all function in angiogenesis, but in unique and synergistic ways.

Indeed, several studies have shown that angiogenesis requires coordinated signaling of angiogenic factors for functional network development. For example, simultaneous delivery of VEGF and PDGF can initiate vessel sprouting, but is associated with reduced coverage of pericyte support cells, leading to vessel destabilization due to negative regulation of pericyte function by VEGF [250]. Likewise, sequential delivery of pro-angiogenic factors, VEGF and angiopoietin-1 (ANGPT1), with pro-maturation factors, PDGF and ANGPT2, has been shown to enhance vascular development, while simultaneous delivery inhibited vessel formation [43]. Based on the known interplay of the inflammatory response and angiogenesis, coupled with the data collected in the previous aim, it is conceivable that M1 and M2a macrophages act sequentially in angiogenesis to initiate sprouting and stabilize newly forming vessels, while M2c macrophages act at early and late stages to initiate sprouting and remodeling of the extracellular matrix.

Therefore, the goal of this aim was to elucidate the impact of macrophage phenotype on vascular development *in vitro*. A previously established *in vitro* 3-dimensional (3D) model of vascularization, developed by Frieman *et al*. [251], was

systematically adapted to facilitate the study of macrophage phenotype in angiogenesis. By self-assembly of ECs and MSCs on porous scaffolds *in vitro*, elongated immature vessels can be obtained within 4 days post-seeding, and well-developed vascular networks can be achieved by day 7 [251]. Importantly, these pre-vascularized constructs not only successfully anastomose with host tissue upon implantation, but also allow vascular morphogenesis to be studied *in vitro* [40] via live cell imaging. Therefore, these pre-vascularized constructs can be used not only *in vitro* by adding macrophages to this 3D model of vascularization, but also *in vivo* to confirm the contribution of macrophages to angiogenesis and anastomosis between engineered and host tissue.

In this work, an *in vitro* tri-culture system of ECs, MSCs and macrophages was first developed with the overarching goals of (1) probing the effects of macrophage phenotype on vascular morphogenesis, and (2) characterizing the crosstalk among macrophages, ECs and support cells required for blood vessel formation. The final 3D model of vascularization was expected to meet the following pre-established criteria:

Criterion 1: Facilitates long-term culture of ECs and support cells that leads to vessel formation and allows for the addition of macrophage post-vasculogenesis.

Criterion 2: Supports quantitative analysis of repeated measures, with respect to macrophage-blood vessel interactions, in 3 dimensions.

Criterion 3: Enables isolation of individual cell populations for gene expression analysis as a means to characterize the effects of cellular crosstalk during angiogenesis.

Thereafter, this tri-culture system was used to assess the effects of macrophage phenotype on tissue vascularization *in vitro*, and to test the hypothesis that temporal control over macrophage activation enhances angiogenesis. This work was completed in collaboration with the Stem Cell & Tissue Engineering Laboratory at the Technion-Israel Institute of Technology (PI: Prof. Shulamit Levenberg).

5.2. Experimental Section

5.2.1. Cell Culture

Endothelial Cells: Human adipose microvascular endothelial cells expressing either dTomato (HAMEC-dTom) or ZsGreen fluorescent protein (HAMEC-ZsGreen) were generously provided by the Levenberg Lab (Technion, Israel) and cultured at 5,000-7,000 cells/cm^2 in Endothelial Cell Medium (ECM, ScienCell, #1001) supplemented with 5% fetal bovine serum (FBS), 1% endothelial cell growth supplement, and 1% penicillin/streptomycin solution. Human umbilical vein endothelial cells expressing green fluorescent protein (HUVEC-GFP) were generously provided by the Levenberg Lab (Technion, Israel) and cultured at 5,000-7,000 cells/cm^2 in Endothelial Cell Growth Medium (EGM-2^{TM}-BulletKit^{TM}, Lonza, #CC-3162). All endothelial cells were routinely subcultured via trypsinization at 90% confluency and used within 9 passages.

Vascular Support Cells: Human adipose-derived mesenchymal stem cells (MSC) were purchased from Lonza and cultured at 5,000 cells/cm^2 in Human Adipose Derived Stem Cell Growth BulletKit^{TM} medium (Lonza, #PT-4503) according to the manufacturer's instructions. MSC were routinely subcultured via trypsinization at 90% confluency and used within 7 passages. Human neonatal dermal fibroblasts (HNDF) were cultured in Dulbecco's modified Eagle's medium (DMEM) supplemented with 10% FBS, 1% non-essential amino acids, 1% penicillin-streptomycin solution, and 0.2% β-mercaptoethanol. HNDF were routinely subcultured via trypsination at 90% confluency and used within 8 passages.

THP-1: Human THP-1 monocytes, which are thought to closely mimic the function of monocytes and macrophages [252], were used to study macrophage regulation of angiogenesis; the limited number of monocytes that can be obtained from a single donor

precluded the initial use of primary macrophages in this work, as the scale of each study required a large number of monocytes and donor-to-donor variability of pooled monocytes could diminish the effects of phenotype. THP-1 cells were generously provided by the Admon Lab (Technion, Israel), and expanded in suspension flasks at 200,000 – 400,000 cells/mL in RPMI 1640 medium supplemented with 10% fetal bovine serum and 1% penicillin/streptomycin solution. Media was replenished every 2-3 days by centrifugation of the cells at 200×g for 5 min. Following expansion, THP-1 cells were transferred to ultra-low attachment culture flasks and stimulated with Phorbol 12-myristate-13-acetate (PMA, 320 nM final concentration) for 16-24 h at 37°C and 5% CO_2, to induce differentiation to M0 macrophages as previously described [160]. Following PMA treatment, M0 macrophages were washed in 1X PBS. For differentiation into the M1, M2a, or M2c phenotypes, the cells were incubated for an additional 48 h in media supplemented with IFN-γ (100 ng/mL) and LPS (100 ng/mL) for M1 activation, IL-4 (40 ng/mL) and IL-13 (20 ng/mL) for M2a activation, or IL-10 (40 ng/mL) for M2c activation. Post-differentiation, the cells were gently scraped and collected for use, as indicated, in the studies described below.

GFP-THP1: To visualize macrophages, THP-1 cells expressing Green Fluorescent Protein (GFP-THP1) were purchased from Angio-Proteomie (Boston, MA). GFP-THP1 were expanded in ultra-low attachment flasks at 200,000 – 400,000 cells/mL in RPMI 1640 media, supplemented with 10% fetal bovine serum and 1% penicillin/streptomycin solution. Media was replenished every 2-3 days by centrifugation of the cells at 200×g for 7 min. Differentiation into the M0, M1, M2a and M2c phenotypes was accomplished using the same procedure as described above for unlabeled THP-1 cells.

All cells were cultured in a humidified chamber at 37°C and 5% CO_2.

5.2.2. Development of *In Vitro* 3D Model of Vascularization with Macrophages

5.2.2.1. Vascular Network Formation

Previous work has demonstrated that endothelial cells and support cells can be seeded onto PLLA/PLGA scaffolds to generate self-assembled vascular networks *in vitro* [40, 251]; however, the ability to seed macrophages onto pre-vascularized PLLA/PLGA constructs may be hindered by the fibrin gel used during the initial endothelial and support cell seeding. Therefore, three different porous constructs were investigated in this work for their ability to generate vascular networks that facilitate macrophage seeding during later stages of vascularization. Specifically, PLLA/PLGA was compared to RGD-modified Alginate and Gelfoam® constructs; there were selected based on previous work demonstrating their utility as scaffolds that support vascular formation [253-255].

PLLA/PLGA Constructs: Three-dimensional (3D) porous poly-L-lactic acid (PLLA)/poly-lactic-co-glycolic acid (PLGA) constructs were fabricated using a salt-leaching technique, as described previously [251]. Briefly, a 50% PLLA (Polysciences) 50% PLGA (Boehringer Ingelheim) solution was prepared in chloroform and 0.24 mL of this solution was added to 0.4 g sodium chloride particles (200-600 μm diameter) maintained in Teflon-coated molds. The molds were sealed for 1 h, after which the chloroform was allowed to evaporate overnight. The polymer matrix was then removed from the molds and the salt was leached out in distilled water for 6-8 h, changing the water hourly. The resulting porous 3D scaffolds were stored at -80°C overnight, lyophilized and cut using an 8-mm diameter biopsy punch. PLLA/PLGA scaffolds were sterilized under UV for 15 min prior to cell seeding, and pre-wet in 1X PBS. Vascular networks were formed using previously established procedures [251]. First, a 5:1 ratio of HAMEC to MSC or

HUVEC to HNDF were mixed in 3.5 μL thrombin, followed by addition of 3.5 μL fibrinogen to the cell suspension. The suspension was mixed, seeded directly onto the PLLA/PLGA scaffolds, and incubated in a humidified chamber at 37°C and 5% CO_2 for 30 min for cell attachment. Post-seeding, the scaffolds were transferred to a clean tissue-culture dish, and 2 mL of 1:1 endothelial cell media and support cell media were added to each scaffold. The scaffolds were incubated for 14 days, with media exchange every 2-3 days.

Alginate-RGD and Gelfoam® Constructs: Alginate constructs were modified with RGD peptide by the Levenberg Lab. Sulfo-NHS, EDC, and RGD peptide were added to 1% alginate in MES buffer and the reaction was allowed to proceed for 20 h with stirring. Hydroxyl amine was used to quench the reaction and the alginate was dialyzed for several days. The modified alginate was then mixed in a 2:1 ratio with active charcoal, filtered, frozen overnight and lyophilized. Alginate-RGD scaffolds were subsequently fabricated by mixing 2.5% alginate-RGD in MES buffer with adipic acid dihydrazide, 1-hydroxybenzotriazole, and EDC crosslinkers. The mixture was cast between two glass slides and polymerized for 3 h. The resulting 3D scaffolds were cut using an 8-mm diameter biopsy punch, washed in distilled water, frozen and lyophilized. Alginate-RGD scaffolds were sterilized under UV for 15 min prior to cell seeding, and pre-wet in 1X PBS. Commercially available Size 100 Compressed Gelfoam® Sponge was purchased from Pfizer (New York, NY), cut using a sterile 8-mm diameter biopsy punch, and pre-wet in 1X PBS or media.

Vascular networks were formed on Alginate-RGD and Gelfoam® scaffolds by seeding a 5:1 ratio of HAMEC to MSC or HUVEC to HNDF directly onto the scaffolds in 10 μL endothelial cell media. The cell-seeded scaffolds were incubated for at least 30 min in a humidified chamber at 37°C and 5% CO_2 to facilitate cell attachment; this processed

was repeated to achieve seeding on both sides of Gelfoam® scaffolds for all macrophage studies described in this aim. Post-seeding, all scaffolds were transferred to clean tissue-culture dishes and immersed in a 1:1 solution of endothelial cell media and support cell media. The scaffolds were incubated for 14 days, with media exchange every 2-3 days.

All vascular networks were cultured in endothelial and support cell co-culture media, which was verified to support THP-1 viability (> 99.5%) after 3 days *in vitro* via trypan blue exclusion. Macrophage media was omitted because its effects vessel development within the systems explored in this work are unknown.

5.2.2.2. Visualization of Macrophages During Vascular Network Formation

In order to visualize macrophage interactions with blood vessels, the ability to stain THP-1 cells using a Vybrant® DiD Cell Labeling solution was investigated. During later stages of this work, THP-1 cells expressing green fluorescent protein (GFP-THP1) became commercially available and were characterized as an alternative to DiD labeling.

DiD: Where indicated, macrophages were labeled with Vybrant® DiD Cell Labeling solution (Thermo Fisher Scientific, Waltham, MA), according to the manufacturer's instructions, immediately before seeding onto scaffolds. Effects of DiD on THP-1 viability were tested via trypan blue exclusion after 3 days of culture *in vitro* on tissue-culture plastic and the ability to visualize DiD-labeled M0 macrophages seeded on Gelfoam® scaffolds was assessed using confocal microscopy and image analysis tools.

GFP-THP1: The ability to visualize GFP-macrophages was confirmed by differentiating GFP-THP1 cells into the M0 phenotype and seeding the cells directly onto Gelfoam® constructs in 10 μL media; GFP-M0 were visualized via confocal microscopy. To determine the effects of GFP-transfection on THP-1 cells, GFP-THP1 and THP-1 cells

were differentiated into the M0, M1 and M2a phenotypes *in vitro*, and lysed in 250 μL Buffer RLT (Qiagen) for gene expression analysis using a panel of markers indicative of the M1 and M2a phenotypes. RNA was extracted from cells, DNA was inactivated with DNAse I, and cDNA was prepared as previously described [83]. Quantitative RT-PCR was performed using 20 ng cDNA and Fast SYBR Green Master Mix (Applied Biosystems) according to the manufacturer's protocol, with n=2 technical replicates. Mean quantification cycle (C_q) values were calculated and the expression of target genes was normalized to the reference gene, *GAPDH*. Data shown represent the mean fold change ± SEM (n≥4). All primers (**Table 3.1**) were synthesized by Life Technologies; *NRP1* Forward (5'-3'): TGAGCCCTGTGGTTTATTCC, *NRP1* Reverse (5'-3'): CGTACTCCTCTGGCTTCTGG; *TIE2* Forward (5'-3'): TCCGCTGGAAGTTACTCAAGA, *TIE2* Reverse (5'-3'): GAACTCGCCCTTCACAGAAATAA.

5.2.2.3. Identification of Macrophage Seeding Density

A range of macrophage concentrations was explored to determine the number of macrophages to seed on the scaffolds that would allow for visualization and characterization of macrophage-vessel interactions, as well as downstream gene expression analysis. THP-1 cells were differentiated to the M0 phenotype and stained for visualization with Vybrant® DiD fluorescent dye (Thermo Fisher Scientific, Waltham, MA) according to the manufacturer's instructions. High (1:1 ratio of HAMEC to M0, corresponding to 300,000 M0), medium (2:1 ratio of HAMEC to M0, corresponding to 150,000 macrophages), and low (1:1 ratio of MSC to M0, corresponding to 60,000 M0) macrophage densities, together with a 5:1 ratio of HAMEC-ZsGreen to MSC, were seeded on Alginate-RGD and Gelfoam® scaffolds. The scaffolds were maintained in co-culture

media, refreshed every 2-3 days, and incubated at 37°C and 5% CO_2 for 14 days. Changes in vascularization were assessed via confocal microscopy; n = 3 scaffolds per group.

5.2.2.4. Identification of Macrophage Seeding Time

Macrophages were seeded on Gelfoam® scaffolds at different stages of vessel development to determine the effects of seeding time on vascularization. In this work, three time points were evaluated: Day 0, Day 3, and Day 6 of vessel development. For Day 0 seeding, THP-1 cells were differentiated to the M0 phenotype and mixed with HAMEC-ZsGreen and MSC in a ratio of 5:1:2.5 (HAMEC: MSC: M0), based on the previous study, in endothelial cell media. The cell suspension was seeded directly onto the scaffolds as described above. For Day 3 and Day 6 seeding, Gelfoam® scaffolds were pre-seeded with a 5:1 ratio of HAMEC to MSC on day 0, and incubated in the absence of macrophages. On day 3 or 6, the media was aspirated from these scaffolds and M0 macrophages were seeded in a 2:1 ratio of HAMEC to M0. All samples were maintained in co-culture media, refreshed every 2-3 days, and incubated at 37°C and 5% CO_2 for 14 days. Changes in vascularization were assessed via confocal microscopy; n = 3 scaffolds per group.

5.2.3. Contribution of Macrophage Phenotype to Vascularization

To test the hypothesis that M1 macrophages stimulate vessel sprouting and M2a macrophages promote vessel branching and stabilization, the contribution of macrophage phenotype on vascularization was explored using the *in vitro* tri-culture system developed through earlier work, as described above. THP-1 macrophages were differentiated into

the M0, M1 and M2a phenotypes. Gelfoam® scaffolds were pre-seeded with a 5:1 ratio of HAMEC-dTom and MSC to initiate vessel formation, and, on day 3, the scaffolds were imaged via confocal microscopy as a baseline measurement of vessel growth. Post-imaging, M0, M1, or M2a macrophages were seeded directly onto the constructs in 10 μL of co-culture media. Control scaffolds without macrophages were seeded with 10 μL of media alone. All samples were incubated for 30 min to allow cell attachment, and subsequently transferred to clean 24-well tissue culture plastic for continued incubation in co-culture media. Changes in vascular network formation were monitored over 10 days *in vitro* using confocal microscopy. In an effort to capture effects of macrophages on angiogenesis, rather than vasculogenesis, this study was repeated with macrophage seeding on day 6 of vascularization, at which point elongated vessels were visible. M2c macrophages were also included in this follow-up investigation. For both studies $n \geq 3$ scaffolds were included per group.

Additionally, to visualize macrophage morphology and co-localization with developing blood vessels, GFP-macrophages differentiated into the M0, M1, M2a and M2c phenotypes were seeded on Gelfoam® scaffolds on day 6 of vascularization in the same manner as described above. Confocal microscopy was performed after 1 and 3 days of macrophage-vessel interactions ($n \geq 3$ scaffolds for M0, M1 and M2a; $n = 1$ scaffold for M2c).

5.2.4. Effects of Sequential M1-to-M2a Activation on Vascularization

To test the hypothesis that sequential M1-to-M2a activation enhances vascularization, macrophages differentiated into the M1 and M2a phenotypes were seeded on Gelfoam® scaffolds on day 3 and 6 of vascularization, respectively. Gelfoam®

scaffolds were pre-seeded with a 5:1 ratio of HAMEC-dTom and MSC to initiate vessel formation, and, on day 3, the scaffolds were imaged via confocal microscopy as a baseline measurement of vessel growth. Post-imaging, 50,000 M1 or M2a macrophages, or media alone, were seeded directly onto the constructs in 10 μL of co-culture media. All samples were incubated for 30 min to allow cell attachment, and subsequently transferred to clean 24-well tissue culture plastic for continued incubation in co-culture media. Scaffolds were imaged on days 4 and 6. Post-imaging on day 6, 50,000 M1 or M2a macrophages, or media alone, were again seeded directly onto the scaffolds in 10 μL of co-culture media and incubated for cell attachment. The effects of this sequential seeding were measured on days 7 and 10 using confocal microscopy. Experimental groups included: Control (no macrophages), M1-media, M1-M1, M1-M2a, media-M2a, M2a-M2a; n=3 per group.

This sequential study was repeated to confirm preliminary findings, as well as to include additional controls (M1-M0, M0-M2a, M1+M2a). Scaffolds (n = 3 per group) were prepared under the same conditions as described above. For both studies, aliquots of differentiated macrophages were lysed in 250 μL Buffer RLT (Qiagen) at the time of macrophage seeding to confirm phenotype via gene expression analysis, as described earlier.

5.2.5. Confocal Microscopy

Network development within the scaffolds was monitored over 14 days using live confocal imaging. Prior to imaging, each scaffold was rinsed in 1X PBS and transferred to a sterile glass-bottom dish. Images were captured using a Zeiss LSM700 inverted laser scanning confocal microscope (Zeiss, Germany) equipped with 10x and 20x objectives.

The z-stack was defined to capture the maximum field-of-view in the z-axis. Tiled z-stack images were acquired and stitched using Zen software (Zeiss, Germany).

5.2.6. Quantitative Image Analysis

Confocal images were processed in Fiji [256] to adjust brightness and contrast, with gamma set to 0.65. Maximum intensity projections of the z-stacks were analyzed in 2D using AngioTool software [257], in terms of vessel area, length, diameter, number of junctions and number of endpoints. Where indicated, Matlab® (MathWorks, Natick, MA) was also used to measure network complexity (vessel elongation) in 2D as described previously [251].

Although AngioTool is commonly used to assess vascularization, its limit to 2D analysis may not accurately represent the 3D network morphology. Therefore, z-stacks were also analyzed in 3D in Matlab® (MathWorks, Natick, MA) using a custom computational image analysis code developed by the Computational Image Sequence Analysis Lab at Drexel University (PI: Dr. Andrew Cohen) [258]. Briefly, metadata from z-stack images were extracted, and images were converted to a binary image using media filter to remove background noise and Otsu thresholding in 3D. Images were then skeletonized using Phi Max tools and vessel structures were quantified. Original and skeletonized images were then concatenated to inspect the accuracy of the skeleton in 3D. Structures were characterized in terms of total number of vessels, number of connected vessels, vessel diameter, number of nodal connections (vessels attached at the same junction), and average connected vessel size.

Imaris software (Bitplane, Switzerland) was also explored as a tool to quantify vascularization dynamics in 3D. Although Imaris is effective in reconstructing and

segmenting z-stacks, the software is not widely available and data interpretation in terms of angiogenesis is challenging.

5.2.7. Investigation of Cell Isolation Techniques

To further elucidate the effects of macrophage phenotype on vascularization, it is of interest to investigate changes in cell behavior resulting from crosstalk between endothelial cells, support cells, and macrophages. As a first step in this analysis, methods to isolate enriched populations of HAMEC-dTom, MSC, and macrophages of different phenotypes were investigated.

5.2.7.1. Scaffold Digestion

Collagenase 4 (Worthington, #LS004188) was reconstituted in 1X PBS and diluted to a working concentration of 2.5-5 mg/mL. Prior to digestion, vascularized Gelfoam® scaffolds were washed twice in 1X PBS and transferred to sterile Eppendorf tubes. Collagenase was added to the tubes and the scaffolds were incubated at 37°C for up to 45 min on a Thermo Scientific™ Tube Revolver/Rotator set to 12 rpm with oscillation. Post-digestion, cold media containing serum was added to each sample to terminate enzymatic activity, and the samples were centrifuged at 200×g for 5 min. The supernatant was aspirated and cells were re-suspended in cold sorting buffer for further processing, as described below.

5.2.7.2. Bead-Based Sorting

To test the hypothesis that THP1-derived macrophage could be positively isolated, S-pluribeads (PluriSelect, San Diego, CA) against CD11b were used, according to the

manufacturer's protocol, to target CD11b+ macrophages from CD11b- endothelial and support cells. However, due to poor macrophage expression of CD11b (< 30% via flow cytometric analysis), as well as CD14 (< 16%), alternative targets were identified using flow cytometry. M0, M1, and M2a macrophages, as well as HAMEC-dTom and MSC were evaluated for CD31 and CD146 staining via flow cytometry.

Cells were blocked in 80 μL of Blocking Buffer (2% BSA in 1 mM EDTA) and 20 μL FcR Blocking Reagent (Miltenyi Biotec) for 15 min at 4°C, and subsequently washed and re-suspended in FACS Buffer (0.5% BSA in 1 mM EDTA). Cells were incubated with CD31-Biotin (Miltenyi Biotec, #130-098-68, 1:10 dilution) or Mouse Anti-IgG1-Biotin isotype control (Miltenyi Biotech, # 130-093-018) for 20 min at 4°C, washed and re-suspended in FACS Buffer. Anti-Biotin-APC (Miltenyi Biotec, #130-098-679, 1:10 dilution) was added to the suspension and incubated for 40 min at 4°C with periodic vortexing. CD146 was detected via labeling with Alexa Fluor®488 anti-human CD146 (Biolegend, #342007, 1:20 dilution) or Alexa Fluor®488 Mouse IgG2a, κ isotype control (Biolegend, #400114) for 40 min at 4°C. Post-staining, cells were fixed in BD CytoFix for 15 min at 4°C, washed, and re-suspended in FACS Buffer. Unstained controls were included for all cells. Labeled cells were analyzed using a BD FACSCanto Flow Cytometer (BD Biosciences, Franklin Lakes, NJ) and data were processed using FlowJo Software.

Based on the flow cytometry data, it was hypothesized that sequential targeting of CD31 and CD146 would yield enriched populations of MSC, HAMEC, and macrophages. To test this hypothesis, pre-vascularized scaffolds containing macrophages were digested and labeled with biotinylated CD31 (Miltenyi Biotec) and magnetically labeled using an Anti-Biotin MultiSort Kit (Miltenyi Biotec), according to the manufacturer's instructions. Labeled cells were magnetically sorted through LS columns via a MidiMacs separator

(Miltenyi Biotec), yielding CD31- and CD31+ cell fractions, and the MultiSort MicroBeads were removed from the cells. Subsequently, magnetic labeling with CD146 MicroBeads (Miltenyi Biotec) was performed on the CD31+ cell fraction, and the labeled cells were magnetically sorted, yielding CD31+CD146- and CD31+CD146+ cell populations. All fractions were analyzed via flow cytometry.

5.2.7.3. FACS-Based Sorting

As an alternative to bead-based sorting, fluorescence-activated cell sorting (FACS) was investigated for scaffolds seeded with HAMEC-dTom, MSC, and GFP-expressing macrophages. It was hypothesized that the cells could be sorted based on their inherent fluorescence, without the need for additional processing. Single cell suspensions obtained after scaffold digestion were incubated with LIVE/DEAD Fixable Dead Cell Stain (Thermo Fisher Scientific, Waltham, MA) for 15 min on ice. The cells were washed and sorted on a BD FACSAria Fusion flow cytometer (BD Biosciences, Franklin Lakes, NJ), with the assistance of Dr. El Haddad's Lab (Drexel University). Pure populations of HAMEC-dTom, MSC, and GFP-expressing macrophages were cultured *in vitro* and used as compensation controls. Sorted cells were collected directly into lysis buffer for subsequent gene expression analysis.

To determine the minimum number of cells needed to obtain detectable levels of RNA for multiplex gene expression analysis, serial dilutions ranging from 500,000 to 976 THP-1 cells were prepared and lysed in Buffer RLT. Lysates were mixed with an equal volume of 70% ethanol and loaded directly onto an RNeasy mini-spin column (RNeasy Micro Kit, Qiagen) for purification, according to the manufacturer's instructions. RNA was eluted in a final volume of 14 μL RNase-free water and stored at -80°C. RNA was later thawed on ice and quantified using a BioAnalyzer 2100 RNA 6000 Nano kit (Agilent

Technologies, Santa Clara, CA), according to the manufacturer's protocol. For all samples, RNA Integrity Number exceeded 9.0.

5.2.7.4. Effects of Collagenase and FACS on Gene Expression

The extent to which collagenase digestion and subsequent FACS isolation of the cells alters their gene expression profiles was analyzed to confirm the efficacy of this approach in assessing crosstalk among HAMEC-dTom, MSC, and GFP-macrophages during vascularization. Gelfoam® scaffolds were pre-vascularized for 6 days *in vitro*, as described above, and seeded with M1 or M2a macrophages derived from GFP-THP1 cells on day 6. The scaffolds were incubated at 37°C and 5% CO_2 for an additional 2 days, after which the samples were digested and processed for FACS isolation of the cells. Sorted cells were collected directly in Buffer RLT (Qiagen) and re-pooled for gene expression analysis; lysates were thawed on ice, vortexed briefly, mixed with an equal volume of 70% ethanol and directly loaded onto an RNeasy mini-spin column (Qiagen) for purification.

As a control, scaffolds prepared in the same manner were immersed in TRIzol for rapid lysis of the entire cell population. TRIzol-treated scaffolds were homogenized using a Mini BeadBeater-16 (BioSpec Products, Bartlesville, OK) with two 2.3 mm stainless steel beads for 2 cycles of 10 s. Chloroform was added to the suspensions and vigorously shaken by hand for 15 s. After an additional 3 min at room temperature, the samples were centrifuged at 12,000×g and 4°C for 15 min. The aqueous layer was collected, mixed with an equal volume of 70% ethanol and the precipitated RNA was purified on an RNeasy mini-spin column (Qiagen).

RNA was quantified using a NanoDrop 1000 (Thermo Scientific) and BioAnalyzer 2100 RNA 6000 Nano kit (Agilent Technologies, Santa Clara, CA), and multiplex gene

expression analysis was performed via NanoString using an nCounter® Myeloid Innate Immunity Panel (NanoString Technologies, Seattle, WA), inclusive of 730 immunology-related endogenous genes, 40 housekeeping genes, 8 External RNA Control Consortium (ERCC) negative controls, and 6 ERCC positive controls. Hybridization reactions were prepared with 100 ng RNA for all samples, according to the manufacturer's instructions. Raw count data were extracted using nSolver™ Analysis Software 3.0 (NanoString Technologies, Seattle, WA), imported into R studio and normalized using the *voomWithQualityWeights* function within the *limma* package, which assigns a weight factor to each sample before performing a global normalization [184]. Prior to analysis, genes not expressed above the ERCC negative controls were identified via a 1-tailed 2-sample Welch's t-test with $p < 0.05$. Differential expression analysis between samples subjected to digestion and sorting vs. TRIzol-treated controls was performed via linear modeling within *limma*, and gene expression comparisons were performed with a global Benjamini-Hochberg adjusted multiple comparisons t-test. Genes with adjusted $p < 0.05$ were considered significant. In addition, PCA was performed using Matlab® software (MathWorks, Natick, MA) on all genes not differentially expressed between the sorted and untreated groups to confirm data clustering by macrophage phenotype.

5.2.8. Statistical Analysis

All data are represented as mean ± SEM. Statistical analysis was performed in GraphPad Prism 7.0 (GraphPad Software, Inc., La Jolla, CA). Quantitative image analysis was assessed using repeated measures (RM) two-way ANOVA, with Tukey's or Bonferroni's multiple comparisons test, as indicated. Macrophage gene expression data were analyzed using one-way ANOVA, with Tukey's post-hoc analysis. For all studies, $n \geq 3$ and $p < 0.05$ was considered significant.

5.3. Results and Discussion

5.3.1. Development of *In Vitro* 3D Model of Vascularization with Macrophages

5.3.1.1. Identification of 3D Scaffold and Cell Combination for Vascular Formation

In order to assess the contribution of macrophage phenotype to angiogenesis, a previously established 3D model of vascularization within PLLA/PLGA scaffolds was modified. It was anticipated that the ability to seed macrophages onto these pre-vascularized constructs would be hindered by the fibrin gel used during the initial endothelial and support cell seeding. As a result, two alternative porous constructs to PLLA/PLGA, Alginate-RGD and Gelfoam®, were tested for their ability to both support the self-assembly of vascular networks and support macrophage seeding onto the scaffolds several days after vascularization is initiated. In addition, previous work has demonstrated that co-culture of HAMEC and MSC on 3D scaffolds *in vitro* yields more organized and complex vasculature, in a reduced period of time, relative to scaffolds seeded with HUVEC and HNDF support cells [251]; however, the effects of this cell combination on Alginate-RGD or Gelfoam® constructs are unknown. In this work, vessel networks generated via fluorescently labeled HAMEC/MSC or HUVEC/HNDF cell combinations on PLLA/PLGA, Alginate-RGD, or Gelfoam® scaffolds were examined over 14 days *in vitro* using confocal microscopy.

Consistent with earlier findings, HUVEC/HNDF appeared to initially form cell clusters, which subsequently sprouted to generate vessel networks on all scaffolds (**Figure 5.1**). While these clusters were absent from PLLA/PLGA scaffolds seeded with HAMEC/MSC, cells seeded in this combination tended to form large agglomerates on both Alginate-RGD and Gelfoam® from which vessels began to sprout after 7 days *in vitro*; however, cell agglomerates were still visible after 14 days. These differences were

quantified in terms of network complexity, representing the extent of vessel elongation, based on a previously described algorithm [251]. As shown in **Figure 5.1**, vessel structures generated by HUVEC/HNDF exhibited significantly greater weighted mean complexity when seeded on PLLA/PLGA constructs, relative to those on Alginate-RGD or Gelfoam® after 3 days *in vitro*. In contrast, the HAMEC/MSC combination produced more complex structures on Gelfoam®, and to a lesser extent on Alginate-RGD, compared to vessels generated on PLLA/PLGA scaffolds after 3 days *in vitro*. For both cell combinations, differences in vessel elongation among the scaffolds were abolished as vascularization progressed. Given the ability of HAMEC/MSC to produce more elongated vessel structures relative to HUVEC/HNDF, this cell combination was selected for the development of an *in vitro* 3D model of vascularization with macrophages.

To determine if PLLA/PLGA scaffolds can be used to introduce macrophages at later stages of vessel development, these constructs were seeded with additional endothelial cells labeled with a different fluorescent protein, allowing these cells to be distinguished from those already present in the tissue, after 14 days of vascularization *in vitro*. As expected, the newly seeded cells were not detectable via confocal microscopy at any location on or within the scaffolds (data not shown). Therefore, PLLA/PLGA scaffolds were not suitable constructs for studying the role of macrophages in biomaterial vascularization, and were excluded from further model development.

5.3.1.2. Visualization of Macrophages During Vascular Network Formation

In order to visualize macrophage distribution throughout the scaffolds during angiogenesis, the ability to label the THP1-derived macrophages was first assessed using a fluorescent Vybrant® DiD cell-labeling solution, which integrates into phospholipid cell membranes. Confocal microscopy of the cells 3 days post-treatment revealed uniform

uptake of DiD by THP-1 cells, which was clearly absent from untreated cells (**Figure 5.2a**). Visualization of the cells on 3D scaffolds was also confirmed using THP-1 derived M0 macrophages labeled with DiD; these cells were visible post-seeding on Gelfoam® scaffolds and appeared distributed throughout the entire construct. Moreover, Trypan blue exclusion of THP-1 cells treated with DiD was performed to confirm cell viability, which was determined to be 92.7%, compared to 99.5% for untreated THP-1 after 3 days *in vitro* on ultra-low attachment plastic.

Although DiD labeling is a rapid (requires less than 30 min) and effective approach to visualize macrophages via confocal microscopy, it is possible for DiD to leak from non-viable cells and localize to other adjacent cells [259]. This was observed in preliminary studies investigating macrophage-vessel interactions. As a result, commercially available GFP-expressing THP-1 macrophages were investigated as an alternative approach. GFP-THP1 consistently exhibited viability comparable to unlabeled THP-1 cells *in vitro*, and were visible and uniformly distributed following seeding on Gelfoam® scaffolds (**Figure 5.2b**).

To confirm that GFP-labeling does not alter the phenotypic behavior of the cells, GFP-THP1 cells were differentiated into M1 and M2a macrophages and gene expression analysis was performed for a panel of markers indicative of macrophage phenotype [70]. Importantly, the gene expression profiles of GFP-THP1 were consistent with unlabeled THP-1 cells (**Figure 5.2c**), suggesting that transfection of the cells with GFP does not alter phenotype. As expected, GFP-THP1 stimulated with LPS and IFN-γ up-regulated M1 markers, *TNF*, *IL1B*, and *CCR7*; whereas, stimulation with IL4 and IL13 induced up-regulation of M2a markers, *CCL22* and *PDGFB*. Although not established as markers of macrophage phenotype, *NRP1* and *TIE2* were included in this panel because of reports implicating their association with macrophages interacting with blood vessels [25, 246].

While these markers were not differentially expressed between M0, M1 or M2a macrophages stimulated *in vitro*, it is possible that *NRP1* and *TIE2* expression are induced by other stimuli present *in vivo* or by hybrid M1/M2 phenotypes not included in this assay.

Overall, these data suggest that GFP-THP1 cells can be used to study the contribution of macrophage phenotype to angiogenesis.

5.3.1.3. Effects of Macrophage Seeding Density

Though it is well established that a 5:1 ratio of endothelial cells to support cells are optimal to generate self-assembled vascular structures on porous scaffolds [40, 251, 260], this work represents the first time that incorporation of macrophages into this system has been explored. Prior to seeding macrophages in combination with HAMEC and MSC, the ability of macrophages to survive in the co-culture media necessary for vascular development was tested. Trypan blue exclusion confirmed that M0 macrophages cultured in equal parts HAMEC media and MSC media displayed > 99.9% viability. Therefore, a 1:1 ratio of endothelial cell and support cell media was used for all vascularization studies described in this work.

Next, the seeding density of macrophages was investigated on both Alginate-RGD and Gelfoam® scaffolds in combination with HAMEC and MSC. Three seeding densities were examined, including a 1:1 ratio of HAMEC to macrophages (defined as high), a 2.5:1 ratio of HAMEC to macrophages (defined as low), and a 5:1 ratio of HAMEC to macrophages (defined as low). The numbers of HAMEC and MSC were held constant for all scaffolds. As shown in **Figure 5.3a**, vascular networks assembled on Gelfoam® appeared to develop uniformly across all seeding densities; in contrast, vessel networks generated on Alginate-RGD scaffolds appeared less developed and displayed inconsistent organization both within and between groups (**Figure 5.3b**). Regardless of

seeding density, DiD-labeled M0 macrophages appeared dispersed throughout the scaffolds, with visible localization to endothelial cell clusters within Alginate-RGD. Analysis of vessel structures revealed only a minor increase on day 3 in vessel complexity for medium densities on both Gelfoam® and Alginate-RGD scaffolds, relative to the same scaffold seeded with a high or low number of macrophages (**Figure 5.3c**). However, vascular structures within Gelfoam® scaffolds were significantly more complex than those within Alginate-RGD after 3 days *in vitro* when seeded with a medium or low number of macrophages.

Based on these findings, a 2.5:1 ratio of HAMEC to macrophages was selected for further investigation, coupled with commercially available Gelfoam® constructs as the scaffolding for vessel formation by HAMEC and MSC. Given the uncontrollable variability in network formation observed for Alginate-RGD scaffolds, these constructs were not considered reliable for the study of macrophages in angiogenesis. Variability in vascular development may have resulted from batch effects in preparing and modifying these constructs with RGD peptide. As a commercially available medical device, Gelfoam® is expected to meet strict quality control standards, which would minimize scaffold-induced batch effects on vascularization and facilitate experimental reproducibility.

5.3.1.4. Effects of Macrophage Seeding Time

The dynamics of macrophage seeding in combination with HAMEC and MSC on Gelfoam® scaffolds were also studied with respect to seeding time. M0 macrophages were seeded on day 0, 3, or 6 of vascularization and network formation was compared to HAMEC/MSC control constructs without macrophages. Interestingly, simultaneous seeding of all three cell populations on day 0 inhibited network development (**Figure 5.4**);

whereas, addition of macrophages on days 3 and 6, when vessels were already formed, appeared to cause vessel regression over 14 days *in vitro*.

Since the goal of this investigation was to delineate the contribution of macrophages to angiogenesis, which involves the sprouting of new blood vessels from pre-existing vessels, all future studies involved pre-seeding HAMEC and MSC on Gelfoam® on day 0 to initiate vessel formation, with subsequent addition of macrophages to the pre-vascularized scaffolds after at least 3 days of network development. Additionally, the presence of elongated vessel structures was confirmed via confocal microscopy prior to macrophage seeding for all succeeding experiments.

5.3.2. Effects of Macrophage Phenotype on Vascularization

Following the development of the 3D tri-culture model of tissue vascularization described above, this system was then applied to elucidate the effects of macrophage phenotype on angiogenesis; a representative schematic of the study design for this investigation is provided in **Figure 5.5**.

5.3.2.1. Early Effects of Macrophage-Vessel Interactions

THP1-derived M0, M1, and M2a macrophages were seeded on Gelfoam® scaffolds pre-vascularized for 3 days, and changes in network morphology were evaluated after 1-3 days of macrophage-vessel interactions, as shown in **Figure 5.6a**. For all groups, HAMEC-dTom formed small clusters from which vessels were sprouting on day 4 (1-day post-macrophage seeding). While differences in network morphology were difficult to discern from the z-stack projections, M1-seeded macrophages appeared to enhance vascularization, within 1-day post-seeding, relative to the HAMEC/MSC control and scaffolds treated with the M0 and M2a phenotypes. Analysis in 2D of the projected z-stack

images using AngioTool confirmed a significant increase in both vessel density and the density of junctions/nodes by M1 macrophages, relative to control vessels without macrophages and those treated with an unactivated M0 phenotype, after 1 day (**Figure 5.6b**). Vessels treated with M1 macrophages also exhibited significantly more endpoints than control constructs, which may correspond to increased vessel sprouting. Interestingly, these phenotypic differences were abolished by day 6 (3-days post-macrophages seeding), at which point there were no significant differences in vessel density or the number of junctions among the groups. However, M1-treated vessels were significantly shorter in length relative to control vessels and those treated with M2a macrophages, and had significantly more vessel endpoints than vasculature treated with other macrophage phenotypes.

Extending this analysis to 3 dimensions using a custom algorithm further established the contribution of the M1 phenotype vascularization, and also revealed morphological changes in vessel structure induced by M2a macrophages after 1 day of macrophage-vessel interaction (**Figure 5.6c**). For example, both M1 and M2a macrophages increased the total number of vessels within the scaffolds and the number of connected vessels throughout the network on day 4. Consistent with these changes, both phenotypes also reduced the average vessel length relative to control networks without macrophages, as well as the number of vessels joined by the same junction/node relative to M0-treated scaffolds. These findings suggest that both M1 and M2a macrophages are pro-angiogenic and can enhance tissue vascularization in terms of vessel sprouting and branching.

To verify the effects of macrophage phenotype on angiogenesis, this study was repeated with macrophage addition on day 6 rather than day 3 and M2c macrophages were included in the analysis. Additionally, changes in network morphology were

normalized to baseline morphology imaged on day 6, and compared after 1, 3 and 4 days post-macrophage seeding. Allowing HAMEC-dTom and MSC to organize into vessels for 6 days *in vitro* provided more developed networks than those of the previous study (**Figure 5.7**). However, in contrast to seeding macrophages on day 3, incorporation of macrophages on day 6 of vascularization appeared to reduce vessel growth relative to control scaffolds without macrophages. Quantification via image analysis revealed reduced (though not significantly) vessel density, junctions density, and vessel length for M1-, M2a, and M2c-treated vasculature (**Figure 5.8a**). M2a macrophages caused the greatest reduction in vessel length and, correspondingly, a significant increase in the number of vessel endpoints relative to control scaffolds over time, which is consistent with the visible vessel regression in the confocal images (**Figure 5.7**).

Similarly, analysis of the z-stacks in 3D showed a significant reduction in vessel length caused by M2a macrophages 1-3 days post-seeding (**Figure 5.8b**), in addition to significant reductions in the mean connected vessel size 3-days post-seeding (day 9), and the number of vessels connected at the same junction 4-days post-macrophage seeding (day 10).

In general, analysis in 3D of the confocal z-stacks was consistent with the findings of the 2D AngioTool analysis, though analysis in 3D would be expected to have greater accuracy in characterizing the three-dimensional network morphology. Indeed, by preserving the native structures of the vessels, changes in vascular dynamics induced by both M1 and M2a phenotypes were detected. Though these trends resembled that of the 2D analysis, many of the differences between macrophage phenotypes were undiscovered via AngioTool tracing. These findings emphasize the importance of analyzing vascular structures in their intrinsic 3D form.

These data are consistent with the changes in gene expression observed in aim 2, which suggested that M1 and M2c macrophages promote tip cell behavior, as well as previous work demonstrating the angiogenic potential of M1, M2a, and M2c macrophages in a tube formation assay [70]. More recently, an *in vitro* bead-based capillary sprouting assay was used to demonstrate that pro-inflammatory macrophages increase the number and density of endothelial sprouts, dependent on Notch signaling [261]. However, in the present study, M1 and M2 macrophages were associated with a decrease in vessel length that corresponding with an increase in the extent of branching and number of connections, suggesting that macrophages both stimulated sprouting and fusion of vessels. The beneficial effects induced by M2a could be due to the elevated levels of PDGFB that are characteristic to this phenotype; indeed, PDGFB is known to enhance angiogenesis, and plays a role in directing the differentiation of MSCs into vascular support cells [262].

The differences in vascularization when seeding macrophages on day 6 versus day 3 were interesting. The data suggest that seeding macrophages at earlier times of vessel development has a greater impact on vascular formation compared to seeding on day 6. It is possible that by day 6, the extensive vessel growth precludes the ability to detect subtle changes induced by macrophages, and perhaps a greater number of macrophages are needed to visualize their contributions.

5.3.2.2. Late Effects of Macrophage-Vessel Interactions

In addition to the studies above, which highlight the immediate changes in vessel development in response to macrophages, network morphology was assessed after prolonged times of M0 macrophage-vessel interactions. In this study, M0 macrophages were seeded on Gelfoam® scaffolds pre-vascularized for 6 days *in vitro*, and vascular dynamics were assessed after 1 (day 7), 4 (day 10), and 8 (day 14) days later.

Similar to the earlier results described above, a dramatic reduction in the extent of vascularization was observed after 4 days of vessel exposure to M0 macrophages (**Figure 5.9a**). These changes were strikingly obvious after an extended period of time, especially compared to vessels formed in the absence of macrophages, which appeared well-developed. Quantification of the vessel structures corroborated these observations, confirming a significant reduction in vessel density, the number of vessel junctions, and average vessel length after prolonged exposure to M0 macrophages (**Figure 5.9b**). Consistent with the changes, M0 macrophages also caused a significant increase in the number of vessel endpoints over time, which correlates with the vessel fragmentation and regression visible in the images. While similar changes were observed in other studies for M1 and M2a macrophages, discussed below, these effects were not thoroughly characterized in this work. Nevertheless, these findings suggest a role of macrophages in vessel regression and remodeling, which occurs during angiogenesis as vessels mature [35, 263]. Though it is not known if the changes induced in this case are beneficial or harmful for biomaterial-mediated tissue regeneration, unpublished *in vivo* work indicates an indispensable role of macrophages in vascular remodeling and integration between pre-vascularized constructs and host tissue (data collected by the Levenberg Lab). This is consistent with early work revealing the macrophages are recruited to sites of remodeling during developmental angiogenesis [247]. However, these findings seem to be controversial, or perhaps context-dependent, as other work suggests that macrophages play a protective role in limiting remodeling induced by TGFB2 *in vivo*. Therefore, additional work is needed to ascertain the interplay of EC apoptosis, vessel remodeling, and macrophage phenotype.

5.3.2.3. Co-localization of Macrophages During Vascular Formation

To gain a better understanding of how macrophage phenotype contributes to the changes in network morphology observed in this work, macrophage-vessel interactions were visualized over 1-3 days using GFP-expressing M0, M1, M2a, and M2c macrophages. Phenotypic differences in macrophage morphology, as well as co-localization and interactions with vessel structures were apparent after both 1 day (**Figure 5.10**) and, to a lesser extent, 3 days (**Figure 5.11**) *in vitro*. In general, M0, M1 and M2c macrophages appeared more rounded in structure compared to M2a macrophages, which tended to form large clusters of elongated cells surrounding the vessels. M0 macrophages were seen in both close proximity with and positioned on top of vessels, and occasionally displaying an elongated morphology, perhaps to guide vessel formation. Similarly, M1 macrophages appeared rounded when localized on top of the vessels, but also displayed occasional elongation between vessels, which may suggest a role for M1 in bridging sprouting vessels. In contrast, M2a macrophages were more frequently found wrapping around vessels and extending between endothelial vessels. M2c macrophages also appeared to be in direct contact with the vessels, as well as in close proximity, and were found to elongate with extended processes between vessel structures, with occasional wrapping around vessels, though less frequently compared to the M2a phenotype.

These phenotypic patterns were still present 3 days post-seeding (**Figure 5.11**). M0 and M1 macrophages appeared predominantly rounded in morphology, but elongation between and near vessels was clearly visible. In some cases, macrophages formed what appeared to be tube-like structures, but the presence of a lumen was not tested. M2a macrophages were still seen wrapping around vessels, and what appeared to be bridging

between adjacent structures. M2c macrophages were also still interacting directly with the vessels after 3 days.

These data are consistent with observations reported by others. Macrophages have been observed on several occasions to wrap around vessels and bridge nearby tip cells [25, 45]. The findings shown here suggest that M2a macrophages play a more predominant role in these actions relative to other macrophage phenotypes. Studies have also shown that macrophages may form tunnels to direct leading tip cells [92], which may be related to the actions of M1 and M2c macrophages. Finally, it was recently demonstrated that macrophages can form functional vascular channels in the absence of ECs [246]; however, macrophage-derived channels were not apparent for the phenotypes investigated in the present study.

5.3.3. Effects of Sequential M1-to-M2 Activation on Vascularization

Based on the data presented in this work and by others [70], suggesting that macrophage phenotypes play unique but synergistic roles in angiogenesis, it was hypothesized that temporal control over macrophage activation would lead to enhanced tissue vascularization. To test this hypothesis, M1 and M2a macrophages, along with the corresponding controls, were added sequentially to pre-vascularized Gelfoam® scaffolds after 3 and 6 days, respectively. These time points were selected based on earlier studies demonstrating phenotypic-differences induced in vessel structures by macrophages seeded on day 3 of vascularization.

Remarkably, all constructs seeded with macrophages, regardless of phenotype, appeared to have greater vessel density relative to untreated vessels over time (**Figure 5.12a-b**). Moreover, constructs seeded with macrophages at both time points, appeared to have greater vascular development compared to those with macrophage

seeded on only day 3 or 6, suggesting that macrophages promoted vessel growth. The most notable difference in vascularization was observed by sequentially adding M1 to M2a macrophages. Image analysis corroborated these qualitative observations (**Figure 5.12c**). Sequential M1 and M2a activation significantly increased vessel density and the extent of vessel branching, in terms of number of junctions, relative to vessels exposed to M2a at either time point. M1-to-M2a addition also enhanced vessel length on average, relative to scaffolds vascularized without macrophages or those exposed to M2a on only day 6. Likewise, vessels exposed to M1 macrophages, without M2a addition, had significantly more endpoints than those exposed to M2a macrophages, without M1 addition. For all scaffolds seeded with M2a macrophages at any time, the number of endpoints was significantly lower than those of the control vessels. These data are consistent with the previous findings that M1 macrophages promote sprouting and M2a macrophages increase vessel length, and suggest that temporal control over macrophage behavior can be used to manipulate biomaterial vascularization.

This study was later repeated with additional controls, including simultaneous addition of M1 and M2a macrophages at both time points, to test the importance of temporal regulation on the synergistic effects of these phenotypes. Surprisingly, the effects of sequential M1 and M2a activation were not consistent with the previous study. In this case, vessels were well-developed in the absence of macrophages, and sequential incorporation of either M0, M1, or M2a macrophages appeared to reduce vascularization regardless of phenotype (**Figure 5.13a**), though M1-to-M1 appeared to retain more vascular structures relative to all other macrophage-treated scaffolds on day 7. By day 10, vessels exposed sequentially to M1 and M2a phenotypes displayed significant vessel regression relative to all other groups investigated (**Figure 5.13b**). Image analysis in both 2D (**Figure 5.14a**) and 3D (**Figure 5.14b**) confirmed these qualitative observations. Only

modest differences in vessel development were detected by day 7; whereas, by day 10, all macrophage-seeded scaffolds had reduced vessel densities, numbers of junctions, and average vessel lengths compared to untreated vessels via AngioTool analysis. M1-treated scaffolds induced these changes to a greater extent, though not significantly, than those with M2a addition. These differences were more apparent via 3D image analysis, which indicated a significant reduction in vessel length for vessels exposed to only M1 macrophages first.

In an effort to identify the discrepancy in the results between these two studies, gene expression analysis was performed on all macrophage lysates collected immediately prior to seeding on both days 3 and 6, using a panel of markers indicative of macrophage phenotype to confirm the successful differentiation of M1 and M2a. As **Figure 5.15** shows, gene expression profiles for M1 and M2a macrophages were consistent between study 1 (S1) and study 2 (S2) for both time points, and in line with respect to phenotype. M1 macrophages up-regulated M1 markers, *TNF*, *CCR7,* and *IL1B*, while M2a macrophages up-regulated M2a markers, *CCL22*, and *PDGF*, in addition to *TIE2*. These data suggest that the discrepancies between the two sequential studies were not attributed to altered macrophage behavior at the time of seeding.

There are several other possible causes for the discrepancies observed between the two studies, many of which were tested. For example, the control scaffolds appeared poorly developed in the first study, which may indicate abnormal behavior of the HAMEC and/or MSC. The passage number of the cells, as well as the Lots from which they were derived, may impact vessel development. To rule out these factors, sequential addition of M1 and M2a macrophages was again tested, using Gelfoam® scaffolds pre-vascularized with HAMEC-dTom and MSC of the same passage as the first study. The first study used MSC at passage 7 (P.7), which was consistently observed to cause cell-aggregation and

inhibit vessel growth. Nevertheless, the original findings were not reproduced. Unfortunately, the HAMEC and MSC, and their corresponding media, used in the original study were kindly provided by the Levenberg Lab (Technion, Israel), for which the lot numbers were not available. Therefore, the cell source (donor) could not be eliminated as a potential source of variability, which could also be related to altered kinetics in vessel development. As an initial step to explore the effects of vascular kinetics, a final study was completed with sequential M1 and M2a macrophages incorporated on days 6 and 9 of vascularization. The results were consistent with those shown in **Figure 5.14**, and did not reproduce the original findings that demonstrated enhanced vascularization with temporal control over macrophage activation. It is also plausible that subtle environmental changes influenced the results, especially considering that the first study was completed in Israel, while all follow-up work was performed at the U.S. at Drexel.

Clearly, additional work is needed to validate the effects of sequential M1 and M2a activation on vascularization. Nevertheless, these preliminary studies demonstrate that temporal control over macrophage phenotype has potential to promote vessel development within 3D scaffolds *in vitro*. These findings are supported by recent *in vivo*, in which sequential delivery of VEGF and PDGFB from a fibrin gel were proven to enhance revascularization of cardiac tissue post-myocardial infarction [42].

5.3.4. Development of Cell Isolation Techniques

To better understand the contributions of macrophage phenotype that lead to changes in vascular formation, the impacts of cell communication need to be explored. While it is not uncommon to use immunohistochemistry (IHC) to assess development and maturation of fixed vessel networks [251, 260], there is a lack of reliable markers that can be used to discern macrophage behavior *in vitro*, thereby prohibiting the use of this

approach. To overcome this limitation, several methods were explored to isolate enriched HAMEC-dTom, MSC and macrophage populations from the vascularized tissue for further characterization. Prior to cell isolation, all Gelfoam® scaffolds were digested in a collagenase solution (**Figure 5.16a**), as reported in literature [254].

5.3.4.1. Magnetic Bead-based Isolation of HAMEC-dTom, MSC, and Macrophages

It was expected that enriched populations of HAMEC, MSC, and macrophages could be obtained by sequentially targeting surface markers specific to the cells. While CD31 is considered to be a robust marker of endothelial cells, preliminary work comparing the gene expression profiles of HAMEC-dTom and macrophages revealed surprisingly high expression of CD31 by macrophages (data not shown here). Though not widely appreciated in literature, these findings were consistent with several other reported studies [246, 264, 265]. Additionally, CD146 is considered to be indicative of endothelial cell lineage [266], and is not expected to be highly expressed by macrophages. Therefore, it was anticipated that CD31 could be used to positively target HAMEC-dTom and macrophages, indirectly isolating MSC from the tri-culture. Then, CD146 could be used to positively target HAMEC-dTom, indirectly isolating macrophages from the co-culture. Before proceeding, surface expression of CD31 and CD146 on HAMEC-dTom, MSC, and M1, M1 and M2a macrophages was compared via flow cytometric analysis.

As shown in **Figure 5.16b**, >99% of endothelial cells stained positively for CD31, while > 80% of M0, M1 and M2a macrophages were positive for CD31. In contrast, approximately 7% of MSC displayed positive CD31 staining. Expectedly, HAMEC-dTom were also positive (roughly 97%) for CD146, but macrophages and MSC exhibited substantially lower levels of CD146 staining, suggesting that CD31 and CD146 can be used to obtain highly enriched cell populations. Hence, magnetic beads targeting CD31,

followed by those targeting CD146 were tested on the tri-culture obtained after digestion of vascularized Gelfoam®, as illustrated in **Figure 5.16c-d**. As anticipated, cells that were not bound by CD31-targeting beads (CD31- fraction) displayed low CD31 intensity, which would be expected of MSC (**Figure 5.16c**). In contrast, the majority of the cells that were collected in the CD31+ fraction displayed positive CD31 staining. Upon removal of the magnetic beads from the CD31+ fraction and subsequent labeling with magnetic beads against CD146, flow cytometric analysis demonstrated distinct CD31+CD146- and CD31+CD146+ cell populations, conceivably representing enriched macrophage and endothelial cell populations, respectively (**Figure 5.16d**). Importantly, this approach provides only enriched, but not pure, cell populations; as a result, gene expression analysis would be needed to confirm that characteristic gene profiles of these populations can be achieved before further analysis is performed. It is possible that cell enrichment could be improved by targeting other surface markers, such as CD18, but this was not tested for the system described here.

This sequential magnetic bead-based cell isolation approach is also associated with other drawbacks. For instance, it takes more than 5 hours to isolate the cells per batch of samples processed together, which in this case was limited to 4 samples because of the magnetic separator utilized. Furthermore, the samples are subjected to a significant amount of processing during this time, including multiple washes and centrifugations, as well as being plunged through multiple separator tubes, which may adversely alter the gene expression profiles of the cells.

5.3.4.2. FACS-Based Isolation of HAMEC-dTom, MSC, and Macrophages

Due to the significant amount of time and processing required to isolate enriched cell populations from the tri-culture used in this work, FACS-based isolation was

investigated as an alternative approach. Since the fluorophores associated with HAMEC-dTom and GFP-macrophages can be excited and detected at different wavelengths, it was expected that FACS could be used to isolate HAMEC and macrophages via their associated fluorophores, with MSC distinguished as unlabeled cells. Therefore, single cell suspensions containing HAMEC-dTom, GFP-macrophages, and MSC were obtained by collagenase digestion of vascularized Gelfoam®, and the cells were subjected to FACS. As shown in **Figure 5.17**, three distinct cell populations were observed based on PE (dTomato) and AlexaFluor488 (GFP) intensities, suggesting that FACS is suitable for isolation of the cells used in this work.

Still, FACS is associated with several limitations worth noting. For instance, of the approximate 920,000 cells isolated following scaffold digestion, only about 51% of the cells were retrieved via sorting after selecting for live, singlet cell populations. Of this relatively small cell population, only 1.2% were identified as macrophages based on GFP expression, while 31.7% and 57.6% of the population were identified as HAMEC and MSC, respectively. Consequently, multiple scaffolds may need to be pooled in order to obtain enough RNA for subsequent gene expression analysis. Indeed, a standard curve of detectable RNA concentration as a function of cell number revealed that > 10,000 macrophages are needed to achieve adequate RNA concentrations using the methods described in this work (**Figure 5.18**). Aside from these challenges, it takes approximately 30-45 min per sample to complete the sorting process, which limits the number of samples that can be processed within a single day, especially considering the time required to prepare the cytometer.

On the other hand, FACS requires significantly less processing relative to the bead-based approach described above, and would thus be expected to have less impact on gene expression of the cells. Moreover, the purity of cells isolated using this strategy

is likely greater than that obtained via magnetic beads, which rely on efficient antibody targeting. Despite these advantages, this approach requires access to a FACS sorter, which is not readily available at all institutions.

5.3.4.3. Effects of Cell Isolation on Gene Expression

Based on the ease and efficiency of cell sorting using FACS, this method was further validated to determine the extent that collagenase digestion of the scaffolds and FACS isolation of the cells affects gene expression, which was compared to vascularized Gelfoam® tri-cultures immersed directly in lysis buffer (**Figure 5.19a**). From a myeloid panel of 730 genes, 588 genes were expressed above the negative controls and were included in the analysis. As **Figure 5.19b** illustrates, gene expression between cells subjected to digestion and sorting was strongly and positively correlated with that of TRIzol-treated controls for both M1- and M2a- seeded constructs, though M2a macrophages appeared marginally more affected ($r = 0.89$) by the treatment relative to M1 macrophages ($r = 0.93$). Still, several genes were observed in distant proximity from these linear correlations, suggesting an impact of the isolation approach. Analysis of differentially expressed genes via a global Benjamini-Hochberg adjusted multiple comparisons *t*-test revealed that 297 genes were altered ($p < 0.05$) in M1-seeded scaffolds, and 357 genes were affected in M2a-seeded scaffolds. Consequently, only 194 genes (33% of the 588 genes expressed) were determined to be unaffected by collagenase digestion together with FACS treatment. Removing the genes differentially expressed between the treated and control groups resulted in high positive correlations, with all genes localized to the linear correlations (**Figure 5.19c**). For additional validation, gene expression for all remaining genes was visualized using PCA, which showed that the data clustered along PC 1 by macrophage phenotype, representing 27.6% of the

variance within the data. However, differences in treatment were still notable even after removal of the differentially expressed genes, as the data clustered by treatment along PC 2, representing 14.6% of the variance within the data (**Figure 5.19d**). Collectively, these findings confirm that collagenase digestion, together with FACS sorting, can alter gene expression; therefore, it is prudent to perform this analysis for all genes of interest in future studies.

It should be acknowledged that there were several limitations in this investigation. First and foremost, the effects of macrophages on vascularization were only studied within the *in vitro* 3D system developed in this aim, which utilized a gelatin-based material. Though Gelfoam® has been shown to support the viability, attachment and proliferation of ECs *in vitro* [254], as well as angiogenesis *in vivo* [253], the effects of Gelfoam on the angiogenic behavior of endothelial cells were not investigated in this work, and it is well established that tissue microenvironment in which the cells are seeded can profoundly influence vascularization [267]. For example, it has been demonstrated that altering substrate stiffness not only affects EC sprouting behavior *in vitro* [268], but also impacts the ability of ECs to respond to angiogenic stimuli, such as VEGF [269]. Consistent with these findings, it has been shown that the ability of ECs to sprout in response to VEGF gradients is related to the density of the surrounding tissue matrix [270]. Based on these findings, it is possible that the Gelfoam system used in this study influenced the response of ECs to difference macrophage phenotypes. Additional work is needed to confirm the translation of these observations, especially in the context of specific tissue applications, such as bone repair.

In addition to these limitations, changes in macrophage phenotype were not measured over time. Although the phenotypic profiles were confirmed prior to seeding on

pre-vascularized Gelfoam® constructs, macrophages would not be expected to retain their phenotype in the presence of polarizing stimuli present in the surrounding microenvironment. This includes signals not only from the cells within the constructs, but also the construct itself. As a result, changes in network morphology may not necessarily result from the macrophage phenotype stimulated on ultra-low attachment plastic. This may, in part, account for the fact that effects of macrophage phenotype were observed at the earliest time investigated post-seeding, but diminished thereafter. Additionally, the co-culture media used to support vascular formation contained growth factors specific to the cells, as well as serum. As in the previous aim, it is possible that the presence of these molecules may interfere and/or mask the effects induced by macrophages on vessel development. Furthermore, the effects of macrophages on supporting MSCs were not explicitly studied, though crosstalk between these cells has been well established [271-273]. It is possible that macrophages play a major role in recruiting and directing the behavior of these vascular support cells, which would be expected to profoundly affect vascular formation.

5.4. Conclusions

In this study, a 3D tri-culture model of vascularization *in vitro* was developed by seeding microvascular ECs together with MSC support cells on Gelfoam® constructs, which supported the addition of a third cell type at later stages of vascular formation. This system was applied to the study of macrophages in angiogenesis in order to better delineate the contributions of different phenotypes to this process. Most notably, addition of M1, and to a lesser extent M2a, macrophages to pre-vascularized constructs enhanced vessel sprouting and the extent of connected vessels relative to vascular formation in the absence of macrophages. These effects were most prominent within 1 day of seeding,

and abolished after 3 days; moreover, long-term culture of macrophages with vascularized constructs induced vessel regression, independent of phenotype, supporting a role for macrophages in vessel remodeling. In addition to these findings, this work has demonstrated the potential for temporal control over M1 and M2a activation to enhance tissue vascularization. The findings presented here are consistent with previous work, suggesting that both M1 and M2 macrophages contribute to angiogenesis, but in unique ways. Additionally, this work provided the foundation needed to characterize cell-specific changes in gene expression and protein secretion with respect to vascular dynamics in 3D.

Given that biomaterial implantation inherently causes an inflammatory response, understanding the complex interplay between macrophages – the regulators of this process, and angiogenesis can provide the insight needed to overcome one of the biggest challenges currently facing regenerative medicine.

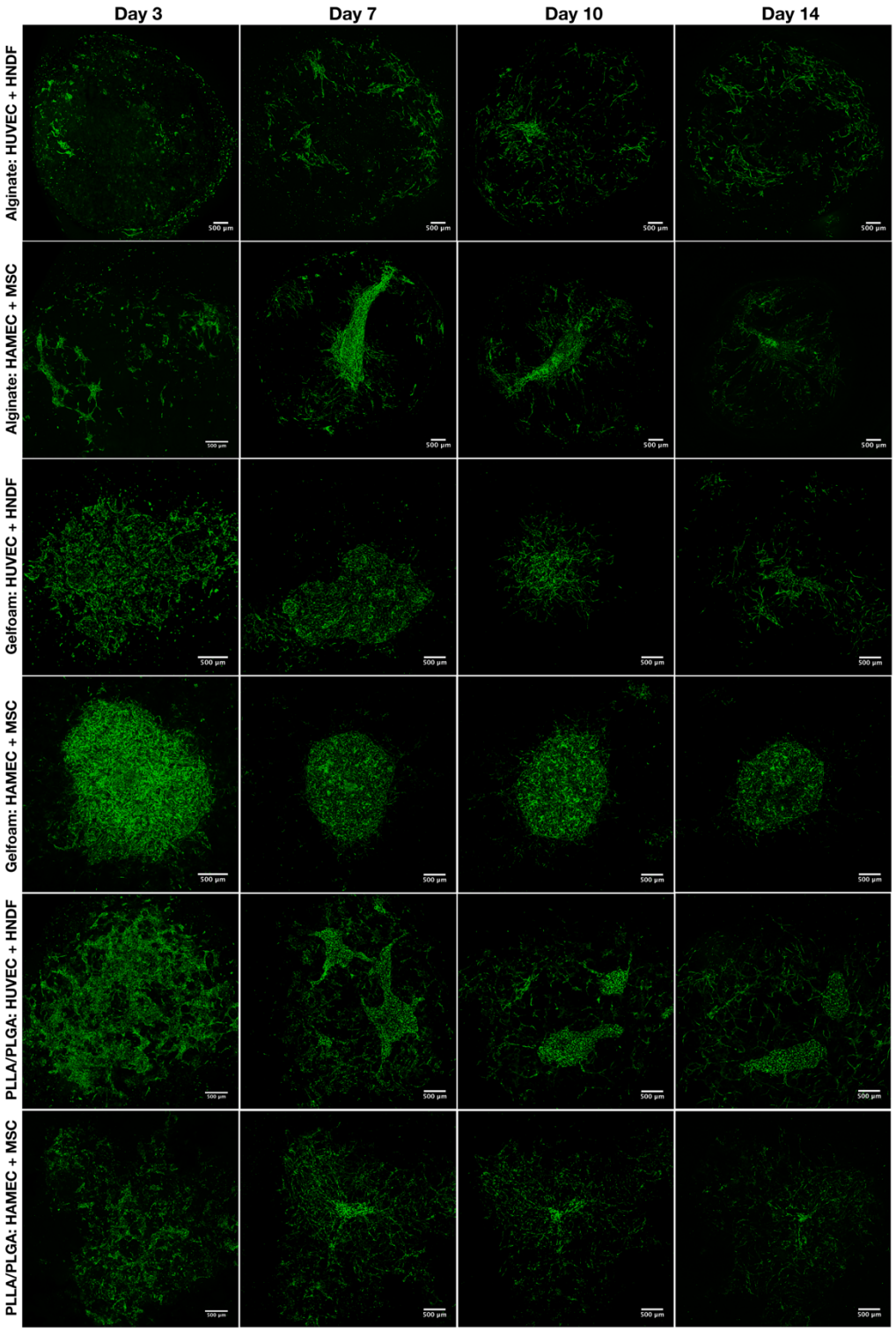

Figure 5.1a. Comparison of vascular formation by HUVEC/HNDF or HAMEC/MSC on RGD-modified alginate, Gelfoam®, and PLLA/PLGA scaffolds over 14 days *in vitro*. Representative maximum intensity projections from n = 3; scale bar = 500 μm.

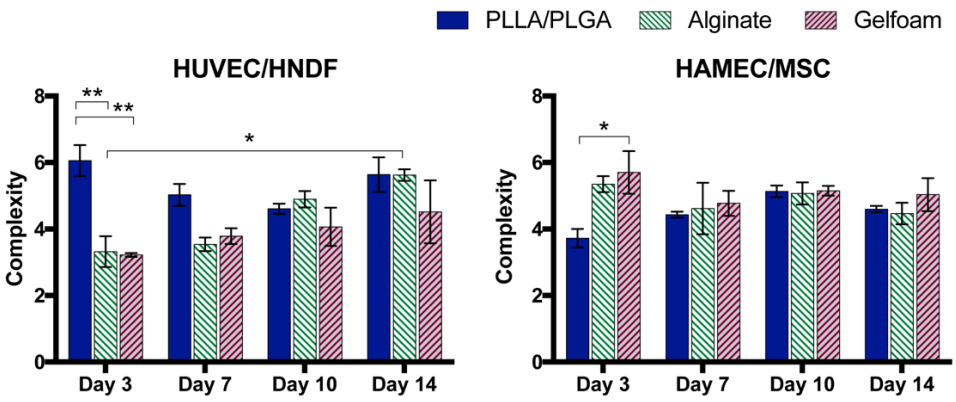

Figure 5.1b. Quantitative comparison of vascular formation by HUVEC/HNDF or HAMEC/MSC on RGD-modified alginate, Gelfoam®, and PLLA/PLGA scaffolds over 14 days *in vitro*. Data represent weighted mean complexity ± SEM (n = 3). Statistical analysis performed using RM two-way ANOVA with Tukey's post-hoc analysis. *$p < 0.05$.

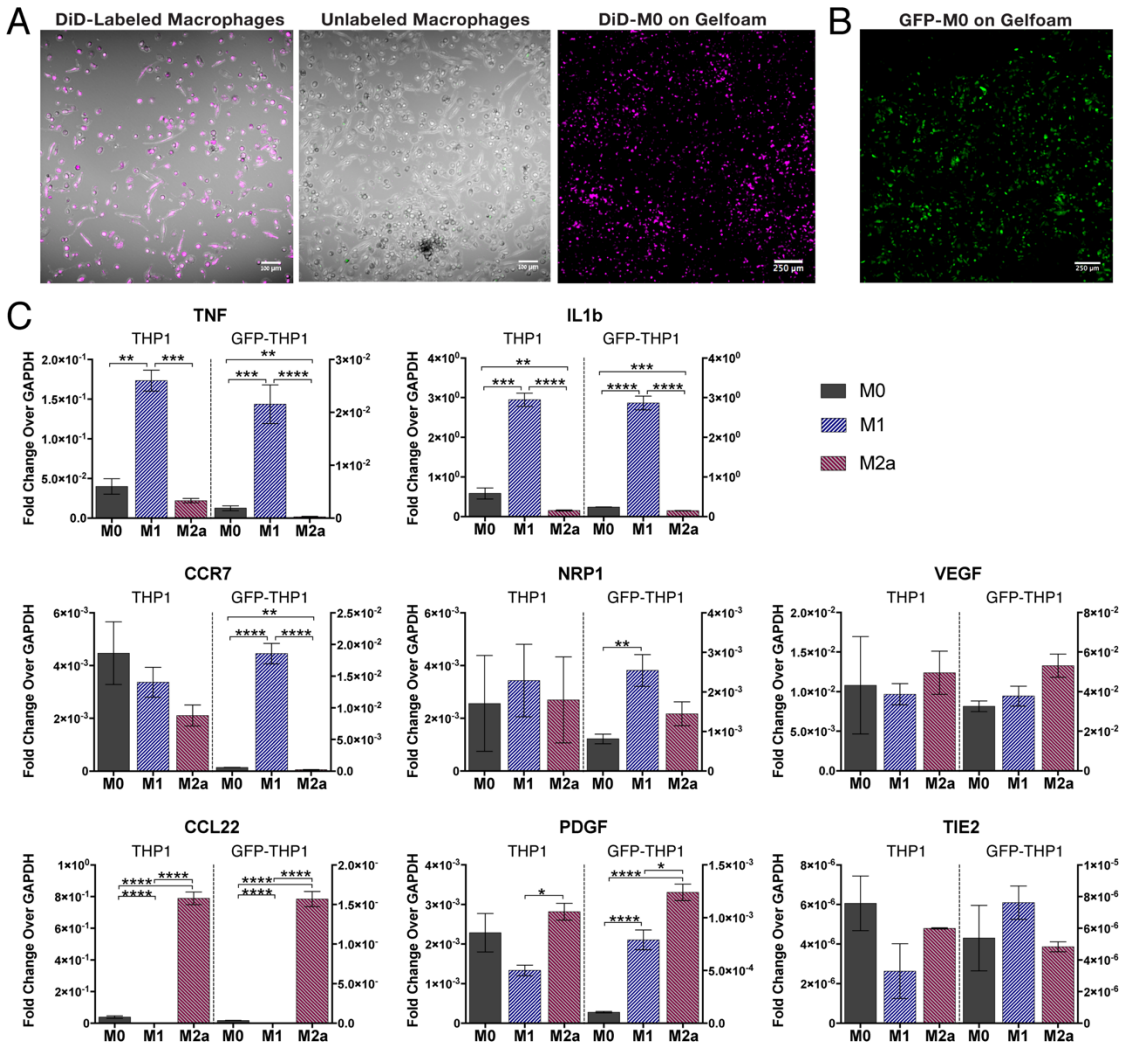

Figure 5.2. (A) Comparison of DiD-labeled and unlabeled THP1-derived macrophages on tissue culture plastic, and maximum intensity projection of DiD-labeled macrophages seeded on Gelfoam®. (B) Maximum intensity projection of GFP-THP1 macrophages seeded on Gelfoam®. (C) Effects of GFP on THP-1 gene expression for a panel of markers indicative of M1 and M2a activation. Statistical analysis performed using one-way ANOVA with Tukey's multiple comparisons test. *$p < 0.05$, **$p < 0.01$, ***$p < 0.001$, ****$p < 0.0001$; $n = 3$.

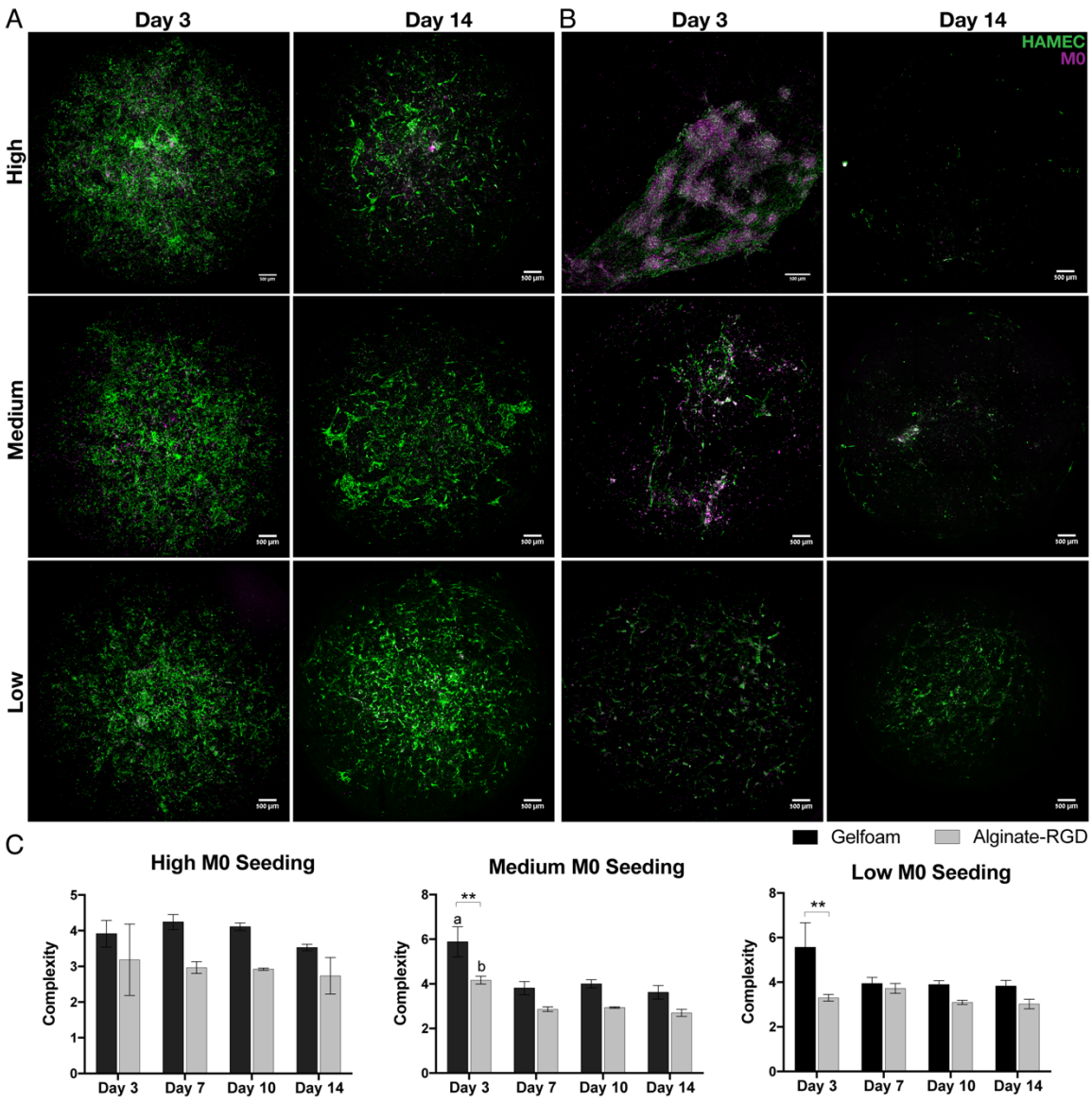

Figure 5.3. Effects of macrophage seeding density on HAMEC/MSC vascular formation on (A) Gelfoam® and (B) RGD-modified alginate scaffolds over 14 days in vitro. M0 macrophages were seeded at a high (5:1:5), medium (5:1:2.5), or low (5:1:1) density of HAMEC: MSC: M0. Representative maximum intensity projections from n = 3. HAMEC-dTom shown in green, DiD-M0 shown in magenta; scale bar = 500 μm. (C) Quantification of vascular formation in terms of weighted mean complexity. Data represent weighted mean complexity ± SEM (n = 3). Statistical analysis performed using RM two-way ANOVA with Tukey's post-hoc analysis. **$p < 0.01$. "a" and "b" denote differences ($p < 0.05$) relative to all other time points.

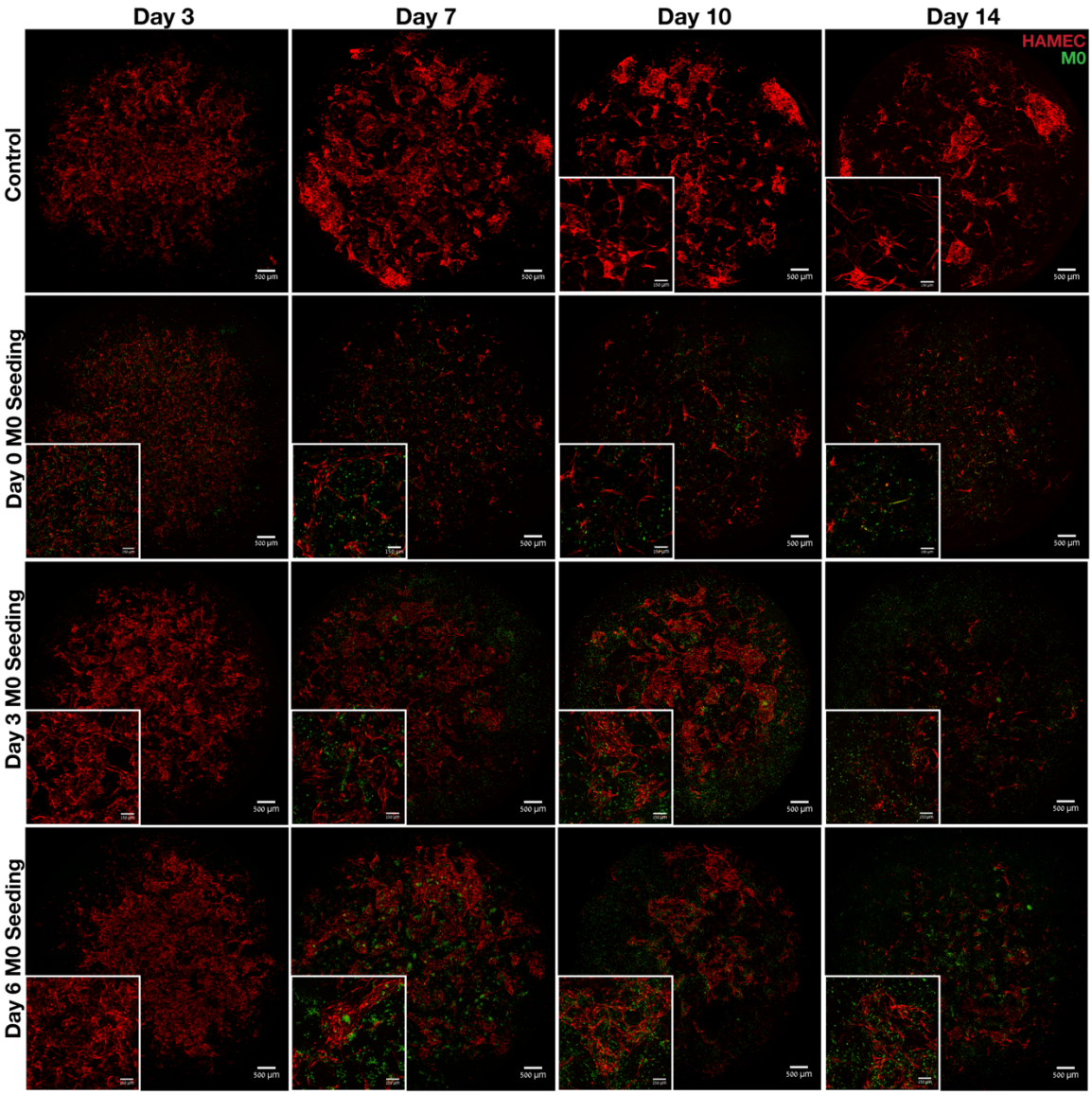

Figure 5.4. Effects of macrophage seeding time on vascular formation by HAMEC/MSC on Gelfoam® scaffolds over 14 days *in vitro*. Representative maximum intensity projections of tile scans from n = 3. HAMEC-dTom shown in red, DiD-M0 shown in green; scale bar = 500 μm for 5x images and 150 μm for 10x images.

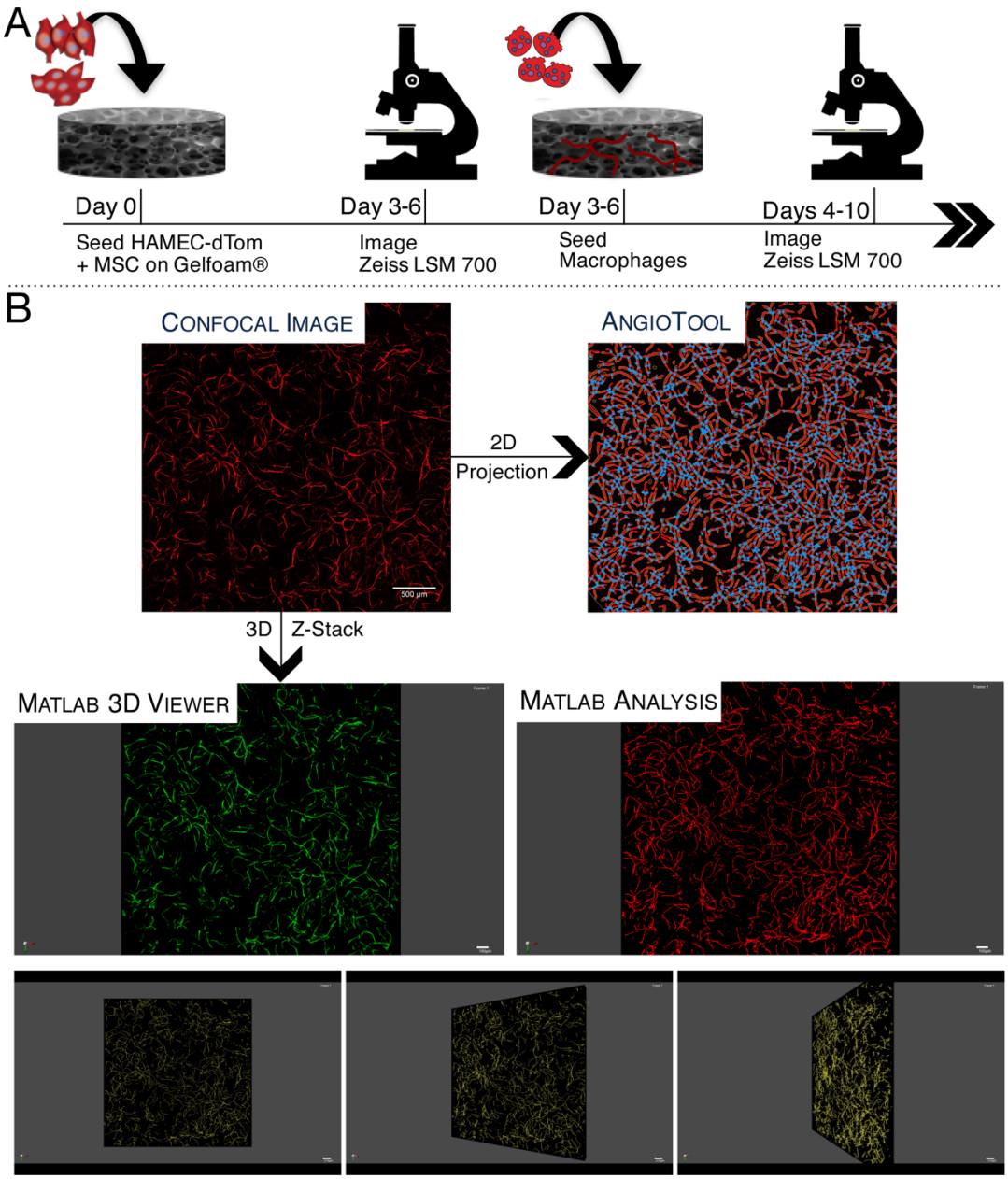

Figure 5.5. (A) Schematic of study design used to investigate macrophages contributions to tissue vascularization. Gelfoam® scaffolds were pre-vascularized using a 5:1 of HAMEC to MSC on day 0. Macrophages were seeded on day 3 or 6 of vessel development, and changes in network morphology were monitored via confocal microscopy over time. (B) Schematic of quantitative image analysis. Maximum intensity projections were analyzed in 2D via AngioTool; z-stacks were analyzed in 3D via a custom code in Matlab. Reconstructed vessels shown in green (3D viewer); skeletonized vessels shown in red (analysis).

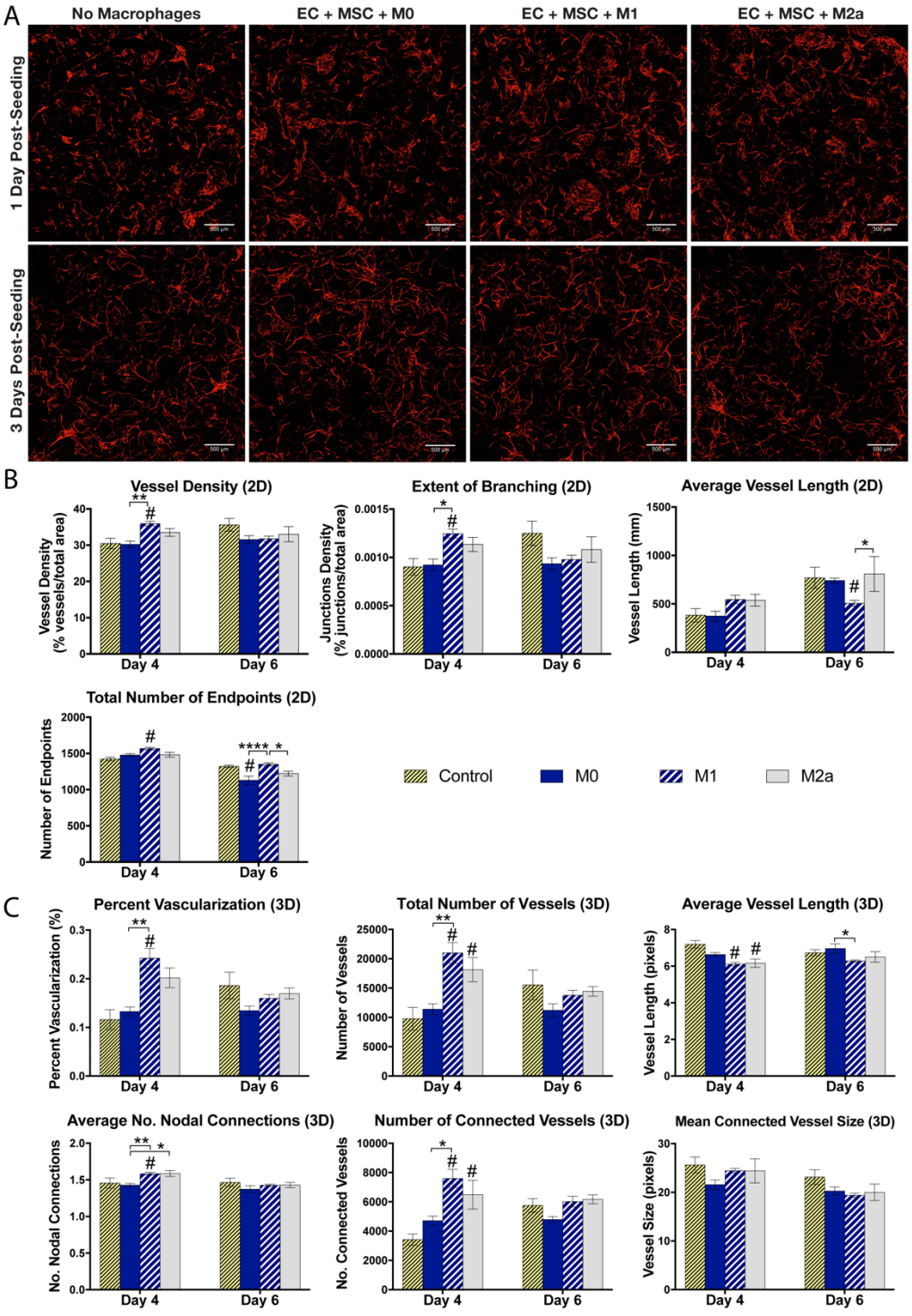

Figure 5.6. Early effects of M0, M1, and M2a on Gelfoam® vascularization in vitro. Macrophages seeded on day 3 of vessel growth. (A) Representative images from n = 3; scale bar = 500 μm. (B) Quantification of vascular development in 2D and (C) 3D. Statistical analysis performed using RM two-way ANOVA with Tukey's post-hoc analysis; $p < 0.05$.

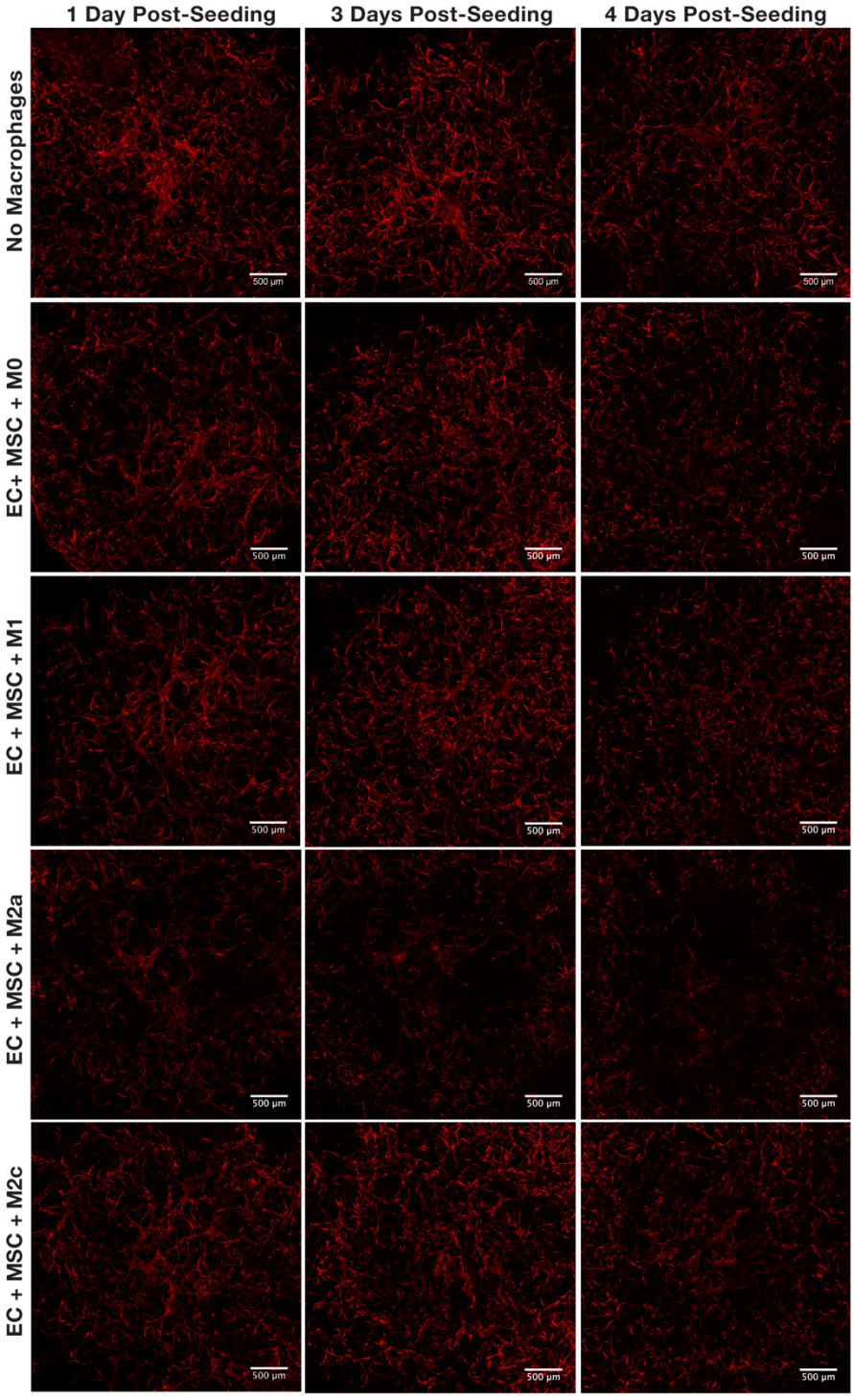

Figure 5.7. Early effects of M0, M1, M2a, and M2c on Gelfoam® vascularization *in vitro*. Macrophages seeded on day 6 of vessel growth. Representative maximum intensity projections from n = 3; scale bar = 500 μm.

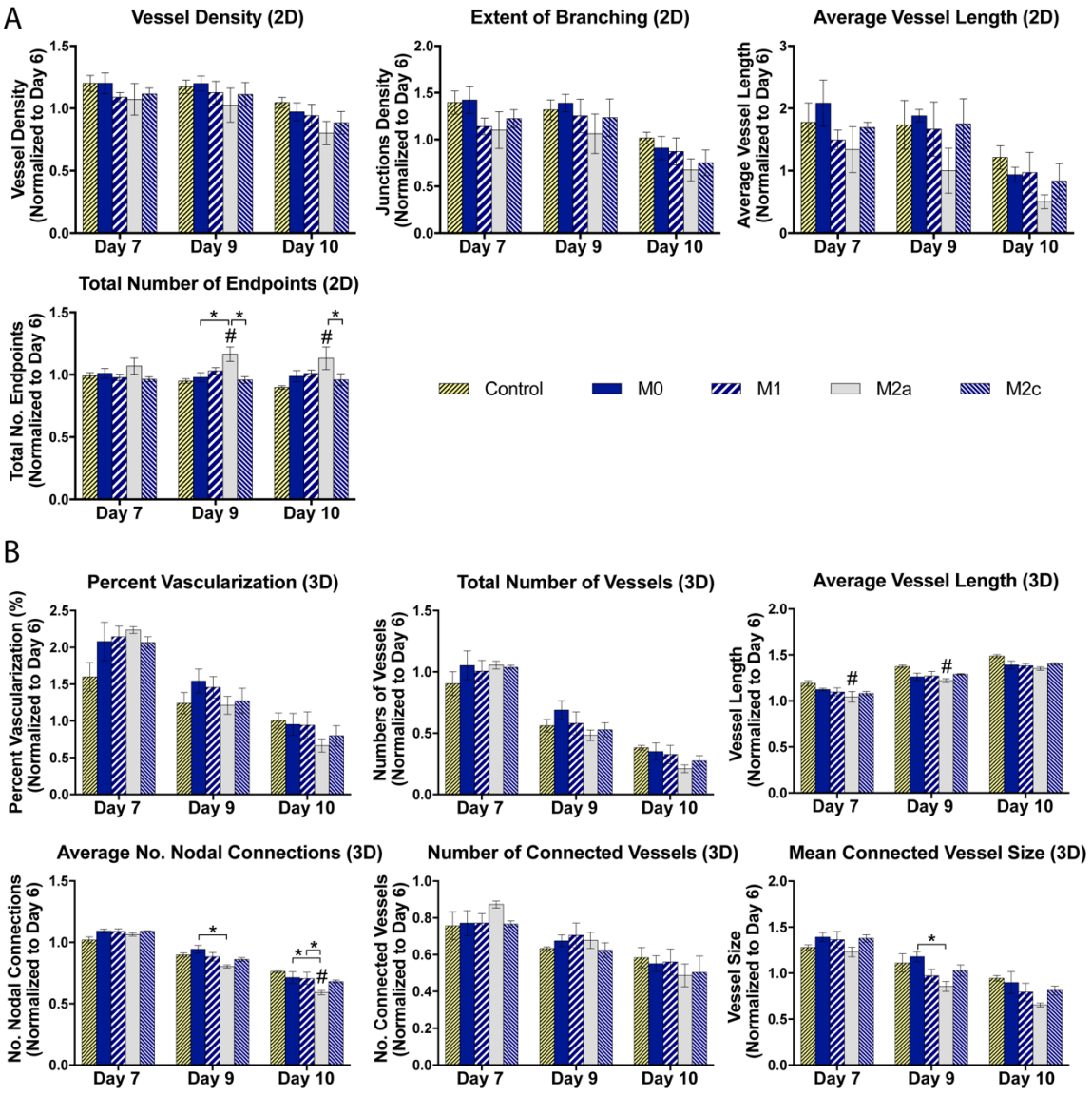

Figure 5.8. Quantification of M0-, M1-, M2a-, and M2c-induced changes in vascular development in (A) 2D and (B) 3D. Macrophages seeded on day 6 of vessel development. Statistical analysis performed using RM two-way ANOVA with Tukey's post-hoc analysis; $n \geq 3$ and $p < 0.05$.

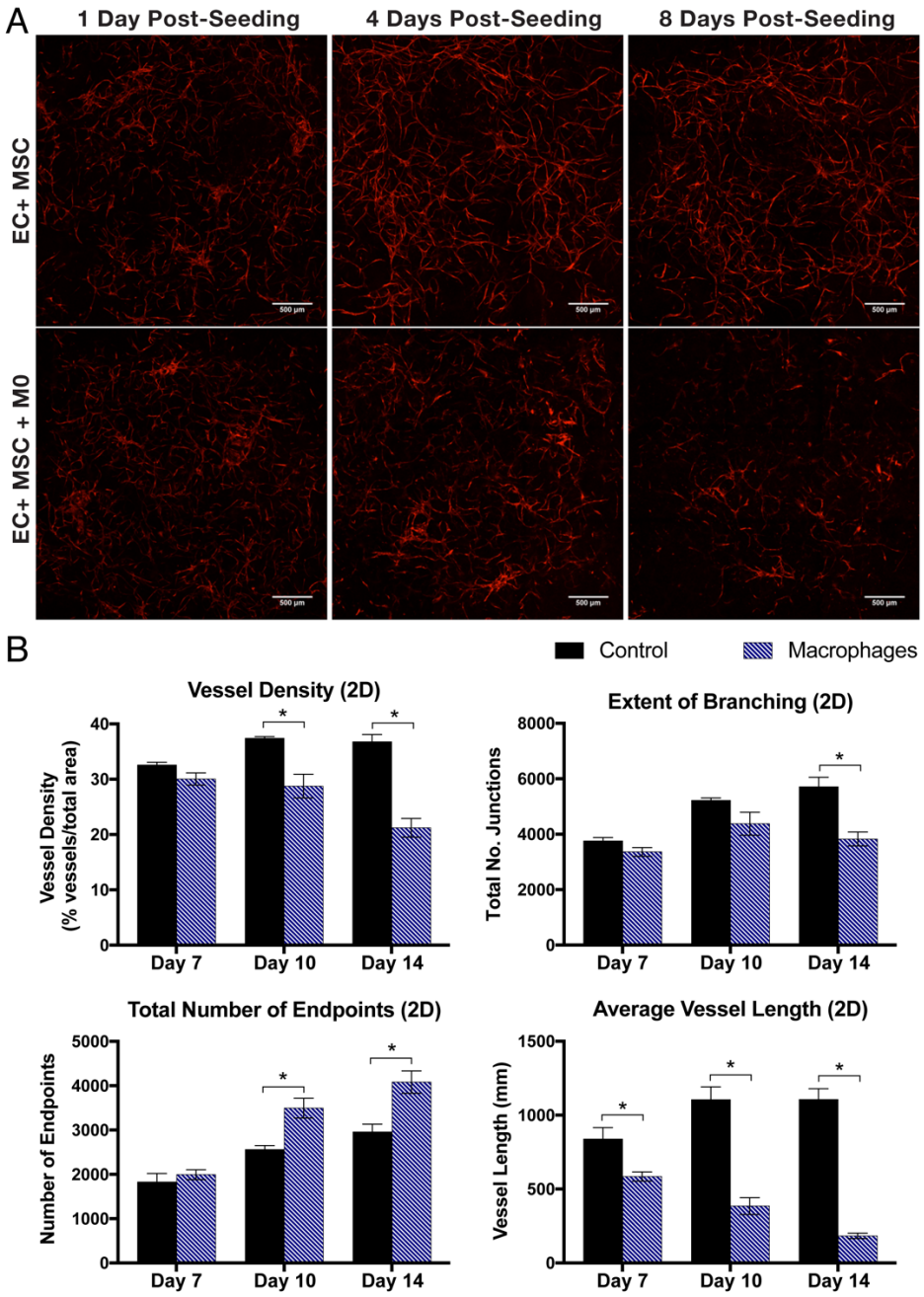

Figure 5.9. Late effects of M0 macrophages on Gelfoam® vascularization *in vitro*. Macrophages seeded on day 6 of vessel growth. (A) Representative images from n = 3; scale bar = 500 μm. (B) Quantification of vascular development in 2D. Statistical analysis performed using RM two-way ANOVA with Bonferroni's multiple comparisons test; $p < 0.05$.

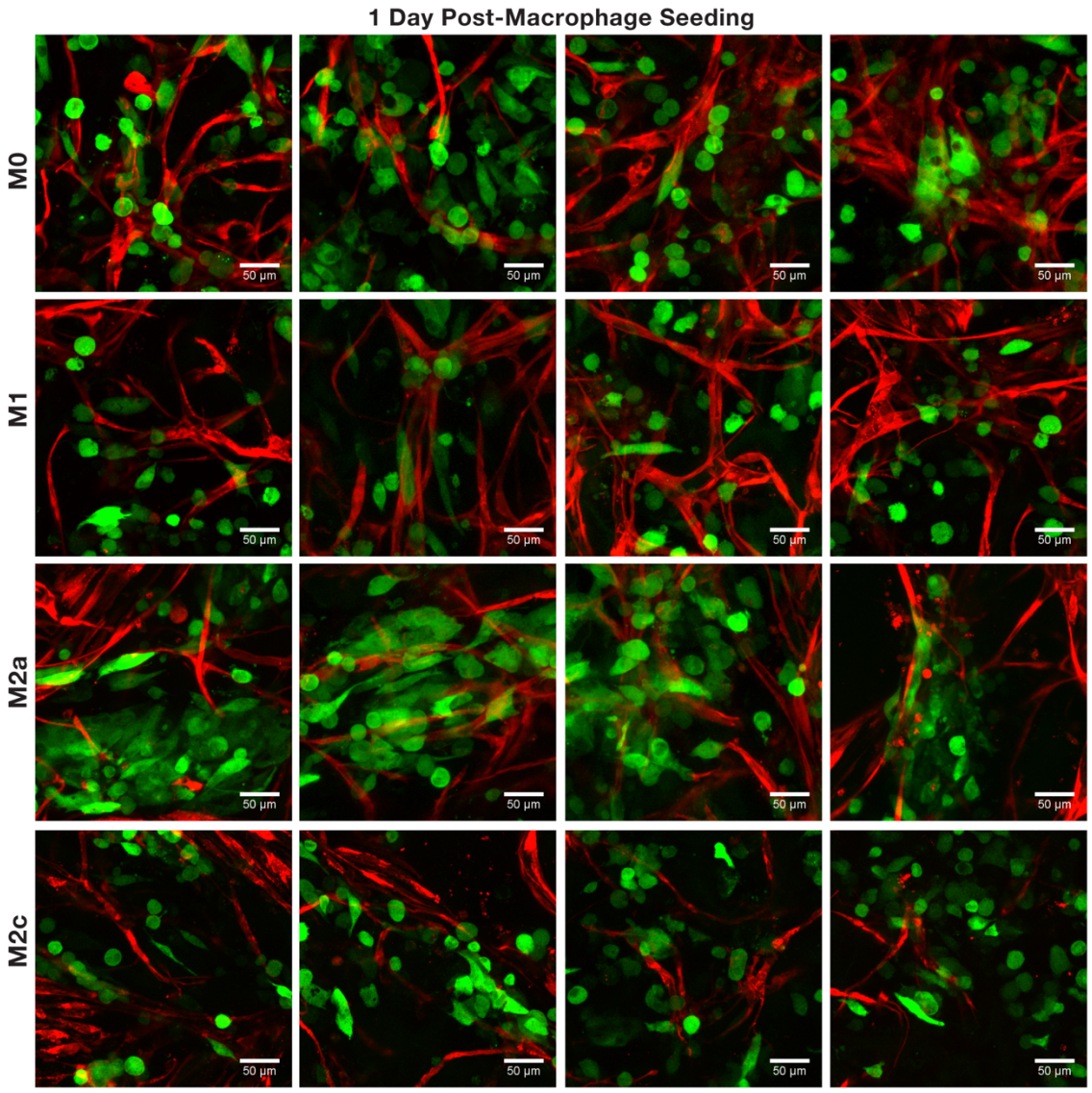

Figure 5.10. Macrophage-vessel interactions 1-day post-seeding. Representation maximum intensity projections of macrophage-vessel interactions from n ≥ 3 scaffolds 1-day post-seeding with M0, M1, M2a or M2c (n = 1 scaffold) macrophages. Macrophages seeded on day 6 of vascular formation; images acquired on day 7. Scale bar = 500 μm. HAMEC-dTom shown in red; GFP-macrophages shown in green.

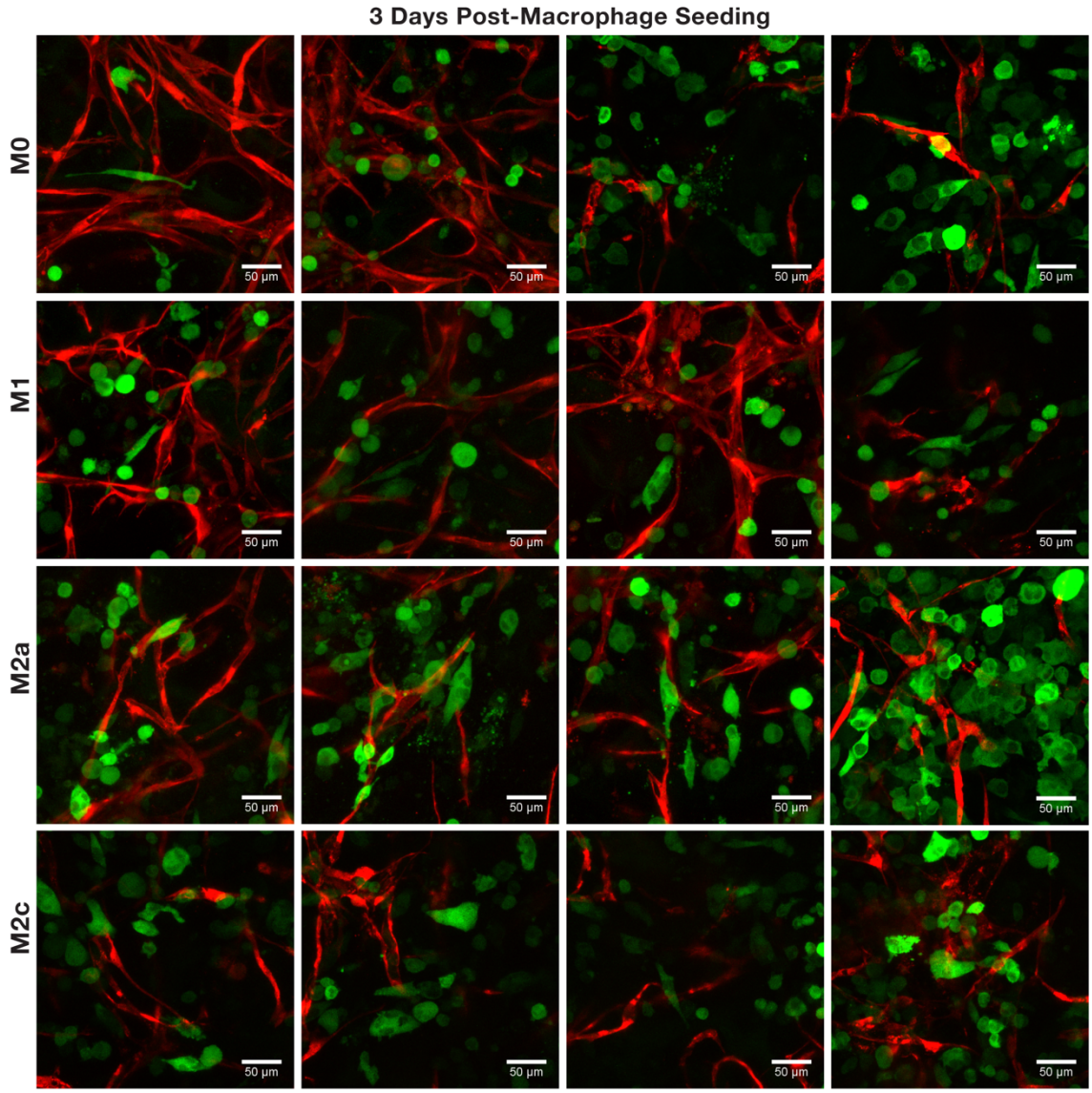

Figure 5.11. Macrophage-vessel interactions 3-days post-seeding. Representation maximum intensity projections of macrophage-vessel interactions from n ≥ 3 scaffolds 3-days post-seeding with M0, M1, M2a or M2c (n = 1 scaffold) macrophages. Macrophages seeded on day 6 of vascular formation; images acquired on day 9. Scale bar = 500 μm. HAMEC-dTom shown in red; GFP-macrophages shown in green.

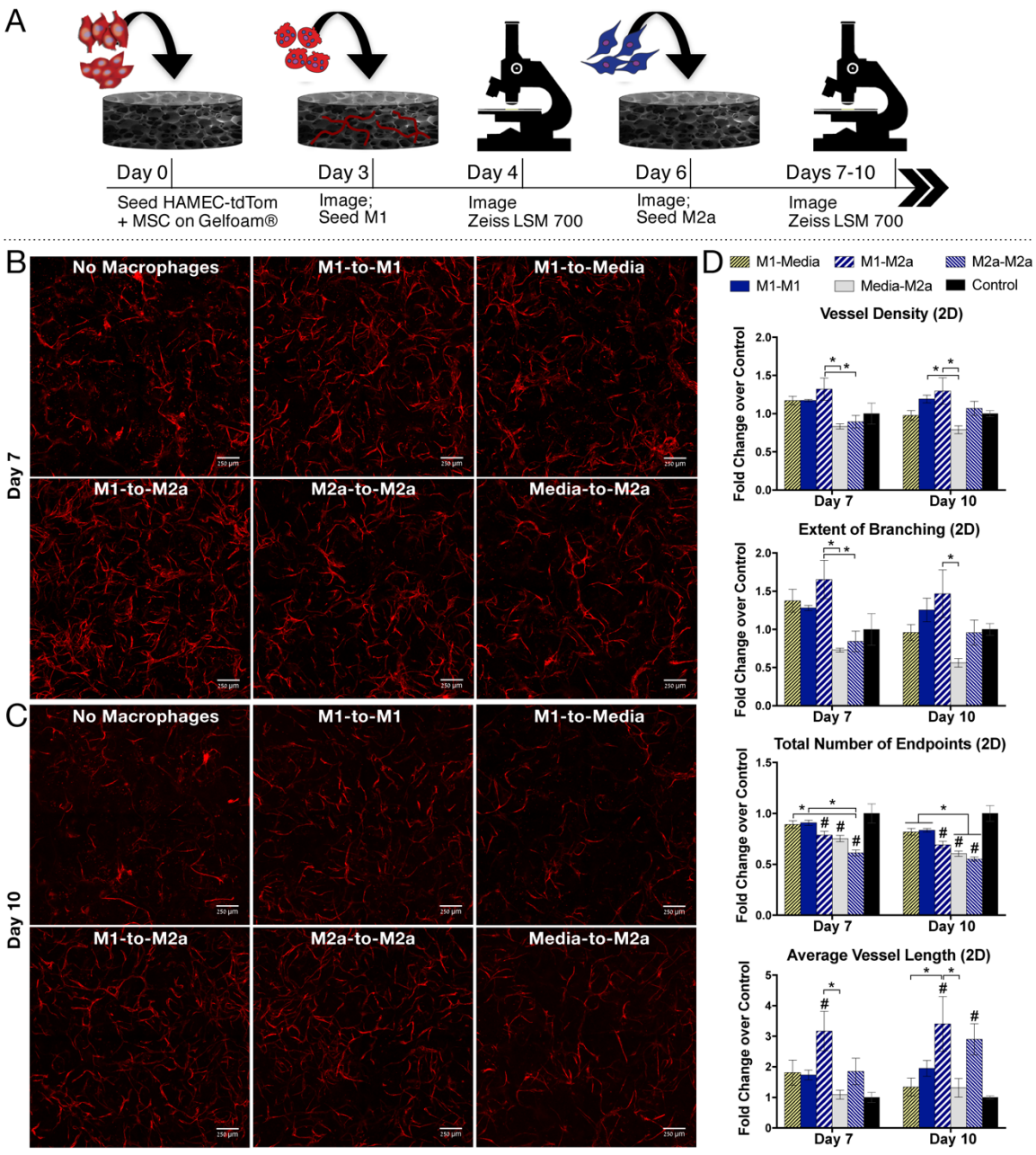

Figure 5.12. Effects of sequential M1 and M2a activation of vascularization (study 1). (A) Schematic of study design; M1 or M2a macrophages, or media alone, seeded on days 3 and 6 of vessel development and changes in network morphology assessed via confocal microscopy over time. (B) Representative images from n = 3 on day 7 and (C) day 10; scale bar = 500 μm. (D) Quantification of vascular development in 2D. Statistical analysis performed using RM two-way ANOVA with Tukey's post-hoc analysis; $p < 0.05$.

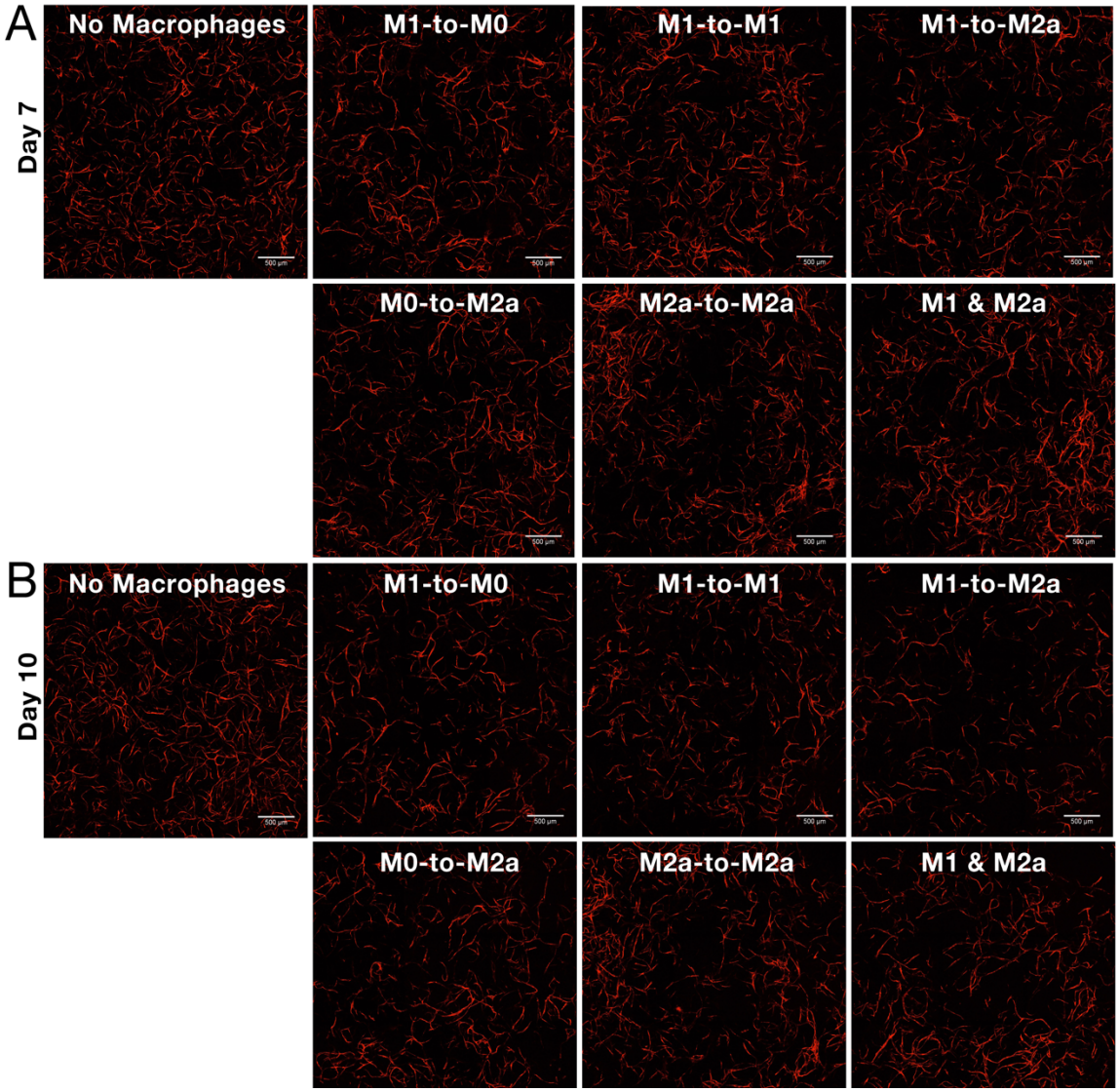

Figure 5.13. Effects of sequential M1 and M2a activation of vascularization (study 2). M0, M1, or M2a macrophages, or media alone, seeded on days 3 and 6 of vessel development and changes in network morphology assessed via confocal microscopy on (A) day 7 and (B) day 10. Representative images from n = 3; scale bar = 500 μm.

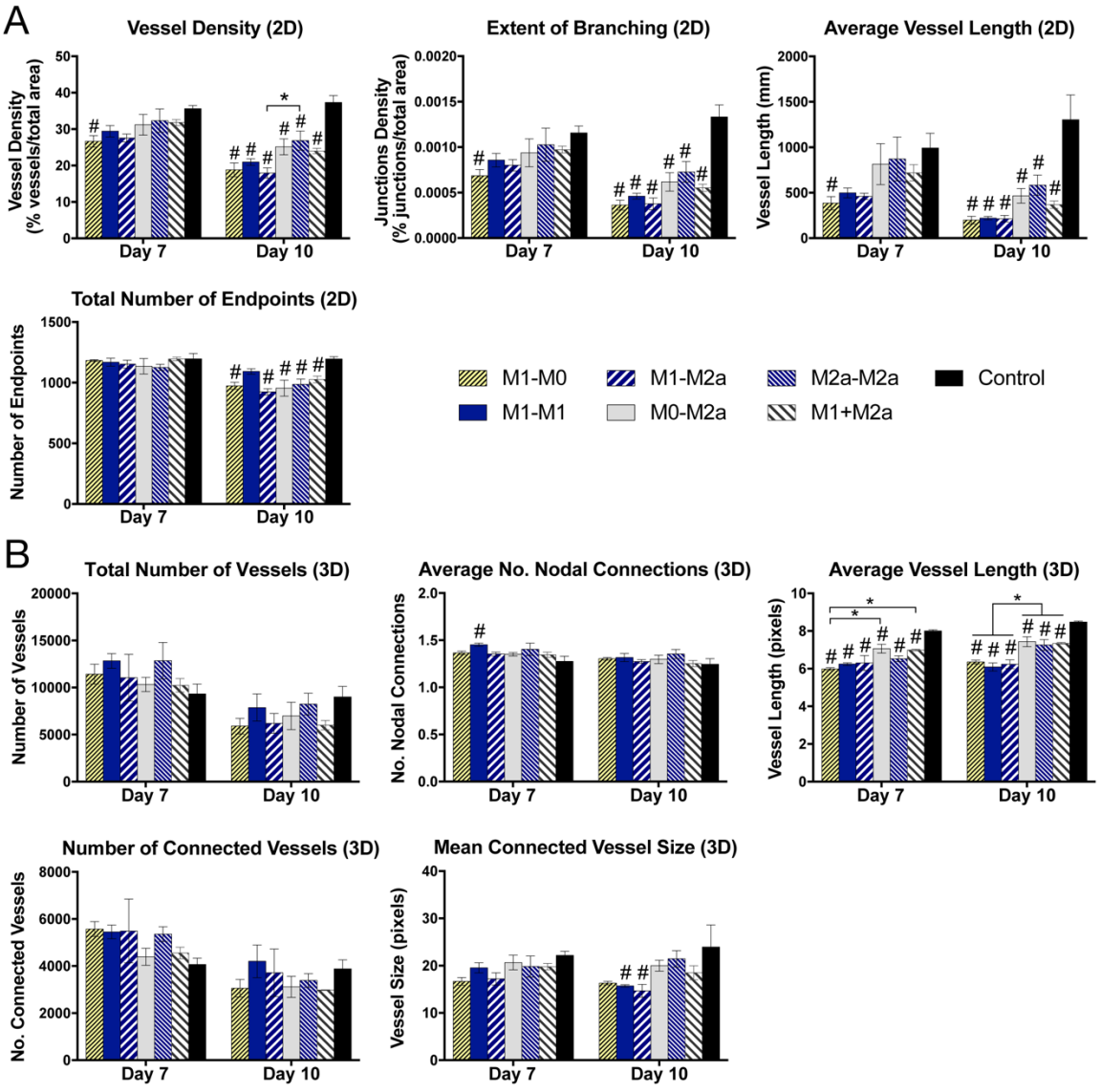

Figure 5.14. Quantification of changes in vascular development induced by sequential M1 and M2a activation (study 2). (A) Analysis of projections in 2D via AngioTool. (B) Analysis of z-stacks in 3D via Matlab. Statistical analysis performed using RM two-way ANOVA with Tukey's post-hoc analysis; $n = 3$ and $p < 0.05$.

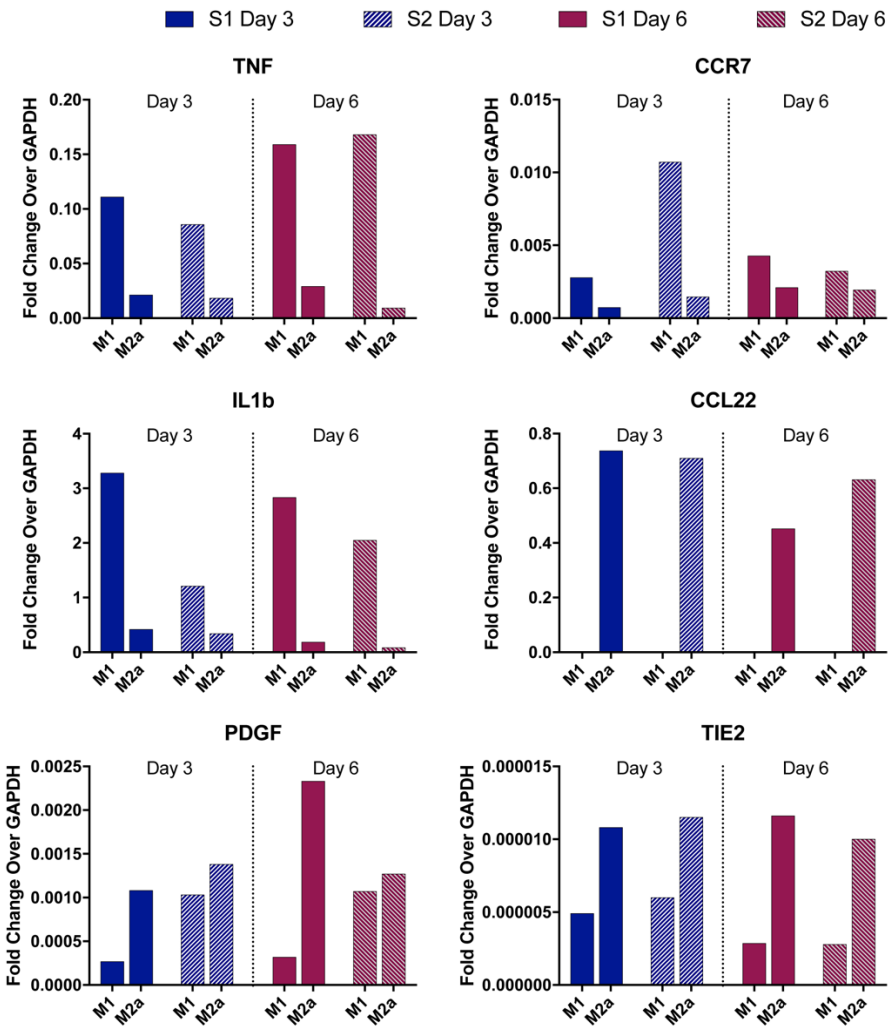

Figure 5.15. Gene expression of M1 and M2a macrophages stimulated *in vitro*, for markers indicative of M1 (*TNF*, *CCR7*, *IL1b*) and M2a activation (*CCL22*, *PDGF*). Data represent macrophage gene expression at the time of seeding on days 3 and 6 for studies investigating sequential M1-to-M2a activation. S1 = study 1; S2 = study 2.

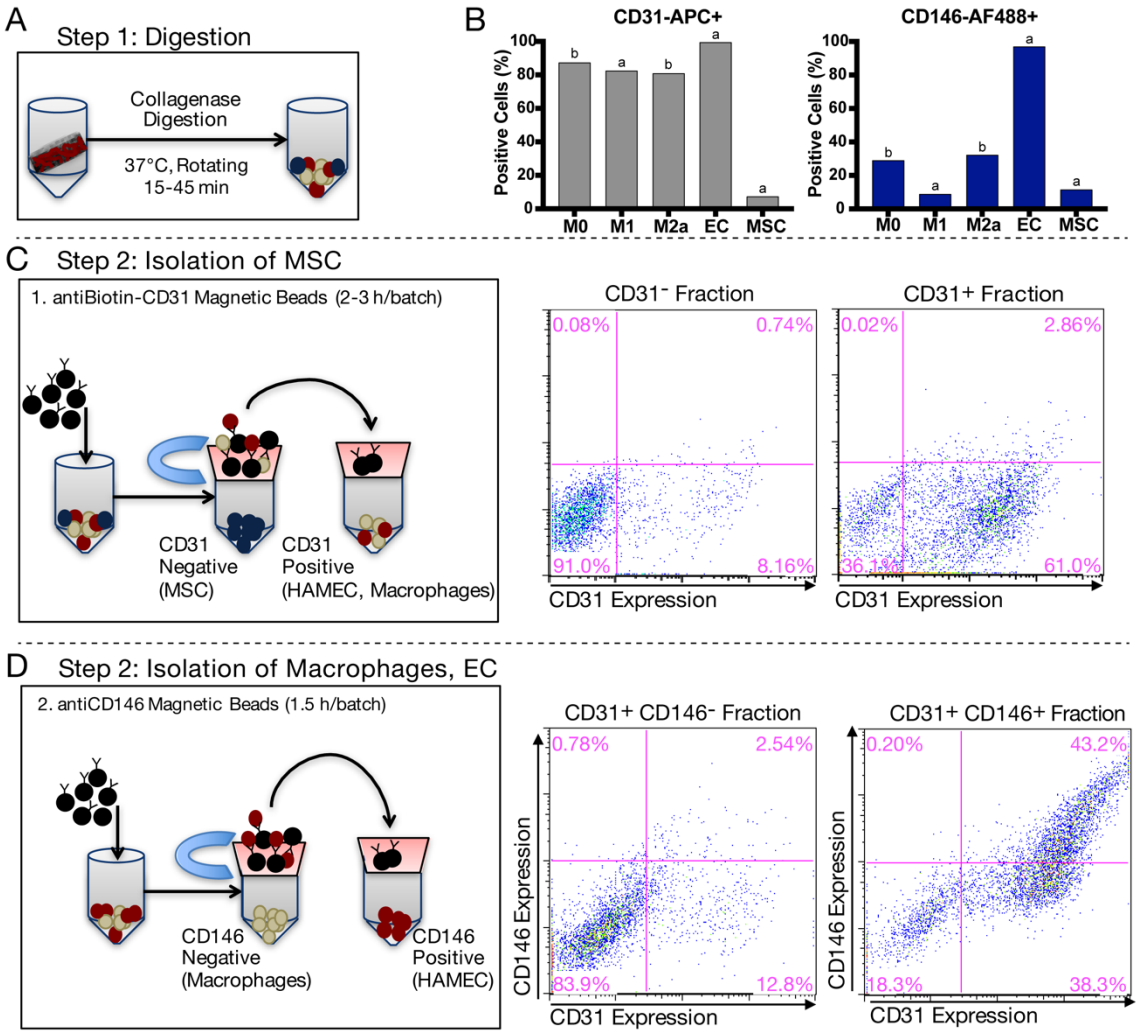

Figure 5.16. Bead-based sorting of HAMEC-dTom, THP1-derived macrophages and MSC. (A) Vascularized Gelfoam® scaffolds digested in collagenase, yielding single cell suspensions. (B) Surface expression of CD31 and CD146 by HAMEC-dTom, THP-1 macrophages and MSC, measured via flow cytometry. (C) Magnetic beads targeting CD31 used to negatively select for CD31- MSC within cell suspension, yielding suspension of CD31+ HAMEC-dTom and macrophages. (D) Beads bound to CD31 removed, and magnetic beads targeting CD146 used to negatively select for CD31+CD146- macrophages, yielding an enriched suspension of CD31+CD146+ HAMEC-dTom. Flow cytometry used to confirm population enrichment in all fractions.

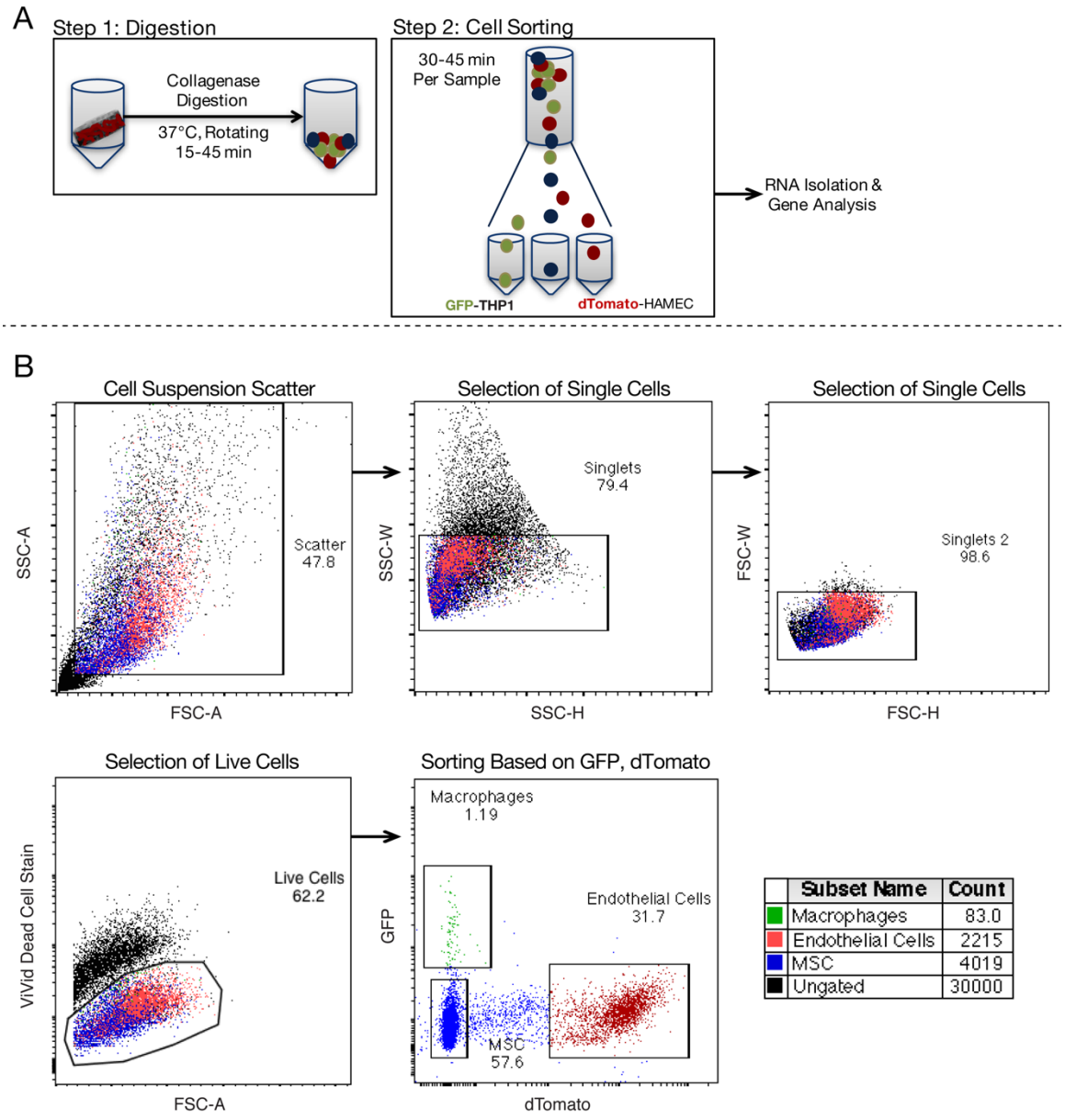

Figure 5.17. FACS-based sorting of HAMEC-dTOM, GFP-THP1-derived macrophages, and MSC. (A) Schematic of sorting process; vascularized Gelfoam® scaffolds digested in collagenase, yielding single cell suspensions, and subsequently sorted based on inherent dTomato and GFP expression. (B) Single cells identified from parent scatter population; live cells distinguished based on intensity of dead cell stain, and subsequently sorted according to dTomato and GFP expression using a BD FACSAria Fusion flow cytometer. Macrophages represented less than 2% of the sorted population collected, while HAMEC-dTOM and MSC represented 31.7% and 57.6% of the sorted cells collected, respectively.

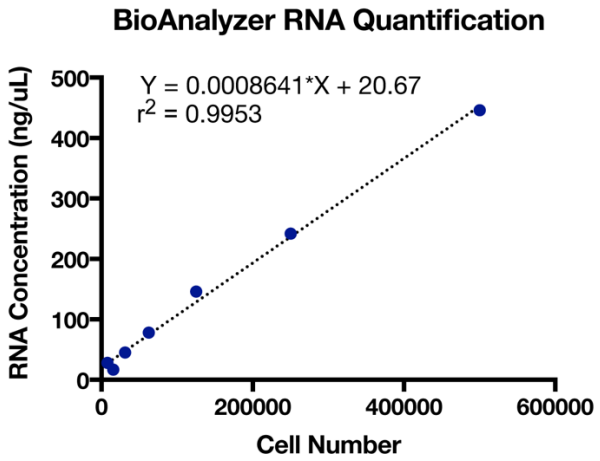

Figure 5.18. Effect of THP-1 cell number on RNA yield according to BioAnalyzer 2100 RNA 6000 Nano kit. Linear regression fit to the data, with $r^2 = 0.9953$, indicating goodness of fit.

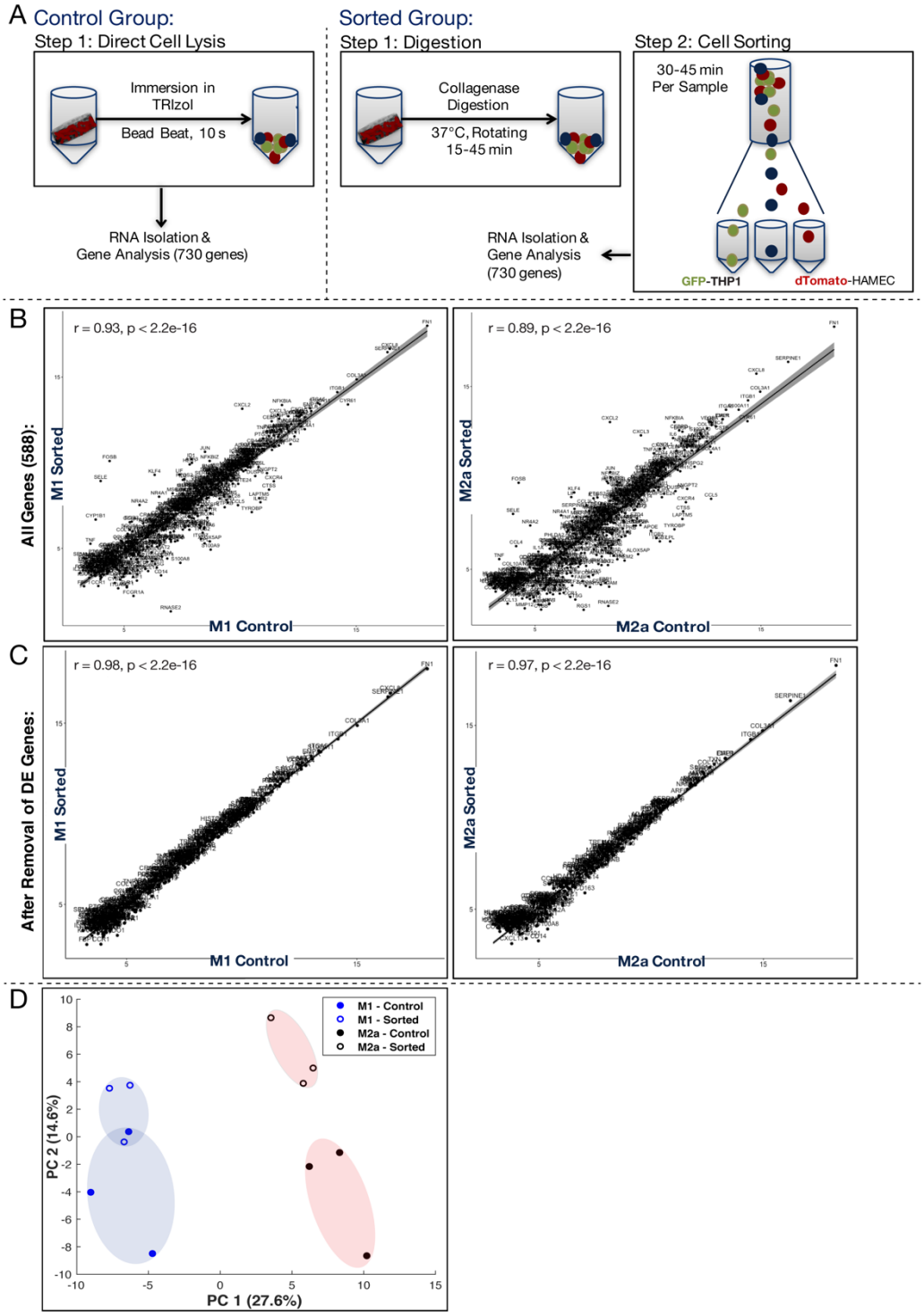

Figure 5.19. Effects of collagenase digestion and FACS-based sorting on gene expression of cells isolated from vascularized Gelfoam® scaffolds containing M1 or M2a macrophages; 730 myeloid genes analyzed. (A) Schematic of isolation process for treated vs. control scaffolds lysed in TRIzol. Correlation analysis comparing gene expression between groups (B) for all genes, and (C) after removal of genes differentially expressed between sorted and control scaffolds. (D) PCA demonstrating clustering of remaining genes according to phenotype by PC 1 and treatment by PC 2, representing 27.6% and 14.6% of the variance, respectively.

CHAPTER 6: CONCLUSIONS AND RECOMMENDATIONS

6.1. Conclusions

The overarching goals of this work were to (1) understand how materials successful in regenerating tissue *in vivo* impact the microenvironment to influence macrophage behavior *in vitro* and (2) determine how changing macrophage phenotype affects biomaterial vascularization. To this end, macrophage activation was examined in response to direct contact with bone substitutes that have been proven to promote regeneration in critical size defects relative to less successful scaffolds. Using cluster analysis to visualize differences among scaffold-induced macrophage activation revealed major changes in gene expression over time for all scaffolds, as well as scaffold-specific effects on macrophage behavior. In contrast to clinically utilized TCP-HA scaffolds that induced sustained up-regulation of pro-inflammatory markers indicative of M1 activation, along with significant down-regulation of M2 activation, Baghdadite and Sr-HT-Gahnite scaffolds demonstrated increased M2a- and M2c-like activation over time.

Because macrophages are known to rapidly change their phenotype in response to different stimuli, including mechanical and structural scaffold properties, and soluble factors present in the microenvironment, a transwell assay was performed to compare macrophage activation when physical contact with the scaffolds was obstructed. Surprisingly, there were few differences in macrophage responses to ions released by the scaffolds despite differences in chemical composition of the scaffolds, indicating that direct cell-scaffold contact was primarily responsible for modulating macrophage phenotype. In an attempt to identify potential mechanisms leading to the M2 responses observed, grain size was varied within Baghdadite scaffolds; however, only modest effects on macrophage

protein production were observed. This work provided evidence that scaffolds more successful in regenerating bone *in vivo* modulate macrophage behavior.

It was not clear how this modulation correlates with vascularization, which plays an indispensable role in biomaterial-mediated tissue repair. Therefore, the next step was to ascertain how changes in macrophage phenotype affect the angiogenic potential of endothelial cells. Primary human monocyte-derived M0, M1, M2a, M2c and M2f phenotypes were co-cultured with microvascular ECs in a transwell system, allowing for cellular crosstalk via paracrine signaling. After 1 and 3 days, gene expression was assessed to identify the physiological state of the cells. ECs had surprisingly modest effects on macrophage phenotype, even after 3 days without exogenous addition of macrophage stimulating factors, which was attributed to differences in cell number between ECs and macrophages.

In contrast, macrophage phenotype induced significant changes in EC expression of genes related to vessel sprouting, stabilization and maturation, and remodeling. M0 macrophages caused down-regulation of genes related to vessel morphogenesis, cell migration, and the positive regulation of vascular smooth muscle cells, which likely signifies an anti-angiogenic contribution to vascularization. M1 macrophages induced up-regulation of several genes associated with positive regulation of chemotaxis, sprouting, and adherens junction organization, suggesting a pro-angiogenic contribution to vascularization that may be related to tip cell regulation. Similar results were observed for M2c macrophages, which also stimulated up-regulation of genes associated with VEGF signaling, the response to VEGF, branching and EC proliferation. Based on these findings, M2c are proposed to mediate pro-angiogenic EC responses related to tip cell selection and regulation. M2a macrophages induced changes related to branching, and M2f affected genes associated with ECM disassembly, EC migration and the response to

mechanical stimuli and hypoxia, which may implicate this phenotype in vessel regression. This study advanced the current understanding of macrophage-EC crosstalk during angiogenesis.

To further ascertain the functional consequences of macrophage control over EC behavior, a 3D *in vitro* model of vascularization was developed. This model utilized microvascular ECs and MSC support cells, which self-assembled into vascular networks on porous Gelfoam® constructs that were selected based on the ability to introduce cells into the system at varying stages of blood vessel development. The seeding ratio of macrophages relative to ECs and MSCs was optimized for quantification of vascular dynamics, from which a 2.5:1 ratio of ECs to macrophages was measured to yield more complex vasculature compared to higher seeding densities. Subsequently, the seeding time of macrophages was varied over days 0-6. Seeding times of day 3 or 6 were chosen based on the presence of tubular structures in combination with the inhibitory effects observed from simultaneous seeding of macrophages with ECs. In order to visualize macrophage-vessel interactions using live cell imaging, the ability to label macrophages with Vybrant® DiD cell labeling solution was explored, and compared to the use of GFP-expressing macrophages. Analysis of GFP-macrophages confirmed that the cells retain the same phenotypic profiles as unlabeled macrophages when stimulated *in vitro*; because of potential DiD leaking and uptake by adjacent cells, GFP-macrophages represent a more stable approach for imaging macrophages in culture over extended periods of time.

With this system, the contributions of M0, M1, M2a and M2c macrophages on network development were investigated. Consistent with the gene expression data resulting from macrophage-EC crosstalk, M1 macrophages enhanced vessel density and branching relative to vessels without macrophages and those exposed to the M0

phenotype. Similar changes were observed for M2a macrophages, but to a lesser extent. Importantly, phenotype-induced changes were rapidly abolished and all macrophage-seeded constructs led to eventual vessel regression. These effects seemed to be accelerated by later seeding times, highlighting the importance of investigating early time points. High-magnification imaging of macrophage-vessel interactions further demonstrated that M2a macrophages wrap around vessels and facilitate bridging between adjacent tip cells, while M1 and M2c macrophages displayed a rounded morphology with only occasional elongation. Nevertheless, M1 and M2c macrophages were also seen on top of vessels, and near branching sites. A preliminary investigation of sequential M1 and M2a activation demonstrated the potential of temporal control over macrophage behavior to improve vascularization relative to constructs without macrophages; however, additional work is needed to confirm these early findings.

Lastly, methods to isolate macrophages, ECs and MSCs from vascularized Gelfoam® identified were explored as a foundation for assessing cellular crosstalk among all three populations of cells at various stages of vascular formation. A magnetic bead-based approach using sequential targeting of CD31 and CD146 was established, yielding enriched but not pure populations of each cell type. Because of extensive processing and time required to achieve this separation, FACS-based isolation of fluorescently-tagged ECs and macrophages were also assessed and found effective in achieving highly enriched cell populations, though only small quantities of cells could be collected from a single scaffold. To confirm that digestion of Gelfoam® and subsequent FACS isolation of ECs, MSCs, and macrophages can be used to measure gene expression profiles without jeopardizing or altering the cells, gene expression was compared between sorted scaffolds and those subjected to immediate lysis of the entire cell population. Based on a myeloid panel of 730 genes, isolation of the cells in this manner significantly altered > 67%

of the genes, emphasizing the importance of testing the effects of processing conditions on cell behavior prior to comparing gene expression profiles of the cells. This investigation has laid the groundwork for future studies to thoroughly characterize crosstalk between ECs, MSCs, and macrophages during tissue vascularization *in vitro*.

6.2. Recommendations for Future Work

This research has exciting implications for controlling vascularization, both in biomaterial-mediated tissue repair and disease. Future work should utilize the tri-culture system developed in aim 3 to characterize the crosstalk between macrophages, ECs and MSCs. Preliminary *in vitro* work in 2D has demonstrated that the angiogenic behavior of ECs is differentially stimulated by macrophage phenotype. Conducting this analysis in 3D, in the presence of developing blood vessels, may shed light on the factor(s) that contribute to macrophage-mediated anastomosis. Functional consequences of silencing or inhibiting potential factors of anastomosis could then be analyzed with respect to network morphology using this system. In addition to characterizing the crosstalk among the cells via gene expression, whole-mount immunohistochemistry should be used on pre-vascularized scaffolds exposed to macrophages of different phenotypes to better elucidate the spatiotemporal effects on MSC support cells, which were not visualized in this work, and EC phenotypes with respect to macrophage localization. Markers of interest include those related to vessel stability (e.g. α-smooth muscle actin, αSMA) and tip and stalk cell differentiation (e.g. DLL4, VEGFR2, NRARP). Alternatively, the phenotypic contributions of macrophages in angiogenesis can also be explored by conducting time-lapse imaging over 24 – 48 h of GFP-expressing macrophages seeded on HAMEC-dTom/MSC-derived vascular networks. This would enable tracking of individual cells with

respect to macrophage phenotype, which would enhance our understanding of the dynamic interactions between macrophages and development vessels.

Other areas that warrant further investigation include the effects of sequential activation of M1 and M2a macrophages. In this work, the time between macrophage seeding was not varied, but it is possible that, because macrophages undergo rapid phenotypic changes, M2a macrophages should be seeded within 1 day of M1 addition. Likewise, temporal control over M2c and M2f was not yet explored. Mounting evidence, collected through this work and by others [70, 80], suggests that M2c macrophages contribute to early stages of vessel sprouting, and perhaps late stages of network remodeling.

Moreover, the consequences of macrophage modulation by regenerative biomaterials in vascularization outcomes is of interest, particularly due to the ability of these biomaterials to induce hybrid phenotypes that are not generally achieved via traditional *in vitro* activation of macrophages. This could be achieved by applying conditioned media collected from macrophage-seeded constructs to the 3D *in vitro* model of vascular formation. However, this would require careful optimization to be able to study vascular dynamics using conditioned media without comprising EC and MSC survival.

Aside from these recommended studies, there are several areas of interest that are known to have a major impact on angiogenesis that should be considered in future analyses. First, the experiments conducted in this work were completed under normal oxygen levels, but it is well established that hypoxia is a major driver of angiogenesis, especially in the context of implanted tissues that lack a functional vasculature supply. Moreover, hypoxia is not only thought to influence macrophage behavior [274] and regulate macrophage-EC interactions during angiogenesis [275], but also plays a role in the recruitment of immune cells [276]. Hypoxia is also affected by mechanical activation,

such as that induced by fluid flow in perfused vessels, which subsequently alters [38, 39]. Therefore, investigating the contribution of macrophages to angiogenesis in a dynamic environment should also be considered. To better understand the mechanisms behind macrophage-vessel crosstalk that lead to the changes observed in this work, future studies should also analyze cell communication through exosomes, or extracellular vesicles. Indeed, recent work has demonstrated that macrophages can be modulated by MSC-secreted vesicles [272], which contribute to vascular regeneration [277]. Exosomes have also been implicated in macrophage-EC crosstalk with respect to angiogenesis [178, 278]; thus, it is conceivable that macrophage-mediated anastomosis and vessel stabilization is related to production of these vesicles, perhaps through production of PDGFB or TGFB [183, 203].

Lastly, the *in vivo* translation of this work should be ascertained; this could be achieved via macrophage depletion at various times post-implantation of pre-vascularized constructs in a dorsal window chamber, allowing for live imaging and tracking of graft-host vascular integration. Then, *in vitro*-stimulated M1 and M2 macrophages could be added locally to the engineered tissue to confirm that contributions of macrophage phenotype observed *in vitro* in the present work.

Ultimately, this work is expected to have important implications for tissue engineering; establishing the role of macrophages in tissue vascularization can be used to both inform the design of biomaterials that promote vascularization, and aid in the treatment of tissues characterized by abnormal vascularization.

CHAPTER 7: SUPPLEMENTAL INVESTIGATION OF MONOCYTE ISOLATION AND CRYOPRESERVATION ON MACROPHAGE BEHAVIOR

7.1. Introduction

The ultimate goal of this work was to extensively characterize the role of human macrophages in the context of tissue regeneration and vascularization. This is commonly performed using primary monocytes, isolated from whole blood and differentiated into macrophages *in vitro*. However, monocytes can also be purchased from a number of different sources and isolated using a variety of different methods, though the cost, effort and ensuing monocyte purity vary substantially. To date, there is a lack of research systematically analyzing the differences in monocyte isolation on macrophage polarization, despite reports that highlight functional differences in macrophages [279] and monocytes [280] with respect to isolation procedures.

Moreover, experiments requiring a large number of macrophages require a large number of monocytes, but only a finite number can be obtained from a single donor. As a result, multiple donors are often used to study macrophage behavior, which may introduce large donor-to-donor variability and potentially confound results, although the effects of donor on macrophage behavior have not been described. One way to circumvent this variability is to cryopreserve monocytes from one donor and use the same donor's cells in multiple studies. Despite their widespread commercial availability, cryopreserved monocytes are not often used, perhaps because of cost (commercially available frozen monocytes are roughly 8 times more expensive than in-house isolation via density gradient centrifugation) and/or a lack of information regarding their robustness in comparison to freshly isolated monocytes. While findings reported in the literature suggest that cryopreservation does not alter the biological activities of monocytes [281-283] or

monocyte-derived dendritic cells [284], others report modified responses [285, 286], and the effects on macrophage phenotype have not been described.

Therefore, the goal of this work was to directly investigate the differences between negatively selected and density gradient centrifugation-derived monocytes on macrophage activation, and further to test the potential to cryopreserve monocytes without adversely impacting their functional differentiation into macrophages. First the level of donor-to-donor variability within each method of isolation on macrophage gene expression was assessed. Then the differences between negative selection and sequential density gradient centrifugation were analyzed. Finally, the effects of monocyte cryopreservation on macrophage function were evaluated to determine if monocytes can be frozen for use in conducting sequential experiments and to minimize donor-to-donor variability.

7.2. Experimental Section

7.2.1. Experimental Design

A schematic of the experimental design is provided in **Figure 7.1**. *Study 1.* Monocytes were isolated from a total of 10 donors by either negative selection or sequential density gradient centrifugation and subsequently differentiated into macrophages *in vitro* for 7 days. The effect of isolation method on macrophage gene expression was evaluated. *Study 2.* The effects of cryopreservation were evaluated by 1) comparing macrophage gene expression from cryopreserved monocytes from 4 donors to that from freshly isolated monocytes, and 2) directly comparing the effect of cryopreservation on macrophage gene expression for monocytes derived from a single donor, to eliminate any potential variability due to donor. Macrophage gene expression and protein secretion were quantified after 7 days.

7.2.2. Monocyte Isolation

7.2.2.1. *Negative selection*

Primary human monocytes isolated via negative selection were purchased from the University of Pennsylvania Human Immunology Core. Monocytes were isolated and purified from a leukapheresis product using a RosetteSep™ Human Monocyte Enrichment Cocktail (STEMCELL Technologies Inc., Vancouver, BC, Canada).

7.2.2.2. *Sequential density gradient centrifugation*

Primary human monocytes were isolated from blood (obtained from the New York Blood Center) using sequential density gradient centrifugation of Ficoll-Paque™ PLUS and 46% Percoll™ PLUS (GE Healthcare, Piscataway, NJ, USA) as we have previously described [70, 83].

7.2.3. Monocyte Cryopreservation and Thawing

Negatively selected monocytes for cryopreservation were resuspended at a density of 1×10^7 cells/mL in cold freezing medium (10% DMSO in fetal bovine serum). Cryovials were transferred to a Cryo 1°C Freezing Container (Thermo Scientific) and stored at -80°C overnight. Later, cryopreserved cells were thawed rapidly in a 37°C water bath and subsequently transferred into pre-warmed RPMI 1640 media containing 10% heat-inactivated human serum and 1% penicillin streptomycin. The cells were washed twice in pre-warmed media and viability was assessed using a Countess® Automated Cell Counter with trypan blue staining; cell viability was typically $\geq$ 98%.

7.2.4. Macrophage Differentiation

Monocytes were seeded in ultra-low attachment flasks (Corning) at a density of 1×10^6 cells/mL and cultured for 5 days in RPMI 1640 media, supplemented with 10% heat-inactivated human serum, 1% penicillin streptomycin and 20 ng/mL macrophage colony stimulating factor (MCSF) for macrophage differentiation. The media was changed on days 3 and 5. On day 5, macrophages were gently scraped, collected and counted using a Countess® Automated cell Counter with trypan blue staining. Macrophages were seeded at 1×10^6 cells/mL in a 24 well ultra-low attachment plate. Differentiation was achieved by addition of IFN-γ (100 ng/mL) and LPS (100 ng/mL) for M1 activation, IL-4 (40 ng/mL) and IL-13 (20 ng/mL) for M2a activation, and IL-10 (40 ng/mL) for M2c activation. M0 macrophages cultured in MSCF alone were used as a control. After 48 h, RNA was extracted for gene expression analysis using RT-PCR.

7.2.5. RNA Extraction and cDNA Synthesis

Extracted RNA was purified on an RNAqueous-Micro Kit spin column (Ambion) according to the manufacturer's instructions. Purified RNA was quantified on a NanoQuant plate (Tecan) and treated with DNAse I, Amplification Grade (Invitrogen) for DNA removal according to the manufacturer's protocol. cDNA was synthesized from 1 μg RNA ($A_{260/280}$ > 1.8) using a High-Capacity cDNA Reverse Transcription Kit (Applied Biosystems) according to the manufacturer's instructions and stored at -80°C until analysis.

7.2.6. Quantitative RT-PCR

Quantitative RT-PCR was performed using 20 ng cDNA and Fast SYBR Green Master Mix (Applied Biosystems) according to the manufacturer's instructions. Mean

quantification cycle, Cq, values were calculated from technical replicates (n = 2). The expression of target genes was then normalized to the reference gene, *GAPDH*, and, where indicated, subsequently normalized to the M0 control ($2^{-\Delta\Delta Ct}$). All primers (**Table 3.1**) were synthesized by Life Technologies.

7.2.7. Principal Component Analysis

Gene expression data were further evaluated using PCA to identify patterns in gene expression and major sources of variation within data sets. PCA was implemented using Matlab® software (The MathWorks, Inc., Natick, MA). Prior to analysis, the data were standardized to enable comparison across the data set. PCA was then performed for each method of isolation and preservation to derive the principal components.

7.2.8. Protein Secretion

Supernatants from cryopreserved and control macrophages were collected on Day 7 of macrophage differentiation and polarization, and analyzed for the presence of human tumor necrosis factor (TNF), vascular endothelial growth factor A (VEGFA), interleukin 10 (IL10) and interleukin 1 receptor antagonist (IL1Ra). Protein secretion was measured using commercially available Mini Enzyme-Linked Immunosorbent Assay (ELISA) Development Kits (PeproTech, NJ, USA) according to the manufacturer's instructions.

7.2.9. Statistical Analysis

Data are represented as mean ± SEM. Prior to analysis, fold change data were log-transformed and statistical analysis was performed in GraphPad Prism 6.0 (GraphPad Software, Inc., La Jolla, CA) using two-way ANOVA with Tukey's multiple comparison post-hoc analysis, as indicated; $p < 0.05$ was considered significant. Inter-donor variability

was assessed by computing the interquartile range (IQR), indicative of data scatter; IQR was calculated as the difference between the 25% percentile and 75% percentile.

7.3. Results and Discussion

7.3.1. Donor-to-Donor Variability

Gene expression by macrophages generated from negatively selected monocytes from multiple donors is shown in **Figure 7.2**. The IQR for all genes ranged from 0.21 to 1.06, indicating variability within the data. Despite this donor-to-donor variability, the expected M1, M2a and M2c gene expression trends were conserved across donors. Pro-inflammatory M1 macrophages were characterized by high expression of the pro-inflammatory markers *CCR7* and *IL1B* (**Figure 7.2a**), while M2a and M2c macrophages upregulated the anti-inflammatory markers *CCL22* (**Figure 7.2b**) and *CD163* (**Figure 7.2c**), respectively. Comparable trends were observed for macrophages derived from monocytes isolated by density gradient centrifugation (**Figure 7.3**), as well as negatively selected monocytes subjected to cryopreservation (**Figure 7.4**). However, density gradient centrifugation resulted in IQR values ranging from 0.33 to 1.75 for all genes, indicating greater spread of the data and inter-donor variability compared to negatively selected monocytes. Similarly, the data were more scattered when negatively selected monocytes were subjected to cryopreservation, resulting in a range of IQR values between 0.50 and 2.38. This variability in scatter may be due to the reduced number of donors used when assessing density gradient centrifugation and the effects of preservation.

To further assess the impact of donor-to-donor variability on macrophage responses and our ability to detect results, we conducted PCA on macrophage responses following isolation and polarization (**Figure 7.2d, Figure** 7.3**d, Figure** 7.4**d**). For all

isolation and preservation methods investigated, PC1 accounted for ≥ 34.0% of the variance in the data and separated M1 and M2a responses. Interestingly, donor variability appeared to confound gene expression by M0 and M2a macrophages derived from negatively selected monocytes (**Figure 7.2d**), as PC2 clearly distinguished donor populations, which accounted for 22.7% of the variance in the data. However, further extending the analysis to PC3 revealed M0 and M2a phenotypes as the third leading source of variance in macrophage differentiation (data not shown). Together, the first three principal components captured 77.2% of the variation in the data from negatively selected monocytes, and grouped macrophage responses into the M0, M1, M2a, and M2c phenotypes.

Although donor variability was also detected in macrophage responses from density gradient centrifugation-derived monocytes, and those that were negatively selected and cryopreserved, this variability did not supersede the separation of M0 and M2a responses by PC1 and PC2 (**Figure 7.3d, Figure 7.4d**). Variability in donor responses did, however, represent the third leading source of variance in density gradient centrifugation-derived macrophages (data not shown). This trend was also observed, to an extent, in negatively selected monocytes subjected to cryopreservation prior to macrophage differentiation and polarization (data not shown). Together, the first three principal components captured 87% and 75% of the variance from density gradient centrifugation and cryopreservation, respectively.

Despite noticeable donor variability in immune responses, the chosen markers differentiated between macrophages polarized to the M0, M1, M2a and M2c phenotypes following isolation and preservation by all methods investigated.

7.3.2. Comparison of Negative Selection and Density Gradient Centrifugation

In order to reduce the donor-to-donor variability in macrophage behavior, gene expression by M1, M2a and M2c macrophages was normalized to the M0 control for each donor (**Figure 7.5a-c**) and log transformed for analysis. Comparison of macrophage phenotypes within each method indicated that gene expression trends were conserved between negative selection and density gradient centrifugation of monocytes. In both cases, M1 macrophages upregulated *CCR7* and *IL1B*, M2a macrophages upregulated *CCL22*, and M2c macrophages upregulated *CD163*.

PCA further confirmed that isolation method did not alter gene expression patterns by M0, M1, M2a and M2c macrophages (**Figure 7.5d**). Indeed, PC1 and PC2 captured macrophage phenotype, which accounted for 53% of the variance in the data. Extending the analysis to PC3 (data not shown) revealed donor variability as another leading source of variation, indicating the importance of normalizing macrophage responses for each donor. Together, these principal components captured 73% of the variance, with no distinction between methods of isolation.

These findings suggest that no difference exists between monocytes isolated by negative selection and density gradient centrifugation with respect to macrophage behavior.

7.3.3. Effects of Cryopreservation on Macrophage Behavior

Cryopreservation of negatively selected monocytes did not alter the gene expression trends of polarized macrophages (**Figure 7.6**). M1 macrophages were still distinguishable by expression of *CCR7*, while M2a macrophages exhibited marked upregulation of *CCL22* and M2c macrophages exhibited prominent expression of *CD163*. Although comparable trends were observed for M1 expression of *IL1B*, the upregulation

was not found to be significant following cryopreservation. However, the lack of significance was attributed to donor-to-donor variability, as opposed to technical variability, because all trends in macrophage behavior were conserved between cryopreserved and control monocytes isolated from a single donor, with considerably less error (**Figure 7.7**).

Again, PCA was applied to the gene expression data to determine if cryopreservation affected gene expression of polarized macrophages (**Figure 7.6d**). PC1 and PC2 captured macrophage phenotype as the main source of variance in gene expression, with no distinction between macrophages differentiated from freshly isolated and cryopreserved monocytes. Donor-to-donor variability accounted for the third major source of variance in the data (not shown). Together, these principal components captured 71% of the variance in macrophage responses. Consistent with earlier findings, macrophage phenotype was captured by PC1 and PC2, and there were no overlaps in macrophage phenotype within each method, confirming the ability to cryopreserve monocytes without subsequent loss of function in polarized macrophages.

To further test the effects of cryopreservation on macrophage behavior, protein secretion by macrophages derived from a single donor was quantified; monocytes from a single donor were used in this analysis to eliminate the influence of donor-to-donor variability. As shown in **Figure 7.8**, cryopreservation did not alter the expected protein secretion profile of macrophages. Pro-inflammatory M1 macrophages exhibited distinct secretion of the angiogenic mediator VEGFA and the inflammatory cytokine TNF, which has been previously described [83], regardless of whether or not they were cryopreserved. Contrary to many publications [287-289], IL1RN (also known as IL1Ra) and IL10 were not secreted at different levels by polarized macrophages; however, these differences may be attributed to variations in macrophage culture conditions and stimulating factors. Notably, reports of IL10 secretion by polarized M2 macrophages measure protein secretion

following LPS stimulation [288, 289], which consequently enhanced secretion of IL10. LPS also induces IL1RN secretion and has been shown to act synergistically with IL4 [290], which may account for elevated production by M2 macrophages. Moreover, it has been shown that media containing serum can reduce cytokine production [291]. Finally, in studies that use MCSF and IL10 to polarize M2c macrophages [291], an IL10 control was not included to verify that the cell secretes the IL10 detected. In this study, there was no increase in IL10 levels in the cell culture media above that of the polarizing media for M2c macrophages.

Overall, these findings indicate that cryopreservation does not impact macrophage behavior, at least for the genes studied here. Although cryopreservation does not overcome the limitation of cell quantity, the ability to freeze monocytes from the same donor enables multiple studies to be conducted with cells without the confounding effect of donor-to-donor variability.

It should be noted that there were several limitations to this investigation. Positive selection was omitted from this work because it was presumed that the presence of magnetic beads would influence macrophage behavior. In addition, ELISA was performed on only a few, select markers related to tissue repair. Moreover, TNF was the only marker also evaluated at the protein level; it is possible that the other genes investigated are not expressed at the level of protein secretion.

7.4. Conclusions

In this study, the effects of monocyte isolation and cryopreservation on expression of prototypical markers of M1, M2a and M2c macrophages were systematically characterized. There were no detectable differences between negatively selected

monocytes and those isolated by density gradient centrifugation; moreover, this work confirmed that monocytes can be cryopreserved without altering macrophage behavior. Most notably, this analysis revealed significant inter-donor variability, which suggests that cells from a single donor should be cryopreserved for use in sequential experiments as a means to abolish donor-to-donor variability and ensure accurate interpretation of data.

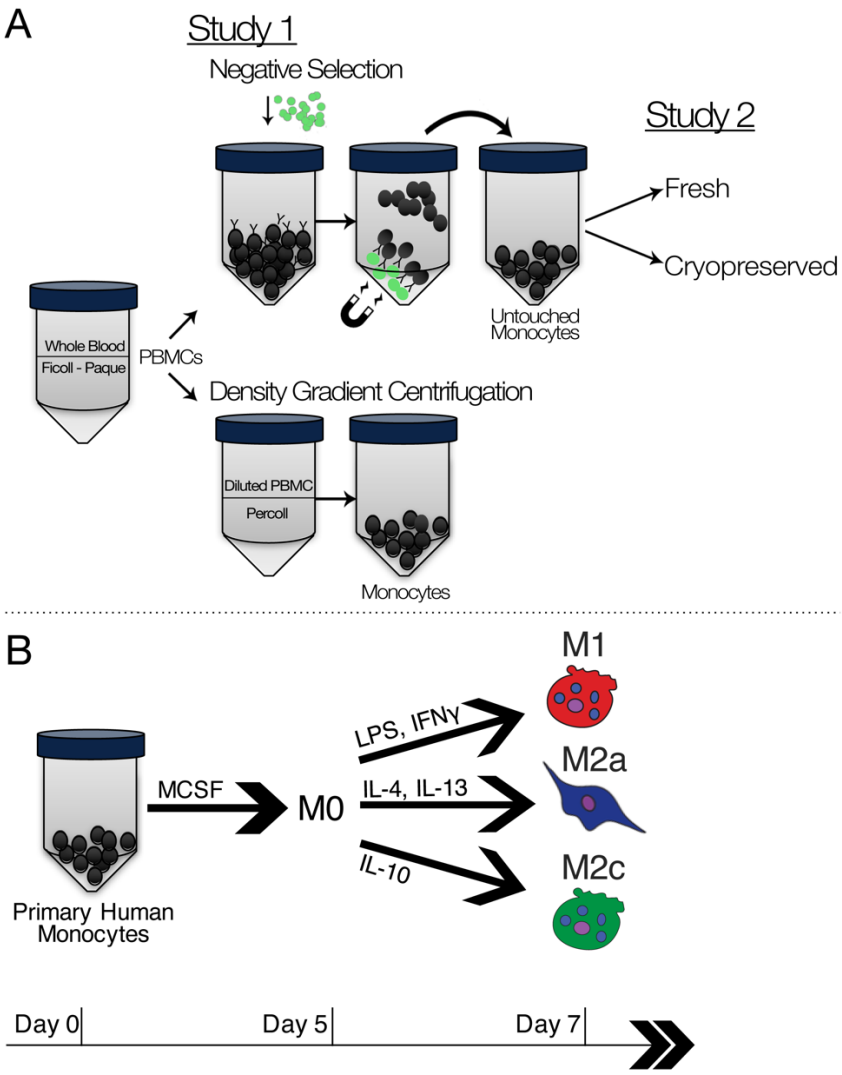

Figure 7.1. Schematic of study design. (A) *Study 1:* Monocytes were isolated by negative selection or sequential density gradient centrifugation and subsequently differentiated into macrophages *in vitro* for 7 days. The effect of isolation method on macrophage gene expression was evaluated. *Study 2:* The effects of cryopreservation were evaluated by 1) comparing macrophage gene expression from cryopreserved monocytes from mulitple donors to that from freshly isolated monocytes, and 2) directly comparing the effect of cryopreservation on macrophage gene expression for monocytes derived from a single donor, to eliminate potential inter-donor variability. (B) Macrophage differentiation scheme; gene expression and protein secretion were quantified after 7 days.

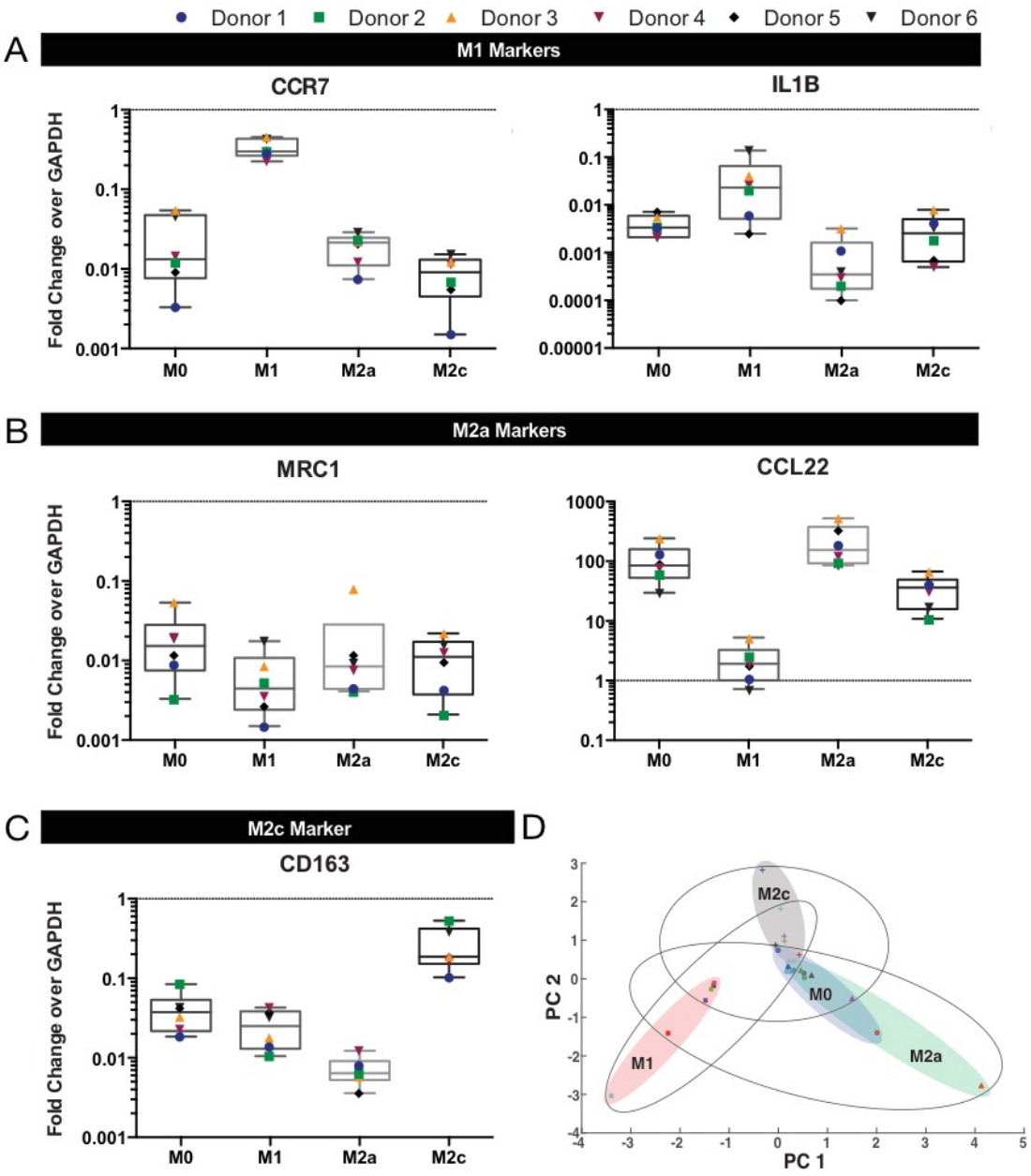

Figure 7.2. (A-C) Tukey box-and-whiskers plots showing donor-to-donor variability in gene expression by macrophages derived from negatively selected monocytes (not cryopreserved). Data represent fold change over *GAPDH*. (D) Principal component analysis of gene expression by macrophages derived from negatively selected monocytes. Score plot of principal components 1 and 2 depicted, capturing 42.8% and 32.3% of the variance within the data, respectively. Macrophage phenotype indicted by black (M0), blue (M1), red (M2a) or green (M2c) shading. Solid line circles indicate variability across donors.

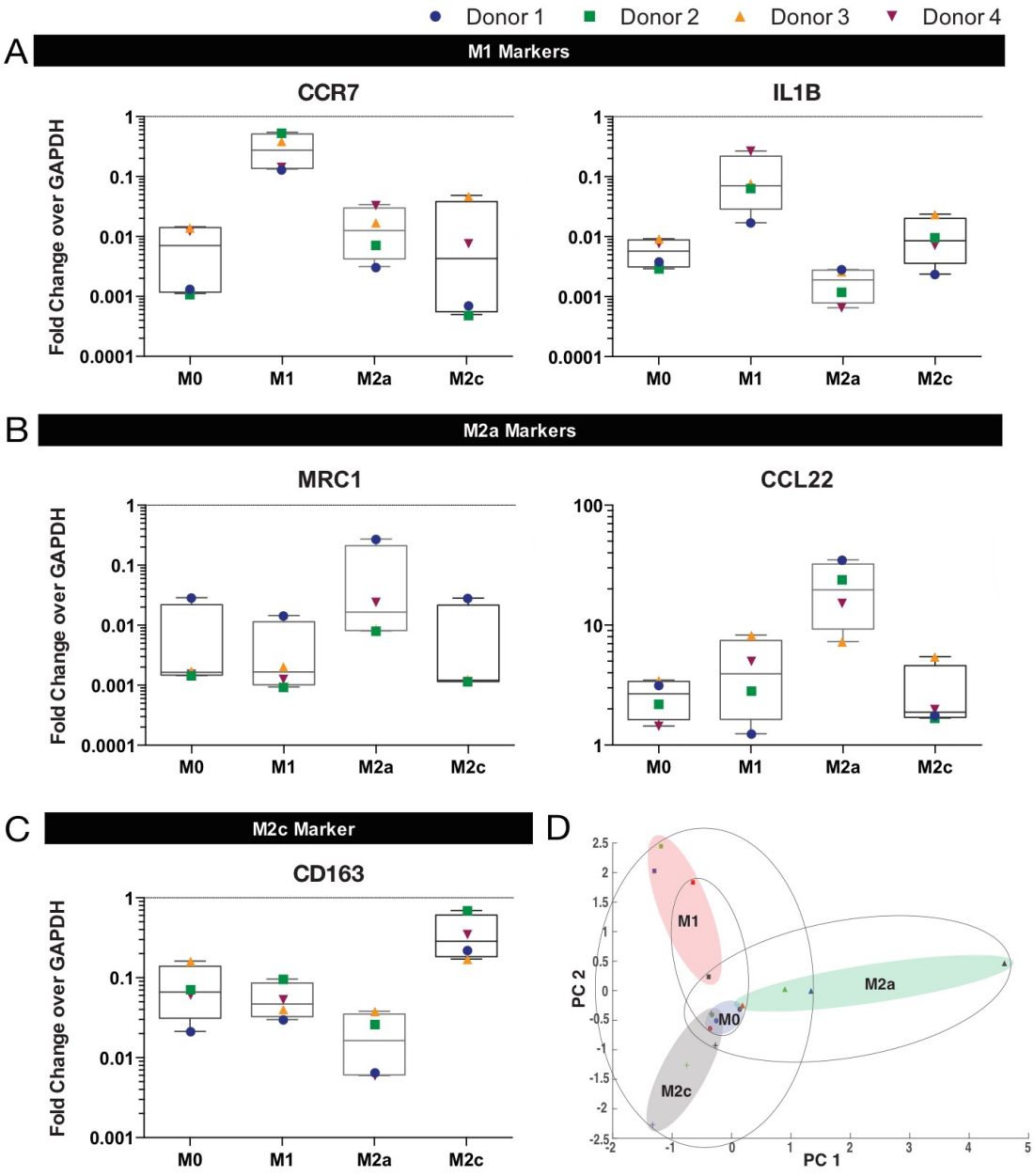

Figure 7.3. (A-C) Tukey box-and-whiskers plots showing donor-to-donor variability in gene expression by macrophages derived from monocytes isolated by density gradient centrifugation (not cryopreserved). Data represent fold change over *GAPDH*. (D) Principal component analysis of gene expression by macrophages derived from monocytes isolated by density gradient centrifugation. Score plot of principal components 1 and 2 depicted, capturing 40.4% and 30.0% of the variance within the data, respectively. Macrophage phenotype indicted by black (M0), blue (M1), red (M2a) or green (M2c) shading. Solid line circles indicate variability across donors.

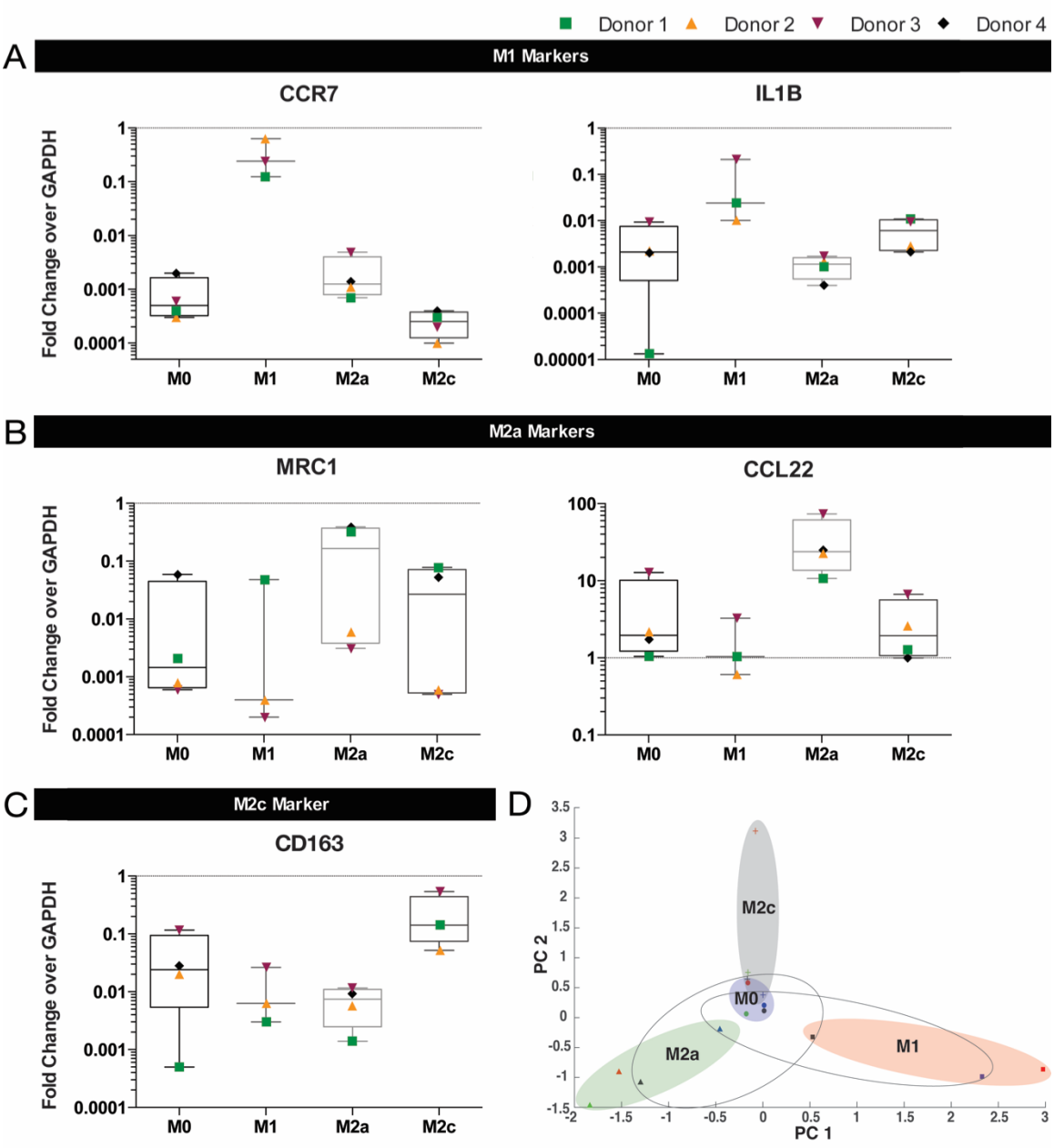

Figure 7.4. (A-C) Tukey box-and-whiskers plots showing donor-to-donor variability in gene expression by macrophages derived from negatively selected monocytes and subjected to cryopreservation. Data represent fold change over *GAPDH*. (D) Principal component analysis of gene expression by macrophages derived from negatively selected monocytes and cryopreserved. Score plot of principal components 1 and 2 depicted, capturing 31.8% and 24.7% of the variance within the data, respectively. Macrophage phenotype indicted by black (M0), blue (M1), red (M2a) or green (M2c) shading. Solid line circles indicate variability across donors.

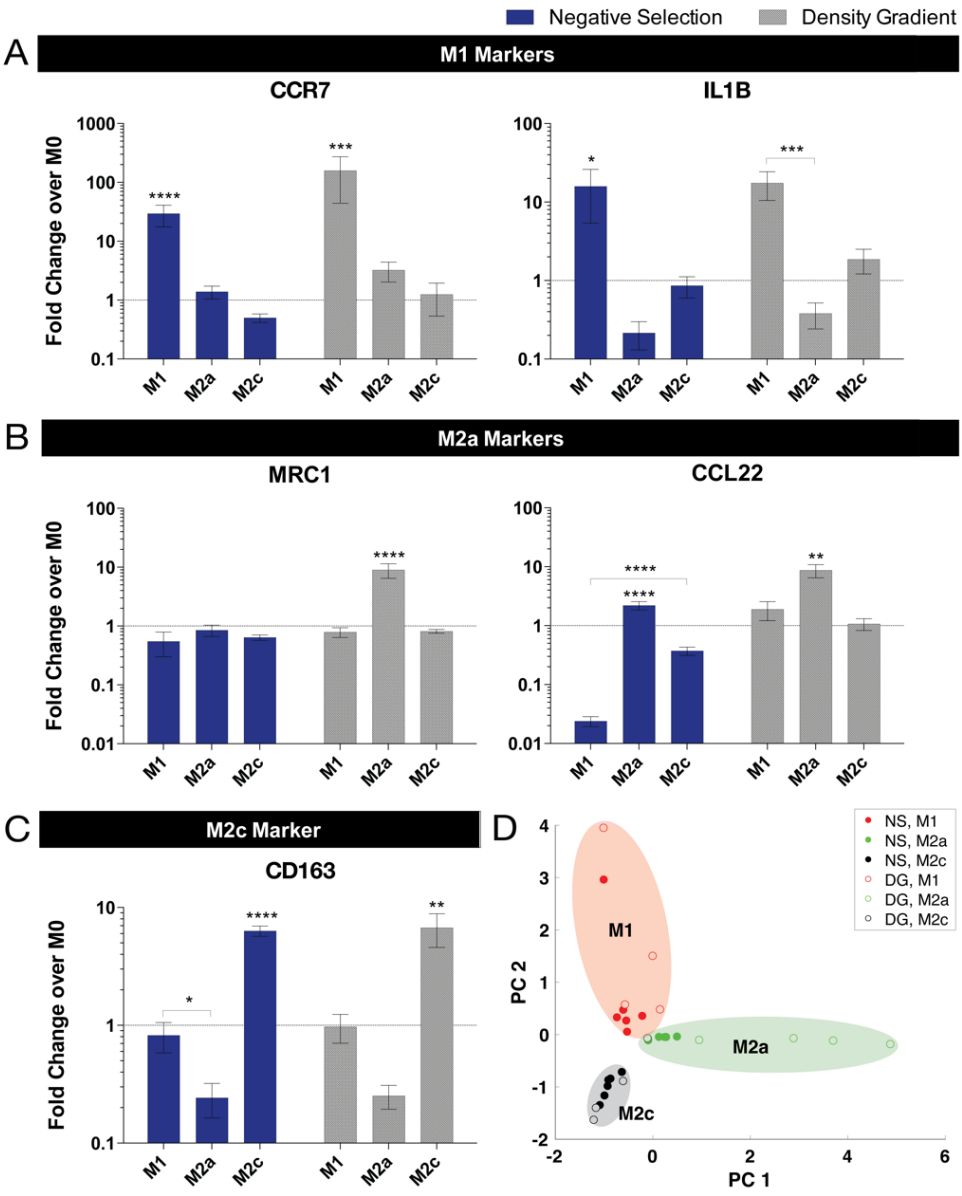

Figure 7.5. (A-C) Comparison between gene expression trends by negatively selected monocytes and monocytes isolated by density gradient centrifugation. Data represent mean fold change over M0 ± SEM. Statistical analysis was performed on log-transformed data using two-way ANOVA with Tukey's post hoc analysis. *$p < 0.05$, **$p < 0.01$, ***$p < 0.001$, ****$p < 0.0001$ relative to all other groups; $n \geq 4$. (D) Principal component analysis comparing gene expression between macrophages derived from negatively selected (NS) monocytes or via density gradient centrifugation (DG). Score plot of principal components 1 and 2 depicted, capturing 40.8% and 27.1% of the variance within the data, respectively. Macrophage phenotype indicted by blue (M0), red (M1), green (M2a) or black (M2c) shading.

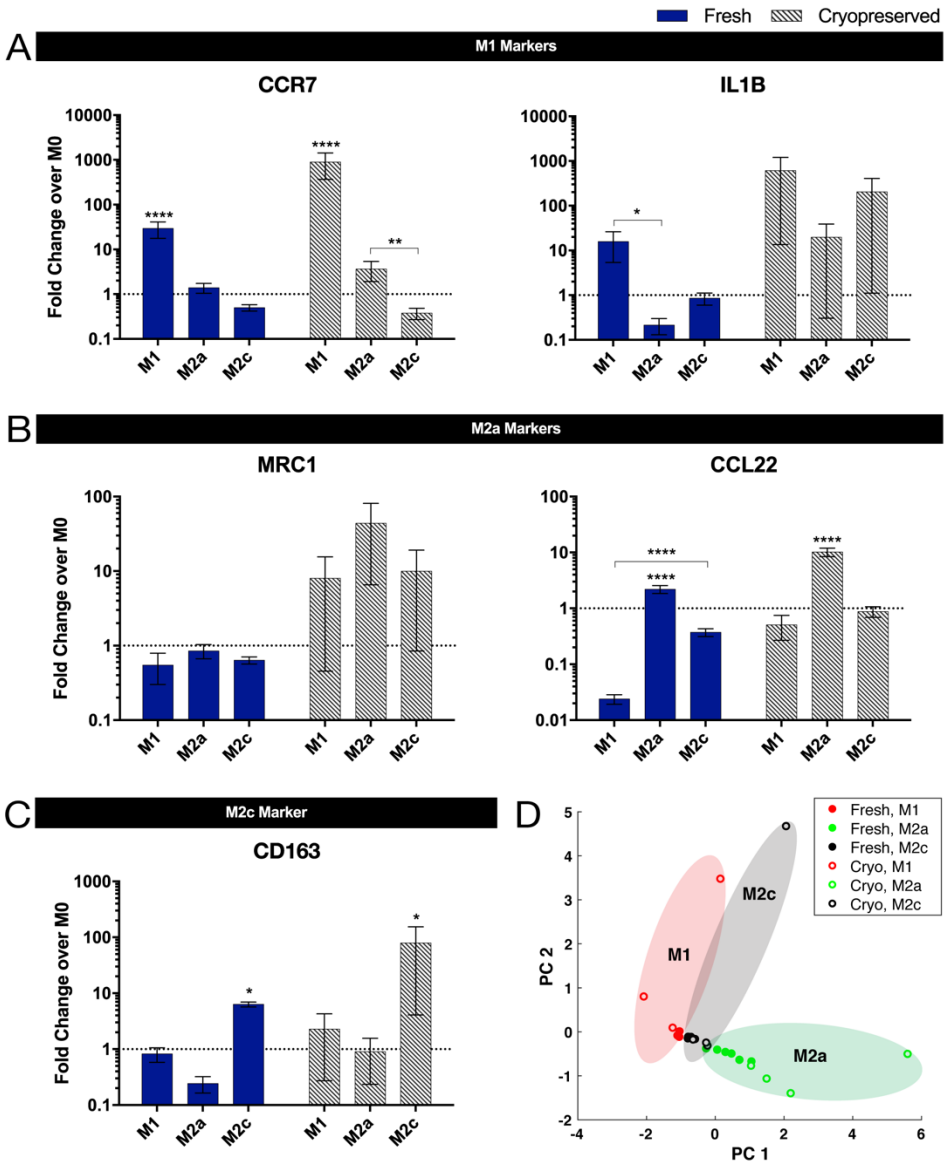

Figure 7.6. (A-C) Comparison between gene expression by cryopreserved macrophages and fresh macrophages from multiple donors; all cells were derived from negatively selected monocytes. Data represent mean change over M0 ± SEM. Statistical analysis was performed on log-transformed data using two-way ANOVA with Tukey's post hoc analysis. *$p < 0.05$, **$p < 0.01$, ****$p < 0.0001$ relative to all other groups; $n \geq 3$. (D) PCA comparing gene expression between freshly isolated and cryopreserved macrophages. Score plot of principal components 1 and 2 depicted, capturing 36.9% and 24.1% of the variance within the data, respectively. Macrophage phenotype indicted by blue (M0), red (M1), green (M2a) or black (M2c) shading.

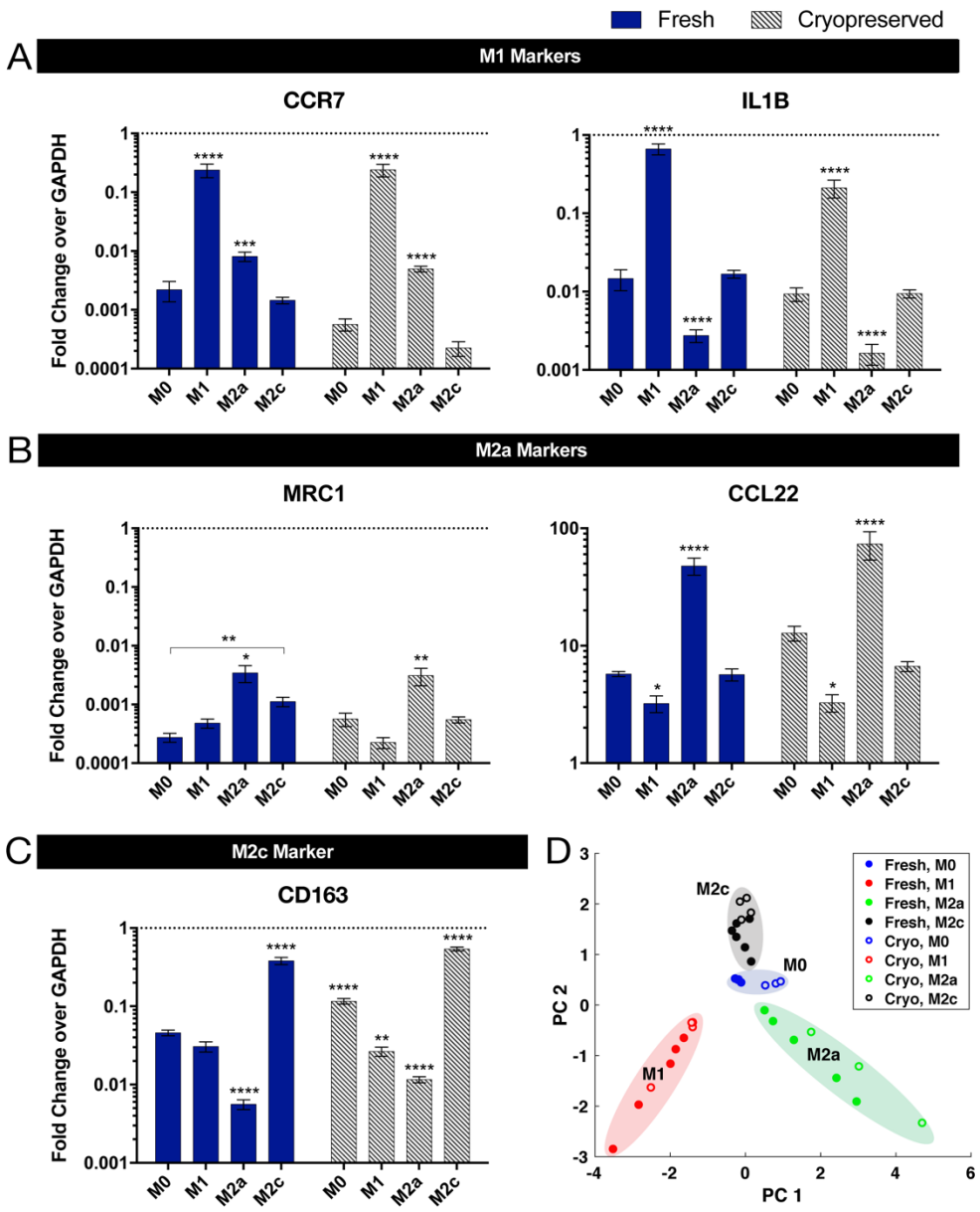

Figure 7.7. (A-C) Effects of cryopreservation on gene expression by macrophages derived from negatively selected monocytes from a single donor. Data represent mean fold change over *GAPDH* ± SEM. Statistical analysis was performed on log-transformed data using two-way ANOVA with Tukey's post hoc analysis. *$p < 0.05$, **$p < 0.01$, ***$p < 0.001$, ****$p < 0.0001$ relative to all other groups; $n \geq 3$. (D) PCA comparing gene expression between freshly isolated and cryopreserved macrophages. Score plot of principal components 1 and 2 depicted, capturing 48.7% and 29.8% of the variance within the data, respectively. Macrophage phenotype indicted by blue (M0), red (M1), green (M2a) or black (M2c) shading.

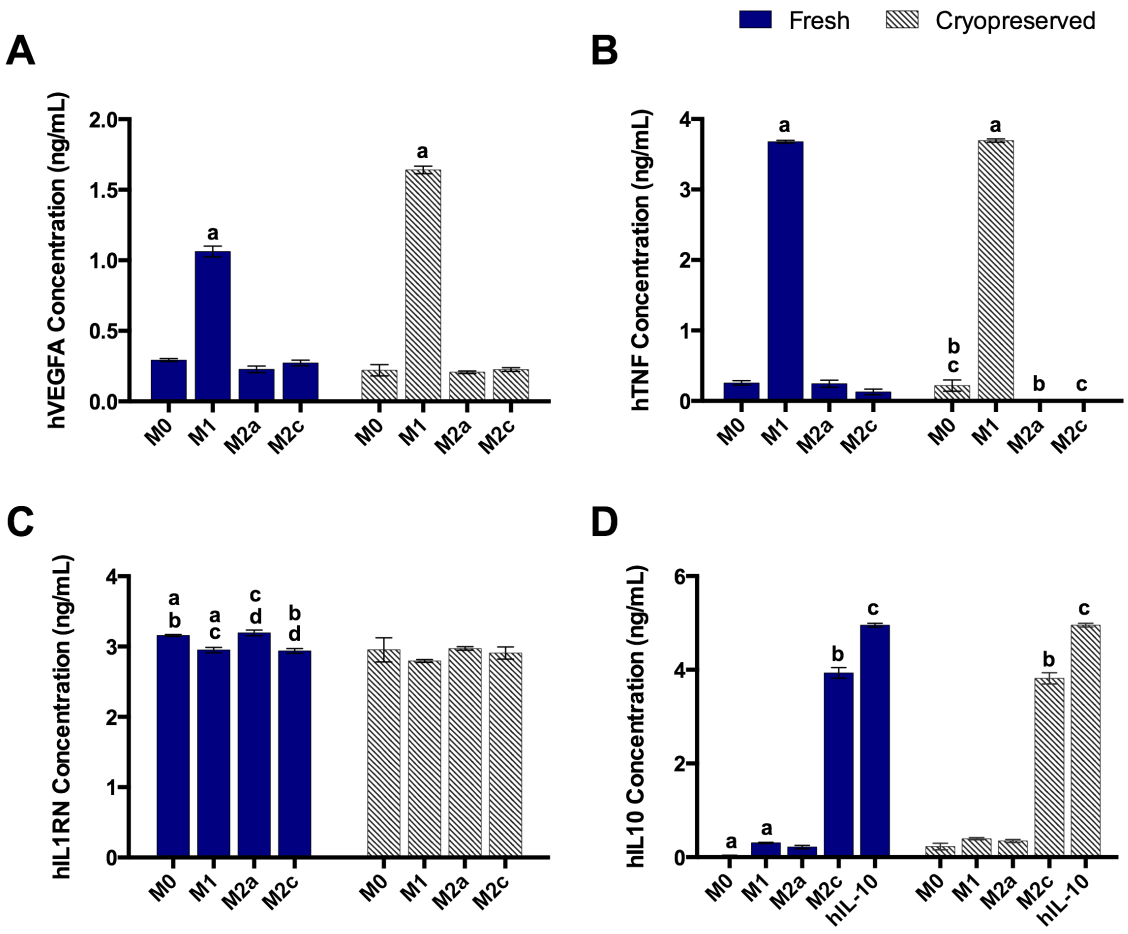

Figure 7.8. Effects of cryopreservation on protein secretion by macrophages derived from negatively selected monocytes. Data represent mean ± SEM. Corresponding letters indicate $p < 0.05$ using two-way ANOVA with Tukey's post hoc analysis; $n \geq 3$.

LIST OF REFERENCES

[1] 2015 Annual Data Report. Scientific Registry of Transplant Recipients. Available: http://srtr.transplant.hrsa.gov/annual_reports/Default.aspx. Accessed Dec 22 2017.

[2] R. Langer and J. P. Vacanti, "Tissue engineering," *Science,* vol. 260, no. 5110, pp. 920-6, May 14 1993.

[3] J. M. Anderson, A. Rodriguez, and D. T. Chang, "Foreign body reaction to biomaterials," *Semin Immunol,* vol. 20, no. 2, pp. 86-100, Apr 2008.

[4] S. Franz, S. Rammelt, D. Scharnweber, and J. C. Simon, "Immune responses to implants - a review of the implications for the design of immunomodulatory biomaterials," *Biomaterials,* vol. 32, no. 28, pp. 6692-709, Oct 2011.

[5] T. N. Demidova-Rice, J. T. Durham, and I. M. Herman, "Wound Healing Angiogenesis: Innovations and Challenges in Acute and Chronic Wound Healing," *Adv Wound Care (New Rochelle),* vol. 1, no. 1, pp. 17-22, Feb 2012.

[6] T. Velnar, T. Bailey, and V. Smrkolj, "The wound healing process: an overview of the cellular and molecular mechanisms," *J Int Med Res,* vol. 37, no. 5, pp. 1528-42, Sep-Oct 2009.

[7] S. J. Lee, J. J. Yoo, and A. Atala, "3.4.1 Acute Response to Biomaterials," in *In situ Tissue Regeneration - Host Cell Recruitment and Biomaterial Design*: Elsevier, 2016.

[8] J. M. Anderson, "Biological Responses to Materials," *Annual Review of Materials Research,* vol. 31, no. 1, pp. 81-110, 2001/08/01 2001.

[9] E. C. Novosel, C. Kleinhans, and P. J. Kluger, "Vascularization is the key challenge in tissue engineering," *Adv Drug Deliv Rev,* vol. 63, no. 4-5, pp. 300-11, Apr 30 2011.

[10] E. A. Phelps and A. J. Garcia, "Engineering more than a cell: vascularization strategies in tissue engineering," *Curr Opin Biotechnol,* vol. 21, no. 5, pp. 704-9, Oct 2010.

[11] J. Rouwkema, N. C. Rivron, and C. A. van Blitterswijk, "Vascularization in tissue engineering," *Trends Biotechnol,* vol. 26, no. 8, pp. 434-41, Aug 2008.

[12] E. C. Watson, Z. L. Grant, and L. Coultas, "Endothelial cell apoptosis in angiogenesis and vessel regression," *Cell Mol Life Sci,* vol. 74, no. 24, pp. 4387-4403, Dec 2017.

[13] I. Geudens and H. Gerhardt, "Coordinating cell behaviour during blood vessel formation," *Development,* vol. 138, no. 21, pp. 4569-83, Nov 2011.

[14] T. Kaully, K. Kaufman-Francis, A. Lesman, and S. Levenberg, "Vascularization--the conduit to viable engineered tissues," *Tissue Eng Part B Rev,* vol. 15, no. 2, pp. 159-69, Jun 2009.

[15] H. M. Eilken and R. H. Adams, "Dynamics of endothelial cell behavior in sprouting angiogenesis," *Curr Opin Cell Biol,* vol. 22, no. 5, pp. 617-25, Oct 2010.

[16] H. Gerhardt *et al.*, "VEGF guides angiogenic sprouting utilizing endothelial tip cell filopodia," *J Cell Biol,* vol. 161, no. 6, pp. 1163-77, Jun 23 2003.

[17] K. L. Marcelo, L. C. Goldie, and K. K. Hirschi, "Regulation of endothelial cell differentiation and specification," *Circ Res,* vol. 112, no. 9, pp. 1272-87, Apr 26 2013.

[18] R. C. Sainson *et al.*, "TNF primes endothelial cells for angiogenic sprouting by inducing a tip cell phenotype," *Blood,* vol. 111, no. 10, pp. 4997-5007, May 15 2008.

[19] R. Blanco and H. Gerhardt, "VEGF and Notch in tip and stalk cell selection," *Cold Spring Harb Perspect Med,* vol. 3, no. 1, p. a006569, Jan 1 2013.

[20] L. Jakobsson *et al.*, "Endothelial cells dynamically compete for the tip cell position during angiogenic sprouting," *Nat Cell Biol,* vol. 12, no. 10, pp. 943-53, Oct 2010.

[21] R. Benedito *et al.*, "The notch ligands Dll4 and Jagged1 have opposing effects on angiogenesis," *Cell,* vol. 137, no. 6, pp. 1124-35, Jun 12 2009.

[22] E. Caussinus, J. Colombelli, and M. Affolter, "Tip-cell migration controls stalk-cell intercalation during Drosophila tracheal tube elongation," *Curr Biol,* vol. 18, no. 22, pp. 1727-34, Nov 25 2008.

[23] L. K. Phng *et al.*, "Nrarp coordinates endothelial Notch and Wnt signaling to control vessel density in angiogenesis," *Dev Cell,* vol. 16, no. 1, pp. 70-82, Jan 2009.

[24] Y. Blum, H. G. Belting, E. Ellertsdottir, L. Herwig, F. Luders, and M. Affolter, "Complex cell rearrangements during intersegmental vessel sprouting and vessel fusion in the zebrafish embryo," *Dev Biol,* vol. 316, no. 2, pp. 312-22, Apr 15 2008.

[25] A. Fantin *et al.*, "Tissue macrophages act as cellular chaperones for vascular anastomosis downstream of VEGF-mediated endothelial tip cell induction," *Blood,* vol. 116, no. 5, pp. 829-40, Aug 5 2010.

[26] H. H. Outtz, I. W. Tattersall, N. M. Kofler, N. Steinbach, and J. Kitajewski, "Notch1 controls macrophage recruitment and Notch signaling is activated at sites of endothelial cell anastomosis during retinal angiogenesis in mice," *Blood,* vol. 118, no. 12, pp. 3436-9, Sep 22 2011.

[27] A. Pabois *et al.*, "Notch signaling mediates crosstalk between endothelial cells and macrophages via Dll4 and IL6 in cardiac microvascular inflammation," *Biochem Pharmacol,* vol. 104, pp. 95-107, Mar 15 2016.

[28] S. B. Coffelt *et al.*, "Angiopoietin-2 regulates gene expression in TIE2-expressing monocytes and augments their inherent proangiogenic functions," *Cancer Res,* vol. 70, no. 13, pp. 5270-80, Jul 1 2010.

[29] R. Lima e Silva *et al.*, "The SDF-1/CXCR4 ligand/receptor pair is an important contributor to several types of ocular neovascularization," *FASEB J,* vol. 21, no. 12, pp. 3219-30, Oct 2007.

[30] P. Lindblom *et al.*, "Endothelial PDGF-B retention is required for proper investment of pericytes in the microvessel wall," *Genes Dev,* vol. 17, no. 15, pp. 1835-40, Aug 1 2003.

[31] A. Armulik, A. Abramsson, and C. Betsholtz, "Endothelial/pericyte interactions," *Circ Res,* vol. 97, no. 6, pp. 512-23, Sep 16 2005.

[32] R. K. Jain, "Molecular regulation of vessel maturation," *Nat Med,* vol. 9, no. 6, pp. 685-93, Jun 2003.

[33] L. E. Benjamin, D. Golijanin, A. Itin, D. Pode, and E. Keshet, "Selective ablation of immature blood vessels in established human tumors follows vascular endothelial growth factor withdrawal," *J Clin Invest,* vol. 103, no. 2, pp. 159-65, Jan 1999.

[34] S. Dimmeler and A. M. Zeiher, "Endothelial cell apoptosis in angiogenesis and vessel regression," *Circ Res,* vol. 87, no. 6, pp. 434-9, Sep 15 2000.

[35] C. Korn and H. G. Augustin, "Mechanisms of Vessel Pruning and Regression," *Dev Cell,* vol. 34, no. 1, pp. 5-17, Jul 6 2015.

[36] E. C. Watson *et al.*, "Apoptosis regulates endothelial cell number and capillary vessel diameter but not vessel regression during retinal angiogenesis," *Development,* vol. 143, no. 16, pp. 2973-82, Aug 15 2016.

[37] C. A. Franco *et al.*, "Dynamic endothelial cell rearrangements drive developmental vessel regression," *PLoS Biol,* vol. 13, no. 4, p. e1002125, Apr 2015.

[38] S. Feng *et al.*, "Mechanical Activation of Hypoxia-Inducible Factor 1alpha Drives Endothelial Dysfunction at Atheroprone Sites," *Arterioscler Thromb Vasc Biol,* vol. 37, no. 11, pp. 2087-2101, Nov 2017.

[39] Y. C. Yung, J. Chae, M. J. Buehler, C. P. Hunter, and D. J. Mooney, "Cyclic tensile strain triggers a sequence of autocrine and paracrine signaling to regulate angiogenic sprouting in human vascular cells," *Proc Natl Acad Sci U S A,* vol. 106, no. 36, pp. 15279-84, Sep 8 2009.

[40] Y. J. Blinder, A. Freiman, N. Raindel, D. J. Mooney, and S. Levenberg, "Vasculogenic dynamics in 3D engineered tissue constructs," *Sci Rep,* vol. 5, p. 17840, 2015.

[41] R. Cao *et al.*, "Angiogenic synergism, vascular stability and improvement of hind-limb ischemia by a combination of PDGF-BB and FGF-2," *Nat Med,* vol. 9, no. 5, pp. 604-13, May 2003.

[42] H. K. Awada, N. R. Johnson, and Y. Wang, "Sequential delivery of angiogenic growth factors improves revascularization and heart function after myocardial infarction," *J Control Release,* vol. 207, pp. 7-17, Jun 10 2015.

[43] Y. Brudno, A. B. Ennett-Shepard, R. R. Chen, M. Aizenberg, and D. J. Mooney, "Enhancing microvascular formation and vessel maturation through temporal control over multiple pro-angiogenic and pro-maturation factors," *Biomaterials,* vol. 34, no. 36, pp. 9201-9, Dec 2013.

[44] Y. Bai, L. Bai, J. Zhou, H. Chen, and L. Zhang, "Sequential delivery of VEGF, FGF-2 and PDGF from the polymeric system enhance HUVECs angiogenesis in vitro and CAM angiogenesis," *Cell Immunol,* Oct 23 2017.

[45] C. W. Hsu *et al.*, "Improved Angiogenesis in Response to Localized Delivery of Macrophage-Recruiting Molecules," *PLoS One,* vol. 10, no. 7, p. e0131643, 2015.

[46] G. Cheng *et al.*, "Engineered blood vessel networks connect to host vasculature via wrapping-and-tapping anastomosis," *Blood,* vol. 118, no. 17, pp. 4740-9, Oct 27 2011.

[47] S. Levenberg *et al.*, "Engineering vascularized skeletal muscle tissue," *Nat Biotechnol,* vol. 23, no. 7, pp. 879-84, Jul 2005.

[48] X. Chen *et al.*, "Prevascularization of a fibrin-based tissue construct accelerates the formation of functional anastomosis with host vasculature," *Tissue Eng Part A,* vol. 15, no. 6, pp. 1363-71, Jun 2009.

[49] A. Lesman *et al.*, "Transplantation of a tissue-engineered human vascularized cardiac muscle," *Tissue Eng Part A,* vol. 16, no. 1, pp. 115-25, Jan 2010.

[50] S. Kusuma, Y. I. Shen, D. Hanjaya-Putra, P. Mali, L. Cheng, and S. Gerecht, "Self-organized vascular networks from human pluripotent stem cells in a synthetic matrix," *Proc Natl Acad Sci U S A,* vol. 110, no. 31, pp. 12601-6, Jul 30 2013.

[51] Q. Zhang *et al.*, "Engineering vascularized soft tissue flaps in an animal model using human adipose-derived stem cells and VEGF+PLGA/PEG microspheres on a collagen-chitosan scaffold with a flow-through vascular pedicle," *Biomaterials,* vol. 73, pp. 198-213, Dec 2015.

[52] D. B. Kolesky, K. A. Homan, M. A. Skylar-Scott, and J. A. Lewis, "Three-dimensional bioprinting of thick vascularized tissues," *Proc Natl Acad Sci U S A,* vol. 113, no. 12, pp. 3179-84, Mar 22 2016.

[53] J. S. Miller *et al.*, "Rapid casting of patterned vascular networks for perfusable engineered three-dimensional tissues," *Nat Mater,* vol. 11, no. 9, pp. 768-74, Sep 2012.

[54] P. J. Murray and T. A. Wynn, "Protective and pathogenic functions of macrophage subsets," *Nat Rev Immunol,* vol. 11, no. 11, pp. 723-37, Nov 2011.

[55] J. W. Godwin, A. R. Pinto, and N. A. Rosenthal, "Macrophages are required for adult salamander limb regeneration," *Proc Natl Acad Sci U S A,* vol. 110, no. 23, pp. 9415-20, Jun 4 2013.

[56] M. Summan *et al.*, "Macrophages and skeletal muscle regeneration: a clodronate-containing liposome depletion study," *Am J Physiol Regul Integr Comp Physiol,* vol. 290, no. 6, pp. R1488-95, Jun 2006.

[57] M. J. van Amerongen, M. C. Harmsen, N. van Rooijen, A. H. Petersen, and M. J. van Luyn, "Macrophage depletion impairs wound healing and increases left ventricular remodeling after myocardial injury in mice," *Am J Pathol,* vol. 170, no. 3, pp. 818-29, Mar 2007.

[58] N. Hibino *et al.*, "A critical role for macrophages in neovessel formation and the development of stenosis in tissue-engineered vascular grafts," *FASEB J,* vol. 25, no. 12, pp. 4253-63, Dec 2011.

[59] Y. Kubota *et al.*, "M-CSF inhibition selectively targets pathological angiogenesis and lymphangiogenesis," *J Exp Med,* vol. 206, no. 5, pp. 1089-102, May 11 2009.

[60] N. Hirose *et al.*, "The local injection of peritoneal macrophages induces neovascularization in rat ischemic hind limb muscles," *Cell Transplant,* vol. 17, no. 1-2, pp. 211-22, 2008.

[61] T. Hisatome, Y. Yasunaga, S. Yanada, Y. Tabata, Y. Ikada, and M. Ochi, "Neovascularization and bone regeneration by implantation of autologous bone marrow mononuclear cells," *Biomaterials,* vol. 26, no. 22, pp. 4550-6, Aug 2005.

[62] L. J. Raggatt *et al.*, "Fracture healing via periosteal callus formation requires macrophages for both initiation and progression of early endochondral ossification," *Am J Pathol,* vol. 184, no. 12, pp. 3192-204, Dec 2014.

[63] K. A. Alexander *et al.*, "Osteal macrophages promote in vivo intramembranous bone healing in a mouse tibial injury model," *J Bone Miner Res,* vol. 26, no. 7, pp. 1517-32, Jul 2011.

[64] L. Vi *et al.*, "Macrophages promote osteoblastic differentiation in-vivo: implications in fracture repair and bone homeostasis," *J Bone Miner Res,* vol. 30, no. 6, pp. 1090-102, Jun 2015.

[65] J. Xue *et al.*, "Transcriptome-based network analysis reveals a spectrum model of human macrophage activation," *Immunity,* vol. 40, no. 2, pp. 274-88, Feb 20 2014.

[66] Y. Lavin *et al.*, "Tissue-resident macrophage enhancer landscapes are shaped by the local microenvironment," *Cell,* vol. 159, no. 6, pp. 1312-26, Dec 4 2014.

[67] K. Brecht *et al.*, "Macrophages programmed by apoptotic cells promote angiogenesis via prostaglandin E2," *FASEB J,* vol. 25, no. 7, pp. 2408-17, Jul 2011.

[68] D. M. Mosser and J. P. Edwards, "Exploring the full spectrum of macrophage activation," *Nat Rev Immunol,* vol. 8, no. 12, pp. 958-69, Dec 2008.

[69] D. M. Schrijvers, G. R. De Meyer, M. M. Kockx, A. G. Herman, and W. Martinet, "Phagocytosis of apoptotic cells by macrophages is impaired in atherosclerosis," *Arterioscler Thromb Vasc Biol,* vol. 25, no. 6, pp. 1256-61, Jun 2005.

[70] K. L. Spiller *et al.*, "The role of macrophage phenotype in vascularization of tissue engineering scaffolds," *Biomaterials,* vol. 35, no. 15, pp. 4477-88, May 2014.

[71] C. A. Gleissner, I. Shaked, K. M. Little, and K. Ley, "CXC chemokine ligand 4 induces a unique transcriptome in monocyte-derived macrophages," *J Immunol,* vol. 184, no. 9, pp. 4810-8, May 1 2010.

[72] P. J. Murray *et al.*, "Macrophage activation and polarization: nomenclature and experimental guidelines," *Immunity,* vol. 41, no. 1, pp. 14-20, Jul 17 2014.

[73] R. M. Taylor, T. G. Kashima, H. J. Knowles, and N. A. Athanasou, "VEGF, FLT3 ligand, PlGF and HGF can substitute for M-CSF to induce human osteoclast formation: implications for giant cell tumour pathobiology," *Lab Invest,* vol. 92, no. 10, pp. 1398-406, Oct 2012.

[74] A. Mantovani, S. Sozzani, M. Locati, P. Allavena, and A. Sica, "Macrophage polarization: tumor-associated macrophages as a paradigm for polarized M2 mononuclear phagocytes," *Trends Immunol,* vol. 23, no. 11, pp. 549-55, Nov 2002.

[75] M. L. Novak, E. M. Weinheimer-Haus, and T. J. Koh, "Macrophage activation and skeletal muscle healing following traumatic injury," *J Pathol,* vol. 232, no. 3, pp. 344-55, Feb 2014.

[76] H. J. Anders and M. Ryu, "Renal microenvironments and macrophage phenotypes determine progression or resolution of renal inflammation and fibrosis," *Kidney Int,* vol. 80, no. 9, pp. 915-25, Nov 2011.

[77] W. J. Kao, A. K. McNally, A. Hiltner, and J. M. Anderson, "Role for interleukin-4 in foreign-body giant cell formation on a poly(etherurethane urea) in vivo," *J Biomed Mater Res,* vol. 29, no. 10, pp. 1267-75, Oct 1995.

[78] L. A. Murray *et al.*, "TGF-beta driven lung fibrosis is macrophage dependent and blocked by Serum amyloid P," *Int J Biochem Cell Biol,* vol. 43, no. 1, pp. 154-62, Jan 2011.

[79] G. Zizzo, B. A. Hilliard, M. Monestier, and P. L. Cohen, "Efficient clearance of early apoptotic cells by human macrophages requires M2c polarization and MerTK induction," *J Immunol,* vol. 189, no. 7, pp. 3508-20, Oct 1 2012.

[80] E. B. Lurier *et al.*, "Transcriptome analysis of IL-10-stimulated (M2c) macrophages by next-generation sequencing," *Immunobiology,* vol. 222, no. 7, pp. 847-856, Jul 2017.

[81] C. Schlundt *et al.*, "Macrophages in bone fracture healing: Their essential role in endochondral ossification," *Bone,* Oct 31 2015.

[82] L. Arnold *et al.*, "Inflammatory monocytes recruited after skeletal muscle injury switch into antiinflammatory macrophages to support myogenesis," *J Exp Med,* vol. 204, no. 5, pp. 1057-69, May 14 2007.

[83] K. L. Spiller *et al.*, "Sequential delivery of immunomodulatory cytokines to facilitate the M1-to-M2 transition of macrophages and enhance vascularization of bone scaffolds," *Biomaterials,* vol. 37, pp. 194-207, Jan 2015.

[84] B. J. Evans, D. O. Haskard, G. Sempowksi, and R. C. Landis, "Evolution of the Macrophage CD163 Phenotype and Cytokine Profiles in a Human Model of Resolving Inflammation," *Int J Inflam,* vol. 2013, p. 780502, 2013.

[85] J. S. Duffield *et al.*, "Selective depletion of macrophages reveals distinct, opposing roles during liver injury and repair," *J Clin Invest,* vol. 115, no. 1, pp. 56-65, Jan 2005.

[86] S. Nassiri, I. Zakeri, M. S. Weingarten, and K. L. Spiller, "Relative Expression of Proinflammatory and Antiinflammatory Genes Reveals Differences between Healing and Nonhealing Human Chronic Diabetic Foot Ulcers," *J Invest Dermatol,* vol. 135, no. 6, pp. 1700-3, Jun 2015.

[87] S. F. Badylak, J. E. Valentin, A. K. Ravindra, G. P. McCabe, and A. M. Stewart-Akers, "Macrophage phenotype as a determinant of biologic scaffold remodeling," *Tissue Eng Part A,* vol. 14, no. 11, pp. 1835-42, Nov 2008.

[88] M. T. Wolf, Y. Vodovotz, S. Tottey, B. N. Brown, and S. F. Badylak, "Predicting in vivo responses to biomaterials via combined in vitro and in silico analysis," *Tissue Eng Part C Methods,* vol. 21, no. 2, pp. 148-59, Feb 2015.

[89] C. Costa, J. Incio, and R. Soares, "Angiogenesis and chronic inflammation: cause or consequence?," *Angiogenesis,* vol. 10, no. 3, pp. 149-66, 2007.

[90] M. Barbeck *et al.*, "Monocyte preseeding leads to an increased implant bed vascularization of biphasic calcium phosphate bone substitutes via vessel maturation," *J Biomed Mater Res A,* vol. 104, no. 12, pp. 2928-2935, Dec 2016.

[91] E. M. Moore, G. Ying, and J. L. West, "Macrophages Influence Vessel Formation in 3D Bioactive Hydrogels," *Advanced Biosystems,* vol. 1, no. 3, pp. 1600021-n/a, 2017, Art. no. 1600021.

[92] M. Anghelina, P. Krishnan, L. Moldovan, and N. I. Moldovan, "Monocytes and macrophages form branched cell columns in matrigel: implications for a role in neovascularization," *Stem Cells Dev,* vol. 13, no. 6, pp. 665-76, Dec 2004.

[93] M. Anghelina, P. Krishnan, L. Moldovan, and N. I. Moldovan, "Monocytes/macrophages cooperate with progenitor cells during neovascularization and tissue repair: conversion of cell columns into fibrovascular bundles," *Am J Pathol,* vol. 168, no. 2, pp. 529-41, Feb 2006.

[94] N. I. Moldovan, P. J. Goldschmidt-Clermont, J. Parker-Thornburg, S. D. Shapiro, and P. E. Kolattukudy, "Contribution of monocytes/macrophages to compensatory neovascularization: the drilling of metalloelastase-positive tunnels in ischemic myocardium," *Circ Res,* vol. 87, no. 5, pp. 378-84, Sep 1 2000.

[95] S. Willenborg *et al.*, "CCR2 recruits an inflammatory macrophage subpopulation critical for angiogenesis in tissue repair," *Blood,* vol. 120, no. 3, pp. 613-25, Jul 19 2012.

[96] N. Jetten, S. Verbruggen, M. J. Gijbels, M. J. Post, M. P. De Winther, and M. M. Donners, "Anti-inflammatory M2, but not pro-inflammatory M1 macrophages promote angiogenesis in vivo," *Angiogenesis,* vol. 17, no. 1, pp. 109-18, Jan 2014.

[97] T. Lucas *et al.*, "Differential roles of macrophages in diverse phases of skin repair," *J Immunol,* vol. 184, no. 7, pp. 3964-77, Apr 1 2010.

[98] R. Mirza, L. A. DiPietro, and T. J. Koh, "Selective and specific macrophage ablation is detrimental to wound healing in mice," *Am J Pathol,* vol. 175, no. 6, pp. 2454-62, Dec 2009.

[99] E. M. Sussman, M. C. Halpin, J. Muster, R. T. Moon, and B. D. Ratner, "Porous implants modulate healing and induce shifts in local macrophage polarization in the foreign body reaction," *Ann Biomed Eng,* vol. 42, no. 7, pp. 1508-16, Jul 2014.

[100] T. Yu *et al.*, "Temporal and spatial distribution of macrophage phenotype markers in the foreign body response to glutaraldehyde-crosslinked gelatin hydrogels," *J Biomater Sci Polym Ed,* vol. 27, no. 8, pp. 721-42, 2016.

[101] P. L. Graney, E. B. Lurier, and K. L. Spiller, "Biomaterials and Bioactive Factor Delivery Systems for the Control of Macrophage Activation in Regenerative Medicine," *ACS Biomaterials Science & Engineering,* 2017/02/15 2017.

[102] A. Vishwakarma *et al.*, "Engineering Immunomodulatory Biomaterials To Tune the Inflammatory Response," *Trends Biotechnol,* vol. 34, no. 6, pp. 470-82, Jun 2016.

[103] H. Laroui *et al.*, "Functional TNFalpha gene silencing mediated by polyethyleneimine/TNFalpha siRNA nanocomplexes in inflamed colon," *Biomaterials,* vol. 32, no. 4, pp. 1218-28, Feb 2011.

[104] S. J. Lee *et al.*, "TNF-alpha gene silencing using polymerized siRNA/thiolated glycol chitosan nanoparticles for rheumatoid arthritis," *Mol Ther,* vol. 22, no. 2, pp. 397-408, Feb 2014.

[105] S. Jain, T. H. Tran, and M. Amiji, "Macrophage repolarization with targeted alginate nanoparticles containing IL-10 plasmid DNA for the treatment of experimental arthritis," *Biomaterials,* vol. 61, pp. 162-77, Aug 2015.

[106] E. C. Leal *et al.*, "Substance P promotes wound healing in diabetes by modulating inflammation and macrophage phenotype," *Am J Pathol,* vol. 185, no. 6, pp. 1638-48, Jun 2015.

[107] D. J. Marks *et al.*, "Defective acute inflammation in Crohn's disease: a clinical investigation," *Lancet,* vol. 367, no. 9511, pp. 668-78, Feb 25 2006.

[108] K. Maruyama, J. Asai, M. Ii, T. Thorne, D. W. Losordo, and P. A. D'Amore, "Decreased macrophage number and activation lead to reduced lymphatic vessel formation and contribute to impaired diabetic wound healing," *Am J Pathol,* vol. 170, no. 4, pp. 1178-91, Apr 2007.

[109] H. Yin *et al.*, "A bioengineered drug-Eluting scaffold accelerated cutaneous wound healing In diabetic mice," *Colloids Surf B Biointerfaces,* vol. 145, pp. 226-231, Sep 1 2016.

[110] D. Hachim, S. T. LoPresti, C. C. Yates, and B. N. Brown, "Shifts in macrophage phenotype at the biomaterial interface via IL-4 eluting coatings are associated with improved implant integration," *Biomaterials,* vol. 112, pp. 95-107, Jan 2017.

[111] T. Harel-Adar, T. Ben Mordechai, Y. Amsalem, M. S. Feinberg, J. Leor, and S. Cohen, "Modulation of cardiac macrophages by phosphatidylserine-presenting liposomes improves infarct repair," *Proc Natl Acad Sci U S A,* vol. 108, no. 5, pp. 1827-32, Feb 1 2011.

[112] S. Minardi *et al.*, "IL-4 Release from a Biomimetic Scaffold for the Temporally Controlled Modulation of Macrophage Response," *Ann Biomed Eng,* vol. 44, no. 6, pp. 2008-19, Jun 2016.

[113] F. Ma *et al.*, "Macrophage-stimulated cardiac fibroblast production of IL-6 is essential for TGF beta/Smad activation and cardiac fibrosis induced by angiotensin II," *PLoS One,* vol. 7, no. 5, p. e35144, 2012.

[114] D. T. Ploeger, N. A. Hosper, M. Schipper, J. A. Koerts, S. de Rond, and R. A. Bank, "Cell plasticity in wound healing: paracrine factors of M1/ M2 polarized macrophages influence the phenotypical state of dermal fibroblasts," *Cell Commun Signal,* vol. 11, no. 1, p. 29, Apr 19 2013.

[115] V. A. Kumar, N. L. Taylor, S. Shi, N. C. Wickremasinghe, R. N. D'Souza, and J. D. Hartgerink, "Self-assembling multidomain peptides tailor biological responses through biphasic release," *Biomaterials,* vol. 52, pp. 71-8, Jun 2015.

[116] R. A. Carano and E. H. Filvaroff, "Angiogenesis and bone repair," *Drug Discov Today,* vol. 8, no. 21, pp. 980-9, Nov 1 2003.

[117] M. R. Hausman and B. D. Rinker, "Intractable wounds and infections: the role of impaired vascularity and advanced surgical methods for treatment," *Am J Surg,* vol. 187, no. 5A, pp. 44S-55S, May 2004.

[118] R. R. Betz, "Limitations of autograft and allograft: new synthetic solutions," *Orthopedics,* vol. 25, no. 5 Suppl, pp. s561-70, May 2002.

[119] M. I. Santos and R. L. Reis, "Vascularization in bone tissue engineering: physiology, current strategies, major hurdles and future challenges," *Macromol Biosci,* vol. 10, no. 1, pp. 12-27, Jan 11 2010.

[120] J. M. Karnes, S. D. Daffner, and C. M. Watkins, "Multiple roles of tumor necrosis factor-alpha in fracture healing," *Bone,* vol. 78, pp. 87-93, Sep 2015.

[121] P. M. Mountziaris, P. P. Spicer, F. K. Kasper, and A. G. Mikos, "Harnessing and modulating inflammation in strategies for bone regeneration," *Tissue Eng Part B Rev,* vol. 17, no. 6, pp. 393-402, Dec 2011.

[122] V. E. Santo, M. E. Gomes, J. F. Mano, and R. L. Reis, "Controlled release strategies for bone, cartilage, and osteochondral engineering--Part I: recapitulation of native tissue healing and variables for the design of delivery systems," *Tissue Eng Part B Rev,* vol. 19, no. 4, pp. 308-26, Aug 2013.

[123] A. Schindeler, M. M. McDonald, P. Bokko, and D. G. Little, "Bone remodeling during fracture repair: The cellular picture," *Semin Cell Dev Biol,* vol. 19, no. 5, pp. 459-66, Oct 2008.

[124] R. Marsell and T. A. Einhorn, "The biology of fracture healing," *Injury,* vol. 42, no. 6, pp. 551-5, Jun 2011.

[125] J. M. Kanczler and R. O. Oreffo, "Osteogenesis and angiogenesis: the potential for engineering bone," *Eur Cell Mater,* vol. 15, pp. 100-14, 2008.

[126] J. Street *et al.*, "Vascular endothelial growth factor stimulates bone repair by promoting angiogenesis and bone turnover," *Proc Natl Acad Sci U S A,* vol. 99, no. 15, pp. 9656-61, Jul 23 2002.

[127] O. Grundnes and O. Reikeras, "The importance of the hematoma for fracture healing in rats," *Acta Orthop Scand,* vol. 64, no. 3, pp. 340-2, Jun 1993.

[128] S. H. Park, M. Silva, W. J. Bahk, H. McKellop, and J. R. Lieberman, "Effect of repeated irrigation and debridement on fracture healing in an animal model," *J Orthop Res,* vol. 20, no. 6, pp. 1197-204, Nov 2002.

[129] L. C. Gerstenfeld *et al.*, "Impaired fracture healing in the absence of TNF-alpha signaling: the role of TNF-alpha in endochondral cartilage resorption," *J Bone Miner Res,* vol. 18, no. 9, pp. 1584-92, Sep 2003.

[130] W. Lehmann *et al.*, "Tumor necrosis factor alpha (TNF-alpha) coordinately regulates the expression of specific matrix metalloproteinases (MMPS) and angiogenic factors during fracture healing," *Bone,* vol. 36, no. 2, pp. 300-10, Feb 2005.

[131] G. E. Glass, J. K. Chan, A. Freidin, M. Feldmann, N. J. Horwood, and J. Nanchahal, "TNF-alpha promotes fracture repair by augmenting the recruitment and differentiation of muscle-derived stromal cells," *Proc Natl Acad Sci U S A,* vol. 108, no. 4, pp. 1585-90, Jan 25 2011.

[132] Z. Lu *et al.*, "Activation and promotion of adipose stem cells by tumour necrosis factor-alpha preconditioning for bone regeneration," *J Cell Physiol,* vol. 228, no. 8, pp. 1737-44, Aug 2013.

[133] K. Schmidt-Bleek *et al.*, "Inflammatory phase of bone healing initiates the regenerative healing cascade," *Cell Tissue Res,* vol. 347, no. 3, pp. 567-73, Mar 2012.

[134] D. L. Hutton, R. Kondragunta, E. M. Moore, B. P. Hung, X. Jia, and W. L. Grayson, "Tumor necrosis factor improves vascularization in osteogenic grafts engineered with human adipose-derived stem/stromal cells," *PLoS One,* vol. 9, no. 9, p. e107199, 2014.

[135] B. J. Kwee and D. J. Mooney, "Manipulating the intersection of angiogenesis and inflammation," *Ann Biomed Eng,* vol. 43, no. 3, pp. 628-40, Mar 2015.

[136] Z. Chen, C. Wu, W. Gu, T. Klein, R. Crawford, and Y. Xiao, "Osteogenic differentiation of bone marrow MSCs by beta-tricalcium phosphate stimulating macrophages via BMP2 signalling pathway," *Biomaterials,* vol. 35, no. 5, pp. 1507-18, Feb 2014.

[137] Z. Chen, J. Yuen, R. Crawford, J. Chang, C. Wu, and Y. Xiao, "The effect of osteoimmunomodulation on the osteogenic effects of cobalt incorporated beta-tricalcium phosphate," *Biomaterials,* vol. 61, pp. 126-38, Aug 2015.

[138] A. L. Gamblin *et al.*, "Bone tissue formation with human mesenchymal stem cells and biphasic calcium phosphate ceramics: the local implication of osteoclasts and macrophages," *Biomaterials,* vol. 35, no. 36, pp. 9660-7, Dec 2014.

[139] E. Seebach, H. Freischmidt, J. Holschbach, J. Fellenberg, and W. Richter, "Mesenchymal stroma cells trigger early attraction of M1 macrophages and endothelial cells into fibrin hydrogels, stimulating long bone healing without long-term engraftment," *Acta Biomater,* vol. 10, no. 11, pp. 4730-41, Nov 2014.

[140] N. J. Lakhkar, I. H. Lee, H. W. Kim, V. Salih, I. B. Wall, and J. C. Knowles, "Bone formation controlled by biologically relevant inorganic ions: role and controlled delivery from phosphate-based glasses," *Adv Drug Deliv Rev,* vol. 65, no. 4, pp. 405-20, Apr 2013.

[141] B. Chehroudi, S. Ghrebi, H. Murakami, J. D. Waterfield, G. Owen, and D. M. Brunette, "Bone formation on rough, but not polished, subcutaneously implanted Ti surfaces is preceded by macrophage accumulation," *J Biomed Mater Res A,* vol. 93, no. 2, pp. 724-37, May 2010.

[142] M. Bartneck, V. A. Schulte, N. E. Paul, M. Diez, M. C. Lensen, and G. Zwadlo-Klarwasser, "Induction of specific macrophage subtypes by defined micro-patterned structures," *Acta Biomater,* vol. 6, no. 10, pp. 3864-72, Oct 2010.

[143] A. K. Blakney, M. D. Swartzlander, and S. J. Bryant, "The effects of substrate stiffness on the in vitro activation of macrophages and in vivo host response to poly(ethylene glycol)-based hydrogels," *J Biomed Mater Res A,* vol. 100, no. 6, pp. 1375-86, Jun 2012.

[144] R. Guo, A. R. Merkel, J. A. Sterling, J. M. Davidson, and S. A. Guelcher, "Substrate modulus of 3D-printed scaffolds regulates the regenerative response in subcutaneous implants through the macrophage phenotype and Wnt signaling," *Biomaterials,* vol. 73, pp. 85-95, Dec 2015.

[145] C. Cheung, "The future of bone healing," *Clin Podiatr Med Surg,* vol. 22, no. 4, pp. 631-41 viii, Oct 2005.

[146] A. C. Wu, L. J. Raggatt, K. A. Alexander, and A. R. Pettit, "Unraveling macrophage contributions to bone repair," *Bonekey Rep,* vol. 2, p. 373, 2013.

[147] K. A. Barth, J. D. Waterfield, and D. M. Brunette, "The effect of surface roughness on RAW 264.7 macrophage phenotype," *J Biomed Mater Res A,* vol. 101, no. 9, pp. 2679-88, Sep 2013.

[148] E. F. Irwin, K. Saha, M. Rosenbluth, L. J. Gamble, D. G. Castner, and K. E. Healy, "Modulus-dependent macrophage adhesion and behavior," *J Biomater Sci Polym Ed,* vol. 19, no. 10, pp. 1363-82, 2008.

[149] J. Y. Wang, B. H. Wicklund, R. B. Gustilo, and D. T. Tsukayama, "Titanium, chromium and cobalt ions modulate the release of bone-associated cytokines by human monocytes/macrophages in vitro," *Biomaterials,* vol. 17, no. 23, pp. 2233-40, Dec 1996.

[150] W. Zhang *et al.*, "The synergistic effect of hierarchical micro/nano-topography and bioactive ions for enhanced osseointegration," *Biomaterials,* vol. 34, no. 13, pp. 3184-95, Apr 2013.

[151] S. I. Roohani-Esfahani, C. R. Dunstan, B. Davies, S. Pearce, R. Williams, and H. Zreiqat, "Repairing a critical-sized bone defect with highly porous modified and unmodified baghdadite scaffolds," *Acta Biomater,* vol. 8, no. 11, pp. 4162-72, Nov 2012.

[152] S. I. Roohani-Esfahani *et al.*, "Unique microstructural design of ceramic scaffolds for bone regeneration under load," *Acta Biomater,* vol. 9, no. 6, pp. 7014-24, Jun 2013.

[153] S. I. Roohani-Esfahani, P. Newman, and H. Zreiqat, "Design and Fabrication of 3D printed Scaffolds with a Mechanical Strength Comparable to Cortical Bone to Repair Large Bone Defects," *Sci Rep,* vol. 6, p. 19468, 2016.

[154] J. J. Li *et al.*, "Efficacy of novel synthetic bone substitutes in the reconstruction of large segmental bone defects in sheep tibiae," *Biomed Mater,* vol. 11, no. 1, p. 015016, Feb 2016.

[155] Y. Ramaswamy, C. Wu, A. Van Hummel, V. Combes, G. Grau, and H. Zreiqat, "The responses of osteoblasts, osteoclasts and endothelial cells to zirconium modified calcium-silicate-based ceramic," *Biomaterials,* vol. 29, no. 33, pp. 4392-402, Nov 2008.

[156] Z. Lu, G. Wang, I. Roohani-Esfahani, C. R. Dunstan, and H. Zreiqat, "Baghdadite ceramics modulate the cross talk between human adipose stem cells and osteoblasts for bone regeneration," *Tissue Eng Part A,* vol. 20, no. 5-6, pp. 992-1002, Mar 2014.

[157] G. Wang *et al.*, "Effects of Sr-HT-Gahnite on osteogenesis and angiogenesis by adipose derived stem cells for critical-sized calvarial defect repair," *Sci Rep,* vol. 7, p. 41135, Jan 20 2017.

[158] P. L. Graney, S. I. Roohani-Esfahani, H. Zreiqat, and K. L. Spiller, "In vitro response of macrophages to ceramic scaffolds used for bone regeneration," *J R Soc Interface,* vol. 13, no. 120, Jul 2016.

[159] E. Quinlan, S. Partap, M. M. Azevedo, G. Jell, M. M. Stevens, and F. J. O'Brien, "Hypoxia-mimicking bioactive glass/collagen glycosaminoglycan composite scaffolds to enhance angiogenesis and bone repair," *Biomaterials,* vol. 52, pp. 358-66, Jun 2015.

[160] C. E. Witherel, P. L. Graney, D. O. Freytes, M. S. Weingarten, and K. L. Spiller, "Response of human macrophages to wound matrices in vitro," *Wound Repair Regen,* Feb 13 2016.

[161] M. Ringner, "What is principal component analysis?," *Nat Biotechnol,* vol. 26, no. 3, pp. 303-4, Mar 2008.

[162] K. L. Spiller, S. Nassiri, P. Raman, R. Rajagopalan, M. Sarmandy, and M. S. Weingarten, "Discovery of a novel M2c macrophage gene expression signature indicates a major role in human wound healing [abstract]," *Wound Repair and Regeneration,* vol. 23, no. 2, p. A40, Mar 2015.

[163] C. Colnot, Z. Thompson, T. Miclau, Z. Werb, and J. A. Helms, "Altered fracture repair in the absence of MMP9," *Development,* vol. 130, no. 17, pp. 4123-33, Sep 2003.

[164] M. M. McDonald *et al.*, "Matrix metalloproteinase-driven endochondral fracture union proceeds independently of osteoclast activity," *J Bone Miner Res,* vol. 28, no. 7, pp. 1550-60, Jul 2013.

[165] C. E. Pedraza, L. G. Nikolcheva, M. T. Kaartinen, J. E. Barralet, and M. D. McKee, "Osteopontin functions as an opsonin and facilitates phagocytosis by macrophages of hydroxyapatite-coated microspheres: implications for bone wound healing," *Bone,* vol. 43, no. 4, pp. 708-16, Oct 2008.

[166] C. L. Duvall, W. R. Taylor, D. Weiss, A. M. Wojtowicz, and R. E. Guldberg, "Impaired angiogenesis, early callus formation, and late stage remodeling in fracture healing of osteopontin-deficient mice," *J Bone Miner Res,* vol. 22, no. 2, pp. 286-97, Feb 2007.

[167] H. Mohammadi *et al.*, "Bioinorganics in bioactive calcium silicate ceramics for bone tissue repair: bioactivity and biological properties," *J Ceram Sci Tech,* vol. 5, no. 1, pp. 1-12, 2014.

[168] G. A. Obando-Pereda, L. Fischer, and D. R. Stach-Machado, "Titanium and zirconia particle-induced pro-inflammatory gene expression in cultured macrophages and osteolysis, inflammatory hyperalgesia and edema in vivo," *Life Sci,* vol. 97, no. 2, pp. 96-106, Mar 3 2014.

[169] E. Gentleman *et al.*, "The effects of strontium-substituted bioactive glasses on osteoblasts and osteoclasts in vitro," *Biomaterials,* vol. 31, no. 14, pp. 3949-56, May 2010.

[170] B. Bao, A. S. Prasad, F. W. Beck, and M. Godmere, "Zinc modulates mRNA levels of cytokines," *Am J Physiol Endocrinol Metab,* vol. 285, no. 5, pp. E1095-102, Nov 2003.

[171] W. G. Brodbeck, Y. Nakayama, T. Matsuda, E. Colton, N. P. Ziats, and J. M. Anderson, "Biomaterial surface chemistry dictates adherent monocyte/macrophage cytokine expression in vitro," *Cytokine,* vol. 18, no. 6, pp. 311-9, Jun 21 2002.

[172] N. E. Paul *et al.*, "Topographical control of human macrophages by a regularly microstructured polyvinylidene fluoride surface," *Biomaterials,* vol. 29, no. 30, pp. 4056-64, Oct 2008.

[173] H. Duan *et al.*, "Transcriptome analyses reveal molecular mechanisms underlying functional recovery after spinal cord injury," *Proc Natl Acad Sci U S A,* vol. 112, no. 43, pp. 13360-5, Oct 27 2015.

[174] M. Becker *et al.*, "Integrated Transcriptomics Establish Macrophage Polarization Signatures and have Potential Applications for Clinical Health and Disease," *Sci Rep,* vol. 5, p. 13351, 2015.

[175] F. O. Martinez, S. Gordon, M. Locati, and A. Mantovani, "Transcriptional profiling of the human monocyte-to-macrophage differentiation and polarization: new molecules and patterns of gene expression," *J Immunol,* vol. 177, no. 10, pp. 7303-11, Nov 15 2006.

[176] H. He *et al.*, "Endothelial cells provide an instructive niche for the differentiation and functional polarization of M2-like macrophages," *Blood,* vol. 120, no. 15, pp. 3152-62, Oct 11 2012.

[177] M. Bohgaki and H. Kitaguchi, "Conversion of cultured monocytes/macrophages into endothelial-like cells through direct contact with endothelial cells," *Int J Hematol,* vol. 86, no. 1, pp. 42-8, Jul 2007.

[178] M. S. Njock *et al.*, "Endothelial cells suppress monocyte activation through secretion of extracellular vesicles containing antiinflammatory microRNAs," *Blood,* vol. 125, no. 20, pp. 3202-12, May 14 2015.

[179] A. N. Stratman, M. J. Davis, and G. E. Davis, "VEGF and FGF prime vascular tube morphogenesis and sprouting directed by hematopoietic stem cell cytokines," *Blood,* vol. 117, no. 14, pp. 3709-19, Apr 7 2011.

[180] J. Capote *et al.*, "Osteopontin ablation ameliorates muscular dystrophy by shifting macrophages to a pro-regenerative phenotype," *J Cell Biol,* vol. 213, no. 2, pp. 275-88, Apr 25 2016.

[181] J. Dai *et al.*, "Osteopontin induces angiogenesis through activation of PI3K/AKT and ERK1/2 in endothelial cells," *Oncogene,* vol. 28, no. 38, pp. 3412-22, Sep 24 2009.

[182] V. A. Fadok, D. L. Bratton, A. Konowal, P. W. Freed, J. Y. Westcott, and P. M. Henson, "Macrophages that have ingested apoptotic cells in vitro inhibit proinflammatory cytokine production through autocrine/paracrine mechanisms involving TGF-beta, PGE2, and PAF," *J Clin Invest,* vol. 101, no. 4, pp. 890-8, Feb 15 1998.

[183] M. Climent, M. Quintavalle, M. Miragoli, J. Chen, G. Condorelli, and L. Elia, "TGFbeta Triggers miR-143/145 Transfer From Smooth Muscle Cells to Endothelial Cells, Thereby Modulating Vessel Stabilization," *Circ Res,* vol. 116, no. 11, pp. 1753-64, May 22 2015.

[184] C. W. Law, Y. Chen, W. Shi, and G. K. Smyth, "voom: precision weights unlock linear model analysis tools for RNA-seq read counts," *Genome Biology,* journal article vol. 15, no. 2, p. R29, February 03 2014.

[185] M. Ashburner *et al.*, "Gene ontology: tool for the unification of biology. The Gene Ontology Consortium," *Nat Genet,* vol. 25, no. 1, pp. 25-9, May 2000.

[186] H. Mi *et al.*, "PANTHER version 11: expanded annotation data from Gene Ontology and Reactome pathways, and data analysis tool enhancements," *Nucleic Acids Res,* vol. 45, no. D1, pp. D183-D189, Jan 4 2017.

[187] C. The Gene Ontology, "Expansion of the Gene Ontology knowledgebase and resources," *Nucleic Acids Res,* vol. 45, no. D1, pp. D331-D338, Jan 4 2017.

[188] Y. Benjamini, A. M. Krieger, and D. Yekutieli, "Adaptive Linear Step-up Procedures That Control the False Discovery Rate," *Biometrika,* vol. 93, no. 3, pp. 491-507, 2006.

[189] S. Yang, J. Graham, J. W. Kahn, E. A. Schwartz, and M. E. Gerritsen, "Functional roles for PECAM-1 (CD31) and VE-cadherin (CD144) in tube assembly and lumen formation in three-dimensional collagen gels," *Am J Pathol,* vol. 155, no. 3, pp. 887-95, Sep 1999.

[190] H. M. DeLisser *et al.*, "Involvement of endothelial PECAM-1/CD31 in angiogenesis," *Am J Pathol,* vol. 151, no. 3, pp. 671-7, Sep 1997.

[191] G. Cao, M. L. Fehrenbach, J. T. Williams, J. M. Finklestein, J. X. Zhu, and H. M. Delisser, "Angiogenesis in platelet endothelial cell adhesion molecule-1-null mice," *Am J Pathol,* vol. 175, no. 2, pp. 903-15, Aug 2009.

[192] M. De Palma *et al.*, "Tie2 identifies a hematopoietic lineage of proangiogenic monocytes required for tumor vessel formation and a mesenchymal population of pericyte progenitors," *Cancer Cell,* vol. 8, no. 3, pp. 211-26, Sep 2005.

[193] M. A. Venneri *et al.*, "Identification of proangiogenic TIE2-expressing monocytes (TEMs) in human peripheral blood and cancer," *Blood,* vol. 109, no. 12, pp. 5276-85, Jun 15 2007.

[194] A. S. Patel *et al.*, "TIE2-expressing monocytes/macrophages regulate revascularization of the ischemic limb," *EMBO Mol Med,* vol. 5, no. 6, pp. 858-69, Jun 2013.

[195] T. N. Sato *et al.*, "Distinct roles of the receptor tyrosine kinases Tie-1 and Tie-2 in blood vessel formation," *Nature,* vol. 376, no. 6535, pp. 70-4, Jul 6 1995.

[196] S. Patan, "TIE1 and TIE2 receptor tyrosine kinases inversely regulate embryonic angiogenesis by the mechanism of intussusceptive microvascular growth," *Microvasc Res,* vol. 56, no. 1, pp. 1-21, Jul 1998.

[197] R. del Toro *et al.*, "Identification and functional analysis of endothelial tip cell-enriched genes," *Blood,* vol. 116, no. 19, pp. 4025-33, Nov 11 2010.

[198] N. Oda, M. Abe, and Y. Sato, "ETS-1 converts endothelial cells to the angiogenic phenotype by inducing the expression of matrix metalloproteinases and integrin beta3," *J Cell Physiol,* vol. 178, no. 2, pp. 121-32, Feb 1999.

[199] C. Iwasaka, K. Tanaka, M. Abe, and Y. Sato, "Ets-1 regulates angiogenesis by inducing the expression of urokinase-type plasminogen activator and matrix metalloproteinase-1 and the migration of vascular endothelial cells," *J Cell Physiol,* vol. 169, no. 3, pp. 522-31, Dec 1996.

[200] Y. Sato *et al.*, "Role of transcription factors in angiogenesis: Ets-1 promotes angiogenesis as well as endothelial apoptosis," *Ann N Y Acad Sci,* vol. 947, pp. 117-23, Dec 2001.

[201] J. Chen *et al.*, "VEGF amplifies transcription through ETS1 acetylation to enable angiogenesis," *Nat Commun,* vol. 8, no. 1, p. 383, Aug 29 2017.

[202] E. J. Battegay, J. Rupp, L. Iruela-Arispe, E. H. Sage, and M. Pech, "PDGF-BB modulates endothelial proliferation and angiogenesis in vitro via PDGF beta-receptors," *J Cell Biol,* vol. 125, no. 4, pp. 917-28, May 1994.

[203] T. Lopatina, S. Bruno, C. Tetta, N. Kalinina, M. Porta, and G. Camussi, "Platelet-derived growth factor regulates the secretion of extracellular vesicles by adipose mesenchymal stem cells and enhances their angiogenic potential," *Cell Commun Signal,* vol. 12, p. 26, Apr 11 2014.

[204] V. W. van Hinsbergh and P. Koolwijk, "Endothelial sprouting and angiogenesis: matrix metalloproteinases in the lead," *Cardiovasc Res,* vol. 78, no. 2, pp. 203-12, May 1 2008.

[205] M. V. Rojiani, J. Alidina, N. Esposito, and A. M. Rojiani, "Expression of MMP-2 correlates with increased angiogenesis in CNS metastasis of lung carcinoma," *Int J Clin Exp Pathol,* vol. 3, no. 8, pp. 775-81, Oct 16 2010.

[206] H. Zheng *et al.*, "Expressions of MMP-2, MMP-9 and VEGF are closely linked to growth, invasion, metastasis and angiogenesis of gastric carcinoma," *Anticancer Res,* vol. 26, no. 5A, pp. 3579-83, Sep-Oct 2006.

[207] A. H. Webb *et al.*, "Inhibition of MMP-2 and MMP-9 decreases cellular migration, and angiogenesis in in vitro models of retinoblastoma," *BMC Cancer,* vol. 17, no. 1, p. 434, Jun 20 2017.

[208] M. Aitkenhead, S. J. Wang, M. N. Nakatsu, J. Mestas, C. Heard, and C. C. Hughes, "Identification of endothelial cell genes expressed in an in vitro model of angiogenesis: induction of ESM-1, (beta)ig-h3, and NrCAM," *Microvasc Res,* vol. 63, no. 2, pp. 159-71, Mar 2002.

[209] J. Glienke *et al.*, "Differential gene expression by endothelial cells in distinct angiogenic states," *Eur J Biochem,* vol. 267, no. 9, pp. 2820-30, May 2000.

[210] H. G. Augustin, G. Y. Koh, G. Thurston, and K. Alitalo, "Control of vascular morphogenesis and homeostasis through the angiopoietin-Tie system," *Nat Rev Mol Cell Biol,* vol. 10, no. 3, pp. 165-77, Mar 2009.

[211] J. Holash *et al.*, "Vessel cooption, regression, and growth in tumors mediated by angiopoietins and VEGF," *Science,* vol. 284, no. 5422, pp. 1994-8, Jun 18 1999.

[212] I. B. Lobov, P. C. Brooks, and R. A. Lang, "Angiopoietin-2 displays VEGF-dependent modulation of capillary structure and endothelial cell survival in vivo," *Proc Natl Acad Sci U S A,* vol. 99, no. 17, pp. 11205-10, Aug 20 2002.

[213] M. De Palma and L. Naldini, "Angiopoietin-2 TIEs up macrophages in tumor angiogenesis," *Clin Cancer Res,* vol. 17, no. 16, pp. 5226-32, Aug 15 2011.

[214] A. K. Nalla, N. Estes, J. Patel, and J. S. Rao, "N-cadherin mediates angiogenesis by regulating monocyte chemoattractant protein-1 expression via PI3K/Akt signaling in prostate cancer cells," *Exp Cell Res,* vol. 317, no. 17, pp. 2512-21, Oct 15 2011.

[215] H. Gerhardt, H. Wolburg, and C. Redies, "N-cadherin mediates pericytic-endothelial interaction during brain angiogenesis in the chicken," *Dev Dyn,* vol. 218, no. 3, pp. 472-9, Jul 2000.

[216] E. Tillet, D. Vittet, O. Feraud, R. Moore, R. Kemler, and P. Huber, "N-cadherin deficiency impairs pericyte recruitment, and not endothelial differentiation or sprouting, in embryonic stem cell-derived angiogenesis," *Exp Cell Res,* vol. 310, no. 2, pp. 392-400, Nov 1 2005.

[217] G. A. Strasser, J. S. Kaminker, and M. Tessier-Lavigne, "Microarray analysis of retinal endothelial tip cells identifies CXCR4 as a mediator of tip cell morphology and branching," *Blood,* vol. 115, no. 24, pp. 5102-10, Jun 17 2010.

[218] Z. Liang *et al.*, "CXCR4/CXCL12 axis promotes VEGF-mediated tumor angiogenesis through Akt signaling pathway," *Biochem Biophys Res Commun,* vol. 359, no. 3, pp. 716-22, Aug 3 2007.

[219] H. Yoshiji *et al.*, "KDR/Flk-1 is a major regulator of vascular endothelial growth factor-induced tumor development and angiogenesis in murine hepatocellular carcinoma cells," *Hepatology,* vol. 30, no. 5, pp. 1179-86, Nov 1999.

[220] Y. Sakurai, K. Ohgimoto, Y. Kataoka, N. Yoshida, and M. Shibuya, "Essential role of Flk-1 (VEGF receptor 2) tyrosine residue 1173 in vasculogenesis in mice," *Proc Natl Acad Sci U S A,* vol. 102, no. 4, pp. 1076-81, Jan 25 2005.

[221] P. Carmeliet, F. De Smet, S. Loges, and M. Mazzone, "Branching morphogenesis and antiangiogenesis candidates: tip cells lead the way," *Nat Rev Clin Oncol,* vol. 6, no. 6, pp. 315-26, Jun 2009.

[222] J. G. Teodoro, S. K. Evans, and M. R. Green, "Inhibition of tumor angiogenesis by p53: a new role for the guardian of the genome," *J Mol Med (Berl),* vol. 85, no. 11, pp. 1175-86, Nov 2007.

[223] M. Farhang Ghahremani *et al.*, "p53 promotes VEGF expression and angiogenesis in the absence of an intact p21-Rb pathway," *Cell Death Differ,* vol. 20, no. 7, pp. 888-97, Jul 2013.

[224] M. Corada *et al.*, "The Wnt/beta-catenin pathway modulates vascular remodeling and specification by upregulating Dll4/Notch signaling," *Dev Cell,* vol. 18, no. 6, pp. 938-49, Jun 15 2010.

[225] A. Cattelino *et al.*, "The conditional inactivation of the beta-catenin gene in endothelial cells causes a defective vascular pattern and increased vascular fragility," *J Cell Biol,* vol. 162, no. 6, pp. 1111-22, Sep 15 2003.

[226] A. Fantin *et al.*, "NRP1 acts cell autonomously in endothelium to promote tip cell function during sprouting angiogenesis," *Blood,* vol. 121, no. 12, pp. 2352-62, Mar 21 2013.

[227] I. M. Aspalter *et al.*, "Alk1 and Alk5 inhibition by Nrp1 controls vascular sprouting downstream of Notch," *Nat Commun,* vol. 6, p. 7264, Jun 17 2015.

[228] A. Casazza *et al.*, "Impeding macrophage entry into hypoxic tumor areas by Sema3A/Nrp1 signaling blockade inhibits angiogenesis and restores antitumor immunity," *Cancer Cell,* vol. 24, no. 6, pp. 695-709, Dec 9 2013.

[229] F. P. Limbourg, K. Takeshita, F. Radtke, R. T. Bronson, M. T. Chin, and J. K. Liao, "Essential role of endothelial Notch1 in angiogenesis," *Circulation,* vol. 111, no. 14, pp. 1826-32, Apr 12 2005.

[230] K. Takeshita *et al.*, "Critical role of endothelial Notch1 signaling in postnatal angiogenesis," *Circ Res,* vol. 100, no. 1, pp. 70-8, Jan 5 2007.

[231] E. A. Korhonen *et al.*, "Tie1 controls angiopoietin function in vascular remodeling and inflammation," *J Clin Invest,* vol. 126, no. 9, pp. 3495-510, Sep 1 2016.

[232] S. Savant *et al.*, "The Orphan Receptor Tie1 Controls Angiogenesis and Vascular Remodeling by Differentially Regulating Tie2 in Tip and Stalk Cells," *Cell Rep,* vol. 12, no. 11, pp. 1761-73, Sep 22 2015.

[233] G. Ferrari, B. D. Cook, V. Terushkin, G. Pintucci, and P. Mignatti, "Transforming growth factor-beta 1 (TGF-beta1) induces angiogenesis through vascular endothelial growth factor (VEGF)-mediated apoptosis," *J Cell Physiol,* vol. 219, no. 2, pp. 449-58, May 2009.

[234] E. Boscolo *et al.*, "JAGGED1 signaling regulates hemangioma stem cell-to-pericyte/vascular smooth muscle cell differentiation," *Arterioscler Thromb Vasc Biol,* vol. 31, no. 10, pp. 2181-92, Oct 2011.

[235] F. A. High, M. M. Lu, W. S. Pear, K. M. Loomes, K. H. Kaestner, and J. A. Epstein, "Endothelial expression of the Notch ligand Jagged1 is required for vascular smooth muscle development," *Proc Natl Acad Sci U S A,* vol. 105, no. 6, pp. 1955-9, Feb 12 2008.

[236] A. R. Pedrosa *et al.*, "Endothelial Jagged1 antagonizes Dll4 regulation of endothelial branching and promotes vascular maturation downstream of Dll4/Notch1," *Arterioscler Thromb Vasc Biol,* vol. 35, no. 5, pp. 1134-46, May 2015.

[237] H. E. Tzeng *et al.*, "Interleukin-6 induces vascular endothelial growth factor expression and promotes angiogenesis through apoptosis signal-regulating kinase 1 in human osteosarcoma," *Biochem Pharmacol,* vol. 85, no. 4, pp. 531-40, Feb 15 2013.

[238] G. Gopinathan *et al.*, "Interleukin-6 Stimulates Defective Angiogenesis," *Cancer Res,* vol. 75, no. 15, pp. 3098-107, Aug 1 2015.

[239] C. Fang *et al.*, "An important role of matrix metalloproteinase-8 in angiogenesis in vitro and in vivo," *Cardiovasc Res,* vol. 99, no. 1, pp. 146-55, Jul 1 2013.

[240] Q. Xiao *et al.*, "Matrix metalloproteinase-8 promotes vascular smooth muscle cell proliferation and neointima formation," *Arterioscler Thromb Vasc Biol,* vol. 34, no. 1, pp. 90-8, Jan 2014.

[241] R. Cao *et al.*, "Angiogenesis stimulated by PDGF-CC, a novel member in the PDGF family, involves activation of PDGFR-alphaalpha and -alphabeta receptors," *FASEB J,* vol. 16, no. 12, pp. 1575-83, Oct 2002.

[242] L. Chen, E. E. Tredget, P. Y. Wu, and Y. Wu, "Paracrine factors of mesenchymal stem cells recruit macrophages and endothelial lineage cells and enhance wound healing," *PLoS One,* vol. 3, no. 4, p. e1886, 2008.

[243] D. I. Cho *et al.*, "Mesenchymal stem cells reciprocally regulate the M1/M2 balance in mouse bone marrow-derived macrophages," *Exp Mol Med,* vol. 46, p. e70, 2014.

[244] C. Liu *et al.*, "Macrophages Mediate the Repair of Brain Vascular Rupture through Direct Physical Adhesion and Mechanical Traction," *Immunity,* vol. 44, no. 5, pp. 1162-76, May 17 2016.

[245] L. E. Hind, E. B. Lurier, M. Dembo, K. L. Spiller, and D. A. Hammer, "Effect of M1-M2 Polarization on the Motility and Traction Stresses of Primary Human Macrophages," *Cell Mol Bioeng,* vol. 9, no. 3, pp. 455-465, Sep 2016.

[246] F. H. Barnett *et al.*, "Macrophages form functional vascular mimicry channels in vivo," *Sci Rep,* vol. 6, p. 36659, Nov 11 2016.

[247] S. Al-Roubaie, J. H. Hughes, M. B. Filla, R. Lansford, S. Lehoux, and E. A. Jones, "Time-lapse microscopy of macrophages during embryonic vascular development," *Dev Dyn,* vol. 241, no. 9, pp. 1423-31, Sep 2012.

[248] A. O. Awojoodu *et al.*, "Sphingosine 1-phosphate receptor 3 regulates recruitment of anti-inflammatory monocytes to microvessels during implant arteriogenesis," *Proc Natl Acad Sci U S A,* vol. 110, no. 34, pp. 13785-90, Aug 20 2013.

[249] K. Lolmede *et al.*, "Inflammatory and alternatively activated human macrophages attract vessel-associated stem cells, relying on separate HMGB1- and MMP-9-dependent pathways," *J Leukoc Biol,* vol. 85, no. 5, pp. 779-87, May 2009.

[250] J. I. Greenberg *et al.*, "A role for VEGF as a negative regulator of pericyte function and vessel maturation," *Nature,* vol. 456, no. 7223, pp. 809-13, Dec 11 2008.

[251] A. Freiman *et al.*, "Adipose-derived endothelial and mesenchymal stem cells enhance vascular network formation on three-dimensional constructs in vitro," *Stem Cell Res Ther,* vol. 7, p. 5, 2016.

[252] Z. Qin, "The use of THP-1 cells as a model for mimicking the function and regulation of monocytes and macrophages in the vasculature," *Atherosclerosis,* vol. 221, no. 1, pp. 2-11, Mar 2012.

[253] Y. Amoh, L. Li, K. Katsuoka, M. Bouvet, and R. M. Hoffman, "GFP-expressing vascularization of Gelfoam as a rapid in vivo assay of angiogenesis stimulators and inhibitors," *Biotechniques,* vol. 42, no. 3, pp. 294, 296, 298, Mar 2007.

[254] M. Centra *et al.*, "Culture of bovine pulmonary artery endothelial cells on Gelfoam blocks," *FASEB J,* vol. 6, no. 12, pp. 3117-21, Sep 1992.

[255] J. Yu, Y. Gu, K. T. Du, S. Mihardja, R. E. Sievers, and R. J. Lee, "The effect of injected RGD modified alginate on angiogenesis and left ventricular function in a chronic rat infarct model," *Biomaterials,* vol. 30, no. 5, pp. 751-6, Feb 2009.

[256] J. Schindelin *et al.*, "Fiji: an open-source platform for biological-image analysis," *Nat Methods,* vol. 9, no. 7, pp. 676-82, Jun 28 2012.

[257] E. Zudaire, L. Gambardella, C. Kurcz, and S. Vermeren, "A computational tool for quantitative analysis of vascular networks," *PLoS One,* vol. 6, no. 11, p. e27385, 2011.

[258] M. Winter, W. Mankowski, E. Wait, S. Temple, and A. R. Cohen, "LEVER: software tools for segmentation, tracking and lineaging of proliferating cells," *Bioinformatics,* vol. 32, no. 22, pp. 3530-3531, Nov 15 2016.

[259] K. Yumoto, J. E. Berry, R. S. Taichman, and Y. Shiozawa, "A novel method for monitoring tumor proliferation in vivo using fluorescent dye DiD," *Cytometry A,* vol. 85, no. 6, pp. 548-55, Jun 2014.

[260] A. Lesman, J. Koffler, R. Atlas, Y. J. Blinder, Z. Kam, and S. Levenberg, "Engineering vessel-like networks within multicellular fibrin-based constructs," *Biomaterials,* vol. 32, no. 31, pp. 7856-69, Nov 2011.

[261] I. W. Tattersall *et al.*, "In vitro modeling of endothelial interaction with macrophages and pericytes demonstrates Notch signaling function in the vascular microenvironment," *Angiogenesis,* vol. 19, no. 2, pp. 201-15, Apr 2016.

[262] K. Dhar *et al.*, "Tumor cell-derived PDGF-B potentiates mouse mesenchymal stem cells-pericytes transition and recruitment through an interaction with NRP-1," *Mol Cancer,* vol. 9, p. 209, Aug 5 2010.

[263] J. E. Nor and P. J. Polverini, "Role of endothelial cell survival and death signals in angiogenesis," *Angiogenesis,* vol. 3, no. 2, pp. 101-16, 1999.

[264] S. J. Kim *et al.*, "Circulating monocytes expressing CD31: implications for acute and chronic angiogenesis," *Am J Pathol,* vol. 174, no. 5, pp. 1972-80, May 2009.

[265] J. K. McKenney, S. W. Weiss, and A. L. Folpe, "CD31 expression in intratumoral macrophages: a potential diagnostic pitfall," *Am J Surg Pathol,* vol. 25, no. 9, pp. 1167-73, Sep 2001.

[266] X. Yan *et al.*, "A novel anti-CD146 monoclonal antibody, AA98, inhibits angiogenesis and tumor growth," *Blood,* vol. 102, no. 1, pp. 184-91, Jul 1 2003.

[267] J. Rouwkema and A. Khademhosseini, "Vascularization and Angiogenesis in Tissue Engineering: Beyond Creating Static Networks," *Trends Biotechnol,* vol. 34, no. 9, pp. 733-45, Sep 2016.

[268] B. N. Mason, A. Starchenko, R. M. Williams, L. J. Bonassar, and C. A. Reinhart-King, "Tuning three-dimensional collagen matrix stiffness independently of collagen concentration modulates endothelial cell behavior," *Acta Biomater,* vol. 9, no. 1, pp. 4635-44, Jan 2013.

[269] L. Santos *et al.*, "Extracellular Stiffness Modulates the Expression of Functional Proteins and Growth Factors in Endothelial Cells," *Adv Healthc Mater,* Aug 13 2015.

[270] A. Shamloo and S. C. Heilshorn, "Matrix density mediates polarization and lumen formation of endothelial sprouts in VEGF gradients," *Lab Chip,* vol. 10, no. 22, pp. 3061-8, Nov 21 2010.

[271] D. O. Freytes, J. W. Kang, I. Marcos-Campos, and G. Vunjak-Novakovic, "Macrophages modulate the viability and growth of human mesenchymal stem cells," *J Cell Biochem,* vol. 114, no. 1, pp. 220-9, Jan 2013.

[272] C. Lo Sicco *et al.*, "Mesenchymal Stem Cell-Derived Extracellular Vesicles as Mediators of Anti-Inflammatory Effects: Endorsement of Macrophage Polarization," *Stem Cells Transl Med,* vol. 6, no. 3, pp. 1018-1028, Mar 2017.

[273] A. Navarro, S. Marin, N. Riol, F. Carbonell-Uberos, and M. D. Minana, "Human adipose tissue-resident monocytes exhibit an endothelial-like phenotype and display angiogenic properties," *Stem Cell Res Ther,* vol. 5, no. 2, p. 50, Apr 14 2014.

[274] N. Dehne, M. Tausendschon, S. Essler, T. Geis, T. Schmid, and B. Brune, "IL-4 reduces the proangiogenic capacity of macrophages by down-regulating HIF-1alpha translation," *J Leukoc Biol,* vol. 95, no. 1, pp. 129-37, Jan 2014.

[275] C. Gerri, R. Marin-Juez, M. Marass, A. Marks, H. M. Maischein, and D. Y. R. Stainier, "Hif-1alpha regulates macrophage-endothelial interactions during blood vessel development in zebrafish," *Nat Commun,* vol. 8, p. 15492, May 19 2017.

[276] G. Christoffersson, J. Lomei, P. O'Callaghan, J. Kreuger, S. Engblom, and M. Phillipson, "Vascular sprouts induce local attraction of proangiogenic neutrophils," *J Leukoc Biol,* vol. 102, no. 3, pp. 741-751, Sep 2017.

[277] T. Kang *et al.*, "Adipose-Derived Stem Cells Induce Angiogenesis via Microvesicle Transport of miRNA-31," *Stem Cells Transl Med,* vol. 5, no. 4, pp. 440-50, Apr 2016.

[278] J. Li *et al.*, "Microvesicle-mediated transfer of microRNA-150 from monocytes to endothelial cells promotes angiogenesis," *J Biol Chem,* vol. 288, no. 32, pp. 23586-96, Aug 9 2013.

[279] C. Neu *et al.*, "CD14-dependent monocyte isolation enhances phagocytosis of listeria monocytogenes by proinflammatory, GM-CSF-derived macrophages," *PLoS One,* vol. 8, no. 6, p. e66898, 2013.

[280] L. Zhou *et al.*, "Impact of human granulocyte and monocyte isolation procedures on functional studies," *Clin Vaccine Immunol,* vol. 19, no. 7, pp. 1065-74, Jul 2012.

[281] L. J. Appleby, N. Nausch, N. Midzi, T. Mduluza, J. E. Allen, and F. Mutapi, "Sources of heterogeneity in human monocyte subsets," *Immunol Lett,* vol. 152, no. 1, pp. 32-41, Apr 2013.

[282] J. B. Hansen, D. S. Halvorsen, B. C. Haldorsen, R. Olsen, H. Sjursen, and P. Kierulf, "Retention of phagocytic functions in cryopreserved human monocytes," *J Leukoc Biol,* vol. 57, no. 2, pp. 235-41, Feb 1995.

[283] J. Seager Danciger *et al.*, "Method for large scale isolation, culture and cryopreservation of human monocytes suitable for chemotaxis, cellular adhesion assays, macrophage and dendritic cell differentiation," *J Immunol Methods,* vol. 288, no. 1-2, pp. 123-34, May 2004.

[284] S. Hori *et al.*, "Freeze-thawing procedures have no influence on the phenotypic and functional development of dendritic cells generated from peripheral blood CD14+ monocytes," *J Immunother,* vol. 27, no. 1, pp. 27-35, Jan-Feb 2004.

[285] M. Meijerink, D. Ulluwishewa, R. C. Anderson, and J. M. Wells, "Cryopreservation of monocytes or differentiated immature DCs leads to an altered cytokine response to TLR agonists and microbial stimulation," *J Immunol Methods,* vol. 373, no. 1-2, pp. 136-42, Oct 28 2011.

[286] G. F. Silveira, P. F. Wowk, A. M. Machado, C. N. Duarte dos Santos, and J. Bordignon, "Immature dendritic cells generated from cryopreserved human monocytes show impaired ability to respond to LPS and to induce allogeneic lymphocyte proliferation," *PLoS One,* vol. 8, no. 7, p. e71291, 2013.

[287] M. Jaguin, N. Houlbert, O. Fardel, and V. Lecureur, "Polarization profiles of human M-CSF-generated macrophages and comparison of M1-markers in classically activated macrophages from GM-CSF and M-CSF origin," *Cell Immunol,* vol. 281, no. 1, pp. 51-61, Jan 2013.

[288] F. A. Verreck, T. de Boer, D. M. Langenberg, L. van der Zanden, and T. H. Ottenhoff, "Phenotypic and functional profiling of human proinflammatory type-1 and anti-inflammatory type-2 macrophages in response to microbial antigens and IFN-gamma- and CD40L-mediated costimulation," *J Leukoc Biol,* vol. 79, no. 2, pp. 285-93, Feb 2006.

[289] W. Xu, A. Roos, N. Schlagwein, A. M. Woltman, M. R. Daha, and C. van Kooten, "IL-10-producing macrophages preferentially clear early apoptotic cells," *Blood,* vol. 107, no. 12, pp. 4930-7, Jun 15 2006.

[290] E. Vannier, L. C. Miller, and C. A. Dinarello, "Coordinated antiinflammatory effects of interleukin 4: interleukin 4 suppresses interleukin 1 production but up-regulates gene expression and synthesis of interleukin 1 receptor antagonist," *Proc Natl Acad Sci U S A,* vol. 89, no. 9, pp. 4076-80, May 1 1992.

[291] F. Rey-Giraud, M. Hafner, and C. H. Ries, "In vitro generation of monocyte-derived macrophages under serum-free conditions improves their tumor promoting functions," *PLoS One,* vol. 7, no. 8, p. e42656, 2012.

VITA

Pamela Leigh (Kubinski) Graney was born on January 22, 1987 in Staten Island, New York. She completed her undergraduate education at Rowan University in Glassboro, NJ, and graduated *cum laude* in 2009 with a Bachelor of Science in Chemical Engineering and minors in chemistry and mathematics. She also earned a Masters of Science in Chemical Engineering from Rowan in 2013, under the guidance of Dr. Jennifer Vernengo. Pamela interned at Novartis Pharmaceuticals in 2008, and served as a teaching assistant for chemical reaction engineering. She was the recipient of several AIChE poster competition awards, as well as the Zeisberg outstanding laboratory report award in 2008 and 2009. Pamela was also inducted into the Tau Beta Pi National Engineering Honor Society, and is a member of the Society For Biomaterials and the Association for Women in Science. During her graduate career at Drexel, Pamela has served as Vice President for the Drexel Biomed Graduation Association, and as a teaching assistant for senior level biomaterials courses. Pamela has also obtained extensive international research experience; she spent 4 months at the University of Sydney, Australia, advised by Prof. Hala Zreiqat, and was awarded a Stein Fellowship and a U.S.-Israel Binational Science Foundation travel award to support a 6-month research exchange at the Technion-Israel Institute of Technology under the guidance of Prof. Shulamit Levenberg. Pamela has presented her work at many national and international conferences, and received a Trainee Award from the World Biomaterials Congress in 2016, and an honorable mention STAR award from the Society For Biomaterials in 2017. Pamela has one patent and numerous publications. While pursuing her PhD, she also completed 4 terms of Hebrew coursework and earned a minor in undergraduate STEM education. Pamela defended her doctoral dissertation on January 9th, 2018.